



SAPIENZA
UNIVERSITÀ DI ROMA

Sapienza University of Rome

Department of Physics
Ph.D. in Physics

THESIS FOR THE DEGREE OF DOCTOR OF PHILOSOPHY

**Study of the critical dynamics
of active matter models to
explain anomalous relaxation in
natural swarms**

Advisors

Dr. Andrea Cavagna
Prof. Tomas S. Grigera

Candidate

Giulia Pisegna
matricola 1536866

Academic Year 2021-2022 (XXXIV cycle)
Author's email: giulia.pisegna@uniroma1.it

Dedicated to my rock,
my strength, my sister Simona.

"Galileo: Le città sono piccole, le teste altrettanto. Piene di superstizioni e di pestilenze. Ma ora noi diciamo: visto che così è, così non deve rimanere. Perché ogni cosa si muove, amico mio. Molto è già stato trovato, ma quello che è ancora da trovare, è di più."

Vita di Galileo, Bertolt Brecht

Contents

Introduction	ix
1 Statistical Physics of collective behavior	1
1.1 When statistical physics meets biology	1
1.2 The Vicsek model	2
1.3 Correlation in biological systems	4
1.4 A paradigmatic example: birds flocks	5
1.5 Midges swarms: collective behavior in absence of collective order .	8
1.6 Near-criticality of natural swarms	9
1.7 Theory of dynamical scaling	11
1.8 Experimental evidence of dynamical scaling in natural swarms . .	14
1.9 The core of the thesis: two crossovers to explain the swarming behavior	16
2 The Dynamical Renormalization Group	21
2.1 From microscopic to mesoscopic equations of motion	21
2.2 The fundamental steps of DRG	24
2.2.1 Martin-Siggia-Rose action	25
2.2.2 Study of the Gaussian theory	27
2.2.3 Shell-integration	28
2.2.4 Rescaling	31
2.3 Fixed points: the dynamical critical exponent	32
2.4 Dynamical scaling from DRG	33
3 Renormalization of the incompressible Vicsek Model	35
3.1 Vicsek Model and Toner and Tu theory	35
3.2 Adding incompressibility	38
3.3 Field dynamical equations	40
3.4 MSR action and Gaussian theory	41
3.5 Vertices and perturbation expansion	42
3.6 Renormalization of the linear dynamics	44
3.7 Vertices corrections	45
3.8 RG flow and fixed points	47
4 The first crossover: from an equilibrium to an off-equilibrium universality class	51
4.1 Activity drives the crossover in parameters space	52
4.2 How to tune activity	56
4.3 Numerical simulations	59

4.3.1	Static behavior and correlation length	60
4.3.2	Dynamical behavior and relaxation time	63
4.4	Dynamical crossover in numerical experiments	63
4.5	Checking homogeneity	67
4.6	Breakdown of hydrodynamics for large speed	68
4.7	Conclusions on the Vicsek Model	69
5	Reinstating inertia in the microscopic dynamics	71
5.1	From the Vicsek Model to the Inertial Spin Model	72
5.1.1	The double role of velocity	75
5.1.2	Rotational symmetry and spin	76
5.2	Spin dissipation and overdamped limit	79
5.3	Another derivation of the ISM equations	81
5.4	Why ISM for natural swarms?	83
6	Renormalization of the Inertial Spin Model in a fixed network approximation	87
6.1	ISM in the fixed network approximation	87
6.1.1	Coarse-grained field theory	89
6.2	MSR action and Gaussian theory	93
6.3	Vertices and perturbative expansion	95
6.4	Renormalization of the parameters	97
6.5	Vertices corrections and Ward identities	102
6.6	RG flow and fixed points	105
7	The second crossover: from a conservative to a dissipative universality class	109
7.1	The crucial role of dissipation	110
7.2	More details on the stable dissipative fixed point	114
7.3	Numerical simulations	115
7.3.1	Static behavior and correlation length	116
7.3.2	Dynamical behavior and relaxation time	120
7.4	Dynamical crossover in numerical experiments	120
7.5	Dynamical scaling at $k\xi = 1$	123
7.6	Conclusions on the equilibrium Inertial Spin Model	125
8	In the crossfires of the two crossovers	127
8.1	How do the crossovers relate to natural swarms?	128
8.2	Next: swarms in 3.99 dimensions	130
8.3	Incompressible ISM	131
9	Collateral projects	137
9.1	A new model to explain anomalous correlations in bird flocks	138
9.1.1	Linear speed control	139
9.1.2	Marginal speed control	142
9.2	Violation of Fluctuation-Dissipation Relations in soft-speed active matter models	144
9.2.1	Biological motivations: perturbation-response study in swarms of insects	146

9.2.2	The model: speed perturbations	148
9.2.3	Response function and equilibrium study	149
9.2.4	Out-of-equilibrium preliminary results	155
9.3	How to spatially confine ISM swarms	158
9.3.1	Force on the angular momentum	162
Conclusions		167
A Angular averages		171
B Numerical implementation of ISM algorithm		173
Bibliography		174

Introduction

A major challenge of modern physics and mathematics is the theoretical modeling of living systems. Recently, methods of condensed matter physics have been successfully applied to biological systems, providing an accurate description of the statistical laws governing active matter.

Systems of interest in active matter are made of a large number of entities interacting locally and leading to large-scale collective behavior. Manifestations of this appear at multiple scales of living systems, from cell migration to swarming of insects and flocking of birds. Interestingly, though these systems are microscopically very different, they exhibit common macroscopic features. The study of active matter through the lens of statistical physics aims at developing a unified description of these behaviors.

A fruitful approach uses the theory of critical phenomena, developed in condensed matter physics to study phase transitions in inanimate systems. This theory has allowed a systematic description of equilibrium phenomena through the introduction of concepts like long-range correlations, scaling laws, and renormalization. A major result states that an equilibrium system close to a second-order phase transition exhibits a macroscopic behavior independent of the microscopic details. This notion of *universality* has inspired the use of the same methods to study non-equilibrium collective behaviors in biology. Hydrodynamics, active matter models, and non-equilibrium statistical physics became paramount to the study of self-organization in biological systems.

Several questions are still open. To what extent can the search for universality be applied to biological collective behavior? How should equilibrium theories be transformed in order to study non-equilibrium living systems? Only a combination of theory and experiments can provide answers to these problems.

In this thesis I try to tackle these questions, focusing on the collective behavior of natural swarms. Recent field experiments unveiled long-range correlations in swarms of midges in absence of collective motion [1], thus suggesting that this system is disordered but with a near-critical phenomenology [2]. Moreover, experiments confirmed the emergence of dynamical scaling laws in the spatio-temporal correlation functions of different swarms [3], providing additional evidence about the universality of their behavior.

Dynamical scaling stems from the study of time-dependent critical phenomena of equilibrium systems [4]. It affirms that, close to criticality, the correlation length ξ is the only relevant length scale of the system, ruling also its dynamical

relaxation [4]. This phenomenon is known as critical slowing down, and it is expressed by the power-law $\tau \sim \xi^z$, where τ is the characteristic time scale and z is called *dynamical critical exponent* [5]. When this property holds, the exponent determines the dynamical universality class of the system, containing all the information on its macroscopic dynamical behavior. Natural swarms obey this law with a dynamical critical exponent $z \simeq 1.2$, value not found in any other statistical model [3]. Moreover, the relaxation reflects an anomalous underdamped decay of velocity correlation functions, which is not compatible with standard models. This thesis proposes to combine classic and novel active matter models with standard statistical field theory tools, with the purpose of rationalizing this experimental finding. The validity of scaling laws suggests that a description in terms of out-of-equilibrium critical phenomena is legitimate, therefore our study will employ Renormalization Group (RG) techniques and numerical simulations of active matter models in a near-critical regime.

The investigation focuses on the analysis of two models. The first is the Vicsek model that describes a self-propelled dissipative dynamics in the velocities. An analytical calculation on the related hydrodynamic incompressible field theory reveals that activity lowers the value of the dynamical critical exponent with respect to the equilibrium universality class through a mechanism of crossover. Numerical simulations confirm that this result is valid also for compressible systems. The second studied theory is the Inertial Spin Model, which formulates a second-order dynamics in the velocities able to qualitatively reproduce the swarms' relaxation. A fixed-network RG calculation highlights the role of inertia in determining the critical dynamics of weakly damped systems: through a dynamical crossover they can exhibit a $z = 1.5$ critical exponent, a value lower than the dissipative case. The information acquired with these studies is combined in a theoretical model that includes self-propulsion and inertial dynamics, ingredients that both contribute to lower the value of the critical exponent finally arriving at consistency with experimental data.

The thesis is organized as follows. We start with chapter 1 by providing an overview of collective animal behaviors and by explaining which are the statistical physics tools used to quantitatively describe them. We focus on the concept of correlation and we give a summary of experimental observations about the collective behavior of flocks of birds and insect swarms. We introduce the dynamical properties of natural swarms and discuss the experimental findings that stimulated this entire project. In chapter 2 we present the methods used for the theoretical analysis carried out in this thesis, namely: how to write field-theory dynamical equations of motion starting from microscopic models, and how to perform a Dynamical Renormalization Group (DRG) calculation on them.

In chapter 3 we study the dynamical universality class of the Vicsek model under incompressibility conditions. It is the first model we investigate to explain the anomalous relaxation found in natural swarms. We report the analytical calculation already performed by Chen, Toner, and Lee in [6], from which we unveil

a dynamical crossover between an equilibrium to an off-equilibrium universality class that interests active polar systems. We study it in chapter 4, where we find out that activity plays a fundamental role with the correlation length in determining the critical relaxation of a macroscopic system. In regimes of strong self-propulsion or very large sizes, the system exhibits a dynamical critical exponent lower than the standard equilibrium value. We verify this phenomenon on the original Vicsek model without imposing any incompressibility constraint and by means of extensive numerical simulations. We fully confirm that the same crossover dynamics can be found in compressible yet homogeneous systems [7].

The Vicsek model is not suitable to reproduce the behavior of natural swarms: the active dynamical critical exponent, $z = 1.7$, is not consistent with the experimental data. Moreover, the exponential decay of the dynamical correlation functions does not match with the underdamped swarming relaxation. Following these observations, we introduce in chapter 5 the Inertial Spin Model, an active matter model with second-order dynamics in the velocity, originally developed to explain turning movements in bird flocks [8]. Due to its inertial nature, we believe it is a good candidate to explain swarming behavior too. Chapter 6 is dedicated to the one-loop DRG calculation we perform on the corresponding field theory under a fixed network approximation. The theory involves coupling between the order parameter and a conjugated momentum in the presence of dissipation.

In chapter 7 we show that the violation of momentum conservation generates a crossover between an unstable fixed point with $z = 1.5$ in three dimensions, reflecting a conservative dynamics, and a stable fixed point with $z = 2$, corresponding to a dissipative dynamics. We report on-lattice numerical simulations of the original microscopic model that confirm this crossover. We also verify that finite-size and weakly damped systems with inertial dynamics experience a lower dynamical exponent even at the equilibrium level [9, 10]. Even though the best estimate of z obtained with this model is not consistent with experimental data, the relaxation is qualitatively well reproduced.

In chapter 8 we summarize the results obtained and we explain the next steps to take to conclude our analysis. To be consistent with experimental data it is necessary to reinstate activity in the hydrodynamic field theory of the ISM. We, therefore, close our investigation anticipating the results of the DRG calculation on this out-of-equilibrium inertial model, but details will not be available in this thesis. The outcome is a new RG fixed-point to which the active and the inertial crossovers contribute, producing a dynamical critical exponent $z = 1.3$ fairly consistent with experimental data [11].

Concluding, chapter 9 collects a series of side projects realized in collaboration with other members of the group and not related to RG calculations. They focus on the role of speed fluctuations in bird flocks and swarms, and how they can be used to quantify the violation of the Fluctuation-Dissipation theorem in active systems. We also investigate the role of external landmarks in swarming behavior. Most of them are still ongoing projects, thus opening and stimulating interesting future research.

Chapter 1

Statistical Physics of collective behavior

1.1 When statistical physics meets biology

From ferromagnets to simple water, many materials of everyday experience are characterized by phenomena of phase transition. This latter describes a process during which systems composed of a large number of interacting particles undergo a transition from one state of matter to another. The complex cooperative behavior shown by equilibrium second-order phase transitions has been studied in great detail during the past sixty years, culminating in the 1970s with the formulation of the Renormalization Group method [12, 13]. The outstanding achievement of this theory was to formally demonstrate that the main features of equilibrium systems at the transition point are not sensitive to the details of microscopic interactions between the constituents. Scaling laws and critical exponents rule instead the phenomena [14], describing in a universal way properties of a large variety of different systems.

Condensed matter materials are not the only ones to develop complex collective behavior. Recently, particular attention has been devoted to systems which are far from equilibrium and undergo processes of aggregations, collective motion or complex pattern formations. Examples can be drawn from the living and the non-living world spanning several order of spatial scales, just to name few of them: self-propelled rods [15], nematic liquid crystals [16], molecular motors [17], cells migration and bacteria [18–20], insects swarms [1, 21] fish schools [22, 23] and flocks of birds [24–26].

All these systems display cooperative and collective macroscopic behaviors, spontaneously emerging from local interactions in absence of leaders or external driving forces. The main feature of these systems is that the action of one individual in the group is strongly influenced by the others, even if they do not directly interact [27, 28]. The similar phenomenology with critical phenomena raised statistical physics to the appropriate science for a quantitative description of this behavior. Indeed, since widely different biological realms are involved, the idea that it is possible to develop minimal models to reproduce common fea-

tures comes into play. A relevant boost in this direction was given by Vicsek and coworkers with the introduction of the well-known Vicsek model [29].

1.2 The Vicsek model

In their seminal paper [29], Vicsek and coauthors introduced a model for self-driven particles, able to describe a novel type of phase transition and to reproduce the phenomenology of various active and living systems. It can be interpreted as the non-equilibrium analog of classical ferromagnetic models, with the main difference that it is inherently dynamic [29]. Every particle is identified by a velocity vector $\mathbf{v}_i(t)$ that determines the direction of motion, and by a positional vector $\mathbf{r}_i(t)$ implementing the dynamical change of positions. The equations in $d = 3$ for a system of N particles read [30],

$$\mathbf{v}_i(t+1) = \mathcal{R}_\eta \left(\sum_j^N n_{ij}(t) \mathbf{v}_j(t) \right) \quad (1.1)$$

$$\mathbf{r}_i(t+1) = \mathbf{r}_i(t) + \mathbf{v}_i(t+1) \quad (1.2)$$

$$|\mathbf{v}_i(t)| = v_0 \quad \forall i, t. \quad (1.3)$$

The rules are simple: at every time step the direction of motion of a particle is determined by the average direction of agents in its neighborhood of radius r_c , with some random perturbation added, eq (1.1); the particles are driven by a constant value of speed v_0 , eq (1.3), and the positions are updated straightforwardly, eq (1.2) [29]. The first equation of the model describes a direct alignment interaction between the velocity vectors, which is mediated by the connectivity matrix $n_{ij}(t)$. The entries of this matrix are 1 if the particles interact with each other, while are zero if they do not. The noise operator \mathcal{R}_η applies a source of scalar noise, rotating randomly and normalizing its argument within a cone of angle $4\pi\eta$ around its original direction, with $\eta \in [0, 1]$ the amplitude of the noise playing the role of temperature [30].

The main difference with equilibrium systems is that particles are allowed to move and the alignment interaction can be seen as a "collision event" in which the momentum is not conserved, namely the momentum of two particles before and after the interaction is not the same. The implementation of this statement lies in the constraint on the value of the speed v_0 , which describes the source of activity in the system, injecting energy and sustaining the self-propelled motion at a particle level [28]. A direct consequence of it is that the interaction matrix depends on time $n_{ij}(t)$: particles are free to move, producing a continuous reshuffling of the interaction network. This condition violates a fundamental requirement to reach equilibrium, namely the validity of detailed balance [31].

Despite these relevant differences, more analogies in methods and phenomenology can be found with equilibrium statistical physics systems, rather than with pure non-equilibrium phase transitions, as those involving absorbing states [32]

or interface growth models [33]. The scenario presented by the Vicsek model is a kinetic phase transition occurring from states of disordered to ordered collective motion, through a spontaneous symmetry breaking of rotational invariance. In the limit of $v_0 \rightarrow 0$, the model recovers the classical Heisenberg class, while for finite values of velocity, the observed phase transition is that of Fig 1.1: it can describe disordered swarms, aggregating and flocking events depending on the thermodynamic phase. The order parameter is the normalized average velocity, which plays the role of polarization,

$$\phi = \frac{1}{N} \left| \sum_i^N \frac{\mathbf{v}_i}{|\mathbf{v}_i|} \right|. \quad (1.4)$$

It measures the degree of collective order and global alignment: when the system moves in a highly polarized pattern, its value is close to 1 (panel d of Fig 1.1), while values close to zero reflect a disordered nature of the system (panel a of Fig 1.1). The first studies of [29] reported a second-order phase transition in noise or in density (panels e,f of Fig 1.1), however its nature has been debated for a long time [34, 35]. Finally, recent works agree that, in the thermodynamic limit, the phenomenology is described by a first-order transition with microphase separation [30, 35].

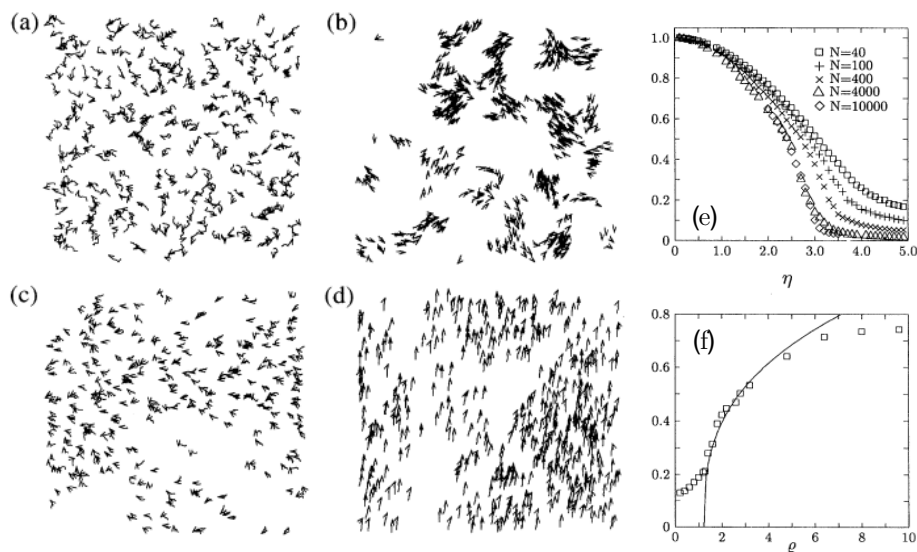


Figure 1.1: Thermodynamic phases and polarization of the Vicsek model. Panels a-d: snapshots of Vicsek model configurations from the high noise phase (a), to low noise phase (d). The system passes from a disordered motion, to an aggregated state and then performs ordered collective movement. Panel e,f: polarization for different sizes of the system as a function of noise strength and polarization as a function of density at fixed noise strength, respectively. Figure reprinted from [29].

Thanks to its simplicity and its ability in describing different phenomenologies of active and living systems, the model became the paradigm of active motion. In the last years, deep theoretical studies have been performed on it, ranging

from hydrodynamic theories [36–38] to modified interaction rules [39]. And still, it stimulates novel frontiers of theoretical investigations and applications to living systems. Success lies in translating into a very simple physical model the evidence that collective behavior emerges only due to local imitation between agents. Certainly, this class of models assumes that imitation happens through a direct interaction between particles' velocities, while it has been demonstrated that an effective similar mechanism can stem also from basic positional rules [40, 41].

1.3 Correlation in biological systems

The Vicsek model paved the way for a quantitative analysis of collective behavior in biological systems. The degree of polarization, the average speed, or the density distribution are examples of measurements of the system's global properties quantifying the emergence of collective motion's patterns in the group. However, the key characteristic of systems displaying cooperative behavior is the strong correlation between elements. A necessary condition for a large number of individuals to behave as a whole is that information spans rapidly across the group through the propagation of local interactions. The outcome is that the behavior of one individual is statistically influenced by others even at large spatial distances.

A significant link between the world of biology and physics is therefore provided by the measure of *correlation*. This feature is always a product of local interaction, namely when elements exchange information within short ranges in a direct and instantaneous way (e.g. alignment interaction). On the other hand, correlation can extend very far in space and time and it describes how much the behavior of an element *indirectly* influences that of others in the group [42].

The correlation functions are the statistical physics tool measuring this phenomenon, and they can be classified in *static* and *dynamical*. The former simply indicates how much the behavior of a part of the system influences that of another part, distant in space but at the same instant of time [42]. The dynamical processes that connect the two different areas are averaged out over all the possible configurations realized by the system. If instead, the interest lies in the mechanism of information propagation, the right tool to adopt is the dynamical correlation function, which measures to what extent a part of the system is correlated to another part at a different time [42].

More precisely, what is really interesting is the evaluation of the average fluctuations around the mean behavior of the group. Common external and environmental factors can produce global effects in the movement, giving trivial degrees of correlation to the system. Once these effects are eliminated, it is possible to evaluate how fluctuations influence each other on large temporal and spatial scales, thus producing a reliable measure of correlation. We therefore better refer to connected correlation functions, which are the principal quantities to identify properties of collective behavior.

We are interested in the degree of freedom of velocity, for which the fluctuation

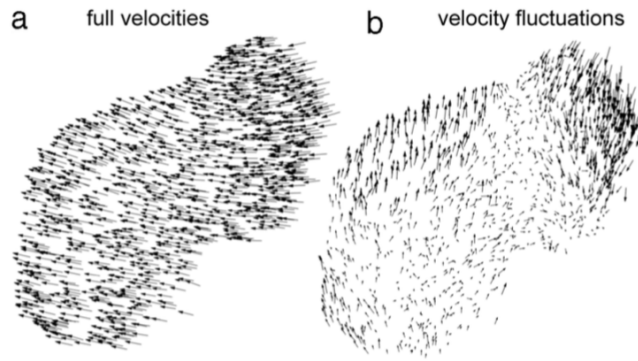


Figure 1.2: Flocks velocities and fluctuations. Two dimensional projection of a real flock of size $L = 36.5m$. Panel a: full velocity vectors of all the individuals, they all point in the same direction showing a high degree of global order. Panel b: fluctuations of the velocities computed according to eq (1.5), two large correlated domains are clearly visible. Figure reprinted from [43].

of one individual i at time t , with respect to the average of the group, is defined as [42],

$$\delta\mathbf{v}_i(t) = \mathbf{v}_i(t) - \frac{1}{N} \sum_k \mathbf{v}_k . \quad (1.5)$$

This quantity represents the building block for the calculation of the correlation functions that, in its static version, reads as [42],

$$C(r) = \frac{\sum_{ij}^N \langle \delta\mathbf{v}_i(t) \cdot \delta\mathbf{v}_j(t) \delta(r - r_{ij}) \rangle}{\sum_{kl}^N \delta(r - r_{kl})} , \quad (1.6)$$

where, for a given particles pair i and j , the product $\delta\mathbf{v}_i(t) \cdot \delta\mathbf{v}_j(t)$ measures the degree of similarity between the corresponding fluctuations. Additionally, since biological systems are clearly out-of-equilibrium, a statistical ensemble over which performing averaging operations is not attainable, therefore the mutual distance is used to perform spatial averages over the number of particles at the same distance. Finally, everything is averaged over the trajectories' evolution [42]. The power of the connected correlation functions is to capture connections that go beyond the simple global behavior of the system, and to distinct collective properties as emergent self-organized phenomena from externally driven processes. The knowledge on animal behavior found relevant progress by the use of these tools on experimental data of bird flocks and midges swarms, the biological systems we are going to focus on.

1.4 A paradigmatic example: birds flocks

One of the most studied biological systems composed of groups of animals is represented by bird flocks. Several works have been dedicated to their investigation from a theoretical and an experimental point of view [25, 44, 45]. Recently, novel

stereometric and computer vision techniques allowed large-scale experiments on starling flocks containing up to 2600 birds. The analysis consisted in the 3D reconstruction of individuals' trajectories, thanks to which an original characterization of the system has been possible [24, 46–48]. The main result of the first data acquisitions concerned the nature of the alignment interaction among birds and the spatial organization of the flock. In [49], authors discovered that starlings interact with 6 – 7 neighbors, exhibiting topological interactions instead of a metric rule. Moreover, density does not play the role one would expect for an equivalent system with metric interaction [49].

In panel a of Fig 1.2, the two-dimensional projection of a flocking event is reported [43]: the global order of the system is visible, all the velocity vectors are polarized along a well-defined direction reflecting a polarization of $\phi \simeq 0.9$. The computation of individuals' fluctuations is shown in panel b of the same figure, from which the presence of two major correlated domains emerges. The spatial connected correlation function (1.6) computed on this data, properly measures the extension of these correlated regions and reveals that they are much larger than the typical interaction distance. Panels a and b of Fig 1.3 present the connected correlation functions of the full velocity vector and of the speed of the birds, respectively. For very short distances the degree of correlation is relevant and positive, then it decays till crossing the zero at a length scale playing the role of the correlation length ξ . Due to the definition (1.5), this quantity measures the size of correlated domains, namely when fluctuations become anti-correlated since summing pairs of individuals that fluctuate in the opposite way with respect to the mean direction [43] [42].

The same data elaboration has been done on several different flocks, from which the correlation length has been extrapolated and plotted against the linear size of the system L . Panels c and d of Fig 1.3 reveal that this quantity scales with the linear size $\xi \sim L$, both for the velocity and the speed [43]. The shown phenomenology recalls the *scale-free* behavior of a statistical physics model [43], for which there is no typical length scale in the system rather than the system's size itself. Moreover, in the limiting case of an infinite physical system with $L \rightarrow \infty$, also the correlation length extends indefinitely $\xi \rightarrow \infty$, reflecting the maximum degree of correlation.

This evidence indicates that elements within a flock are able to influence each other at very large distances, regardless of the system's size. A possible biological interpretation of the directional scale-free behavior is that strong correlations achieve a fast collective response to external perturbations. With this, we mean the way the group as a whole reacts to its environment. In analogy with statistical systems, the maximum degree of correlation could be linked to high susceptibility, thus yielding a significant adaptive advantage against external predators [43, 50].

The phenomenon appears not unusual from a physical perspective and we can understand it looking at a reference equilibrium system: the Heisenberg ferromagnet in the deeply polarized regime [51]. The main ingredients of a flocking model are the alignment interaction among the velocities, and the consequent ro-

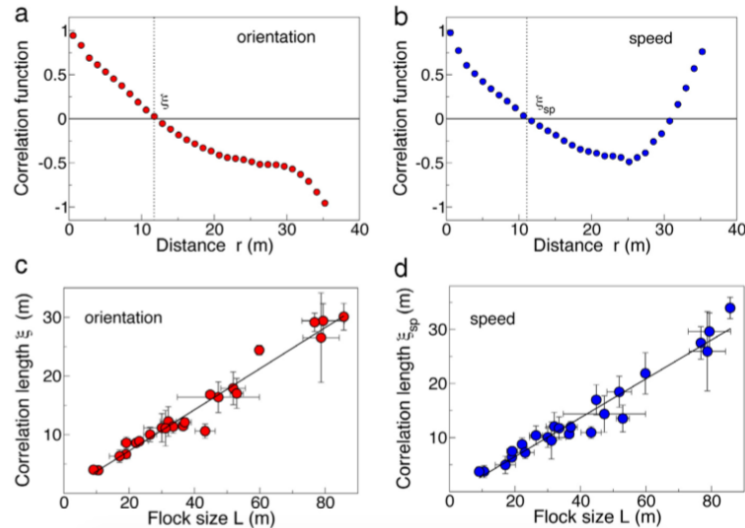


Figure 1.3: Spatial correlation functions of flocks' velocities and speeds. Panels a,b: static correlation function of a flocking event for the velocity and for the speed, respectively. The first one, computed following eq (1.6), reflects how much the fluctuations of the orientations are correlated. The intercept point is a measure of correlation length ξ , namely the size of correlated domains. The $C(r)$ for the speed of panel b, is computed with the same formula of eq (1.6) but using the moduli of velocities. Panels c,d: extrapolation of the correlation length for different flocks, plotted against the size of the system. The linear trend manifests a scale-free behavior for both the degrees of freedom. Figure reprinted from [43].

tational symmetry, both affecting also Heisenberg's spins. In the low-temperature phase, the equilibrium system spontaneously breaks the symmetry and chooses a particular direction of polarization. In this phase, modes of fluctuations that cost zero energy and that are scale-free emerge, and they are properly called the Goldstone's modes [52]. Even if flocks of birds are clearly out of equilibrium, under reasonable conditions, we can affirm that this general theorem can provide a natural explanation for their velocities' scale-free behavior [42, 43].

Different is the situation for the flocks' speed. This is a scalar quantity not subject to any continuous symmetry, therefore Goldstone's theorem cannot be invoked in its case. The explanation of this experimental evidence requires more subtle and novel investigations which have been conducted in [53, 54] and completed in [55]. A summary of the discoveries can be found in chapter 9 since the author of this manuscript contributed to the achievement of the results.

The broken symmetry phase is not the only situation in which a system can manifest a diverging correlation length. A typical scenario is in fact represented by the critical point of an ordering phase transition, for instance, when the temperature in the Heisenberg model reaches its critical value T_c [51]. This phenomenology obviously does not apply to the case of deeply polarized flocks, but it becomes useful when studying other strong correlated biological systems that live in a disordered but correlated phase, namely swarms of insects, the main players of our dissertation.

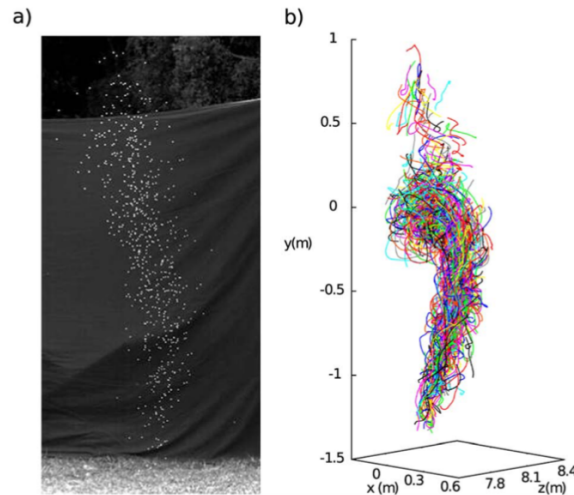


Figure 1.4: Experiment on natural swarms. Panel a: a natural swarm of midges (*Cladotanytarsus atridorsum*, Diptera:Chironomidae), in Villa Ada, Rome. Panel b: three dimensional reconstruction of each individual's trajectory for the same event of panel a. Figure reprinted from [1].

1.5 Midges swarms: collective behavior in absence of collective order

When thinking about collective behavior in biological systems, it is natural to imagine scenarios of all individuals of a group acting in a synchronized way and moving coherently. However, collective motion is only one of the possible manifestations of collective behavior, since the true hallmark relies on high correlation between the individuals, for which global order is not a necessary condition. An example confirming this statement is given by the biological system of midges swarms.

Several species of midges form swarms in the natural environment for reproductive purposes: groups are composed of male individuals which dance above natural landmarks to attract females (Fig. 1.4) [1, 56]. Their movement appears completely disordered and erratic, as if there were no interaction among them but only between the insects and the marker. However, a quantitative analysis of experimental data acquired with the same technology used for birds flocks, revealed that this is actually false [1].

The first result is achieved by the computation of the system's polarization. The definition of eq (1.4) gives an average value of $\phi \simeq 0.21$, confirming the intrinsic disordered nature of the swarming motion [1]. The second important evidence is shown by the calculation of the connected correlation function (1.6) of midges' velocities. Results are reported in Fig 1.5 for three different swarms. The exhibited trend is similar to the one observed for birds flocks: at short distances, there is a strong positive correlation, then it decays at larger distances crossing the zero at the correlation length ξ [1]. This latter quantity happens to be 4 times larger than the mean inter particles distance r_1 , affirming that, contrary to what

expected, also insects in a swarm are strongly correlated.

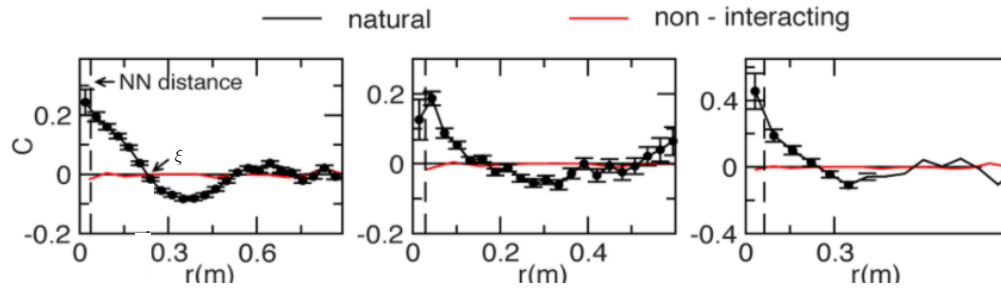


Figure 1.5: Static correlation functions of natural swarms. Black dots and lines stand for the static correlation functions computed on experimental data of three different swarms. For short distances the correlation is relevant and positive and then it crosses the zero at the correlation length ξ . The red lines show the result of the same calculation on numerical data of non-interacting harmonic swarms: interaction is necessary to reproduce strong correlation. Figure reprinted from [1].

In the previous section, we explained that correlation is a product of local interaction. This is indeed verified for this system: in Fig. 1.5, the $C(r)$ are compared to those of simulated non-interacting swarms (in red), composed by particles performing a three-dimensional random walk in a harmonic potential [1]. When the interaction is switched off, the correlation is null. Therefore, to explain these experimental data, it is necessary to suppose a local alignment interaction among the individuals, like that modeled for flocks. Certainly, there could be other different ways of modeling interaction that go beyond a direct alignment force [57] and, besides that, single individuals feel attracted by the landmark. It has been shown that introducing this confining interaction does not change the behavior of the velocity correlation function [1], but we will go back to this topic from a theoretical point of view in chapter 9.

Additional analyses have also provided more in-depth evidence on the type of interaction characterizing the system: denser swarms are more correlated. This fact can be explained by referring to a *metric* short-range interaction: midges tend to align their direction of motion to those of the neighbors within a fixed interaction radius r_c [1]. Consequently, the density or the rescaled mean first neighbor distance $x = r_1/r_c$, can be assumed as the control parameter, since it regulates the amount of correlation and then the state of the system.

1.6 Near-criticality of natural swarms

The application of statistical physics to strong correlated biological systems was recently powered by the hypothesis that some of them can be poised close to a critical point. Namely, special points of parameters space that provide large correlations and high susceptibility [58, 59]. From a biological point of view, a near-critical setting could provide robustness against external perturbations and

agility in collective response [59]. To support this statement, relevant experimental evidence has been recognized also in natural swarms of insects [2].

A more extended analysis of spatial correlation functions, like those of Fig 1.5, allowed an evaluation of the correlation length ξ for swarms of different sizes, from $N = 100$ to $N = 600$ individuals [2]. The result is that this system shows similar behavior to that of bird flocks, confirming a scale-free trend of the correlation length with the system's size $\xi \sim L$ (panel b of Fig 1.6) [2]. If, on the one hand, this phenomenon for flocks finds a reasonable explanation in the picture of Goldstone modes, on the other this appears not applicable to the disordered nature of the swarming behavior, for which a different mechanism has to be invoked.

The degree of correlation is measured by the correlation function, but also by its integrated version that gives a proxy of the standard susceptibility,

$$\chi = \frac{1}{N} \sum_{i \neq j}^N \delta \mathbf{v}_i \cdot \delta \mathbf{v}_j \theta(\xi - r_{ij}) . \quad (1.7)$$

Experimental values of this quantity confirm a relevant extent of correlation in the biological system and show an increasing trend with the system's size, panel a of Fig 1.6. Both these pieces of evidence can be explained by a physical mechanism.

Let's assume that the phase of the system is regulated by a control parameter x , which determines a bulk correlation length ξ_{bulk} . Computing ξ for many system's sizes at the same value of x , one would observe a linear growth of it as long as $L < \xi_{bulk}$, and then a saturation for the opposite condition $L > \xi_{bulk}$. The first regime could explain an effective scale-free behavior, which happens only for small enough sizes. However, this scenario does not fit with experimental data: the quantities χ and ξ do not show levels of saturation for very large L . Moreover, it seems unlikely to assume that different swarms are regulated by a single value of control parameter.

A more reasonable mechanism provides that natural systems are able to tune x with respect to the linear size L , such that they always maintain the maximum degree of correlation [2]. We are basically describing a process of finite-size scaling of a near-critical regime, in which, calling x_c the critical point of a phase transition, the following relations must hold [60],

$$x \sim x_c + N^{-1/3\nu} \quad (1.8)$$

$$\chi \sim N^{\gamma/3\nu} \quad (1.9)$$

$$\xi \sim L . \quad (1.10)$$

Here γ and ν are the exponents describing the finite-size divergence of the susceptibility and the correlation length, respectively [51].

The experimental data of Fig 1.6 support this reasoning, and a further confirmation arrives by numerical simulations of the Vicsek model (1.1) (1.2). The disordered sparse phase of this active theory is able to reproduce the static phe-

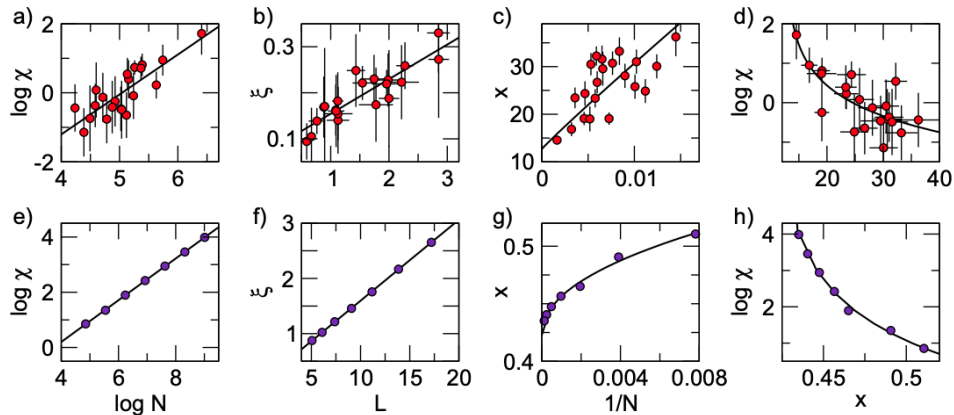


Figure 1.6: Comparison between natural swarms and Vicsek model. Top: experimental data, each dot represents a different swarm. Bottom: numerical simulations of the Vicsek model in the near-critical disordered phase. Panels a, e: susceptibility as a function of N ; panels b, f: correlation length as a function of L ; panels c, g control parameter (mean first interparticle distance) x as a function of $1/N$; panels d, h: susceptibility as a function of the control parameter. The comparison confirms a scale-free behavior of the natural system, following arguments of finite-size scaling in a near critical regime. Figure reprinted from [2].

nomenology of swarms, not only from a qualitative point of view but also from a quantitative one. A finite-size scaling approach has been performed on numerical simulations in the near-critical regime, and the calculation of χ and ξ is shown in panels e-h of Fig 1.6. The comparison with experimental data is straightforward, confirming that a near-critical phase of the Vicsek model well reproduces the scale-free behavior of swarms' static quantities [2].

These results support the hypothesis that a description of natural swarms in terms of quasi-critical active matter models is legitimate [2]. From a theoretical perspective, they also suggest that tools like field theories and scaling laws, typical of critical phenomena, could be successful in explaining additional experimental evidence on the same system. Our attention wants to focus on the dynamical properties of natural swarms that still urge a theoretical explanation. However, before introducing the experimental results that stimulated our research, we need to explain some fundamental topics of classical statistical field theory, namely the scaling hypothesis.

1.7 Theory of dynamical scaling

The scaling hypothesis was formulated to study critical phenomena in equilibrium statistical systems [4, 14]. Firstly introduced as a plausible conjecture, it found later a solid theoretical demonstration within the Renormalization Group framework [12, 61]. The core of the idea is that, when a system undergoes a second-order phase transition and it approaches the critical point, the divergence of the correlation length ξ is the only one responsible for singularities in other

statistical physical quantities [14, 62]. Scaling laws are the fundamental tool that allows predictions on these diverging elements. They have been mathematically expressed in several ways and formulated for static and dynamical critical phenomena [4, 14, 63].

We start studying the statics of a system close to a critical point, where the correlation length ξ is much larger than the microscopic lattice spacing a . Under the additional condition of exploring large spatial scales $r \gg a$, the scaling hypothesis states that the correlation length is the only relevant length scale of the system and it is the quantity that determines the singular behavior of all the others [14, 64]. Moreover, considering for simplicity a one-dimensional order parameter ψ , the hypothesis states that its spatial correlation function has to be a homogeneous function of the ratio r/ξ [64], namely:

$$C(\mathbf{r}) = \langle \delta\psi(\mathbf{r})\delta\psi(0) \rangle = r^y g(r/\xi) \quad (1.11)$$

where $\delta\psi(\mathbf{r}) = \psi(\mathbf{r}) - \langle \psi \rangle$, y is an exponent that needs to be determined and g is a scaling function [64]. This latter does not have to present singularities, except exactly at T_c and in the thermodynamic limit. Therefore, for finite \mathbf{r} , the function does not show discontinuities but changes smoothly along with all the thermodynamic phases. A direct consequence of this hypothesis is the scaling invariance of the functions at criticality when $\xi \rightarrow \infty$, which leads to the characteristic power-law of correlation. It gives also important information about relations linking the static critical exponents, e.g. $y = 2 - d - \eta$ with η the anomalous dimension of the field [14, 63].

The static hypothesis directly reflects on the dynamical behavior of the system. All the information to describe it is contained in the dynamical correlation functions and in the characteristic relaxation of the order parameter. At the core of the dynamical extension, there is the concept that the correlation length determines the relaxation time of the critical quantities: the system is as spatially correlated as it is temporally [4, 64]. To better formulate the discussion we need to introduce the dynamical correlation function of the order parameter,

$$C(\mathbf{r}, t) = \langle \delta\psi(\mathbf{r}, t)\delta\psi(0, 0) \rangle \quad (1.12)$$

that, in Fourier space, is directly connected to the static one via the sum rule [61]

$$C(\mathbf{k}) = \int \frac{d\omega}{2\pi} C(\mathbf{k}, \omega) . \quad (1.13)$$

The dynamical scaling hypothesis then formulates in two major assumptions [4, 5]:

1. the correlation function is a homogeneous function of the product $k\xi$,

$$C(\mathbf{k}, \omega) = \frac{2\pi}{\omega_c(\mathbf{k})} C(\mathbf{k}) f\left(\frac{\omega}{\omega_c(\mathbf{k})}, k\xi\right) \quad (1.14)$$

2. $\omega_c(\mathbf{k})$ is the characteristic frequency, the principal quantity characterizing the relaxation of the dynamics. This is also a homogeneous function of the product $k\xi$,

$$\omega_c(\mathbf{k}) = k^z \Omega(k\xi) . \quad (1.15)$$

The last equation defines z , the dynamical critical exponent, whose value discriminates between different dynamical universality classes [61]. Additionally, we can translate eq (1.15) in the time domain, obtaining

$$\tau_c(\mathbf{k}) = k^{-z} g(k\xi) \quad \text{or also} \quad \tau_c(\mathbf{k}) = \xi^z g'(k\xi) \quad (1.16)$$

with τ_c the characteristic time scale, namely the inverse of the characteristic frequency [5]. The quantities f, Ω, g and g' are all generic scaling functions.

Halperin and Hohenenberg provide a standard definition of the characteristic frequency in [5]: ω_c is the quantity which realizes that half of the total integrated area of the dynamic correlation functions is included in the interval $-\omega_c \leq \omega \leq \omega_c$,

$$\frac{\int_{-\omega_c}^{\omega_c} \frac{d\omega}{2\pi} C(\mathbf{k}, \omega)}{\int_{-\infty}^{+\infty} \frac{d\omega}{2\pi} C(\mathbf{k}, \omega)} = \int_{-\omega_c}^{\omega_c} \frac{d\omega}{2\pi} \frac{C(\mathbf{k}, \omega)}{C(\mathbf{k})} = \frac{1}{2} \quad (1.17)$$

Inserting here the definition (1.14), a relation for the shape function f directly follows:

$$\int_{-1}^1 dx f(k\xi, x) = \frac{1}{2} \quad (1.18)$$

where $x = \omega/\omega_c$. In time domain it reads,

$$\int_0^{\infty} dt \frac{1}{t} \sin(t/\tau_c) f(k\xi, t/\tau_c) = \frac{\pi}{4} \quad (1.19)$$

from which it is possible to extrapolate the value of τ_c just knowing the normalized dynamical correlation function [3].

The power of this hypothesis is to state that all the dependence on control parameters and microscopic details enter in the dynamical correlation functions only through the correlation length, especially determining its temporal decorrelation. What really matters to determine the long-wavelength and small frequency behavior is the dimension of space, the dimension of the order parameter, and the existence of symmetries and conservation laws that identify a specific dynamical universality class and therefore the value of the exponent z [64]. The homogeneity of the shape functions guarantees the scale invariance property at the critical point also at a dynamical level. This is the main core of the concept of universality and of the Dynamical Renormalization Group's idea, properly studying how dynamical laws change under a rescaling of space and time [61]. Within this framework, we will be able to provide proof of the dynamical scaling hypothesis (see chapter 2).

An immediate consequence of the dynamic scaling is that correlation functions

of critical systems, described by different sets of parameters, collapse on the same shape function once space is measured in units of correlation length and time in units of characteristic time scale [5]. This can be understood considering

$$k\xi = b \quad (1.20)$$

in the correlation function $C(k, \omega)$, implying:

$$\frac{C(k, \omega)}{C(k)} = \frac{2\pi}{k^z \Omega(b)} f\left(\frac{\omega}{k^z \Omega(b)}, b\right) \quad (1.21)$$

thus,

$$\frac{C(k, \omega)}{C(k)} = 2\pi k^{-z} h(\omega k^{-z}) \quad (1.22)$$

where h is another scaling function that absorbs the constant terms. In the time domain, this finally reads:

$$\frac{C(k, t)}{C(k)} = \hat{C}(tk^z) \quad (1.23)$$

where $\hat{C}(tk^z)$ represents the shape function on which the collapse realizes, provided that time is rescaled with the proper dynamical critical exponent z . This property can be used as proof of the validity of dynamical scaling in a system, and indeed we are going to make extensive use of it in the following.

1.8 Experimental evidence of dynamical scaling in natural swarms

We can now go back to the system of natural swarms for the last experimental evidence we are going to show at this stage. In a more recent work [3], the investigation focuses on the system's dynamical properties, analyzed by means of the spatio-temporal velocity correlation functions both from an experimental and a theoretical perspective. Assuming isotropy in the 3d Fourier momentum space, these quantities have been calculated as,

$$C(k, t) = \left\langle \frac{1}{N} \sum_{i,j} \frac{\sin(kr_{ij}(t))}{(kr_{ij}(t))} \delta \hat{\mathbf{v}}_i(t_0) \cdot \delta \hat{\mathbf{v}}_j(t_0 + t) \right\rangle_{t_0} \quad (1.24)$$

where k is the wave-number and the fluctuations of the velocity are always computed according to eq (1.5) and then normalized to,

$$\delta \hat{\mathbf{v}}_i(t) = \frac{\delta \mathbf{v}_i(t)}{\sqrt{\frac{1}{N} \sum_k \delta \mathbf{v}_k(t) \cdot \delta \mathbf{v}_k(t)}} . \quad (1.25)$$

The positions are expressed in the center of mass reference frame and the mutual distance $r_{ij}(t)$ stands for $r_{ij}(t, t_0) = |\mathbf{r}_i(t_0) - \mathbf{r}_j(t_0 + t)|$. Additionally, everything

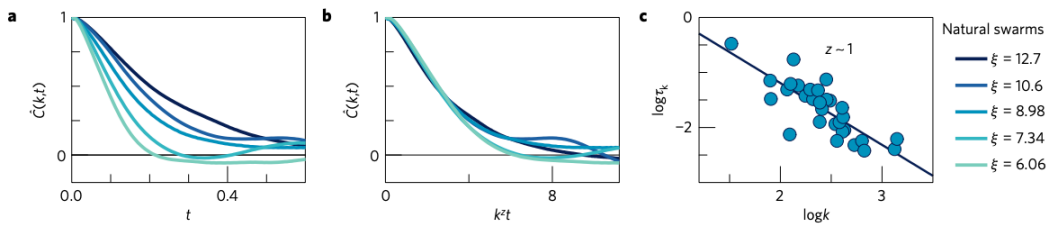


Figure 1.7: Dynamical scaling in natural swarms. Panel a: normalized dynamical correlation functions of 5 different swarms of different size. Panel b: same functions of panel a, when time is rescaled $t \rightarrow tk^z$, with $k = 1/\xi$ and $z = 1.2$ the value that realizes the best collapse. Panel c: relaxation time τ_k against wave-number, the slope of the linear fit gives $z = 1.12$. Figure reprinted from [3]

is averaged on time t_0 ,

$$\langle \cdot \rangle_{t_0} = \frac{1}{T_{max} - t_0} \sum_{t=t_0}^{T_{max}-t_0} \cdot \quad (1.26)$$

As we already mentioned, this correlation function measures how the behavior of one insect at time t_0 influences that of another element distant r_{ij} in space, and t in time. In panel a of Fig. 1.7 curves are reported for several swarms: they are normalized at the value $\hat{C}(k, t) = C(k, t)/C(k, 0)$ and computed at wave-number equal to $k = 1/\xi$. The correlation length is extrapolated according to the static analysis explained in the previous section.

These quantities are calculated on experimental data of different natural swarms, therefore each function embodies all the microscopic details and parameters of the system under consideration. In absence of general laws, all these details could affect the observed dynamics in terms of the shape of the dynamical correlation functions and dependence on the typical decay rate τ_k . However, the quasi-critical nature of the system discovered in [2] suggests referring to universality also at the dynamical level, testing the validity of the dynamical scaling hypothesis. Therefore, assuming that the characteristic time scale behaves like $\tau_k = k^{-z}g(k\xi)$ for fixed $k\xi = 1$, time has been rescaled in tk^z searching for the aforementioned characteristic collapse of the dynamical correlation functions. In panel b of Fig. 1.7 one can appreciate that this happens to be verified by using a particular value of the exponent, namely $z = 1.2$ [3]. This result can be interpreted as a surprising proof of the validity of the scaling hypothesis in the out-of-equilibrium biological system of natural swarms.

To confirm this evidence, from the same functions the characteristic time scale τ_k has been extrapolated according to eq (1.19) and plotted against k , which simply represents the inverse of the correlation length. In the plane $(\log k, \log \tau_k)$, the relation between these two quantities (1.16) has to be linear and the slope of the line represents an estimate of the dynamical critical exponent. From a direct linear fit of experimental data $z \simeq 1.12$ is obtained (panel c of Fig. 1.7 [3]).

This result is remarkable for two reasons: first, it is not obvious that a bi-

ological system satisfies a property formulated for equilibrium standard critical systems; second, the value of the exponent z is original of the system since there are no equilibrium or out-of-equilibrium models that can predict such a value. In the next chapters, we will study a theoretical model that reproduces qualitatively and quantitatively this dynamical behavior of natural swarms.

1.9 The core of the thesis: two crossovers to explain the swarming behavior

The Vicsek model (VM) is the first model we will investigate to explain experimental findings on the dynamical scaling in natural swarms. Its main ingredients, alignment force, and self-propulsion proved to be necessary to reproduce the scale-free behavior of this system [2]. For these reasons, its critical dynamics has been studied looking for consistency also on dynamical properties.

In [3] a numerical study of the model in $d = 3$ and in the near-critical disordered phase was carried out. Following a finite-size scaling analysis, with methods that we are going to extensively explain in the next sections, the authors verified that the model satisfies the dynamical scaling hypothesis showing the characteristic collapse of the velocity's correlation functions [3]. This feature is reported in Fig 1.8, from which we deduce that the value of the critical exponent was found to be $z \simeq 2$.

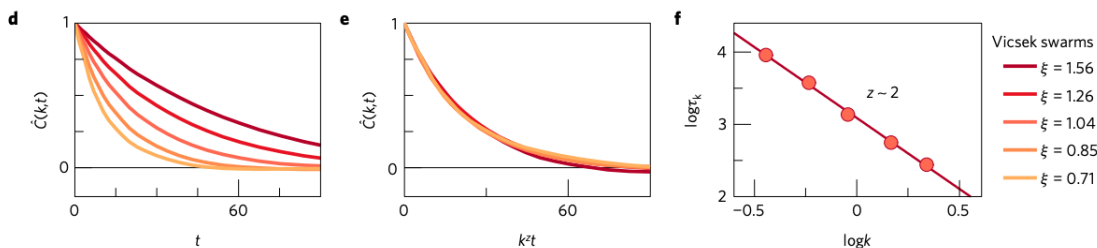


Figure 1.8: Dynamical scaling in the Vicsek model. Panel d: Normalized dynamical correlation functions in the near critical regime, evaluated at $k = 1/\xi$ and for sizes $N = 128, 256, 516, 1024, 2048$. Panel e: same functions of panel d, when time is rescaled $t \rightarrow k^z t$ using $z = 1.96$, value extrapolated from the linear fit of panel f: relaxation time τ_k against wave-number. Reprinted from [3].

In contrast to the good agreement reached for the static behavior, the dynamical critical exponent of the VM appears quite far from the value discovered in natural swarms $z \simeq 1.2$. What is more, this numerical estimate suspiciously recalls the universality class typical of equilibrium dissipative dynamics [61].

This result opened several questions about the origin of the out-of-equilibrium nature of the VM. The emergence of aggregates and heterogeneity at the edge of the phase transition is a clear out-of-equilibrium manifestation of the model. However, the above analysis of finite-size scaling to extrapolate critical exponents requires homogeneous configurations, in which quantitative non-equilibrium ef-

fects are not trivial. The dynamical scaling with $z = 2$ seemed to confirm that the VM in a continuous phenomenology belongs to an effective equilibrium universality class, suggesting, in a misleading way, that activity does not play a relevant role in determining the value of the model's dynamical critical exponent.

To investigate this issue, we study here the hydrodynamic theory of the VM under an incompressibility constraint. This theory was introduced in [6], where an RG calculation was also performed. The result is that the out-of-equilibrium critical dynamics is described by a stable fixed point characterized by $z = 1.7$, a value different from the one found numerically for the original microscopic model [3]. At that stage, the constraint of incompressibility could be addressed as the only relevant difference between the theoretical calculation and the numerical result.

With a deeper study on the hydrodynamic theory, we reveal that these apparent contradictions are solved by a dynamical crossover between the equilibrium, $z = 2$, and the out-of-equilibrium universality class with $z = 1.7$. The main players are the level of the activity and the correlation length of the system. If these quantities are really large, out-of-equilibrium effects can be quantified by the slower relaxation. On the contrary, if the effective activity or the size is small, the equilibrium critical dynamics rules all the physical scales even if the system is microscopically active. Additionally, by performing numerical simulations on the original VM in $d = 3$, we are able to demonstrate this crossover phenomenon also in compressible but homogeneous systems.

With this study, we unveil the importance of crossovers between universality classes in application to natural and finite-size systems. We prove that incompressibility does not affect the value of the dynamical critical exponent and that this latter can be used to quantify out-of-equilibrium effects in active homogeneous systems. Finally, we demonstrate that the effect of self-propulsion on critical dynamics is to lower the value of the exponent with respect to the equilibrium case [7].

An additional important experimental evidence stimulated the second part of this project. It concerns the shape of the dynamical correlation functions of natural swarms. What emerged from the study of [3], is that swarms show an underdamped dynamical decay, which is not compatible with the dissipative and exponential relaxation of the VM. The difference is evident when computing the relaxation form factor:

$$h(t/\tau_k) = \frac{\dot{C}(t/\tau_k)}{C(t/\tau_k)} \quad (1.27)$$

where τ_k is the relaxation time extrapolated from correlations of Fig 1.8, and 1.7. For $t \rightarrow 0$, the limit of this function is equal to one when the decay is purely exponential, while it is equal to zero for higher-order dynamical rules. Fig 1.9 shows the comparison between Vicsek and natural swarms: the dynamics of insects is different from the one of VM, the former reflecting more non-dissipative dynamics rather than a dissipative one [3].

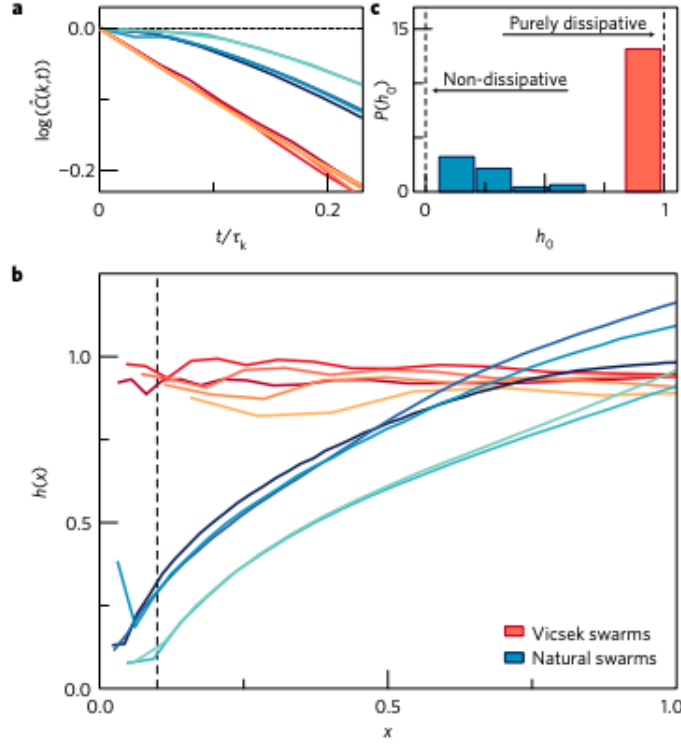


Figure 1.9: Dynamical relaxation in VM and natural swarms. Panel a: comparison of the dynamical correlation functions of swarms and of the VM in semi-log scale; the latter have a linear decay, while the former reflect a non-exponential behavior. Panel b: form factor $h(x)$ computed for all the natural and numerical functions: it goes to zero for small times confirming a non-dissipative dynamics for real swarms, while it goes to 1 for the VM as for purely-dissipative dynamics. Panel c: histograms of $h_0 = h(x = 0.1)$, the value of the form factor for very small times; for the dissipative dynamics is peaked on 1, while it assumes small values for the natural system.

From a quantitative and a qualitative point of view, we conclude that the VM is not suitable to reproduce the dynamics of this natural system. Our main goal is therefore to find a theoretical model able to rationalize these experimental findings. The model we propose is called the Inertial Spin Model (ISM), whose equations we report here for clarity [8]:

$$\begin{aligned}
 \frac{d\mathbf{v}_i}{dt} &= \frac{\mathbf{s}_i \times \mathbf{v}_i}{\chi} \\
 \frac{d\mathbf{s}_i}{dt} &= \frac{\mathbf{v}_i}{v_0} \times \left(\frac{J}{v_0} \sum_j n_{ij} \mathbf{v}_j - \frac{\eta}{v_0} \frac{d\mathbf{v}_i}{dt} + \boldsymbol{\zeta}_i \right) \\
 \frac{d\mathbf{r}_i}{dt} &= \mathbf{v}_i .
 \end{aligned} \tag{1.28}$$

The main difference with the VM is already appreciable: the dynamics is of second order in the velocity, being mediated by an additional variable \mathbf{s}_i called spin that is also dissipated by a friction η . This is the generator of the internal rotational symmetry of the velocity and it is directly connected to the radius of curvature

of the particles.

We develop the hydrodynamic theory related to this microscopic model and we study it under a fixed network approximation. The aim is to understand, separately from the activity, how the introduction of inertial dynamics with dissipation can affect the dynamical universality class and the critical exponent of a system. We discover that also this equilibrium theory is characterized by a crossover. The phenomenon involves an unstable RG fixed point, reflecting a conservative critical dynamics with $z = 3/2$ and a stable fixed point with a dissipative dynamics and $z = 2$ [9, 10]. In the asymptotic limit, relaxation is dissipative, but thanks to the same mechanism of the previous crossover, weakly damped and limited systems can experience a faster relaxation with smaller critical exponent. To this aim, spin's effective friction and size of the system are paramount to determine its critical macroscopic behavior. Moreover, ISM well reproduces the underdamped decay of experimental correlation functions.

Even though these studies do not achieve fully consistent results with experimental evidence of natural swarms, they are crucial to unveil the crossovers of equilibrium and out-of-equilibrium theories of active matter. The main achievement is that both the phenomena describe processes that go in the right direction to explain anomalous relaxation in natural swarms: activity and inertial dynamics have separated effects in lowering the value of the dynamical critical exponent with respect to dissipative dynamics. The combination of these two ingredients will finally fill the gap on the value of the dynamical critical exponent, thus reconciling theory and experiments.

Before getting to the crux of the matter, we reserve the next chapter to methods and analytical tools necessary to understand the study of models' critical dynamics.

Chapter 2

The Dynamical Renormalization Group

In this chapter, we turn our attention to time-dependent equilibrium critical phenomena, i.e. to the dynamics of systems at the critical point of a second order phase transition. We present methods and tools, useful to understand the technical part of the subsequent chapters mostly relying on basic concepts of statistical field theory. We start with a section dedicated to the passage from a microscopic description to a coarse-grained mesoscopic version of the dynamical evolution of a system, necessary to understand the long-time and large-scale physics of a critical phase. Thus we introduce the technique of the Dynamical Renormalization Group (DRG) and its connection with dynamical scaling properties.

This branch of theoretical physics raised in the '70s after the fruitful advancement of the Renormalization Group technique to study the statics of critical systems [12, 13, 65]. Leading representatives were Halperin, Hohenberg, and Ma, from whose works we draw the material for the following discussion [61, 64].

2.1 From microscopic to mesoscopic equations of motion

When studying the statics of a critical phenomenon, one is mainly interested in the properties of the equilibrium distribution of the system's configurations: the problem of statics thus reduces to a problem of statistics and its consequences. On the contrary, the study of the dynamics is much more complicated: one wants to describe the evolution in time of these system's configurations, how those reach the stationary probability distributions, and how the system reacts to external perturbations [64]. A more varied scenario spreads out in different models that distinguish for symmetries, conservation laws, and slow quantities involved, all constructed with the final purpose to study the time variation properties of large-scale fluctuations of the system [61].

Crucial players are the *slow* modes, namely those quantities that have a very long relaxation time. Certainly, the order parameter is always included in this set

and it is easy to understand why: when a system is close to a critical point, it is composed of large correlated domains in which most of the spins have the same orientations, thermal agitations usually flip some of them, but the time to reverse the entire patch is the longer the larger the correlated areas are. This phenomenon is called *critical slowing down* and it can affect other quantities as those conserved [66]. The purpose of the critical dynamics theory is to explain how these long relaxation time behaviors come out in terms of small-scale interactions.

To study the dynamics, we need to consider equations of motion for the time evolution of the system. If we want to discover its long-wavelength behavior, it is useful to carry out a description in terms of fields that we can define starting from a set of microscopic variables and coarse-graining them, namely:

$$\psi(\mathbf{x}, t) = \frac{1}{V(\mathbf{x})} \sum_{i \in V(\mathbf{x})} \sigma_i(t) \quad (2.1)$$

where $\sigma_i(t)$ are the microscopic degrees of freedom belonging to the small volume V centered in the point space \mathbf{x} . For this operation to be meaningful, the linear size l corresponding to the volume must be larger than the microscopic length scale $l \gg a$ and smaller than the size of correlated regions $l \ll \xi$. This operation identifies the field $\psi(\mathbf{x}, t)$ that, for simplicity, we are here considering as the order parameter of one dimension.

As we mentioned before, other coarse-grained fields can also participate as slow modes to the critical dynamics of the system, therefore we can imagine collecting all these quantities in a vector ψ^a , indicating with the index a the identity of the field. Writing down mesoscopic fields from the microscopic degrees of freedom certainly has the consequence of losing some information on the system itself: the limit of the knowledge is fixed by the size of the coarse-grained volume l which is better indicated in momentum space as the natural cutoff $\Lambda = (2\pi)/l$. This means that fluctuations on scales larger than the cutoff are neglected and that the Fourier transform of the fields can be computed as,

$$\psi^a(\mathbf{x}, t) = \int_{|\mathbf{k}| < \Lambda} d^d k e^{i\mathbf{k} \cdot \mathbf{x}} \psi^a(\mathbf{k}, t) . \quad (2.2)$$

Once determined the relevant fields, we can write down the respective equations of motion, also called the *kinetic equations*. They are generally composed by two different parts: i) the reversible forces $F_{rev}^a[\psi](\mathbf{x}, t)$, namely those terms representing the deterministic evolution of the dynamics and describing a time-reversal regular motion, they are also called mode-coupling terms; ii) the dissipative forces, that are the responsible for time-irreversible effects [67]. The latter originate from the random thermal agitations over the length scale of the coarse-graining, and appear in the equations of motion with decay rates and noises of usual thermal baths of stochastic dynamics [64]. A prototype equation then reads,

$$\frac{\partial \psi^a(\mathbf{x}, t)}{\partial t} = -\Gamma_0^a \frac{\partial \mathcal{H}}{\partial \psi^a(\mathbf{x}, t)} + F_{rev}^a[\psi](\mathbf{x}, t) + \zeta^a(\mathbf{x}, t) , \quad (2.3)$$

where the last term is a Gaussian white noise satisfying $\langle \zeta^a(\mathbf{x}, t) \rangle = 0$ with variance

$$\langle \zeta^a(\mathbf{x}, t) \zeta^b(\mathbf{x}', t') \rangle = 2T\Gamma_0^a \delta^d(\mathbf{x} - \mathbf{x}') \delta(t - t') \delta_{ab}, \quad (2.4)$$

the amplitude Γ_0^a is called kinetic coefficient. Moreover \mathcal{H} corresponds to an effective Hamiltonian (properly an effective free-energy), that identifies the stationary state at which the system relaxes when it is at the equilibrium. It can be obtained imposing that,

$$\frac{\partial \mathcal{H}}{\partial \psi^a(\mathbf{x}, t)} = 0. \quad (2.5)$$

This happens because the thermal bath of eq (2.3) ensures the achievement of an equilibrium Boltzmann probability distribution, whose weight is represented by the effective Hamiltonian itself,

$$P[\psi] \sim e^{-\beta \mathcal{H}[\psi]} \quad (2.6)$$

assuming $k_B = 1$ and $\beta = 1/T$. Another important consequence of being at equilibrium is the validity of the Fluctuation Dissipation Theorem [68], thanks to which the amplitude of the noise and the damping term depends on the same quantity Γ_0^a , as expressed in eq (2.3). On the contrary, in out-of-equilibrium systems these two quantities become independent and stochastic fluctuations decouple from dissipation.

The deterministic part of the dynamics can be expressed in terms of Poisson-brackets between the fields and the Hamiltonian, as in the classic Heisenberg representation [67],

$$F_{rev}^a[\psi](\mathbf{x}, t) = \{\psi^a, \mathcal{H}[\psi]\} \quad (2.7)$$

that can be expanded as,

$$\{\psi^a, \mathcal{H}[\psi]\} = \int d^d x' \sum_b \frac{\delta \mathcal{H}}{\delta \psi^b(\mathbf{x}')} \{\psi^a(\mathbf{x}), \psi^b(\mathbf{x}')\}. \quad (2.8)$$

From this last expression it is visible that the Poisson-brackets between the slow fields crucially determine the reversible dynamics of the system. Calling indeed $\{\psi^a(\mathbf{x}), \psi^b(\mathbf{x}')\} = Q^{ab}(\mathbf{x}, \mathbf{x}')$, we have

$$F_{rev}^a[\psi](\mathbf{x}, t) = \int d^d x' \sum_b \frac{\delta \mathcal{H}}{\delta \psi^b(\mathbf{x}')} Q^{ab}(\mathbf{x}, \mathbf{x}'). \quad (2.9)$$

However, this last expression is not totally complete. To understand better the onset of these reversible terms and how to explicitly compute them, we can consider a zero temperature dynamics which simply reads,

$$\frac{\partial \psi^a(\mathbf{x}, t)}{\partial t} = F_{rev}^a[\psi](\mathbf{x}, t) \quad (2.10)$$

The probability distribution associated to this process has to fulfill the stationary condition $\partial_t P = 0$ that, passing through the related Fokker-Planck equation [69],

becomes

$$\frac{\partial}{\partial \psi^a} [F_{rev}^a[\psi] e^{-\beta \mathcal{H}[\psi]}] = 0 . \quad (2.11)$$

It can be shown that eq (2.9) does not solve the last relation but that an additional term is needed to correctly fulfill it, namely:

$$F_{rev}^a[\psi](\mathbf{x}, t) = \int d^d x' \sum_b \left[\frac{\delta \mathcal{H}}{\delta \psi^b(\mathbf{x}')} Q^{ab}(\mathbf{x}, \mathbf{x}') - \frac{1}{\beta} \frac{\delta Q^{ab}(\mathbf{x}, \mathbf{x}')}{\delta \psi^b(\mathbf{x}, \mathbf{x}')} \right] . \quad (2.12)$$

However, if for the hydrodynamic fields considered it happens that

$$\frac{\delta Q^{ab}(\mathbf{x}, \mathbf{x}')}{\delta \psi^b(\mathbf{x}, \mathbf{x}')} = 0 , \quad (2.13)$$

and this will be always our case, we recover the simple dynamics given by (2.9).

Finally, a last comment on the relaxation term is in order. In eq (2.3) we consider a pure dissipative mechanism described by the kinetic coefficient Γ_0^a : in absence of reversible forces, starting from some initial conditions, it describes an exponential decay to the stationary state of the field ψ^a . In fact, another situation has to be taken into account: if ψ^a indicates a field that is also a conserved quantity of the dynamics, the relaxation cannot be the one described by (2.3), but the kinetic coefficient has to transform in a transport coefficient of the type,

$$\frac{\partial \psi^a(\mathbf{x}, t)}{\partial t} = \lambda_0^a \nabla^2 \frac{\partial \mathcal{H}}{\partial \psi^a(\mathbf{x}, t)} + \zeta^a(\mathbf{x}, t) \quad (2.14)$$

with appropriate noise variance

$$\langle \zeta^a(\mathbf{x}, t) \zeta^b(\mathbf{x}', t') \rangle = -2T \lambda_0^a \nabla^2 \delta^d(\mathbf{x} - \mathbf{x}') \delta(t - t') \delta_{ab} . \quad (2.15)$$

This last equation, indeed, can be read as a continuity equation which ensures that the total integral of ψ^a is preserved along with the time evolution.

The kinetic equations thus presented are the basis of the study of dynamical critical phenomena, the presence of different dynamical rules and conservation laws acts on the determination of various mode-coupling terms and types of relaxation, giving rise to great zoology of models which have been analyzed in [61] and [67].

2.2 The fundamental steps of DRG

Our final objective is to find a suitable theoretical model for a good explanation of experimental data of natural swarms [3]. To achieve this goal we need to propose theories that can qualitatively reproduce the behavior of swarms and to study their critical dynamics, in order to compare with experiments the value of the dynamical critical exponent and their dynamical universality class. The way to perform this analysis follows the path of the Dynamical Renormalization Group

(DRG).

This is a powerful technique that consists in a set of scale transformations that, applied to a system close to a critical point, allows a quantitative determination of its universal and scale-invariant behavior [67]. The approach we are going to use is the one known as *momentum-shell*, introduced by Wilson and Kogut in [70] and formulated by these scientists as a strategy for dealing with complicated problems involving many length scales, such as critical phenomena. The scheme plans to divide the problem into subsequent steps, each one representing a different length scale of observation that grows as the number of iterations increases. Technically, this is made by carrying out statistical averages over thermal fluctuations on smaller scales, with the purpose to deduce the long-range physics of the system from the behavior of a few quantities incorporating the effects of the microscopic degrees of freedom.

An RG transformation is practically composed of two steps, which have to be applied to an effective theory describing the system like the one reported in eq (2.3), namely [61]:

1. *coarse-graining*: the first procedure stands for integration over the short wavelengths and over the microscopic details of the system; in momentum space, it means that the modes within the interval $\Lambda/b \leq |\mathbf{k}| \leq \Lambda$ are averaged out, where $b \sim 1$ is called the scaling factor and $\Lambda \sim 1/l$ is the inverse of the microscopic length scale;
2. *rescaling*: since the first step changes the starting effective theory, to compare the system before and after the coarse-graining, a procedure of rescaling of fields, space, and time is needed.

The combination of the two actions describes how the field theory of a system modifies when it is explored at larger scales and, indeed, all the physical meaning of this transformation has to be found in the way the parameters of the theory change within the steps. These two passages have then to be iterated many times, such that to make the parameters flow along with the scale transformations till eventually reach some fixed points, namely when the effective theories do not change with a further increase of the observation's scale. These points, therefore, encapsulate the property of scale-invariance of a critical system and contain all the information about the critical phenomenon, including the set of the critical exponents [70].

2.2.1 Martin-Siggia-Rose action

The starting point of a DRG application is to build up an effective theory from the dynamical equations of motion. This can be done by using a response function formalism that is valid for equilibrium and out-of-equilibrium processes [67]; it allows to define an action \mathcal{S} , called the Martin-Siggia-Rose (MSR) [71] or Janssen-De Dominicis action [72], with which expressing the weight of the probability distribution of the system $P \sim e^{-\mathcal{S}}$. The purpose of this technique is to transform

averages of physical quantities over the stochastic processes in functional averages, a procedure that appears quite convenient since once obtained \mathcal{S} , the RG machinery can follow the same steps of the static calculation.

Let's illustrate this formalism considering a simple dynamical equation of motion in generic dimension d ,

$$\mathcal{F}[\psi] - \theta = 0 \quad (2.16)$$

where we mean with θ the source of stochastic noise and with $\mathcal{F}[\psi]$ all the deterministic part of the equation. Indicating with greek letters the components of the n dimensional fields involved in (2.16), we can generically write the variance of the Gaussian white noise as,

$$\langle \theta_\alpha(\mathbf{x}, t) \theta_\beta(\mathbf{x}', t') \rangle = 2L_{\alpha\beta} \delta^d(\mathbf{x} - \mathbf{x}') \delta(t - t') \quad (2.17)$$

where $L_{\alpha\beta}$ has to be meant as an operator, for instance: $\Gamma_0 \delta_{\alpha\beta}$ for a dissipative dynamics or $-\lambda_0 \nabla^2 \delta_{\alpha\beta}$ for a conservative dynamics.

We now want to compute a thermal average of a generic operator $\langle A[\psi] \rangle_\theta$, but selecting only those configurations of the field which evolve according to (2.16). This average can be firstly written as,

$$\langle A[\psi] \rangle_\theta \sim \int \mathcal{D}_\theta P[\theta] A[\psi] \quad (2.18)$$

where $P[\theta]$ is the noise's Gaussian probability distribution:

$$P[\theta] \sim \exp \left(-\frac{1}{4} \int d^d x \int dt \theta_\alpha(\mathbf{x}, t) (L_{\alpha\beta})^{-1} \theta_\beta(\mathbf{x}, t) \right) \quad (2.19)$$

with the repetition of indices indicating a sum over the components.

To select the right field's trajectories in the measure, we can exploit the identity:

$$\int \prod_\alpha \prod_{(\mathbf{x}, t)} \mathcal{D}\psi_\alpha \delta(\mathcal{F}_\alpha[\psi] - \theta_\alpha) = 1 \quad (2.20)$$

where now we substitute the integral representation of the delta function using the additional response field $\hat{\psi}$ ¹,

$$\delta(\mathcal{F}_\alpha[\psi] - \theta_\alpha) = \int \prod_\alpha \mathcal{D}[i\hat{\psi}_\alpha] e^{-\int \hat{\psi}_\alpha (\mathcal{F}_\alpha[\psi] - \theta_\alpha)} . \quad (2.21)$$

The integral in the exponential is written in a simplified version and stands for $\int = \int d^d x \int dt$. Eq (2.20), in a more compact notation, then becomes:

$$\int \mathcal{D}[\psi] \int \mathcal{D}[\hat{\psi}] e^{-\sum_\alpha \int \hat{\psi}_\alpha (\mathcal{F}_\alpha[\psi] - \theta_\alpha)} = 1 \quad (2.22)$$

¹This expression is indeed valid only in the Ito stochastic scheme, where the Jacobian $|\det(\delta\mathcal{F}_\alpha/\delta\psi_\alpha)| = 1$.

Inserting this 1 in the expression of (2.18) we get,

$$\langle A[\boldsymbol{\psi}] \rangle_{\theta} \sim \int \mathcal{D}[\boldsymbol{\psi}] \mathcal{D}[\hat{\boldsymbol{\psi}}] \mathcal{D}_{\theta} e^{-\int \hat{\psi}_{\alpha} (\mathcal{F}_{\alpha}[\boldsymbol{\psi}] - \theta_{\alpha})} P[\boldsymbol{\theta}] A[\boldsymbol{\psi}] \quad (2.23)$$

Finally, using (2.19) and performing on it the Gaussian integral of the noise, we obtain the expression,

$$\langle A[\boldsymbol{\psi}] \rangle_{\theta} \sim \int \mathcal{D}[\boldsymbol{\psi}] \mathcal{D}[\hat{\boldsymbol{\psi}}] e^{-\mathcal{S}[\hat{\boldsymbol{\psi}}, \boldsymbol{\psi}]} A[\boldsymbol{\psi}] \quad (2.24)$$

where the action,

$$\mathcal{S}[\hat{\boldsymbol{\psi}}, \boldsymbol{\psi}] = \int d^d x \int dt \left(\hat{\psi}_{\alpha} \mathcal{F}_{\alpha}[\boldsymbol{\psi}] - \hat{\psi}_{\alpha} L_{\alpha\beta} \hat{\psi}_{\beta} \right) \quad (2.25)$$

defines the new measure of the probability distribution in terms of the two fields $\boldsymbol{\psi}$ and $\hat{\boldsymbol{\psi}}$ [67, 71].

2.2.2 Study of the Gaussian theory

The deterministic part of the dynamics can be generally expressed by the sum of two parts: the linear one in the field, $F_{\alpha\beta}^0 \psi_{\beta}$, plus the non-linear part $\mathcal{F}_{\alpha}^I[\boldsymbol{\psi}]$, which describes the non-trivial interactions in the system. The study of the linear part usually represents the starting point of an RG analysis, since it contains all the information about the mean-field behavior of a system.

We can focus on it neglecting for the moment the interacting terms of the dynamics and of the effective action (2.25). Therefore, writing everything in Fourier space, namely using the complete Fourier transform of the field

$$\psi_{\alpha}(\mathbf{x}, t) = \int \frac{d^d k}{(2\pi)^d} \int \frac{d\omega}{2\pi} e^{i(\mathbf{k}\cdot\mathbf{x} - \omega t)} \psi_{\alpha}(\mathbf{k}, \omega), \quad (2.26)$$

we obtain the Gaussian action,

$$\mathcal{S}_0[\hat{\boldsymbol{\psi}}, \boldsymbol{\psi}] = \int d\tilde{\mathbf{k}} \left(\hat{\psi}_{\alpha}(-\tilde{\mathbf{k}}) \mathcal{F}_{\alpha\beta}^0 \psi_{\beta}(\tilde{\mathbf{k}}) - \hat{\psi}_{\alpha}(-\tilde{\mathbf{k}}) L_{\alpha\beta} \hat{\psi}_{\beta}(\tilde{\mathbf{k}}) \right) \quad (2.27)$$

where we are using the simplified notation $\tilde{\mathbf{k}} = (\mathbf{k}, \omega)$ and $\int d\tilde{\mathbf{k}} = \int_{|\mathbf{k}| < \Lambda} d^d k / (2\pi)^d \int d\omega / 2\pi$. Defining the vector $u_{\alpha} = (\psi_{\alpha}, \hat{\psi}_{\alpha})$, the last equation can be written as,

$$\mathcal{S}_0[\hat{\boldsymbol{\psi}}, \boldsymbol{\psi}] = \int d\tilde{\mathbf{k}} u_{\alpha}(-\tilde{\mathbf{k}})^{\top} M_{\alpha\beta}(\tilde{\mathbf{k}}) u_{\beta}(\tilde{\mathbf{k}}) \quad (2.28)$$

with the introduction of the matrix $M_{\alpha\beta}$, which stands for

$$M_{\alpha\beta}(\tilde{\mathbf{k}}) = \begin{pmatrix} 0 & F_{\alpha\beta}^0(\tilde{\mathbf{k}}) \\ F_{\alpha\beta}^0(-\tilde{\mathbf{k}}) & -2L_{\alpha\beta}(\tilde{\mathbf{k}}) \end{pmatrix}. \quad (2.29)$$

Thanks to this simplification it is possible to easily compute Gaussian averages

of the type,

$$\langle u_\alpha(\tilde{\mathbf{q}})^\top u_\beta(\tilde{\mathbf{k}}) \rangle_0 = (M_{\alpha\beta}(\tilde{\mathbf{k}}))^{-1} \delta(\tilde{\mathbf{q}} + \tilde{\mathbf{k}}) \quad (2.30)$$

just evaluating the inverse of the matrix M , namely:

$$M_{\alpha\beta}(\tilde{\mathbf{k}})^{-1} = \begin{pmatrix} 2G_{\alpha\lambda}^0(-\tilde{\mathbf{k}})L_{\lambda\mu}(\tilde{\mathbf{k}})G_{\mu\beta}^0(\tilde{\mathbf{k}}) & G_{\alpha\beta}^0(-\tilde{\mathbf{k}}) \\ G_{\alpha\beta}^0(\tilde{\mathbf{k}}) & 0 \end{pmatrix} \quad (2.31)$$

where

$$G_{\alpha\beta}^0(\tilde{\mathbf{k}}) = (F_{\alpha\beta}^0(\tilde{\mathbf{k}}))^{-1} \quad (2.32)$$

is the Gaussian propagator of the theory. Moreover, if we recognize the correlator $C_{\alpha\beta}^0(\tilde{\mathbf{k}}) = 2L_{\alpha\beta}(\tilde{\mathbf{k}})|G^0(\tilde{\mathbf{k}})|^2$, we directly obtain generic forms for these basic two-points correlation functions,

$$\begin{aligned} \langle \hat{\psi}_\alpha(\tilde{\mathbf{q}})\psi_\beta(\tilde{\mathbf{k}}) \rangle_0 &= G_{\alpha\beta}^0(\tilde{\mathbf{k}})\delta(\tilde{\mathbf{q}} + \tilde{\mathbf{k}}) = (F_{\alpha\beta}^0(\tilde{\mathbf{k}}))^{-1}\delta(\tilde{\mathbf{q}} + \tilde{\mathbf{k}}) \\ \langle \psi_\alpha(\tilde{\mathbf{q}})\psi_\beta(\tilde{\mathbf{k}}) \rangle_0 &= C_{\alpha\beta}^0(\tilde{\mathbf{k}})\delta(\tilde{\mathbf{q}} + \tilde{\mathbf{k}}) = 2L_{\alpha\beta}(\tilde{\mathbf{k}})/|F^0(\tilde{\mathbf{k}})|^2\delta(\tilde{\mathbf{q}} + \tilde{\mathbf{k}}). \end{aligned} \quad (2.33)$$

To conclude, from the last expressions we can understand the physical meaning of the response field and the reason of its name: if we add a magnetic field coupled to ψ_α in the equation of motion and consequently in the effective action, the kinetic response function can be computed as,

$$\frac{\delta\langle\psi_\alpha(\tilde{\mathbf{k}})\rangle}{\delta h_\beta(\tilde{\mathbf{q}})} = \langle \hat{\psi}_\alpha(\tilde{\mathbf{q}})\psi_\beta(\tilde{\mathbf{k}}) \rangle \quad (2.34)$$

which is directly given by the dynamical propagator of (2.33) [67].

2.2.3 Shell-integration

We are now going to explain in more detail the operations that form an RG step. Once determined the effective action of a theory, the first thing to do is perform the coarse-graining on the system, namely averaging out the short-wavelength details and writing the theory for the resulting degrees of freedom. It is more useful to operate these passages in the Fourier space, in which the small length scales become large momenta. We already met b , the scaling factor, which is the quantity determining the range of modes we want to integrate out, namely those included in the interval $\Lambda/b < |\mathbf{k}| < \Lambda$, properly the momentum shell. Clearly $b \simeq 1$ corresponds to an infinitesimal operation and Λ is the natural cutoff of the theory [65].

We can then separate the modes of the field on the shell and outside the shell (to be done also for the response field):

$$\psi_\alpha(\tilde{\mathbf{k}}) = \begin{cases} \psi_\alpha^<(\tilde{\mathbf{k}}) & \text{for } |\mathbf{k}| < \frac{\Lambda}{b} \\ \psi_\alpha^>(\tilde{\mathbf{k}}) & \text{for } \frac{\Lambda}{b} < |\mathbf{k}| < \Lambda \end{cases} \quad (2.35)$$

In this way each integral over the momentum appearing in the effective action

can be splitted as,

$$\int_{|\mathbf{k}|<\Lambda} d\tilde{\mathbf{k}} f(\tilde{\mathbf{k}}) \psi_\alpha(\tilde{\mathbf{k}}) = \int_{|\mathbf{k}|<\Lambda/b} d\tilde{\mathbf{k}} f(\tilde{\mathbf{k}}) \psi_\alpha^<(\tilde{\mathbf{k}}) + \int_{\Lambda/b<|\mathbf{k}|<\Lambda} d\tilde{\mathbf{k}} f(\tilde{\mathbf{k}}) \psi_\alpha^>(\tilde{\mathbf{k}}) \quad (2.36)$$

where f is just an example function. The result is that the action is also affected by this division,

$$\mathcal{S}[\psi, \hat{\psi}] = \mathcal{S}_0[\psi^<, \hat{\psi}^<] + \mathcal{S}_0[\psi^>, \hat{\psi}^>] + \mathcal{S}_I[\psi^<, \hat{\psi}^<, \psi^>, \hat{\psi}^>] \quad (2.37)$$

and it separates in two Gaussian parts: one only for the small modes and one for the large modes; and in a non-linear part in which all the modes interact with each other. The latter indeed represents the complicated part of the theory, namely that describing fluctuations of the fields at every length scale.

To integrate out the modes on the shell we have to consider the probability distribution associated with the system, where now, to simplify the notation, we indicate with ϕ the couple $(\psi, \hat{\psi})$,

$$P[\phi] \sim e^{-\mathcal{S}[\phi]} \sim e^{-\mathcal{S}_0[\phi^<]-\mathcal{S}_0[\phi^>]-\mathcal{S}_I[\phi^<,\phi^>]} . \quad (2.38)$$

Coarse-graining practically means marginalizing this distribution with respect to the large modes, thus obtaining a probability distribution for the remaining small modes,

$$P[\phi^<] \sim \int \mathcal{D}\phi^> P[\psi] \sim e^{-\mathcal{S}_0[\phi^<]} \int \mathcal{D}\phi^> e^{-\mathcal{S}_0[\phi^>]-\mathcal{S}_I[\phi^<,\phi^>]} . \quad (2.39)$$

These algebraic calculations have to be performed also in the partition function normalizing the distribution $Z = \int \mathcal{D}\phi \exp(-\mathcal{S}[\phi])$, thanks to which it is possible to rewrite the previous equation in

$$\begin{aligned} P[\phi^<] &\sim e^{-\mathcal{S}_0[\phi^<]} \langle e^{-\mathcal{S}_I[\phi^<,\phi^>]} \rangle_0 \\ &\sim e^{-\mathcal{S}_R[\phi^<]} \end{aligned} \quad (2.40)$$

where we define the renormalized effective action,

$$\mathcal{S}_R[\phi^<] = \mathcal{S}_0[\phi^<] + \ln(\langle e^{-\mathcal{S}_I} \rangle_0) . \quad (2.41)$$

In this last formula, the $\langle \ \rangle_0^>$ indicates an average over the Gaussian distribution, whose measure is represented by $\mathcal{S}_0[\phi^>]$. The result of this procedure is a probability distribution for the small scale modes whose effective action is composed by the bare starting one, plus a term coming from the interacting part (2.41) [64]. This latter represents the most difficult part to compute analytically and, to achieve this goal, we are going to use the perturbation theory.

Perturbation theory

All the nontrivial part of this first step of calculation comes from the evaluation of the interacting term of (2.41) that cannot be computed exactly but only in an approximated way. If we isolate in this part of the action a common prefactor λ , called *coupling constant*, we can indeed expand the quantity $\langle e^{-\mathcal{S}_I} \rangle_0^>$ in powers of it, obtaining:

$$\langle e^{-\lambda \mathcal{S}_I} \rangle_0^> \simeq e^{-\lambda \langle \mathcal{S}_I \rangle_0 + \frac{1}{2} \lambda^2 (\langle \mathcal{S}_I^2 \rangle_0 - \langle \mathcal{S}_I \rangle_0^2) + \mathcal{O}(\lambda^3)}. \quad (2.42)$$

The expansion in terms of coupling constant, performed thanks to properties of Gaussian distributions, becomes an expansion around the Gaussian theory which is represented by the zeroth-order at $\lambda = 0$. All these averaged terms are usually computed by means of the Feynman-diagrams, that can be drawn remembering (briefly) some rules [51]:

- the terms in \mathcal{S}_I represent the vertices where each line stands for a field;
- the $\psi^<$ fields are the external legs, while the $\psi^>$ are the internal legs;
- the operation of average connects the internal legs forming bare propagators and correlators;
- each loop represents an integral over an internal momentum defined on the shell, and on the frequency defined in all \mathbb{R} ;
- each vertex and diagram has to satisfy a conservation law of momenta and frequencies;
- each diagram has to be multiplied by a multiplicity factor counting all the possible combinations of fields' contractions.

The issue is in fact subtler: the expansion is performed in terms of the coupling constant, thinking to progressively add interaction to the system while increasing the order of expansion; however, the right interpretation is to think about it as an expansion in the continuous space of dimensions [51]. The coupling constants and all the non-linear terms usually become irrelevant when the dimension is large enough: the threshold to make it happen is called upper critical dimension d_c^u and it sets the limit above which the Gaussian theory is exact. Calling ϵ the distance in dimension from this quantity $\epsilon = d_c^u - d$, this becomes the real parameter fixing the order of the expansion, which indeed is better known as ϵ -expansion [70]. Everything is consistent if, at the fixed point, $\lambda^* \simeq \mathcal{O}(\epsilon)$ [62].

The outcome of the diagrams' calculation defines the renormalized effective action \mathcal{S}_R , which appears with the same combination of fields but with a new set of coefficients absorbing the corrections coming from the perturbative expansion. For instance, after this step, a generic coefficient μ_0 of the bare action, belonging with a set of parameters \mathcal{P}_0 , becomes,

$$\mu_R = \mu_0 - \delta\mu \ln b \quad (2.43)$$

where the second term of r.h.s. is the result of the integration, and $\ln b$ is the thickness of the shell for an infinitesimal transformation, since $1 - b^{-1} \simeq \ln b$ for $b \simeq 1$. Moreover, the correction $\delta\mu$ is usually proportional to the set of coupling constants of the theory.

2.2.4 Rescaling

A step further is needed to complete one RG iteration and it is the step of rescaling [64]. After the procedure of coarse-graining, one ends up with a theory described by \mathcal{S}_R with a new upper limit, that is the cutoff Λ/b . To make a direct comparison between the theory before and after the defocusing procedure, and therefore to understand how the theory changes when explored at different length scales, we need to ripristinate the original natural cutoff Λ . Hence, we work out the transformation of momenta,

$$\mathbf{k} \rightarrow \mathbf{k}_b = b\mathbf{k} , \quad (2.44)$$

which inversely affects the correlation length $\xi_b = \xi/b$. As a consequence, also a rescaling of time and frequency is needed [61, 73],

$$\omega \rightarrow \omega_b = b^z \omega \quad (2.45)$$

where z is the critical exponent that verifies the dynamical scaling hypothesis [5], appearing as the wild card to be determined at the end of the scaling procedure. Also the fields of the action have to be replaced, since their space-time dependence is modified according to the previous scaling relations, we then define the new fields,

$$\begin{aligned} \psi_b(\mathbf{k}_b, \omega_b) &= b^{-D_\psi} \psi \left(\frac{\mathbf{k}_b}{b}, \frac{\omega_b}{b^z} \right) \\ \hat{\psi}_b(\mathbf{k}_b, \omega_b) &= b^{-D_{\hat{\psi}}} \hat{\psi} \left(\frac{\mathbf{k}_b}{b}, \frac{\omega_b}{b^z} \right) \end{aligned} \quad (2.46)$$

indicating with D_ψ and $D_{\hat{\psi}}$ the fields' scaling dimensions. Adding those relations together, the renormalized parameters acquire a naive scaling dimension D_μ which can be guessed by simple dimensional analysis,

$$\begin{aligned} \mu_b &= b^{D_\mu} \mu_R \\ &= b^{D_\mu} \mu_0 \left(1 - \frac{\delta\mu}{\mu_0} \ln b \right) . \end{aligned} \quad (2.47)$$

Because the scaling factor is $b \simeq 1$, everything can be expressed in terms of bare parameters as,

$$\mu_b = b^{\chi_\mu} \mu_0 \quad (2.48)$$

where $\chi_\mu = D_\mu - \delta\mu/\mu_0$ is called the total scaling dimension of the parameter μ . It is usually composed of a naive part plus the non-trivial contribution com-

ing from the coarse-graining process. Certainly, this latter is always null in the Gaussian (mean-field) case. Equations as (2.48) have to be written down for all the parameters defining the theory, including the coupling constants. Finally, iterating the total procedure l times one obtains a full set of recursion relations,

$$\begin{aligned}\mu_{l+1} &= b^{\chi_\mu} \mu_l \\ \mu_{l+1} &= b^{l\chi_\mu} \mu_0 ,\end{aligned}\tag{2.49}$$

which determine the RG flow in the parameters space [64].

2.3 Fixed points: the dynamical critical exponent

As it happens for the classical static study, the universality of the dynamic critical behavior is determined by properties of the recursion relations' (2.49) fixed points. Critical exponents are indeed related to the behavior under RG of the set of parameters in their neighborhood [64].

These points can be identified with a special set \mathcal{P}^* in the parameters space, which is invariant under an RG transformation, namely those satisfying

$$\mathcal{R}_b \mathcal{P}^* = \mathcal{P}^*\tag{2.50}$$

where the operator \mathcal{R}_b indicates both the coarse-graining and the rescaling procedure. This relation tells us that the fixed points are that specific combination of parameters realizing the critical scale-invariance property of the system, namely when fluctuations are correlated on every length scale and the system does not change if observed at larger distances.

The solution of eq (2.50), when it exists, can be found directly solving the coupled involved recursion equations, or introducing what are called the β -functions [62]. The latter can be extrapolated by a linearization of the dynamical relation of each parameter, namely:

$$\mathcal{P}_{l+1} = \mathcal{P}_l - \beta_{\mathcal{P}} \ln b\tag{2.51}$$

from which the definition follows,

$$\beta_{\mathcal{P}} = \frac{\partial \mathcal{P}_{l+1}}{\partial (-\ln b)} = -\chi_{\mathcal{P}} \mathcal{P}_l .\tag{2.52}$$

Depending on the scaling dimensions, these quantities describe how the parameters behave along with the RG flow and contain double information: first, their zeros represent the fixed points of the flow:

$$\beta_{\mathcal{P}}(\mathcal{P}^*) = 0 ;\tag{2.53}$$

second, their derivatives draw up the infrared stability or instability of these

points. In our case we assume that, when

$$\frac{\partial \beta_{\mathcal{P}}(\mathcal{P}^*)}{\partial \mathcal{P}} < 0 \quad (2.54)$$

the fixed point is infrared stable, otherwise is unstable [62].

The critical exponents quantitatively describe the singular behavior of the thermodynamic quantities of a system when it approaches the critical point $T \sim T_c$ of a phase transition. In parameters space, this can be represented by a starting point of the flow close to the critical manifold (i.e. when $\xi = \infty$), thus characterized by a large and finite correlation length. In this case, applying the RG transformations, one sees its flow being attracted by the critical fixed point and then escaping towards the other non-critical fixed points. The exponents can be then evaluated by looking at the velocity of this process, of course in terms of parameters and changes of spatio-temporal scales. A deeper discussion can be found in [62, 65], but here we are going to focus only on the determination of the dynamical critical exponent z .

The kinetic coefficient of the order parameter is what plays a fundamental role in the game. If the dynamics follows the general scheme of eq (2.3), this exponent can indeed be found imposing that the recursion relation Γ_l reaches a finite non-zero fixed-point value Γ^* or, in other words, that [64, 74]:

$$\Gamma^* \sim \mathcal{O}(1) \quad (2.55)$$

which implies the condition,

$$\Gamma_{l+1} = b^{l\chi_{\Gamma}} \Gamma_0 \quad \implies \quad \chi_{\Gamma}(z) = 0 . \quad (2.56)$$

Solving the equation on the right, it is, therefore, possible to directly find the dynamical critical exponent of the model. The reason for this derivation lies in the fact that eq (2.55) is equivalent to requiring that eq (2.50) has a non-trivial solution for the dynamics. Indeed, the kinetic coefficient represents a the time-scale under which the time of the dynamical evolution can be rescaled: thus, excluding fixed points values like $\Gamma^* = 0$ and $\Gamma^* = \infty$ means excluding trivial or insignificant dynamics of the order parameter [61, 64].

2.4 Dynamical scaling from DRG

We now dedicate the last section of this chapter to the connection between the technique of the DRG and the dynamical scaling hypothesis introduced in chapter 1 [64].

The dynamical correlation function of a physical system $C_0(\mathbf{k}, \omega, \mathcal{P}_0)$ depends in Fourier space on the wave-number, on the frequency, and on a starting set of bare parameters \mathcal{P}_0 . When we apply the RG scaling procedure on it, we usually

get:

$$C_0(\mathbf{k}, \omega, \mathcal{P}_0) = b^{2z} C_b(b\mathbf{k}, b^z \omega, \mathcal{P}_b) , \quad (2.57)$$

valid until the term $-i\omega$ takes perturbative corrections. To proceed, we can discriminate two different cases,

1. $T \neq T_c$ and $\xi < \infty$. The correlation length decreases as $\xi_{l+1} = \xi/b^l$ till reaching, in the limit of $l \rightarrow \infty$, the smallest possible scale $1/\Lambda$. This imposes a stop condition to the flow, namely when

$$\Lambda \xi = b^l . \quad (2.58)$$

Substituting it in (2.57), we obtain,

$$C_0(\mathbf{k}, \omega, \mathcal{P}_0) = (\Lambda \xi)^{2z} C(\Lambda \xi k, (\Lambda \xi)^z \omega, \mathcal{P}^*) \quad (2.59)$$

where we are assuming that, in this limit, the parameters reach their fixed point values. If now we consider a fixed product $k\xi$, from this latter equation it is evident the emergence of a characteristic frequency, scaling as,

$$\omega_c(k\xi) = \xi^{-z} g(k\xi) \quad (2.60)$$

which directly recalls and validates the dynamical scaling hypothesis [75].

2. $T = T_c$ and $\xi = \infty$. In this case, the maximum number of RG iterations is fixed again by the natural cutoff but it is expressed in terms of the scale observation k ,

$$\frac{\Lambda}{k} = b^l . \quad (2.61)$$

The scaling of the correlation function accordingly reads,

$$C_0(\mathbf{k}, \omega, \mathcal{P}_0) = \left(\frac{\Lambda}{k}\right)^{2z} C\left(\Lambda, \left(\frac{\Lambda}{k}\right)^z \omega, \mathcal{P}^*\right) \quad (2.62)$$

which again defines the appropriate generalization of the scaling hypothesis,

$$\omega_c(k) = k^z f(k\xi) , \quad (2.63)$$

finally closing the connection with the DRG transformations [64].

Chapter 3

Renormalization of the incompressible Vicsek Model

In this chapter, we are going to focus on the first analyzed active matter model of swarming behavior, namely the Vicsek model. The main purpose is to analytically understand its critical dynamics and to find an explanation to the first numerical results shown in Fig 1.8, namely a dynamical scaling with $z = 2$. To start with, we present the explicit DRG calculation of the out-of-equilibrium incompressible case, already performed by Chen, Toner, and Lee in [6]. In this theory density fluctuations, which are also not relevant in natural swarms, are suppressed and it allowing to understand the role of activity in determining the universality class of an active matter model.

3.1 Vicsek Model and Toner and Tu theory

A possible way to approach the research for universal theories of physical systems is to build up minimal models that, with the smallest set of parameters and details, are able to characterize the most important traits of a subject. An example of this approach is represented by the Vicsek model, introduced in 1995 in [29]. We already presented the model in chapter 1, but we report here again some details for clarity [30].

The model describes an overdamped dynamics for active particles and it is formulated in a time discrete domain ($\Delta t = 1$). The equations for the particles' velocities and positions read [28],

$$\mathbf{v}_i(t+1) = \mathcal{R}_\eta \left(\sum_j^N n_{ij}(t) \mathbf{v}_j(t) \right) \quad (3.1)$$

$$\mathbf{r}_i(t+1) = \mathbf{r}_i(t) + \mathbf{v}_i(t+1) \quad (3.2)$$

$$|\mathbf{v}_i(t)| = v_0 \quad \forall i, t. \quad (3.3)$$

Here i, j are the indices of the N particles of the system, and $n_{ij}(t)$ is the connectivity matrix, whose dependence on time is due to the reshuffling of the self-

propelled network. Eq. (3.1) describes the result of the alignment interaction: the direction of motion of one particle at time $(t+1)$ is determined by the average of the neighbors' velocities at time t , to which it tends to be aligned. The number of interacting particles can be fixed, referring to a topological interaction, while it can change over time being determined according to a metric rule: two particles interact only if their mutual distance satisfies $r_{ij} < r_c$ with r_c the interaction radius. The natural system of our interests belongs to this second class so we are going to consider only metric interactions. Finally, the noise operator \mathcal{R}_η applies a scalar noise of amplitude η .

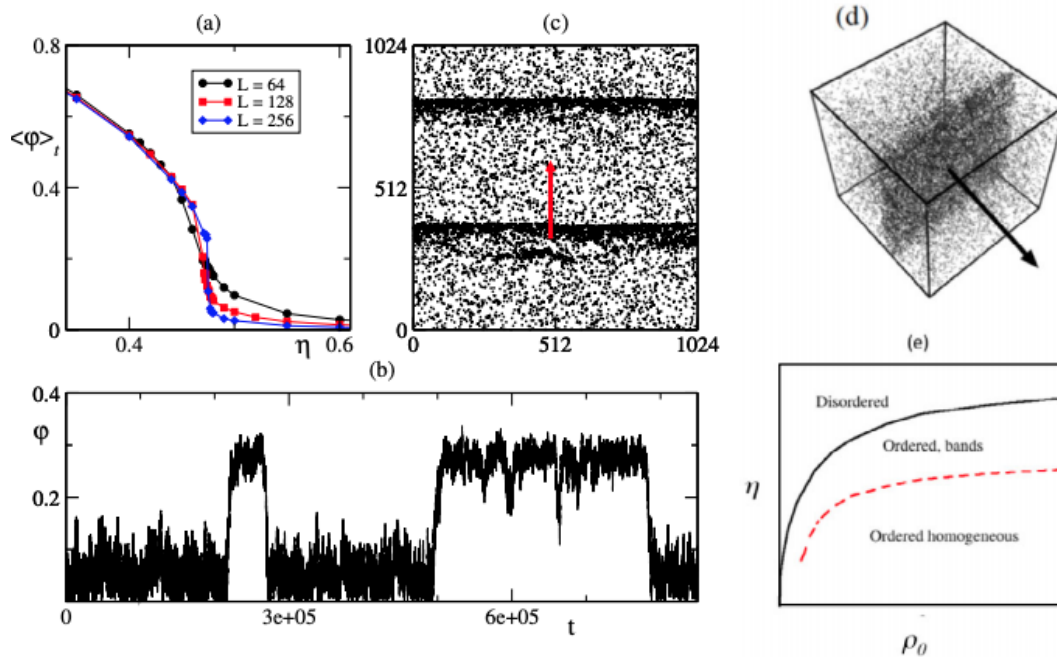


Figure 3.1: Main features of the Vicsek model. Panel a: polarization vs noise for different sizes in $d = 2$, with the increasing of the size the curve becomes steeper passing from a second-order to a first-order phenomenology. Panel b: time series of polarization when the system is at the interface of order and disorder, showing the typical instability. The jumps in the polarization are given by the emergence of order bands as those of panel c (in 2d) and d (in 3d). Panel e: qualitative phase diagram in the (ρ_0, η) plane. Figure reprinted from [30].

This model describes an out-of-equilibrium dynamics, since particles continuously exchange their mutual positions: interactions are thus not reversible in time, clearly violating the detailed balance condition. Moreover, the last equation (3.3) imposes that the speed of each particle is constant and fixed to v_0 , inducing a violation of momentum conservation and making the system properly *active*. The speed v_0 , together with the noise amplitude η and the average density $\rho_0 = N/V$, forms the fundamental set of dynamical parameters which rules the thermodynamics of the system. Indeed, this model exhibits a phase transition from a disordered homogeneous state, where the system has no net motion, to a collective flocking state in which particles move coherently in a symmetry broken phase (Fig. 3.1). The critical point is usually identified as the noise $\eta_c = \eta_c(\rho_0, v_0)$

that clearly depends on the other parameters of the model. Actually, once the value of the speed is fixed, a critical line in the plane (η, ρ_0) exists, for which it is possible to assume as a control parameter of the transition also the density [30, 76]. This is the method we choose to connect this theory to the metric system of swarms.

Several variants of the original model have been studied, and deep numerical and analytical works focused on the investigation of the phase transition's nature [34, 38]. Though for small sizes the exhibited phenomenology recalls a second-order transition, for which scaling and critical phenomena tools can be applied [77], for asymptotically large sizes the phase transition has been shown to be of the first order within a phase separation scenario [78] (Fig 3.1).

In chapter 1, we already discussed the range of applicability of this microscopic model to the biological case of swarms, claiming that its dynamics is not suitable to explain the related experimental data about their dynamical properties. We remind that numerical simulations of the VM realized in [3] found that the disordered critical phase of the model is characterized by a pure exponential relaxation with $z \simeq 2$, a result not consistent with experiments both from a quantitative and a qualitative point of view. However, this evidence opens several general questions about the critical dynamics of the theory that needs to be addressed. The way to do it is to write a hydrodynamic field theory and study its large-scale, long-time physics.

Hydrodynamic theory

Toner and Tu wrote their seminal paper in 1995 introducing a field theory version of the VM [36]. This theory describes the system as an active fluid with ferromagnetic interactions, a picture that proved to be very successful in explaining many large-scale properties of the microscopic model. The equations of motions involve two fields: the particles number density $\rho(\mathbf{x}, t)$ and the velocity $\mathbf{v}(\mathbf{x}, t)$, namely [36, 37]:

$$\partial_t \rho + \nabla \cdot (\rho \mathbf{v}) = 0 \quad (3.4)$$

$$\begin{aligned} \partial_t \mathbf{v} + \lambda_0 (\mathbf{v} \cdot \nabla) \mathbf{v} + \lambda_1 (\nabla \cdot \mathbf{v}) \mathbf{v} + \lambda_2 \nabla |\mathbf{v}|^2 = \\ \Gamma_0 \nabla^2 \mathbf{v} - (a_0 + J_0 v^2) \mathbf{v} - \nabla P + D_1 \nabla (\nabla \cdot \mathbf{v}) + D_2 (\mathbf{v} \cdot \nabla)^2 \mathbf{v} + \mathbf{f} \end{aligned} \quad (3.5)$$

with noise variance

$$\langle \mathbf{f}(\mathbf{x}, t) \mathbf{f}(\mathbf{x}', t') \rangle = 2\tilde{\Gamma}_0 \delta^{(d)}(\mathbf{x} - \mathbf{x}') \delta(t - t') \quad (3.6)$$

The first equation eq (3.4) describes the conservation of particles' number, which is the only conservation law admitted in the system [36]. Unlike simple fluids, active fluids do not conserve the momentum since the velocity field assumes also the role of polarity. A Landau-Ginzburg potential $V(\mathbf{v}) = a_0 v^2 + J_0 v^4$ confines field fluctuations around a reference value, translating the constant speed constraint into a mesoscopic formulation. This fact breaks the Galilean invariance, reflecting

in the presence of multiple terms of advection. In (3.5) we observe an advective term multiplied by the coefficient λ_0 , which also classically appears in the Navier-Stokes equation, and additional advective λ_1, λ_2 terms that are gradient terms of the same order allowed by the violation of Galilean invariance [37].

This latter is a special feature of active systems, and it stems directly from the constraint of constant speed v_0 imposed at a microscopic level. The application of a simple Galilean boost brings to a violation of the constraint, thus breaking the invariance. Hence, the dynamics has to be kinematically interpreted as expressed in a special reference frame, represented by the resistive medium in which the system moves [37]. At the hydrodynamic level, applying a Galilean boost means performing the transformations,

$$\mathbf{v} \rightarrow \mathbf{v} + \hat{\mathbf{v}} \quad (3.7)$$

$$\mathbf{x} \rightarrow \mathbf{x} - \hat{\mathbf{v}}t \quad (3.8)$$

on the eq (3.4) (3.5). A strict invariance would force $\lambda_0 = 1$ and $\lambda_1 = \lambda_2 = 0$, but, due to this violation, all the additional terms are allowed to be different from zero and one [37].

The other players of the theory are: the coefficients Γ_0, D_1 and D_2 , representing diffusion constants of velocity's fluctuations; the amplitude of the Gaussian white noise $\tilde{\Gamma}_0$, which is different from any other kinetic coefficient because of the violation of Fluctuation Dissipation Relations; and finally the parameters a_0 , the mass, and J_0 , the ferromagnetic coupling. These last coefficients describe the ordering transition in polarization: when the mass $a_0 < 0$ the system shows long-range polar order with a mean-field velocity $|\mathbf{v}| = \sqrt{-a_0/J_0}$, while for $a_0 > 0$ the system lives in a disorder phase with $|\mathbf{v}| = 0$. The gradient of pressure ∇P maintains the local density $\rho(\mathbf{x}, t)$ around its mean value ρ_0 [36] and, additionally, all the coefficients appearing in eq (3.5) depend in a non-trivial way on density and on all the microscopic parameters.

This theory was formulated within a phenomenological approach in terms of gradients expansion and, although it initially had not a direct connection with the microscopic starting model, it was able to reproduce its fundamental traits: long-range order in two dimensions [36] (the consequence of a violation of the Mermin-Wagner theorem [79]), giant density fluctuations and propagating density-dependent modes [80]. Most of the performed studies focus on the ordered phase with application to flocking systems. A first investigation on the pure critical phase was carried out in [6] under the incompressibility condition.

3.2 Adding incompressibility

For a long time, the ordering transition described by eq (3.4) (3.5) was believed to be continuous belonging to a new universality class of active matter. However, several theoretical and numerical studies [35, 78] revealed that the phase transition is in fact of the first-order. A phase separation scenario characterizes the change

from a disordered to a homogeneous ordered state, where all the results of Toner and Tu's studies can be applied. This process occurs because density instabilities cause the formation of bands transversal to the direction of motion, which coexist with the disordered state of matter [78]¹.

This phenomenon is one of the most evident manifestations of the out-of-equilibrium nature of the system. The active motion of the agents produces a strong coupling between the density and the velocity fields, establishing a positive feedback that gives birth to the band structure. To condensate this concept: denser regions order more strongly, but since they are more ordered than the rest of the system, they coherently travel recruiting other particles in the path, thus forming the transverse patterns of Fig 3.1 [76]. In the hydrodynamic equations, the coexistence phase reveals itself in the dependence of the mass on the density $a_0 = a_0(\rho)$ [80], whose variations are the main responsible for the first-order transition scenario.

In [6], Chen et al. proposed to suppress density fluctuations making the system incompressible, i.e. imposing $\nabla \cdot \mathbf{v} = 0$. A major effect is that the mechanism being at the core of band instabilities is completely turned off, since the density field ρ_0 becomes homogeneous and constant. Certainly, the condition of incompressibility implies that the system is homogeneous, thus allowing a continuous phenomenological description of its statistical physics. On the other hand, the opposite implication is not always true, a physical system can be homogeneous and compressible at the same time, especially without the long-range interactions entailed in an incompressible active fluid scenario. However, this condition simplifies by a lot the theory that now reads:

$$\begin{aligned} \frac{\partial \mathbf{v}}{\partial t} + \lambda_0(\mathbf{v} \cdot \nabla)\mathbf{v} &= \Gamma_0 \nabla^2 \mathbf{v} - (a_0 + J_0 v^2)\mathbf{v} - \nabla P + \mathbf{f} \\ \langle \mathbf{f}(\mathbf{x}, t) \mathbf{f}(\mathbf{x}', t') \rangle &= 2\tilde{\Gamma}_0 \delta^{(d)}(\mathbf{x} - \mathbf{x}') \delta(t - t') \\ \nabla \cdot \mathbf{v} &= 0 \end{aligned} \tag{3.9}$$

where the pressure P enforces the incompressibility constraint [6].

The authors were able to perform a one-loop DRG analysis at the critical point $a = 0$, discovering a rich scenario and a new dynamical universality class with exponent $z = 1.7$ in three dimensions [6]. The theory produces also an unstable fixed point reached for zero effective activity, which describes an equilibrium dynamics with $z = 2$ thus recalling the numerical exponent found in [3]. To understand better these results and to explore the role of the activity and of the incompressibility constraint in the critical dynamics of the VM, we present the complete DRG calculation.

¹In fact, a recent numerical study [81] demonstrates the existence of an additional thermodynamic phase of the Vicsek model: the cross-sea phase. It is interposed between the bands' and disordered phase and it is characterized by crossing patterns moving into opposite directions. However, a theoretical investigation of this phenomenon is still lacking.

3.3 Field dynamical equations

We want to perform a Dynamical Renormalization Group analysis of the theory (3.9). To do this, we briefly recall which are the main steps of the calculation:

1. start from the stochastic dynamical equation of motion;
2. write the MSR effective action and identify correlators and propagators of the free theory;
3. perform a perturbative expansion in terms of non-linearities around the Gaussian approximation;
4. apply iteratively coarse-graining and space-time rescaling, to write recursion relations for the parameters' flow extracting all the relevant information at the fixed points.

To effectively start the calculation, we must firstly ponder over the incompressibility condition $\nabla \cdot \mathbf{v} = 0$. We consider the Fourier transform of the velocity field in space, namely:

$$v_\alpha(\mathbf{x}, t) = \int \frac{d^d k}{(2\pi)^d} e^{i\mathbf{k} \cdot \mathbf{x}} v_\alpha(\mathbf{k}, t) \quad (3.10)$$

where with α we are indicating the cartesian component of the n dimensional vectorial field, and we are using the same symbol v_α to indicate the field in the x and k space. Applying the incompressibility condition then reads,

$$\partial_\alpha v_\alpha(\mathbf{x}, t) = 0 \quad \rightarrow \quad k_\alpha v_\alpha(\mathbf{k}, t) = 0 . \quad (3.11)$$

The second equation of (3.11) tells us two important things: first, to perform a scalar product between the momentum and the field and to maintain it null, the dimension of the order parameter must be equal to the space's one, namely $n = d$; second, the projection of $\tilde{\mathbf{v}}(\mathbf{k}, t)$ on the direction of \mathbf{k} is always null, meaning that only the transverse modes are significant for the dynamics, while the longitudinal ones are fixed by the constraint.

It is, therefore, useful to introduce the operator of projection along the orthogonal direction to the wavenumber \mathbf{k} , as:

$$P_{\alpha\beta}(\mathbf{k}) \equiv \delta_{\alpha\beta} - \frac{k_\alpha k_\beta}{k^2} \quad (3.12)$$

thanks to which, eq (3.11) becomes

$$P_{\alpha\beta}(\mathbf{k})v_\beta(\mathbf{k}, t) = v_\alpha(\mathbf{k}, t) \quad (3.13)$$

We can now apply the Fourier transform to the two sides of the equation (3.9)

and then the projection operator to obtain:

$$\begin{aligned} \partial_t v_\alpha(\mathbf{k}, t) &= -(\Gamma_0 k^2 + a_0)v_\alpha(\mathbf{k}, t) - i\frac{\lambda_0}{2}P_{\alpha\beta\gamma}(\mathbf{k}) \int d^d q v_\beta(\mathbf{q}, t)v_\gamma(\mathbf{k} - \mathbf{q}, t) \\ &\quad - \frac{J_0}{3}Q_{\alpha\beta\gamma\nu} \int d^d q \int d^d p v_\beta(\mathbf{k} - \mathbf{q} - \mathbf{p}, t)v_\gamma(\mathbf{q}, t)v_\nu(\mathbf{p}, t) + f_\alpha(\mathbf{k}, t) \end{aligned} \quad (3.14)$$

The noise variance becomes,

$$\langle f_\alpha(\mathbf{k}, t)f_\beta(\mathbf{k}', t') \rangle = 2\tilde{\Gamma}_0 P_{\alpha\beta}(\mathbf{k})\delta(\mathbf{k} + \mathbf{k}') \delta(t - t') . \quad (3.15)$$

Additionally, in the non-linear terms of interaction, we needed to symmetrize with respect to the integrals' momenta and projectors, thus obtaining the following additional operators appearing in (3.14):

$$P_{\alpha\beta\gamma}(\mathbf{k}) = P_{\alpha\beta}(\mathbf{k})k_\gamma + P_{\alpha\gamma}(\mathbf{k})k_\beta \quad (3.16)$$

$$Q_{\alpha\beta\gamma\nu}(\mathbf{k}) = P_{\alpha\beta}(\mathbf{k})\delta_{\gamma\nu} + P_{\alpha\gamma}(\mathbf{k})\delta_{\beta\nu} + P_{\alpha\nu}(\mathbf{k})\delta_{\gamma\beta} \quad (3.17)$$

3.4 MSR action and Gaussian theory

Using a Fourier transform in time,

$$v_\alpha(\mathbf{x}, t) = \int d\tilde{\mathbf{k}} e^{-i(\omega t - \mathbf{k} \cdot \mathbf{x})} v_\alpha(\tilde{\mathbf{k}}) \quad (3.18)$$

we derive the Martin-Siggia-Rose effective action with the standard procedure indicated in chapter 2. This action is thus composed by the two canonical parts:

$$\mathcal{S}[\mathbf{v}, \hat{\mathbf{v}}] = \mathcal{S}_0[\mathbf{v}, \hat{\mathbf{v}}] + \mathcal{S}_I[\mathbf{v}, \hat{\mathbf{v}}] \quad (3.19)$$

the Gaussian part:

$$\begin{aligned} \mathcal{S}_0[\mathbf{v}, \hat{\mathbf{v}}] &= \int d\tilde{\mathbf{k}} \left[\hat{v}_\alpha(-\tilde{\mathbf{k}})(-i\omega + \Gamma_0 k^2 + a_0)v_\alpha(\tilde{\mathbf{k}}) \right. \\ &\quad \left. - \tilde{\Gamma}_0 \hat{v}_\alpha(-\tilde{\mathbf{k}})P_{\alpha\beta}(\mathbf{k})\hat{v}_\beta(\tilde{\mathbf{k}}) \right] \end{aligned} \quad (3.20)$$

and the interacting one,

$$\begin{aligned} \mathcal{S}_I[\mathbf{v}, \hat{\mathbf{v}}] &= \int d\tilde{\mathbf{k}} \left[\frac{i\lambda_0}{2} \hat{v}_\alpha(-\tilde{\mathbf{k}})P_{\alpha\beta\gamma}(\mathbf{k}) \int d\tilde{\mathbf{q}} v_\gamma(-\tilde{\mathbf{k}} - \tilde{\mathbf{q}})v_\beta(\tilde{\mathbf{q}}) \right. \\ &\quad \left. + \frac{J_0}{3} \hat{v}_\alpha(-\tilde{\mathbf{k}})Q_{\alpha\beta\gamma\nu}(\mathbf{k}) \int d\tilde{\mathbf{q}} \int d\tilde{\mathbf{p}} v_\beta(\tilde{\mathbf{k}} - \tilde{\mathbf{q}} - \tilde{\mathbf{p}})v_\gamma(\tilde{\mathbf{q}})v_\nu(\tilde{\mathbf{p}}) \right] . \end{aligned} \quad (3.21)$$

From the free part of the action it is easy to recognize the expressions of the

bare propagator and correlator:

$$\langle v_\alpha(-\tilde{\mathbf{k}})\hat{v}_\beta(\tilde{\mathbf{k}})\rangle = \delta_{\alpha\beta}G_0(\tilde{\mathbf{k}}) = \delta_{\alpha\beta}[-i\omega + \Gamma_0(k^2 + a_0)]^{-1} \quad (3.22)$$

$$\langle v_\alpha(-\tilde{\mathbf{k}})v_\beta(\tilde{\mathbf{k}})\rangle = P_{\alpha\beta}(\mathbf{k})C_0(\tilde{\mathbf{k}}) = 2P_{\alpha\beta}(\mathbf{k})\tilde{\Gamma}_0|G_0(\tilde{\mathbf{k}})|^2 \quad (3.23)$$

which can also be easily derived starting from eq (3.14) with null non-linearities coefficients, $u_0 = 0$ and $\lambda_0 = 0$,

$$-i\omega\mathbf{v}(\tilde{\mathbf{k}}) = -\Gamma_0(k^2 + a_0)\mathbf{v}(\tilde{\mathbf{k}}) + \mathbf{f}(\tilde{\mathbf{k}}). \quad (3.24)$$

and then solving it with the Green function method. The solution is indeed

$$\mathbf{v}(\tilde{\mathbf{k}}) = G_0(\tilde{\mathbf{k}})\mathbf{f}(\tilde{\mathbf{k}}) \quad (3.25)$$

with

$$G_0(\tilde{\mathbf{k}}) = \frac{1}{-i\omega + \Gamma_0k^2 + a_0} \quad (3.26)$$

from which the scalar part of the correlator directly follows,

$$C_0(\tilde{\mathbf{k}}) = \frac{2\tilde{\Gamma}_0}{\omega^2 + (\Gamma_0k^2 + a_0)^2}. \quad (3.27)$$

3.5 Vertices and perturbation expansion

From the interacting part of the effective action, we instead deduce the form of the vertices that, together with bare propagator and correlator, will be the building blocks of the perturbative expansion around the Gaussian theory. We recognize two vertices, namely:

$$V_1 = \hat{v}_\alpha \rightarrow \begin{array}{c} v_\beta \\ | \\ v_\gamma \end{array} = -i\frac{\lambda_0}{2}P_{\alpha\beta\gamma}(\mathbf{k})\hat{v}_\alpha(-\tilde{\mathbf{k}})v_\beta(\tilde{\mathbf{q}})v_\gamma(\tilde{\mathbf{k}} - \tilde{\mathbf{q}}) \quad (3.28)$$

$$V_2 = \hat{v}_\alpha \rightarrow \begin{array}{c} v_\beta \\ | \\ v_\gamma \\ | \\ v_\nu \end{array} = -\frac{J_0}{3}Q_{\alpha\beta\gamma\nu}(\mathbf{k})\hat{v}_\alpha(-\tilde{\mathbf{k}})v_\beta(\tilde{\mathbf{k}} - \tilde{\mathbf{q}} - \tilde{\mathbf{p}})v_\gamma(\tilde{\mathbf{q}})v_\nu(\tilde{\mathbf{p}}) \quad (3.29)$$

in which we are indicating with solid lines the fields, distinguishing the response fields with an arrow entering in the vertex. The vertex V_2 is quite similar to the standard ferromagnetic vertex used in equilibrium field theories, indeed it is indicating the fundamental alignment interaction proper of this kind of polar systems.

Incidentally, we could have interpreted the l.h.s. of the velocity's equation (3.9), as a dissipative force coming from a generalized Landau-Ginzburg free-energy:

$$\mathcal{H} = \int d^d x dt \left(\frac{1}{2}(\nabla \mathbf{v})^2 + \frac{1}{2}r_0 v^2 + \frac{u_0}{4}v^4 \right) \quad (3.30)$$

mapping $a_0 \rightarrow r_0\Gamma_0$ and $J_0 \rightarrow u_0\Gamma_0$. On the other hand, the first vertex is the pure out-of-equilibrium element of the theory: it embeds the transport of the velocity and then all the activity of the system.

We are now ready to perform the perturbative expansion in the non-linearities represented by these vertices, which therefore will be determined by the interplay of these two physical components: activity and alignment interaction. The relevant terms of the expansion are built with the use of Feynman's diagrams as explained in chapter 2. However, to finally draw them, we need to fix a graphical representation of the bare propagator and correlator, that we chose as

$$G_0 = \longrightarrow \quad C_0 = \text{---} . \quad (3.31)$$

We use a simple line for the average of two velocity fields, while we use a line with an arrow for the propagator to highlight the presence of the response field and the consequent relevant ordering of time. From a simple power counting, it can be shown that both the non-linearities become irrelevant when $d > 4$, where the Gaussian mean-field theory happens to be exact. Therefore, the real parameter of the expansion is the distance from this upper critical dimension $d_c^u = 4$, that it $\epsilon = 4 - d$. Moreover, calculations are performed at 1-loop, and then at first order in ϵ .

The first corrections we compute regard the two points vertex functions. These contributions can be summarized in the Dyson equation for the propagator [51], which can be expressed as

$$G^{-1}(\tilde{\mathbf{k}})_{\alpha\beta} = G_0^{-1}(\tilde{\mathbf{k}})\delta_{\alpha\beta} - \Sigma_{\alpha\beta}(\tilde{\mathbf{k}}) \quad (3.32)$$

where $\Sigma_{\alpha\beta}$ represents the self-energy, whose graphical representation is:

$$\Sigma_{\alpha\beta} = \hat{v}_\alpha \longrightarrow \text{blob} \text{---} v_\beta \quad (3.33)$$

The blob indicates the sum of all amputated one-particle irreducible diagrams with the same external legs as the propagator and contains the leading contributions to the perturbative expansion.

In the effective action we recognize that the Gaussian part is not only composed by the $\hat{\mathbf{v}}\mathbf{v}$ term, which takes correction in the form of self-energy, but also by the Gaussian part of response fields $\hat{\mathbf{v}}\hat{\mathbf{v}}$ coming from the noise integration. This latter represents the renormalization of the correlation function which, in this case, has to proceed independently from that of the response functions. In-

deed, the system is out-of-equilibrium and there is no Fluctuation-Dissipation Relation valid to connect these two quantities. Therefore, to take into account corrections for the amplitude of the noise $\tilde{\Gamma}_0$, we additionally define the noise strength as,

$$\tilde{\Sigma}_{\alpha\beta} = \begin{array}{c} \text{---} \rightarrow \text{---} \text{---} \left(\text{shaded circle} \right) \text{---} \leftarrow \text{---} \text{---} \\ \hat{v}_\alpha \qquad \qquad \qquad \hat{v}_\beta \end{array} . \quad (3.34)$$

3.6 Renormalization of the linear dynamics

The first step of a Renormalization Group transformation is the coarse-graining, namely averaging the small length scale modes with wave-number in the shell $\Lambda/b < k < \Lambda$, with $b \sim 1$ the scaling factor. This step produces some additional corrections in the effective action that have to be reabsorbed from the coefficients of the theory. In this way, they become what we called renormalized coefficients. In this section, we are going to focus on those characterizing the Gaussian part, whose renormalizing contributions come directly from the self energies we just introduced. Diagrammatically, the one of the propagator appears:

$$\Sigma_{\alpha\beta} = \begin{array}{c} \text{---} \rightarrow \text{---} \left(\text{shaded circle} \right) \text{---} \text{---} \\ \hat{v}_\alpha \qquad \qquad \qquad v_\beta \end{array} = \begin{array}{c} \text{---} \rightarrow \text{---} \left(\text{loop} \right) \text{---} \\ \text{---} \end{array} + \begin{array}{c} \text{---} \rightarrow \text{---} \left(\text{circle} \right) \text{---} \\ \text{---} \end{array} \quad (3.35)$$

thus defining the renormalization of the coefficients of the linear dynamics:

$$a_R \equiv G^{-1} \Big|_{\substack{k=0 \\ \omega=0}} = a_0 \left(1 - \frac{1}{a_0} \Sigma_{\alpha\beta} \Big|_{\substack{k=0 \\ \omega=0}} \right) \quad (3.36)$$

$$\Gamma_R \equiv \frac{\partial G^{-1}}{\partial k^2} \Big|_{\substack{k=0 \\ \omega=0}} = \Gamma_0 \left(1 - \frac{1}{\Gamma_0} \frac{\partial \Sigma_{\alpha\beta}}{\partial k^2} \Big|_{\substack{k=0 \\ \omega=0}} \right) . \quad (3.37)$$

On the other hand, since at one loop

$$\tilde{\Sigma}_{\alpha\beta} = \begin{array}{c} \text{---} \rightarrow \text{---} \left(\text{shaded circle} \right) \text{---} \leftarrow \text{---} \text{---} \\ \hat{v}_\alpha \qquad \qquad \qquad \hat{v}_\beta \end{array} = \begin{array}{c} \text{---} \rightarrow \text{---} \left(\text{circle} \right) \leftarrow \text{---} \\ \text{---} \end{array} = 0 \quad (3.38)$$

we can easily say that the amplitude of the noise does not take any correction, implying $\tilde{\Gamma}_R = \tilde{\Gamma}_0$.

Every loop of the diagrams represents an integral in the internal momentum on the shell and in the unbounded internal frequency $-\infty < \omega < +\infty$. The result

of this integration for equations (3.36) (3.37) reads,

$$a_R = a_0 \left(1 + \frac{J_0 \tilde{\Gamma}_0}{a_0} \frac{(d-1)(d+2)}{d} K_d \Lambda^d \frac{\ln b}{(a_0 + \Gamma_0 \Lambda^2)} \right) \quad (3.39)$$

$$\Gamma_R = \Gamma_0 \left(1 + \frac{\lambda_0^2 \tilde{\Gamma}_0}{2\Gamma_0^3} \frac{(d-2)}{d} K_d \Lambda^{d-4} \ln b \right) \quad (3.40)$$

where we used rules for angular averages that are reported in Appendix A and the fact that in the limit of the scaling factor $b \rightarrow 1$, i.e. for an infinitesimal RG transformation, the shell is also infinitesimal, specifically of thickness $1 - 1/b \sim \ln b$. Moreover, an underlying tensorial structure should be taken into account for the perturbative corrections, coinciding with a $\delta_{\alpha\beta}$ for a_R and a $P_{\alpha\beta}(\mathbf{k})$ for Γ_R , however these are simply reabsorbed by the fields in the effective action.

Finally, one can see that the first equation contains a dependence on the bare mass a_0 , which has been kept in the evaluation of the diagrammatic integral since it is necessary to study the flow of itself. On the other hand, all others graphs are evaluated at the critical point and then at $a_R = 0$. To write down the recursion relations for these quantities, it is clear that we still need to know how to renormalize the parameters λ_0 and J_0 . We gain this information from the vertices corrections.

3.7 Vertices corrections

We represent in a similar way of the self energies the renormalized effective vertices, namely

$$V_1^R = \text{diagram with one incoming and two outgoing lines to a shaded blob} \quad V_2^R = \text{diagram with one incoming, one outgoing, and two diagonal lines to a shaded blob} \quad (3.41)$$

Also here blobs represent the sum of the irreducible one-loop diagrams, directly identified for the vertex of self-propulsion in:

$$V_1^R = \text{diagram with one incoming and one outgoing line to a circle with a clockwise arrow} + \text{diagram with one incoming and two outgoing lines to a circle with a clockwise arrow} \quad (3.42)$$

while in the following one for the ferromagnetic coupling:

$$V_2^R = \begin{array}{c} \begin{array}{c} \text{---} \nearrow \text{---} \\ \text{---} \circlearrowleft \text{---} \\ \text{---} \searrow \text{---} \end{array} \\ \cdot \end{array} \quad (3.43)$$

These contributions have a tensorial structure, which is fundamental to reconstruct the right correction to the terms appearing in the effective action. Let's focus first on the self-propulsion vertex for which the sum of the two diagrams have a dependence on indices that we can display as

$$V_1^R = V_1^{\alpha\beta\gamma}(\tilde{\mathbf{k}}, \tilde{\mathbf{q}}) = P_{\alpha\beta\gamma}(\mathbf{k})q_{\hat{v}vv}(\tilde{\mathbf{k}}, \tilde{\mathbf{q}}) \quad (3.44)$$

where we are indicating with $q_{\hat{v}vv}$ the contribution of the diagrams once the tensorial part is gathered. Therefore, we can express the renormalized active parameter as,

$$\lambda_R = \lambda_0 \left(1 - \frac{2}{i\lambda_0} q_{\hat{v}vv} \Big|_{\substack{\tilde{\mathbf{k}}=0 \\ \tilde{\mathbf{q}}=0}} \right). \quad (3.45)$$

The same considerations are valid for the ferromagnetic vertex, for which we write:

$$V_2^R = V_2^{\alpha\beta\gamma\nu}(\tilde{\mathbf{k}}, \tilde{\mathbf{q}}, \tilde{\mathbf{p}}) = Q_{\alpha\beta\gamma\nu}(\mathbf{k})q_{\hat{v}vvv}(\tilde{\mathbf{k}}, \tilde{\mathbf{q}}, \tilde{\mathbf{p}}) \quad (3.46)$$

where $q_{\hat{v}vvv}$ is the contribution coming from V_2^R without tensorial structure. The coarse-graining corrections to this vertex' parameters are,

$$J_R = J_0 \left(1 - \frac{3}{J_0} q_{\hat{v}vvv} \Big|_{\substack{\tilde{\mathbf{k}}=0 \\ \tilde{\mathbf{q}}=0 \\ \tilde{\mathbf{p}}=0}} \right) \quad (3.47)$$

A direct evaluation of equations (3.45) (3.47) leads to,

$$\lambda_R = \lambda_0 \left(1 - \frac{J_0 \tilde{\Gamma}_0}{\Gamma_0^2} \frac{3d^2 - 8}{d(d+2)} K_d \Lambda^{d-4} \ln b \right) \quad (3.48)$$

$$J_R = J_0 \left(1 - \frac{J_0 \tilde{\Gamma}_0}{\Gamma_0^2} \left(d + 1 + \frac{6(d^2 - 2)}{d(d+2)} \right) K_d \Lambda^{d-4} \ln b \right) \quad (3.49)$$

which concludes the first step of RG for the renormalized parameters of the theory. For a complete discussion we must specify that the diagrams shown in this section are the only resulting non-null diagrams. It is indeed possible to construct other graphs within the 1-loop approximation, that anyway are null by symmetry. A diagrammatic list, for both the two vertices, is reported in the following.

$$(3.50)$$

At this point, we simplify the equations for all the coefficients, defining a set of effective coupling constants read from the prefactors of the perturbative corrections, namely:

$$\alpha_0 = \frac{\lambda_0^2 \tilde{\Gamma}_0}{\Gamma_0^3} K_d \Lambda^{d-4}; \quad u_0 = \frac{J_0 \tilde{\Gamma}_0}{\Gamma_0^2} K_d \Lambda^{d-4}. \quad (3.51)$$

The first quantity α_0 is the coupling constant that describes the *activity* of the system since it is proportional to λ_0 , the coefficient of the advective dynamical term; the second equation identifies, instead, the *ferromagnetic* coupling constant since it depends on J_0 , that is the strength of the alignment interaction.

It is worth noticing that both these quantities are proportional to Λ^{d-4} , confirming that their scaling dimension is $\epsilon = 4 - d$. With this property they assume the role of effective dynamical coupling constants of the theory, namely the expansion's parameters of the perturbative calculation. They here result in a non-trivial combination of dynamical coefficients different from the simple parameters of the non-linear terms. Since we are interested in corrections of order ϵ coming from the RG, we therefore evaluate the rest of the integrals' results at $d = 4$. Finally, we summarize:

$$\begin{aligned} a_R &= a_0 - \frac{9}{2}(a_0 - \Gamma_0 \Lambda^2) u_0 \ln b \\ \Gamma_R &= \Gamma_0 \left(1 + \frac{\alpha_0}{4} \ln b \right) \\ \tilde{\Gamma}_R &= \tilde{\Gamma}_0 \\ \lambda_R &= \lambda_0 \left(1 - \frac{5}{3} u_0 \ln b \right) \\ J_R &= J_0 \left(1 - \frac{17}{2} u_0 \ln b \right) \end{aligned} \quad (3.52)$$

3.8 RG flow and fixed points

Once carried out the stage of coarse-graining, to compare the effective theories before and after this procedure, we need to rescale the space-time. This means applying the scaling relation $k \rightarrow bk$ to the wave-number, and $\omega \rightarrow b^z \omega$ to the frequency. Moreover, we have to define the scaling dimensions of the fields that

transform as:

$$v_\alpha(k/b, \omega/b^z) = b^{\chi_v} v_\alpha^b(k, \omega), \quad \hat{v}_\alpha(k/b, \omega/b^z) = b^{\chi_{\hat{v}}} \hat{v}_\alpha^b(k, \omega) \quad (3.53)$$

Since the term $-i\omega$ in the effective action does not take any perturbative correction, because of $\partial\Sigma_{\alpha\beta}/\partial(-i\omega) = 0$, we can state that the following identity, linking the two fields' scaling dimensions, applies,

$$\chi_v + \chi_{\hat{v}} = 2z + d. \quad (3.54)$$

Using this result and the standard rules of rescaling, we write down the relations for all the parameters,

$$\begin{aligned} a_0 &\rightarrow b^z a_0 \\ \Gamma_0 &\rightarrow b^{z-2} \Gamma_0 \\ \tilde{\Gamma}_0 &\rightarrow b^{3z+d-2\chi_v} \tilde{\Gamma}_0 \\ \lambda_0 &\rightarrow b^{\chi_v-d-1} \lambda_0 \\ J_0 &\rightarrow b^{2\chi_v-2d-z} J_0 \end{aligned} \quad (3.55)$$

which combine in the definitions of the coupling constants to give,

$$\alpha_0 \rightarrow b^{4-d} \alpha_0, \quad u_0 \rightarrow b^{4-d} u_0 \quad (3.56)$$

still confirming themselves as the true couplings of expansion of the model because now their irrelevant behavior for $d > 4$ is manifest.

We now merge (3.52) and (3.55) to obtain the final recursion relations of the dynamical parameters,

$$\begin{aligned} a_{l+1} &= b^z \left[a_l - \frac{9}{2} (a_l - \Gamma_l \Lambda^2) u_l \ln b \right] \\ \Gamma_{l+1} &= b^{z-2} \Gamma_l \left(1 + \frac{\alpha_l}{4} \ln b \right) \\ \tilde{\Gamma}_{l+1} &= b^{3z+d-2\chi_v} \tilde{\Gamma}_l \\ \lambda_{l+1} &= b^{\chi_v-d-1} \lambda_l \left(1 - \frac{5}{3} u_l \ln b \right) \\ J_{l+1} &= b^{2\chi_v-2d-z} J_l \left(1 - \frac{17}{2} u_l \ln b \right) \end{aligned} \quad (3.57)$$

and of the coupling constants,

$$\begin{aligned} \alpha_{l+1} &= b^\epsilon \alpha_l \left(1 - \frac{10}{3} u_l \ln b - \frac{3}{4} \alpha_l \ln b \right) \\ u_{l+1} &= b^\epsilon u_l \left(1 - \frac{17}{2} u_l - \frac{1}{2} \alpha_l \ln b \right) \end{aligned} \quad (3.58)$$

where l indicates the iteration of the RG transformation. These equations il-

illustrate the results of Chen et al's calculations [6] and define the flow of the parameters in the parameters' space. This space coincides with the critical manifold ($a_R = 0$, i.e. $\xi = \infty$), the place of existence of the critical fixed points. These latter can be found from the zeros of the β -functions, computed as,

$$\begin{aligned}\beta_\alpha &= \alpha \left(\frac{10}{3}u - \frac{3}{4}\alpha - \epsilon \right) \\ \beta_u &= u \left(\frac{17}{2}u - \frac{1}{2}\alpha - \epsilon \right) .\end{aligned}\tag{3.59}$$

The above system is solved by a set of three non-trivial solutions, corresponding to three different fixed points (clearly, the null solution $\alpha^* = 0$ and $u^* = 0$ is always admissible and it represents the Gaussian theory, unstable for $d < 4$):

1. the **equilibrium fixed point**, characterized by $\alpha^* = 0$ and $u^* = (2/17)\epsilon$. This is IR-unstable along the α direction for dimensions below the upper critical dimension $d_c^u = 4$, it belongs to the universality class of the isotropic ferromagnet with long-range dipolar interactions [82];
2. the random stirred fluid fixed point, when $\alpha^* = (4/3)\epsilon$ and $u^* = 0$. This is also IR-unstable but in the u direction, it was previously studied in [83] and it describes an incompressible normal fluid subject to random Gaussian forces;
3. the **off-equilibrium, active, fixed point** reached for $\alpha^* = (124/113)\epsilon$ and $u^* = 6/113\epsilon$. This is the only IR-stable fixed point for $d < 4$, and the only one where activity and ferromagnetic interaction combine in an interesting way to originate the universality class of incompressible active matter.

Finally, from these fixed points, one can extrapolate all the information about the critical exponents. We are interested in the dynamical critical one z , which is derived imposing that the kinetic coefficient is finite at the fixed point $\Gamma^* \sim \mathcal{O}(1)$. A condition here satisfied by the equation:

$$z = 2 - \frac{\alpha^*}{4} + \mathcal{O}(\epsilon^2) .\tag{3.60}$$

As a consequence, the equilibrium fixed point presents a $z = 2$ dynamical critical exponent, while the stable active fixed point exhibits $z = 1.7$ in $d = 3$ and in first-digit approximation. The latter exponent characterizes the new out-of-equilibrium dynamical universality class [6], from which we learn that, for incompressible theories, activity has the effect to lower the exponent with respect to an equilibrium counterpart. A summary of the results obtained from this analytical calculation is provided by Fig 3.2.

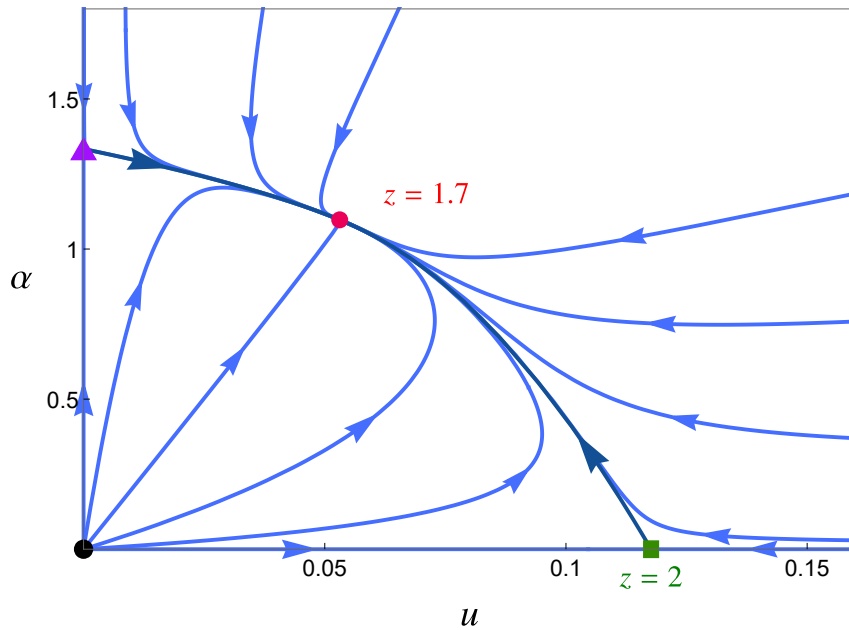


Figure 3.2: Critical manifold in the parameters space. This plane represents the critical manifold of the incompressible Toner and Tu theory. On the axes there are the two coupling constants, u that is the ferromagnetic coupling constant and α that is the active coupling constant. The result of the DRG calculation provides four fixed points, of which three unstable: black circle with $u^* = 0$ and $\alpha^* = 0$ that represents the mean-field theory; purple triangle with $u^* = 0$ and $\alpha^* = (4/3)\epsilon$ that is an incompressible fluid with random forces [83]; green square with $u^* = (2/17)\epsilon$ and $\alpha^* = 0$ with $z = 2$ that describes the universality class of the equilibrium isotropic and dipolar ferromagnet [82]. Finally the red circle identifies the stable fixed point with $u^* = (6/113)\epsilon$ and $\alpha^* = (124/113)\epsilon$ and $z = 1.7$, the fixed point relevant for active matter. Reprinted from [6] and [7]

Chapter 4

The first crossover: from an equilibrium to an off-equilibrium universality class

The ultimate aim of our research is to find a theoretical model able to provide a quantitative explanation to the dynamical scaling evidence in natural swarms of insects [3]. As we explained, the first attempt to achieve this goal concerns the study of the critical dynamics of the Vicsek model, which has already been tackled from two complementary sides. A first numerical approach, reported in [3], performed a finite-scaling analysis in the near-critical paramagnetic phase of the original model of eq (3.1) (3.2). It found out the validity of the dynamical scaling hypothesis for a critical exponent equal to $z = 2$ (Fig. 4.1). On the other hand, the second outlook involved a DRG calculation on the corresponding incompressible hydrodynamic field theory. This study discovered that the critical dynamics of active systems manifests with $z = 1.7$ in $d = 3$, while the exponent $z = 2$ indicates the equilibrium universality class [6].

These two results are apparently in contrast with each other, thus stimulating many questions about the consistency between the two aforementioned approaches. Why do numerical simulations of an active system reproduce an equilibrium-like critical exponent? To what extent is activity important in the critical dynamics of this system?

A first possible answer is based on the most evident difference between the calculation and the numerical simulations: the constraint of incompressibility. Simulations were indeed performed without imposing any condition on the velocities, thus reproducing compressible systems, although homogeneous to justify a finite size-scaling analysis. Conversely, compressibility represented a hard constraint to fulfill in the calculation, leading to think that the active fixed point with $z = 1.7$ is an artifact of the incompressibility requirement. In this chapter, we are going to demonstrate that this hypothesis is in fact false and that both the results can be reconciled together with the introduction of the concept of crossover between an equilibrium to an out-of-equilibrium universality class.

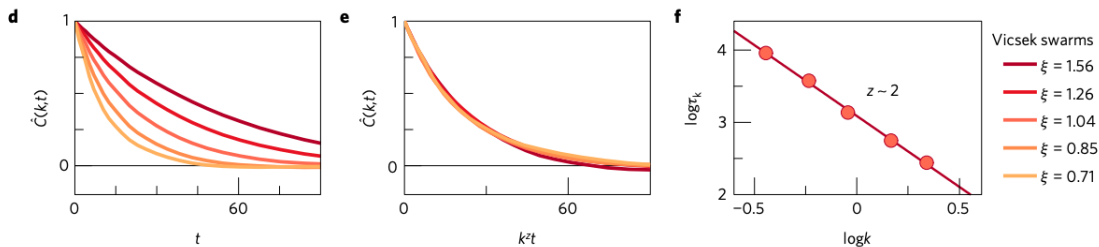


Figure 4.1: Dynamical scaling in the Vicsek model d) Normalized dynamical correlation functions evaluated at criticality for sizes $N = 128, 256, 516, 1024, 2048$ with wave-number $k = 1/\xi$. e) Same functions of panel d) when time is rescaled by $t \rightarrow k^z t$ using $z = 1.96 \pm 0.04$, value extrapolated by the linear fit of panel f) where τ_k indicates the relaxation time of the correlation functions. Reprinted from [3].

4.1 Activity drives the crossover in parameters space

The inspiration to solve this issue comes from the representation of the flow diagram of the hydrodynamic theory, reported again in Fig.4.2. The plane of ferromagnetic and active coupling constants (u, α) contains all the fixed points of the critical manifold. Our attention focuses on the equilibrium ferromagnetic fixed point (green square with $z = 2$) and on the stable active fixed point (red circle with $z = 1.7$) since they contain all the information needed to describe polar active systems.

The idea is that the equilibrium, and unstable, fixed point gives rise to an interplay with the active stable fixed point leading to a dynamical crossover between the respective universality classes. We believe this crossover contains the key information to understand how the level of the activity affects the real critical dynamics of a natural and finite-size system. The analytical result definitely concerns incompressible systems, but we are going to prove with numerical simulations that it characterizes also compressible ones [7].

To develop this concept, we show in Fig 4.2 the numerical integration of the recursion relations (3.58) in three dimensions: the blue oriented lines represent different evolution of the system at various bare conditions of the coupling constants (u_0, α_0) . The red dots, each one representing an RG iteration, picture the case of a physical value of the activity α_0 very small, whose flow starts in the left bottom corner of the phase space. Following the red path, the flow is firstly attracted by the unstable fixed point, lingering in its vicinity for many RG iterations, and then it moves asymptotically towards the stable fixed point. The value of the dynamical critical exponent accordingly changes. We can compute it at every iteration as,

$$z_l = 2 - \frac{1}{4}\alpha_l, \quad (4.1)$$

and follow its RG evolution. The curve z_l shows a plateau at the effective equilibrium value $z = 2$ and then a smooth descend to the active off-equilibrium

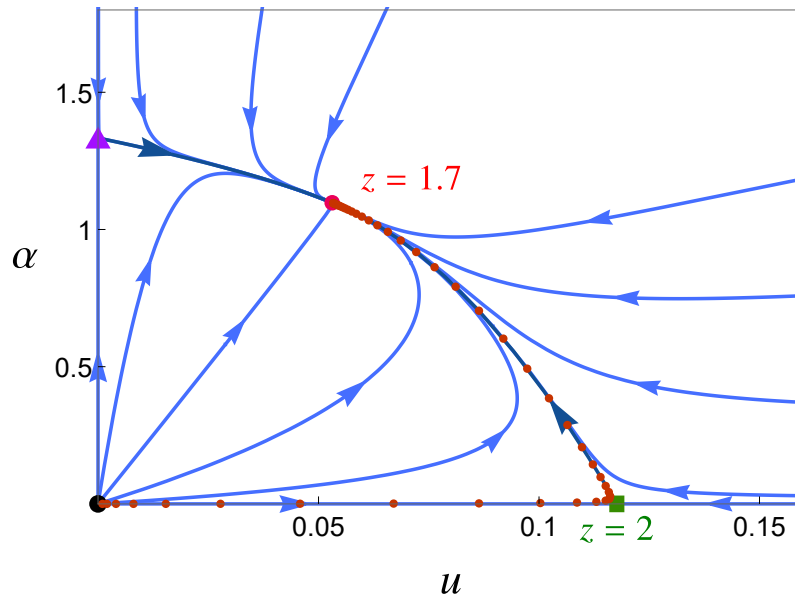


Figure 4.2: RG flow and crossover (I). Critical manifold resulting from the calculation of chapter 3: the fixed points of our interest are the equilibrium ferromagnet with $z = 2$ (green square), and the Vicsek active-ferromagnetic fixed point, with $z = 1.7$ (red circle). They give rise to the equilibrium to off-equilibrium crossover: if the initial value of the activity α_0 is small, the flow, starting from the left bottom corner, quickly approaches the equilibrium fixed point (red dots) and remains around it for many RG iterations, before crossing over to the out-of-equilibrium fixed point. Reprinted from [7].

$z = 1.7$ (Fig.4.3), suggesting that the system indeed experiences both the critical dynamics. Every RG iteration represents a length scale of observation of the system, therefore this result is saying that, for a system microscopically weakly active, there exist some length scales at which an equilibrium-like critical dynamics emerges with the corresponding exponent. On the other hand, if the bare activity is really large, the flow goes directly to explore the stable fixed point exhibiting only an out-of-equilibrium dynamics.

The origin of this crossover can be fully understood by paying attention to the principal quantity characterizing a critical system: the correlation length. Each red dot of Fig.4.2 represents a length scale of observation of the system, but also an effective theory with a corresponding physical correlation length ξ . This quantity is reduced by the RG iterations as $\xi_{l+1} = \xi_l/b = \xi/b^l$, thus setting a maximum limit to the applicability of the scale transformations [74]:

$$\xi_{l+1} = \frac{1}{\Lambda} \quad \Longrightarrow \quad b^{l_{stop}} = \Lambda \xi . \quad (4.2)$$

The largest RG iteration is l_{stop} , namely when the correlation length is decreased till the microscopic length scale $1/\Lambda$. If at this stop condition the physical bare parameters allow the system to reach only the neighborhood of the equilibrium fixed point, then the active system shows a $z = 2$ equilibrium exponent at all its

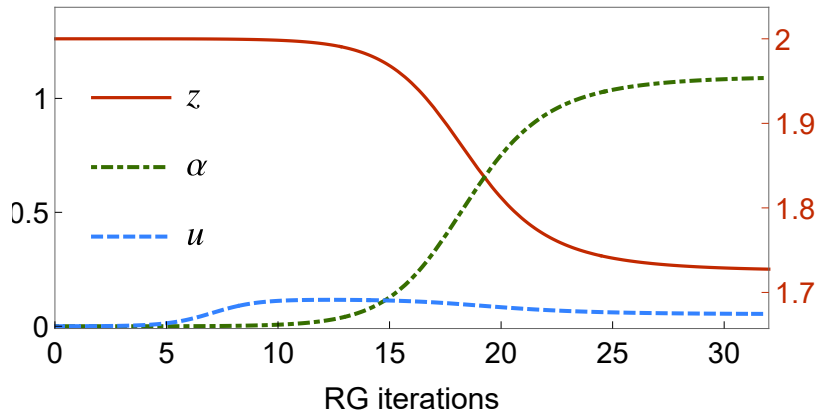


Figure 4.3: RG flow and crossover (II). Numerical integration of the coupling constants recursion relations vs number of RG iterations. The dynamical crossover is evident especially in the trend of the running dynamical critical exponent z_l , which starts from the equilibrium value $z = 2$ to arrive to its off-equilibrium value, $z = 1.7$ (in $d = 3$). Reprinted from [7].

physical scales. Conversely, if the correlation length is very large the flow reaches the stable fixed point, belonging to the $z = 1.7$ universality class.

We can look at the behavior of the dynamical correlation functions and their scaling properties introduced in chapter 1 and 2. At step l of RG, the temporal correlation function has to scale accordingly with:

$$C(t, \xi, k, \mathcal{P}_0) = b^{2lz_l} C(tb^{-lz_l}, \xi/b^l, kb^l, \mathcal{P}_l) \quad (4.3)$$

where \mathcal{P} stands for the set of parameters of the theory, bare and at the transformed level, respectively. When the RG flow arrives at its end, namely when (4.2) is satisfied, we can calculate the correlation function in the neighborhood of the reached fixed point, becoming

$$C(t, \xi, k, \mathcal{P}_0) = (\Lambda\xi)^{2z_{l_{STOP}}} C(t/\xi^{z_{l_{STOP}}}, \Lambda^{-1}, k\Lambda\xi, \mathcal{P}^*) . \quad (4.4)$$

We can appreciate that, when the product $k\xi$ is kept fixed, the function majorly depends on $t/\xi^{z_{l_{stop}}}$, identifying a characteristic time scale that decays as

$$\tau_c \sim \xi^{z_{l_{stop}}} . \quad (4.5)$$

The value of $z_{l_{stop}}$ is therefore determined by the closest fixed point attained by the flow and it represents the quantity that rules the real critical dynamics and the dynamical scaling of the system, even if it is not the exponent of the stable fixed point.

Additionally, we are able to identify what is the condition that separates these two different regimes of the dynamical crossover [7]. If the system explores only

the unstable fixed point, we can expand eq (3.58) around it, obtaining

$$\alpha_{l+1} = \alpha_l b^{\epsilon - (10/3)u^*} = \alpha_l b^\kappa \quad (4.6)$$

with $\kappa = (31/51)\epsilon$. Since the value of the active coupling constant in the vicinity of the stable fixed point is $\alpha^* = \mathcal{O}(\epsilon)$, asking to be away from it, it is equivalent to state that $\alpha_{stop} \ll \epsilon$, which is verified when

$$\alpha_0 b^{\kappa l_{stop}} = \alpha_0 (\Lambda \xi)^\kappa \ll \epsilon . \quad (4.7)$$

If now we define the crossover length scale as

$$\mathcal{R}_c = (\epsilon/\alpha_0)^{1/\kappa} \Lambda^{-1} \quad (4.8)$$

the inequality in (4.7) translates into $\xi \ll \mathcal{R}_c$, which appears as a requirement for the system to visit only the equilibrium fixed point. The crossover scenario can then be measured in terms of an interplay between the correlation length and the value of the physical activity of the system. The crossover length scale is indeed determined once the value of the effective activity is assigned, allowing the following cases:

$$\begin{aligned} \xi \ll \mathcal{R}_c &\implies \tau_c \sim \xi^2 \\ \xi \gg \mathcal{R}_c &\implies \tau_c \sim \xi^{1.7} . \end{aligned} \quad (4.9)$$

This result has interesting applications for physical finite size systems, which are characterized by size L and by a certain extent of self-propulsion. If the activity is so large that $\mathcal{R}_c < 1/\Lambda$, the entire system lives in the off-equilibrium critical regime to all physical scales up to the linear size L . On the other hand, when the value of the bare activity is sufficiently small, the crossover length scale can be arbitrarily large. When $\mathcal{R}_c > L$, the system exhibits only the equilibrium critical dynamics despite being microscopically active. Concluding, it is the effective activity that really drives the crossover, making the system show relevant off-equilibrium dynamics only for very large values of it or for very large system's sizes [7].

The mechanism we just presented would totally explain the result of the numerical simulations performed in [3] if the constraint of incompressibility had been implemented also at the numerical level, while it had not. However, these preliminary simulations can instead suggest that this crossover mechanism is way more general than a strict application to incompressible systems. It could indeed regard compressible but nonetheless homogeneous systems as the ones described by the original Vicsek model with limited system sizes and small values of activity.

This is the idea we are going to explore in detail in this chapter, showing its validity by means of numerical simulations of the original compressible VM. We indeed believe that finding the crossover in the critical dynamics of this active matter model would confirm that the out-of-equilibrium universality class with

$z = 1.7$ is not an artifact of the incompressibility condition but it represents a pure feature of the out-of-equilibrium nature of active systems. Certainly, these considerations apply as long as the phenomenology of the VM's phase transition stays of the second order, while in the thermodynamic limit we expect another crossover ruled by density fluctuations towards a phase-separation scenario. On the other hand, this would also confirm that an incompressibility condition does not change the dynamical universality class of an active model when considering systems of finite-size. To demonstrate this, we need to understand how to practically tune activity in a microscopic system.

4.2 How to tune activity

Our main purpose is to numerically observe the dynamical crossover produced by the RG calculation on the incompressible hydrodynamic theory of the Vicsek model. We saw that what regulates this phenomenon is the active coupling constant, namely $\alpha = \lambda^2 (\tilde{\Gamma}/\Gamma^3)\Lambda^{-\epsilon}$ (to lighten the notation we drop here all the 0 subscripts of the bare parameters). Indeed, when this quantity is different from zero, it grows along with the RG flow, carrying the system from the equilibrium and unstable fixed point, to the stable and out-of-equilibrium one [7].

It is natural to ask what is the microscopic parameter of the original model (4.24) that corresponds to the active coupling constant in the continuous parameters space, and that has to be tuned in order to observe the crossover in finite-size systems. The intuitive candidate is the speed v_0 , since for $v_0 = 0$ the Vicsek model reduces to an equilibrium ferromagnet. We can appreciate it simply reformulating the microscopic model in these terms,

$$\begin{aligned}\varphi_i(t+1) &= \mathcal{R}_\eta \left(\sum_j n_{ij}(t) \varphi_j(t) \right) \\ \mathbf{r}_i(t+1) &= \mathbf{r}_i(t) + v_0 \varphi_i(t+1) ,\end{aligned}\tag{4.10}$$

where we substituted $\mathbf{v}_i = v_0 \varphi_i$ and we wrote the dynamics only for the orientations φ_i . It is clear that, in the limit $v_0 \rightarrow 0$, the network freezes and the dynamics of the orientations becomes an equilibrium dynamics belonging with the universality class of Model A [74]. However, it is not transparent how to connect this limit to the parameters of the incompressible field theory (3.9). For clarity, let's report here the continuous equations for the velocity,

$$\begin{aligned}\frac{\partial \mathbf{v}}{\partial t} + \lambda(\mathbf{v} \cdot \nabla) \mathbf{v} &= \Gamma \nabla^2 \mathbf{v} - (a + Jv^2) \mathbf{v} + \mathbf{f} \\ \langle \mathbf{f}(\mathbf{x}, t) \mathbf{f}(\mathbf{x}', t') \rangle &= 2\tilde{\Gamma} \delta^{(d)}(\mathbf{x} - \mathbf{x}') \delta(t - t') .\end{aligned}\tag{4.11}$$

Each coefficient appearing in these equations contains a non-trivial dependence on the microscopic parameters, which is also coarse-graining dependent. For the compressible case, one can look at [84, 85] for a derivation within the kinetic approach. In our case, we do not know a priori the limit of these quantities for

the speed $v_0 \rightarrow 0$, therefore, to make progress, we can try to write directly the hydrodynamic theory of eq (4.10) and then compare it with (4.11).

To this end, we use the fact that the coarse-grained velocity can be zero for two distinct reasons: *i*) because the microscopic speed v_0 is zero; *ii*) because the system is misaligned and disordered, so that the local average of microscopic vectors gives a zero value. Hence, in terms of fields, we can express these two features writing

$$\mathbf{v}(\mathbf{x}, t) = v_0 \boldsymbol{\varphi}(\mathbf{x}, t) \quad (4.12)$$

where $\boldsymbol{\varphi}(\mathbf{x}, t)$ represents the field of polarization. By using the same exact arguments that lead from (4.24) to (4.11), we can associate to (4.10) its corresponding dynamical field theory,

$$\begin{aligned} \frac{\partial \boldsymbol{\varphi}}{\partial t} + \lambda'(v_0 \boldsymbol{\varphi} \cdot \nabla) \boldsymbol{\varphi} &= \Gamma' \nabla^2 \boldsymbol{\varphi} - (a' + J' \boldsymbol{\varphi}^2) \boldsymbol{\varphi} + \mathbf{f}' \\ \langle \mathbf{f}'(\mathbf{x}, t) \mathbf{f}'(\mathbf{x}', t') \rangle &= 2\tilde{\Gamma}' \delta^{(d)}(\mathbf{x} - \mathbf{x}') \delta(t - t') \end{aligned} \quad (4.13)$$

where we relabeled the coefficients to highlight the original microscopic difference with those of (4.11). The remarkable thing is that now an explicit dependence of the mesoscopic theory on the microscopic speed appears. This is due to the fact that the material derivative always expresses the transport made by the velocity field. We can therefore make a comparison between eq (4.13) and eq (4.11), multiplying the first one for v_0 and getting,

$$\frac{\partial \mathbf{v}}{\partial t} + \lambda'(\mathbf{v} \cdot \nabla) \mathbf{v} = \Gamma' \nabla^2 \mathbf{v} - \left(a' + \frac{J'}{v_0^2} v^2 \right) \mathbf{v} + v_0 \mathbf{f}' . \quad (4.14)$$

This theory must be equal to (4.11), because coarse-graining the microscopic polarizations $\boldsymbol{\varphi}_i$ and then multiplying them by v_0 , must give the same hydrodynamic theory as coarse-graining directly the microscopic velocities, \mathbf{v}_i , as long as v_0 does not fluctuate. Therefore, we can read the parameters of the hydrodynamic theory for \mathbf{v} in terms of that of $\boldsymbol{\varphi}$,

$$\begin{aligned} \lambda &= \lambda' \\ \Gamma &= \Gamma' \\ a &= a' \\ J &= J'/v_0^2 \\ \tilde{\Gamma} &= v_0^2 \tilde{\Gamma}' \end{aligned} \quad (4.15)$$

The great advantage of doing this detour is that now we know the limit for $v_0 \rightarrow 0$ of the primed parameters, since the corresponding microscopic theory has to reflect the standard equilibrium dynamics of the polarization of a Heisenberg ferromagnet [61], that is:

$$\frac{\partial \boldsymbol{\varphi}}{\partial t} = -\Gamma_{\text{eq}} \frac{\partial \mathcal{H}}{\partial \boldsymbol{\varphi}} + \boldsymbol{\zeta} \quad , \quad \langle \boldsymbol{\zeta} \boldsymbol{\zeta} \rangle = 2\Gamma_{\text{eq}} \quad (4.16)$$

where Γ_{eq} is the equilibrium kinetic coefficient and simultaneously the amplitude of the noise. The \mathcal{H} stands for the classic Landau-Ginzburg Hamiltonian,

$$\mathcal{H} = \int d^d x (\nabla\varphi)^2 + r_{\text{eq}}\varphi^2 + u_{\text{eq}}\varphi^4 \quad (4.17)$$

that contains the equilibrium mass r_{eq} and the equilibrium ferromagnetic coupling constant u_{eq} . We can then conclude that,

$$\begin{aligned} a'(v_0 = 0) &= \Gamma_{\text{eq}} r_{\text{eq}} \\ J'(v_0 = 0) &= \Gamma_{\text{eq}} u_{\text{eq}} \\ \Gamma'(v_0 = 0) &= \Gamma_{\text{eq}} \\ \tilde{\Gamma}'(v_0 = 0) &= \Gamma_{\text{eq}} \end{aligned} \quad (4.18)$$

have to be valid in order to respect the correct equilibrium limit. This means that all the parameters of the dynamical field theory for the orientation have a well-defined and non-singular behavior in the limit $v_0 \rightarrow 0$. Only the coefficient of the advective term λ' remains undetermined, but this is reasonable since it is turned off from the explicit dependence on the speed v_0 . By using this information and eq (4.15), we can extrapolate the small $v_0 \rightarrow 0$ behavior of the coefficients of the velocity dynamics, which states

$$\begin{aligned} a &\sim \Gamma_{\text{eq}} r_{\text{eq}} \\ J &\sim \Gamma_{\text{eq}} u_{\text{eq}}/v_0^2 \\ \Gamma &\sim \Gamma_{\text{eq}} \\ \tilde{\Gamma} &\sim v_0^2 \Gamma_{\text{eq}} . \end{aligned} \quad (4.19)$$

By combining them in the definition of the active coupling constant $\alpha = \lambda^2 (\tilde{\Gamma}/\Gamma^3)\Lambda^{-\epsilon}$, we explicitly gain its dependence on the microscopic speed:

$$\alpha = \frac{\lambda^2 v_0^2}{\Gamma_{\text{eq}}^2} \Lambda^{-\epsilon} \sim v_0^2 . \quad (4.20)$$

It is worth noticing that the parameter decisively affecting the result is the amplitude of the noise $\tilde{\Gamma}$ that scales as v_0^2 , while we simply assume a reasonable non-singular behavior for the transport coefficient λ .

Eq (4.20) represents the first important result of this analysis [7]. Dependence of the active coupling constant on the speed v_0 was expected, however, eq (4.20) tells something more. Activity grows with a non-trivial exponent 2, showing a rather rapid increase with v_0 and confirming that small changes in the speed have great effects on the system's critical dynamics. This result demonstrates that the microscopic parameter that has to be tuned in order to verify the dynamical crossover in the numerical simulations is the speed of the particles v_0 . This is the reason why we decide to run simulations fixing all the dynamical parameters and just varying the speed.

To close this section, we can briefly analyze the behavior of the ferromagnetic coupling constant, indeed from the second equation of (4.19), one might be led to think that the parameter J diverges in the limit $v_0 \rightarrow 0$. This is only an apparent problem since this quantity alone does not represent the real effective coupling constant, but rather one must consider the more complete

$$u \sim \frac{\Gamma_{\text{eq}} u_{\text{eq}} v_0^2 \Gamma_{\text{eq}}}{v_0^2 \Gamma_{\text{eq}}^2} \Lambda^{-\epsilon} = u_{\text{eq}} \Lambda^{-\epsilon} \quad (4.21)$$

whose small speed limit is again well defined as it coincides with the equilibrium ferromagnetic relevant parameter.

4.3 Numerical simulations

In order to test the dynamical crossover explained in the previous sections, we perform numerical simulations of the original Vicsek model (3.1) (3.2) in its near-critical regime. However, before going through the numerical results, let's clarify two important points for the discussion.

First of all, we remark that, in contrast to the analytical calculation, we do not explicitly impose any incompressibility condition in our simulated model. Assuming that the divergence of the velocity field is null implies that the system is homogeneous, but also that long-range dipolar interactions can be involved. Here, we decide just to passively monitor the homogeneity of the near-critical system without imposing incompressibility in the system, hence without imposing any long-range interaction. We maintain the more general and original formulation of the Vicsek model, monitoring density fluctuations and considering the system's sizes not too big to ensure a continuous phenomenology of the phase transition. In these conditions, we are sure to be able to apply the dynamical scaling theory to numerical data and, thanks to homogeneity, to compare our results with the RG predictions [6, 7]. Additionally, this situation reflects that of natural swarms, which are of limited sizes and do not show relevant density fluctuations.

Secondly, we decide to treat the numerical data in the same way as the experimental ones are analyzed in [2] and [3], being motivated by the final objective to compare the theoretical critical dynamics of active matter to that of natural swarms. This choice affects the calculation of statistical quantities, first of all, the nature of fluctuations of the order parameter and consequently its correlation functions. Due to the out-of-equilibrium nature of biological systems and of self-propelled particles, we indeed define fluctuations of the velocity at time t like the difference between the velocity of one particle and the velocity of the center of mass at the same time [42], namely:

$$\delta \mathbf{v}_i(t) = \mathbf{v}_i(t) - \frac{1}{N} \sum_{i=1}^N \mathbf{v}_i(t) \quad (4.22)$$

This definition implies what we call *the sum rule*:

$$\sum_i^N \delta \mathbf{v}_i(t) = 0, \quad (4.23)$$

a spatial constraint that simply encodes the fact that there cannot be a global net motion of the system when considered in the center of mass reference frame [42]. Moreover, to make a direct comparison with experimental data of natural swarms we follow the same strategy of [3], namely, in the simulations of the Vicsek model, we use the finite-size scaling method to extrapolate the dynamical critical exponent. Indeed, from the analysis performed in [2], it is evident that this powerful technique can reproduce the quasi-criticality of the natural system into consideration.

We briefly repeat the simulated equations of the Vicsek model [28], which read:

$$\begin{aligned} \mathbf{v}_i(t+1) &= \mathcal{R}_\eta \left(\sum_j n_{ij}(t) \mathbf{v}_j(t) \right) \\ \mathbf{r}_i(t+1) &= \mathbf{r}_i(t) + \mathbf{v}_i(t+1) \\ |\mathbf{v}_i(t)| &= v_0 \quad \forall i, t \end{aligned} \quad (4.24)$$

where the applied noise is scalar and the interaction is metric ($r_c = 1$). The simulated systems live in $d = 3$ and have sizes equal to $N = 128, 256, 384, 512, 1024, 2048$, with N the number of particles. Periodic boundary conditions (PBC) are implemented and all the simulations are run at constant noise, $\eta = 0.45$. As it is believed to happen in the biological system of swarms [1], the density (or, more precisely, the mean first-neighbor distance) is tuned to follow the ordering transition at various N , exploring the near-critical scaling regime. Finally, the parameter v_0 represents the speed, which is identical for all the particles and it is preserved as a constraint along with the evolution of motion. We studied several cases of different values of speed but we report results for $v_0 = 0.05$ and $v_0 = 0.2$. As we have seen, the activity coupling constant grows as the square of the speed; hence we expect this change of a factor of 4 to be sufficient to reproduce the crossover we want to test.

4.3.1 Static behavior and correlation length

To compute the dynamical critical exponent from the simulations the first thing to ascertain is the finite-size criticality of the system. With this sentence, we mean to fix the size of the system N and then identify the critical value of the tuning parameter, namely the density, at which the system is maximally correlated. To locate this finite-size critical point, we compute for each value of density explored

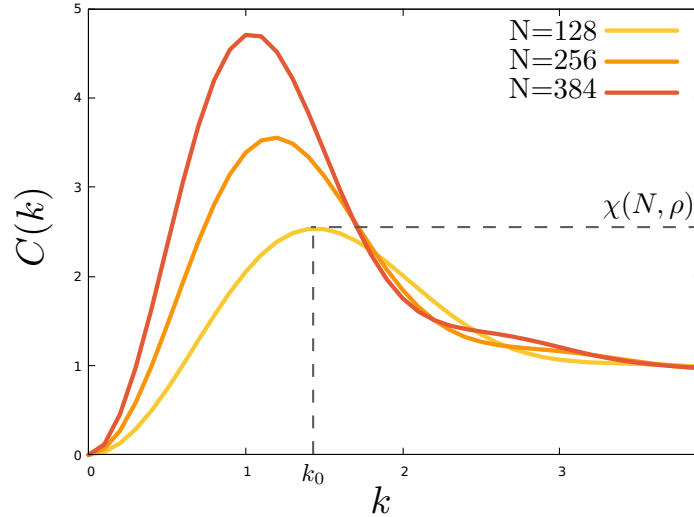


Figure 4.4: Static correlation functions Three static correlation functions of the Vicsek model in $d = 3$ for sizes $N = 128, 256, 384$ and $v_0 = 0.05$. Each curve is a function of the size N and of the tuning parameter, ρ . They all show the same behavior, being null when $k = 0$ and going to 1 for large momenta. The point of maximum k_0 and its value change with N , this latter representing a measure of the susceptibility χ .

the equal time correlation function in wave-number space [42], that is:

$$C(k) = \frac{1}{Nv_0^2} \left\langle \sum_{ij} \frac{\sin(kr_{ij})}{kr_{ij}} \delta \mathbf{v}_i(t) \cdot \delta \mathbf{v}_j(t) \right\rangle, \quad (4.25)$$

where the velocity fluctuations are calculated according to eq (4.22), $r_{ij} = |\mathbf{r}_i(t) - \mathbf{r}_j(t)|$ and $\langle \rangle$ indicates an average in time. Examples of these functions are reported in Fig. 4.4 for three different sizes and densities at the same value of speed. From this graph a particularity emerges: the $C(k)$ computed at $k = 0$ are identically null, and this is due to the sum rule (4.23) since,

$$C(k = 0) = \frac{1}{Nv_0^2} \sum_i \delta \mathbf{v}_i(t) \sum_j \delta \mathbf{v}_j(t) = 0$$

while in the limit $k \rightarrow \infty$ the only self-contribution survives, implying $C(k \rightarrow \infty) = 1/Nv_0^2 \sum_i |\mathbf{v}_i|^2 = 1$.

This fact has the consequence that the usual definition of susceptibility $\chi = C(k = 0) = \int d^d r \tilde{C}(r)$ loses its meaning, being itself null. However, we can take as a measure of this statistical quantity χ the peak of the static correlation function, that is where the correlation is maximum, and that occurs at a particular inverse length scale k_0 (Fig. 4.4). We compute the susceptibility for each value of the control parameter and for each size we analyze, obtaining the graph in Fig 4.5, shown just for one value of the speed, namely $v_0 = 0.05$.

As in normal equilibrium systems, we interpret the point of maximum of susceptibility as the transition point of the system which is located at a critical

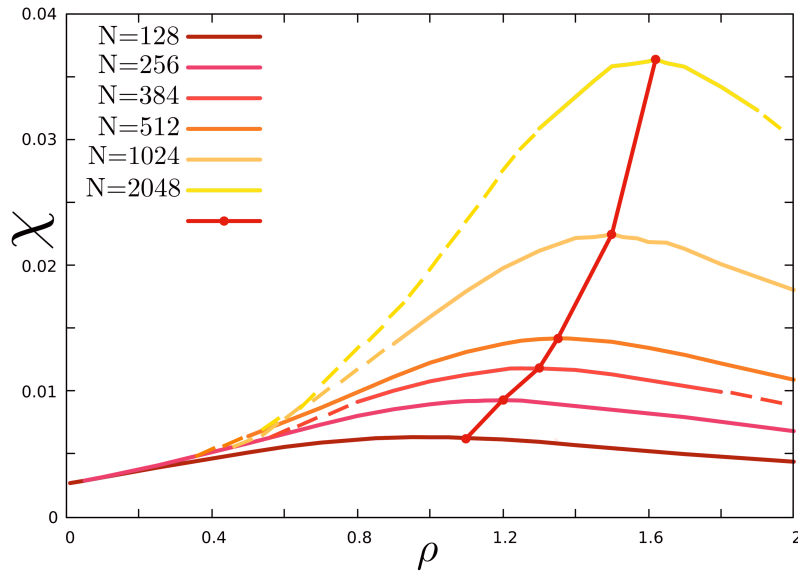


Figure 4.5: Surfing of susceptibility. Susceptibility vs density for Vicsek model simulations in $d = 3$, with $v_0 = 0.05$ and sizes $N = 128, 256, 384, 512, 1024, 2048$. The red dots identify the maxima of susceptibility for each N and correspond to the finite-size critical points ρ_c , which follow the FFS expected trend. Continuous lines are formed by points of simulations, dashes lines are extrapolations of the high and low-density regimes.

value of the density ρ_c (red dots of Fig4.5). Certainly, we can see that this point is size dependent $\rho_c = \rho_c(N)$ and grows as the size of the system increases. This is correct in view of finite size scaling (FSS) analysis [60]: indeed, to be precise, the real control parameter associated to the ordering transition is $x = r_1/r_c$, the mean first-neighbor distance rescaled for the interaction radius, which, for homogeneous systems, is expected to scale as $x \sim 1/\rho^{1/3}$. When the susceptibility reaches its peak, the system is deeply correlated and, if FSS holds, these relations have to be valid

$$\xi \simeq L \quad (4.26)$$

$$x \simeq x_c + N^{-\frac{1}{3\nu}} \quad (4.27)$$

where ν is the static critical exponent that describes the divergence of the correlation length at criticality:

$$\xi \simeq \frac{1}{(x - x_c)^\nu} \quad (4.28)$$

and L is the linear size of the system $L = (N/\rho)^{1/3}$. Combining this information we can appreciate that FFS holds for the peaks of the susceptibility in terms of density as a control parameter (Fig. 4.5). Finally, to extrapolate the correlation length, we go back to analyze the $C(k)$ relative to that particular ρ_c and we interpret $\xi = 1/k_0$ as the maximum correlation length of the system [2].

4.3.2 Dynamical behavior and relaxation time

The second important ingredient we need to analyze the critical dynamics of the model is the relaxation time of the velocity dynamical correlation functions. For these latter, we use a definition always in k -space [86], already used for experimental data (1.24), namely:

$$C(k, t) = \left\langle \frac{1}{N} \sum_{ij} \delta \mathbf{v}_i(t_0) \cdot \delta \mathbf{v}_j(t_0 + t) \frac{\sin(kr_{ij})}{kr_{ij}} \right\rangle_{t_0}, \quad (4.29)$$

where $r_{ij} = |\mathbf{r}_i(t_0) - \mathbf{r}_j(t_0 + t)|$ and

$$\langle \rangle_{t_0} = 1/(T_{max} - t) \sum_{t_0=1}^{T_{max}-t} \quad (4.30)$$

with T_{max} the length of the simulation. From this latter quantity the characteristic time scale can be computed as the value of τ that verifies the condition [5],

$$\frac{1}{2\pi} = \int_0^\infty dt \frac{1}{\tau} \sin\left(\frac{t}{\tau}\right) \frac{C(k, t)}{C(k, 0)}, \quad (4.31)$$

as also explained in the previous chapters.

Being this function k dependent, we have to decide at which length scale looking at the system. In analogy with experimental data of natural swarms [3], we decide to fix the product $k\xi = 1$ and then to evaluate correlations at $k = 1/\xi$. Certainly, this helps in verifying the dynamical scaling hypothesis because, if it holds and this product is kept constant, then the relaxation time has to scale as $\tau(k) = \xi^{-z} f(k\xi)$ and the different correlation functions, computed for different sizes, have to collapse one on each other to the same shape function $C(k, t)/C(k, 0) = F(k^z t)$, when time is also properly rescaled.

4.4 Dynamical crossover in numerical experiments

We now use the tools just introduced to explore and try to verify the dynamical crossover predicted by the RG study [7]. As we explained before, the speed v_0 is a key parameter to move coherently the effective theory in the parameter space and visit the different fixed points. When the speed v_0 is changed at a microscopic level, also the bare activity coupling constant α_0 is changed, determining the well-known RG flow.

From Fig.4.2, we understood that, if this initial value is quite small, the system will show the transition between the two different types of critical dynamics. Therefore, following this reasoning, we should be able to see the crossover fixing a small value of v_0 and then exploring the system at very large sizes: at least two decades in correlation length to appreciate the change of the exponent in a power law. However, this is numerically very hard to implement: we are studying out-of-

equilibrium systems in $d = 3$ and the computational time to evaluate quantities as (4.29) and (4.25) is quite demanding already at $N \sim 2000$. Therefore, we decide to carry out another strategy translating this crossover in size into a crossover in speed.

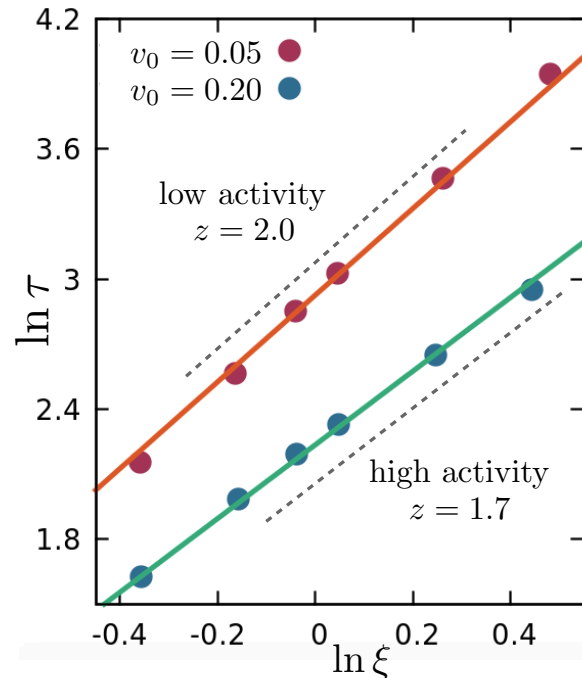


Figure 4.6: Vicsek critical dynamics in three dimensions (I). Relaxation time vs correlation length for the two different values of speed $v_0 = 0.05, 0.20$ and sizes $N = 128, 256, 384, 512, 1024, 2048$. Lines are the best fit to the RG results, $z = 1.7$ (blue, high v_0 , high activity) and $z = 2$ (red, low v_0 , low activity). This result confirms the realization of the dynamical crossover in speed.

To achieve this goal, we remember that once the value of v_0 is assigned, we determine the effective coupling constant but, above all, we fix the crossover length scale (eq. (4.8)) $\mathcal{R}_c \sim 1/\alpha_0$. Choosing very high values for α_0 , i.e. v_0 means reducing this length scale that can eventually shrink to zero or be smaller than the mean interacting distance. If this happens, the system is in the regime where $\xi \sim L \gg \mathcal{R}_c$, directly feeling the attraction of the stable fixed point and exhibiting a $z = 1.7$ off-equilibrium critical dynamics. On the other hand, if the speed is small enough, implying $\mathcal{R}_c \gg L$, then the system will explore solely the neighborhood of the unstable fixed point showing an effective equilibrium critical dynamics with $z = 2$. This is what we test in our simulations, which are performed at two values of the speed, namely $v_0 = 0.05, 0.2$ [7].

In Fig.4.6, we report in the plane $(\ln \xi, \ln \tau)$ the critical quantities we have computed as explained before, at each size N for the two values of speed. The slope of the two lines represents an estimate of the dynamical critical exponent z . Here we show the best fit of data using as fixed slopes the theoretical values of the exponents predicted by RG. For $v_0 = 0.05$, representing the low activity

regime, simulations reproduce a critical dynamical scaling with $z = 2$, belonging to the equilibrium universality class. In the high speed regime $v_0 = 0.20$, the system crosses over to the off-equilibrium class, clearly fitting a $z = 1.7$ critical exponent.

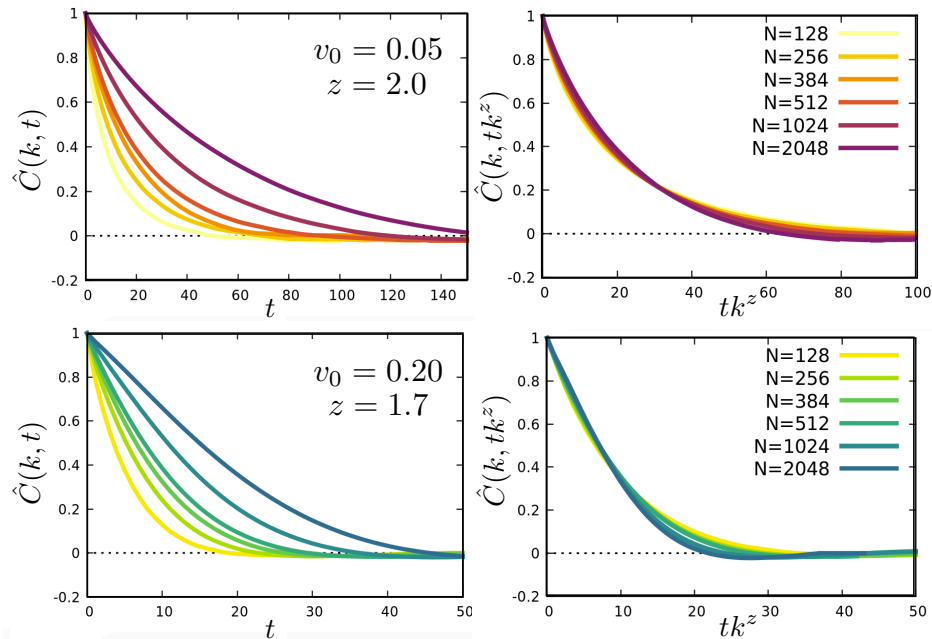


Figure 4.7: Vicsek critical dynamics in three dimensions (II). Left: normalized dynamical correlation functions, $\hat{C}(k, t) = C(k, t)/C(k, 0)$, at $k = 1/\xi$ for $v_0 = 0.05$ (top) and $v_0 = 0.20$ (bottom), respectively. Explored sizes $N = 128, 256, 384, 512, 1024, 2048$. Right: same correlation functions plotted against the scaling variable tk^z , using $z = 2$ (top) and $z = 1.7$ (bottom). The characteristic collapse of the curves states the validity of the dynamical scaling hypothesis for the respective values of dynamical critical exponent.

In order to confirm the numerical crossover and the full validity of the dynamical scaling, we also directly test the collapse of the dynamical correlation functions for these values of the exponents. In Fig.4.7, we show these functions and the same curves when time is rescaled in tk^z , again with $z = 2.0$ for $v_0 = 0.05$ and $z = 1.7$ for $v_0 = 0.20$. The collapse is satisfying and it still confirms the realization of the dynamical crossover in the microscopic and compressible model. Additionally, we report here the opposite scaling of the functions in Fig.4.8, namely exchanging the two values of the exponents in the two different cases: we can appreciate a relevant difference with Fig 4.7.

Statistical tests about the critical exponents' estimate

To enhance the robustness of our critical exponents' evaluation, we perform two additional basic statistical tests on our simulations [87].

Test 1: We examine the consistency of the z values extrapolated by linear fits of the data of Fig 4.6 with the theoretical expectations. First of all, for each

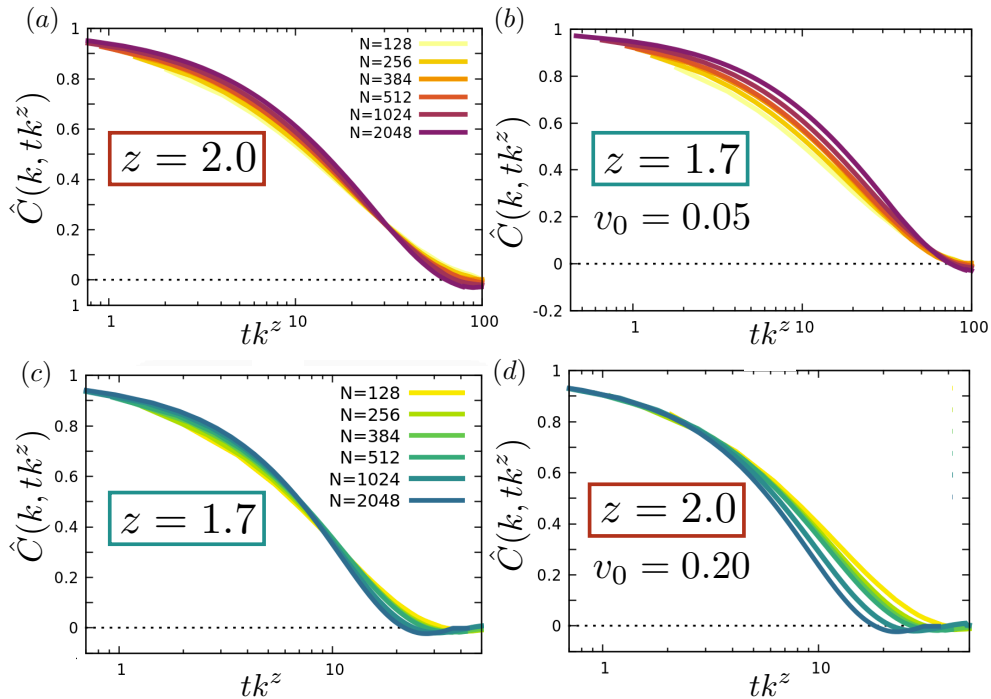


Figure 4.8: Vicsek critical dynamics in three dimensions (III). Panels (a), (c) Scaling of dynamic correlation functions $\hat{C}(k, t)$ in semi-log scale using values of z extrapolated by the linear fits of Fig.4.6: (a), $v_0 = 0.05$ with $z = 2.0$ and (b), $v_0 = 0.20$ with $z = 1.7$. Panels (b), (d) same correlation functions reversing the scaling procedure: (c), $v_0 = 0.05$ with $z = 1.7$ and (d), $v_0 = 0.05$ with $z = 2.0$. The scaling hypothesis is not well verified for (b) and (d).

value of speed v_0 , we fit the data on the plane $(\ln \xi, \ln \tau)$ with the simple linear function $f(x) = mx + c$. Since we know that $\tau \sim \xi^z$, the slope m is the value of z we are looking for. We obtain:

- $v_0 = 0.05$: $z_{\text{sim}} = 2.10 \pm 0.04$
- $v_0 = 0.20$: $z_{\text{sim}} = 1.65 \pm 0.03$

The value of the exponent z_{sim} is affected by an uncertainty σ , which is computed assuming that data on correlation time belong to a Gaussian distribution and that their standard deviation can be determined with the least squares method. Then, we perform a simple hypothesis test to verify the compatibility with the analytical theoretical values z_{th} . We compute the variable

$$t = \frac{z_{\text{sim}} - z_{\text{th}}}{\sigma}, \quad (4.32)$$

which measures the distance between the theoretical and the simulation value of z in units of uncertainty. If $|t| > 3$, the probability that the value extracted from simulations is compatible with the theoretical one is less than 1%. We got:

- $v_0 = 0.05$: $z_{\text{th}} = 2.0 \rightarrow t = 2.5$, *consistent*;
- $z_{\text{th}} = 1.7 \rightarrow t = 10.0$, *not consistent*.

- $v_0 = 0.20$: $z_{\text{th}} = 2.0 \rightarrow t = -11.7$, *not consistent*;
 $z_{\text{th}} = 1.7 \rightarrow t = -1.7$, *consistent*.

This result validates the thesis we found the dynamic crossover in the Vicsek model.

Test 2: We evaluate the quality of the linear fits of Fig.4.6 using theoretical values of the dynamic critical exponents as fixed slope. To achieve this, we carry out a χ^2 -test. For each data set with activity v_0 , we perform a linear regression using both values of $z_{\text{th}} = 2.0, 1.7$ and extrapolating only the intercept c of the linear function from data. With uncertainties on $\ln \tau$ derived by the least square method, as in the point above, we computed the standard χ^2 for $N - 1$ degrees of freedom for both analyses. If this variable results larger than 11, we can say that the probability that the fit is compatible with data is less than 5%, hence

- $v_0 = 0.05$: $z_{\text{th}} = 2.0 \rightarrow \chi^2 = 9.98$, *consistent*;
 $z_{\text{th}} = 1.7 \rightarrow \chi^2 = 415$, *not consistent*.
- $v_0 = 0.20$: $z_{\text{th}} = 2.0 \rightarrow \chi^2 = 131$, *not consistent*;
 $z_{\text{th}} = 1.7 \rightarrow \chi^2 = 7.04$, *consistent*.

Once again, this analysis confirms the result of this work, namely that, increasing the activity of the self-propelled particles in the standard Vicsek model, we can numerically verify the dynamic crossover from the equilibrium to the out-of-equilibrium dynamic universality class.

4.5 Checking homogeneity

As we stressed before, we run simulations of the original Vicsek model without imposing incompressibility. We merely check that homogeneity conditions are preserved along with the analyzed configurations, in order to assert that the only important thing to determine the two different dynamical universality classes is the absence of relevant density fluctuations. These inspections become also more necessary when increasing the speed v_0 of the model, indeed it has been shown in [78] that the threshold size, above which a first-order transition become visible, shows a regime in which it boils down when v_0 grows, and then it increases for very large speed.

We carefully look at the numerical data to primarily exclude the presence of heterogeneous structures like bands, typical of the near-ordering phase of these active systems. For all the simulations collected we examine the temporal series of the polarization $\phi = \frac{1}{N} |\sum \mathbf{v}_i|$, monitoring eventual jumps in its value that can reflect the presence of denser and more ordered zones (Fig.4.9a).

Moreover, for both sets of simulations, we verify the trend of the mean first neighbor distance with the average density: for homogeneous systems, these quantities are expected to behave as $x \sim 1/\rho_0^{1/3}$, and this is also fully confirmed by our

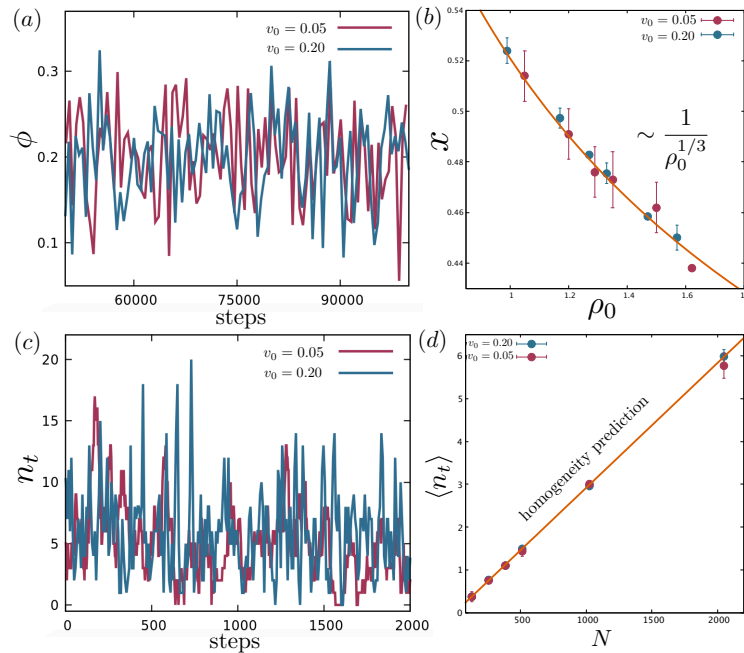


Figure 4.9: Numerical simulations: test of homogeneity. Analysis of homogeneity for data sets with $v_0 = 0.05$ (red) and $v_0 = 0.2$ (blue). (a) Temporal series of polarization ϕ for both activities and for size $N = 2048$ at the critical point. (b) The mean first neighbor distance is computed for each size $N = 128, 256, 384, 512, 1024, 2048$: it scales as $x \sim \rho_0^{1/3}$ as predicted for homogeneous systems. (c) Temporal series of n_t : the number of particles entering in a box of size $l_0 = L/7$ and centered in the middle of the bigger box of size L for $N = 2048$. (d) Average on time of n_t for all the sizes N and speed: this quantity scales linearly with N , as predicted for homogeneous systems $\langle n_t \rangle = N/7^3$ [30].

data (Fig.4.9b). Finally, we localize a small box of size $l_0 = L/7$ in the center of the big box of the simulation and we record the number of particles n_t entering in the first one during the evolution of motion [30]. The temporal series of this quantity does not show consistent fluctuations that can help in identifying denser clusters going through the sample box and, what is more, its time-averaged value verifies:

$$\langle n_t \rangle \sim \rho_0 l_0^3, \quad (4.33)$$

a relation proper of systems traveling without bands or aggregates [30]. Inserting in this expression the fact that $\rho_0 = N/L^3$, we affirm its validity looking at the linear trend $\langle n_t \rangle \sim N/7^3$ (Fig.4.9 c,d). Concluding, all the simulated data presented here reflect a homogeneous second order phenomenology, and can be used to test RG predictions of the original theory.

4.6 Breakdown of hydrodynamics for large speed

To explore the dynamical crossover between an equilibrium to an out-of-equilibrium universality class, we showed results regarding only two values of speed v_0 , one

representing the low activity regime and one the high activity regime. Between the two there is a change of factor 4, that translates into a factor 16 in the activity coupling constant because of their reciprocal squared relation (4.20). This turned out to be a sufficient condition for the manifestation of the crossover, however, one could argue that $v_0 = 0.2$ is not such a high value and we could have performed simulations at a larger speed. This is partly true, but we realized that going to arbitrary large v_0 is not functional for the purpose to make a comparison between numerical data of microscopic models and field theory's predictions.

The reason is that the hydrodynamic and continuous description of a model breaks down for very high values of v_0 . Remembering that the time step, in this discrete model, is $\Delta t = 1$, the condition to preserve the applicability of hydrodynamics reads as $v_0 \ll L$ that, given the sizes under consideration, means for v_0 in the range $0.2 - 0.3$. The quantitative explanation of this statement lies in the kinetic theory of [88], in which the Knudsen number is introduced as,

$$\text{Kn} = \frac{\sigma}{L} \quad (4.34)$$

where σ is the mean free path of a particle, and L is the macroscopic length scale. For hydrodynamics to be consistent, it must be $\text{Kn} \ll 1$, meaning that particles have to undergo many interactions with other active elements within the coarse-grained volume, in order for the coarse-graining procedure to make sense at all. In our case of the Vicsek model, $\sigma \sim v_0 \Delta t = v_0$, therefore one always has to respect the condition

$$v_0 \ll L . \quad (4.35)$$

In the opposite case, namely when v_0 becomes comparable with the linear size L , the rewiring of the interaction's network is so relevant, that the notion of local interaction disappears, and studying the critical dynamics of the simulations appears quite problematic, especially in comparison with RG calculations.

4.7 Conclusions on the Vicsek Model

In the last two chapters, we saw that an active matter model characterized by the presence of self-propulsion and ferromagnetic alignment as the Vicsek model (both in incompressible, but finite-size, or compressible scenarios) belongs to a universality class that is different from its equilibrium counterpart. From the study of the critical dynamics of the incompressible Toner and Tu theory in the near-critical phase, we understood that the off-equilibrium universality class is identified by a dynamical critical exponent $z = 1.7$ in $d = 3$ when the calculation is performed at 1-loop. Moreover, numerical simulations confirm that the same scenario is applicable also to homogeneous compressible systems, and the aforementioned value of z is not an artifact of incompressibility.

Therefore, the main take-home message relies on the result that out-of-equilibrium effects manifest in a lowering of the dynamical critical exponent's value with respect to the corresponding fixed network universality class, and the ingredient

that realizes this is the self-propulsion of the active particles. This fact confirms the intuitive idea that, when individuals are allowed to move and exchange continuously their interaction network, the information spreads more easily across the group reducing the value of the exponent z .

However, the *fil rouge* of this work is to identify the dynamical universality class of natural swarms, therefore it is important to highlight that this result is still far from a complete agreement with experimental data on this system. Swarms exhibit the dynamical scaling property with an exponent in the experimental window $1.1 < z < 1.3$ and, what is no less concerning, the decay of the dynamical correlation functions does not match with the first-order exponential relaxation of the Vicsek model. These discrepancies suggest that this theory is not capable to describe the relevant features that characterize the swarming behavior, and that some fundamental ingredients are missing in our mathematical description.

Chapter 5

Reinstating inertia in the microscopic dynamics

If, on the one hand, the Vicsek model is able to reproduce the quasi-critical phenomenology and the static properties of natural swarms, on the other, its dynamics does not capture some fundamental traits of their dynamical correlation functions. First of all, even taking into consideration relevant levels of activity, the out-of-equilibrium universality class studied in the previous chapter gives the exponent $z = 1.7$ that is quite far from the experimental value $z \simeq 1.2$. Second, the shape of their functions is reproduced by the exponential decay of the VM. We need, therefore, to modify our theoretical approach searching for new mechanisms in addition to the relevant effect of the activity.

The inspiration comes from the world of classical condensed matter physics of equilibrium systems. The literature of critical dynamics [67, 74] provides an overview on the main causes of the lowering of the dynamical critical exponent with respect to the standard dissipative case $z = 2$. These mechanisms emerge in the presence of symmetry and conservation laws that affect the nature of the order parameter's dynamics. The main results are mode-coupling terms that modify the classical dynamics (2.3) making it inertial or of second order. Models in which this effect is visible are the classic Model E, Model G or Model F of [74].

These theories work already on a coarse-grained level, to which we want to arrive starting from a microscopic ground with the aim to continue a comparison with the biological system of interest. What really drives us is the non-exponential decay of the $C(k, t)$ of natural swarms' velocities (Fig 1.9), which represents the key starting point of this investigation. The clear zero derivatives for small times can be explained, in fact, considering a microscopic model with a non-dissipative structure in the dynamics of the velocity, maintaining the main features of the VM: activity and ferromagnetic alignment. The model that has been proposed to fill these gaps is called the Inertial Spin Model (ISM), and it will be the main player of this chapter. We are going to introduce its microscopic derivation from the VM and its main characteristics, while in the next chapter we will proceed with the related field theory RG study.

5.1 From the Vicsek Model to the Inertial Spin Model

The ISM was introduced in [8] with the purpose to explain the phenomenon of information propagation in flocks of birds. Experiments show that starlings' collective turns are described by a linear propagation of purely directional information that does not involve any relevant local change in the density of the system [89]. This means that, when a bird starts to change direction, a wave-front of information, originating from it, rapidly propagates traveling fast and undamped through the whole homogeneous system. This scenario turns out to be quite different from the one predicted by the Toner and Tu theory: in the hydrodynamic limit $k \rightarrow 0$, it shows anisotropic propagating modes coupled to density fluctuations [36], which have not been observed in flocks' experimental data [89]. From this scenario, the introduction of a model with a new dynamics able to capture these traits appeared necessary [90].

We firstly introduce the equations of the model and then comment its derivation starting from the continuous version of the Vicsek model. In three dimensions of space and vectors the ISM reads:

$$\begin{aligned} \frac{d\mathbf{v}_i}{dt} &= \frac{\mathbf{s}_i \times \mathbf{v}_i}{\chi} \\ \frac{d\mathbf{s}_i}{dt} &= \frac{\mathbf{v}_i}{v_0} \times \left(\frac{J}{v_0} \sum_j n_{ij} \mathbf{v}_j - \frac{\eta}{v_0} \frac{d\mathbf{v}_i}{dt} + \boldsymbol{\zeta}_i \right) \\ \frac{d\mathbf{r}_i}{dt} &= \mathbf{v}_i \end{aligned} \quad (5.1)$$

with noise correlator:

$$\langle \boldsymbol{\zeta}_i(t) \cdot \boldsymbol{\zeta}_j(t') \rangle = 2d\eta T \delta_{ij} \delta(t - t') \quad (5.2)$$

Here \mathbf{r}_i identifies the position in space of the particle i , \mathbf{v}_i its velocity with fixed speed $|\mathbf{v}_i| = v_0$ and \mathbf{s}_i is a new variable that represents the generalized momentum connected to the rotation of the particle in its internal space. Due to these features and in analogy with quantum mechanics, it is named *spin*. The parameter χ is the behavioral inertia, η is a friction coefficient acting on the spin and J represents the strength of the alignment. Finally, T is a generalized temperature that fixes the amplitude of the noise.

To explain the origin of this model we can use a more convenient version of VM, which is its continuous-time version [42]. This is characterized by some formal differences with the original model introduced in the previous chapters, however, it preserves all the most important features of the discrete version. Using a Lagrange multiplier to enforce the constraint on the fixed modulus, in the limit

for $dt \rightarrow 0$, the model appears:

$$\eta \frac{d\mathbf{v}_i}{dt} = J \sum_j n_{ij} \mathbf{v}_j + \lambda_i \mathbf{v}_i + \boldsymbol{\zeta}_i \quad (5.3)$$

$$\frac{d\mathbf{r}_i}{dt} = \mathbf{v}_i \quad (5.4)$$

where η now can be interpreted as the timescale of the dynamical update, λ_i is the Lagrange multiplier to fix the condition $|\mathbf{v}_i| = v_0$ and $\boldsymbol{\zeta}_i$ is the same Gaussian noise introduced above. In this formulation the velocity's dynamics is very similar to a Langevin spin dynamics with ferromagnetic interactions, namely:

$$\eta \frac{d\mathbf{v}_i}{dt} = -\frac{\partial H}{\partial \mathbf{v}_i} + \lambda_i \mathbf{v}_i + \boldsymbol{\zeta}_i \quad (5.5)$$

with the force coming from the pseudo-Hamiltonian:

$$H = -J \sum_{\langle ij \rangle} n_{ij} \mathbf{v}_i \cdot \mathbf{v}_j . \quad (5.6)$$

On the other hand, compared to the lattice ferromagnetic case, in this model the network is not fixed, the connectivity matrix depends generally on time $n_{ij} = n_{ij}(t)$ and the system is out of equilibrium [42]. As the original model, also this kind of dynamics generates long-range order and scale-free correlations in the conditions of low noise and high polarization (Goldstone modes), or at the critical point and low polarization.

We said that the flaw of the VM is that it does not correctly reproduce the way collective turns occur in natural flocks and that ISM was formulated to fill this gap. Therefore, to understand its origins, let's focus on the ordered flocking phase of these models, forgetting for a moment the disordered swarming regime.

A useful path to go is the computation of the dispersion relation in the case of fixed network approximation. In the polarized phase, it is indeed reasonable to assume that the connectivity matrix does not depend on time, because flocks' collective turns occur on time scales smaller than the rearrangement scale of the network [91]. To calculate it, we then consider eq (5.3) in the limit of low temperature, where a spin-wave approximation can be used to expand each velocity vector around the mean velocity direction (that here we consider as the x axis) [42]:

$$\mathbf{v}_i = v_i^x \mathbf{n}_x + \boldsymbol{\pi}_i \sim \mathbf{n}_x v_0 \left(1 - \frac{1}{2} \frac{\pi_i^2}{v_0^2} \right) \quad (5.7)$$

where $\boldsymbol{\pi} = v_0(0, \phi^y, \phi^z)$ is the vector of transverse fluctuations with $\boldsymbol{\phi}$ the vector of phases. In this approximation, the equation of motion for the phases, in both the two directions, states:

$$\eta \frac{d\phi_i^\alpha}{dt} = -J \sum_j \Lambda_{ij} \phi_j^\alpha + \zeta_i^\alpha \quad (5.8)$$

where we introduced the discrete Laplacian defined as: $\Lambda_{ij} = -n_{ij} + \delta_{ij} \sum_k n_{ik}$, indicating with α the phase's components. If we look at spatial scales larger than the microscopic ones, we can transform the discrete Laplacian to its continuous counterpart, namely:

$$\sum_j \Lambda_{ij} \rightarrow -J n_c a^2 \nabla^2 \quad (5.9)$$

where a is the mean inter-particle distance, multiplied in order to respect the dimensional analysis, and n_c the number of interacting neighbors. Following this point of view, we can substitute the individual phases with the continuous field:

$$\phi_i^\alpha(t) \rightarrow \phi^\alpha(\mathbf{x}, t) . \quad (5.10)$$

with α indicating the cartesian component. Therefore the equation for the phase becomes:

$$\eta \frac{\partial \phi^\alpha(\mathbf{x}, t)}{\partial t} = J n_c a^2 \nabla^2 \phi^\alpha(\mathbf{x}, t) + \zeta^\alpha(\mathbf{x}, t) \quad (5.11)$$

accompanied by the noise's variance:

$$\langle \zeta^\alpha(\mathbf{x}, t) \zeta^\beta(\mathbf{x}', t') \rangle = 2\eta T a^3 \delta(\mathbf{x} - \mathbf{x}') \delta(t - t') \delta_{\alpha\beta} . \quad (5.12)$$

To study the dispersion relation, we can go to Fourier space and use the Green function method to obtain the modes' frequency, which, in this case, results purely imaginary:

$$\omega(k) = i \frac{J n_c a^2}{\eta} k^2 . \quad (5.13)$$

The last equation identifies a diffusive process of information propagation with $D = J n_c a^2 / \eta$ as diffusion coefficient, meaning that a disturbance that originates in a point of the group spreads diffusely through the system [42]. When few individuals, willing to turn, change direction of motion, turning information is transmitted diffusively and attenuated or, in other words, the turning modes are non-propagating overdamped modes. As a consequence in the long time limit the whole group loses coherence and disperses [8], as represented in Fig. 5.1. To summarize, a diffusion-like equation as the last one is clearly not ideal for the description of propagating information phenomena in flocks of birds.

One could blame the fixed network approximation as the responsible for this behavior. Indeed, reinstating density fluctuations in the system, it is possible to show that propagating modes emerge in the hydrodynamic limit $k \rightarrow 0$ [37], although strictly depending on the density itself. Possibly due to the finite size of real flocks, experimental data of these systems never revealed such a coupling between velocity and density that could justify a proper use of this hydrodynamic theory [89]. A possible way to obtain a real and linear dispersion relation embedding propagating sound modes is to make this theory *inertial* using effective variables, symmetries, and conservation laws.

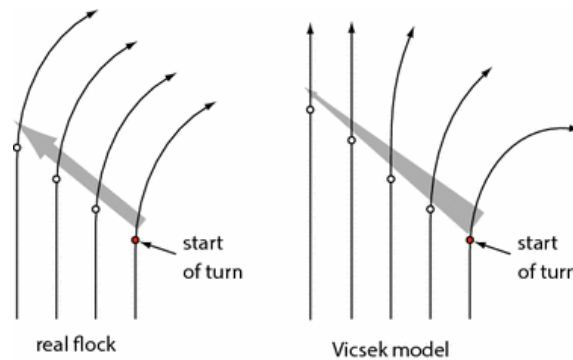


Figure 5.1: Schematic representation of turning events in real and Vicsek flocks. In real flocks, left panel, the information of turning propagates from a bird to the rest of the group, thus allowing a compact and coherent collective movement. In the Vicsek model, right panel, the turning information does not propagate: one element starts to turn and the flock does not follow it, with the consequence that the whole group loses coherence. Reprinted from [8].

5.1.1 The double role of velocity

To make progress, we analyze the role of the velocity in these active models, going back to the hydrodynamic theory of Toner and Tu. We can here briefly recall the equation that identifies the latter in absence of noise,

$$D_t \mathbf{v} = \mathcal{J} \nabla^2 \mathbf{v} - \nabla P + \frac{\partial V}{\partial \mathbf{v}}, \quad (5.14)$$

where with V we are indicating the classic quartic potential. We focus on the physical meaning of the first term of the r.h.s. that, in a usual Navier-Stokes interpretation, represents the dissipation responsible for the diffusive behavior of the fluid, with \mathcal{J} assuming the role of kinematic viscosity. This equation can be therefore interpreted in a mechanistic sense for which $D_t \mathbf{v}$ is the acceleration of the fluid, and the remaining terms of the right side play the role of external dissipative forces.

However, we saw from the previous section that the Laplacian contribution directly comes from a continuous limit of the interaction term $J \sum n_{ij} \mathbf{v}_j$, which describes more a social force than a viscosity. From this perspective, \mathcal{J} is what regulates the dynamics of the velocity acting like a stiffness of an orientation force. As a consequence, the velocity \mathbf{v} assumes the role of the fundamental degree of freedom of the theory. This point of view is already explicit in the microscopic formulation of the model of (5.5), where the force is expressed as the derivative of an effective Hamiltonian with respect to the velocity itself $\mathbf{F}_i = -\partial H / \partial \mathbf{v}_i$.

Under this second interpretation, equation (5.14) can be viewed as an over-damped first order Langevin equation for the orientations, instead of an under-

damped second order Newton equation. To recover propagating orientational modes independent of the density, it seems reasonable to write the velocity underdamped limit of this model [42]. Nevertheless, if going from an inertial equation to its overdamped limit is quite easy, performing the opposite limit can be complicated. Symmetries and conservation laws help us in reaching this goal.

5.1.2 Rotational symmetry and spin

The hint of the existence of a symmetry comes again from the world of flocks of birds. Experimental data highlight that, when the flock performs a collective turn, each individual follows a specific trajectory in space that can be described with an equal-radius turning scenario [92]. This rotation is different from the usual rigid body turning, for which individuals rotate around the same axis with the same angle of rotation but different radii of curvature. In this latter case, from an external observer, the main effect is that particles change their relative positions but do not with respect to the center of the reference frame. On the other hand, in the case of equal-radius turning, the relative positions among individuals do not change from an external observer since all the particles turn with the same radius of curvature but with different centers of rotation (the difference can be appreciated in Fig 5.2, [42]). The biological advantage of this behavior is that flocks maintain stronger cohesion in the group flying at an almost constant speed and preserving the symmetry of invariance under a fixed-radius rotation.

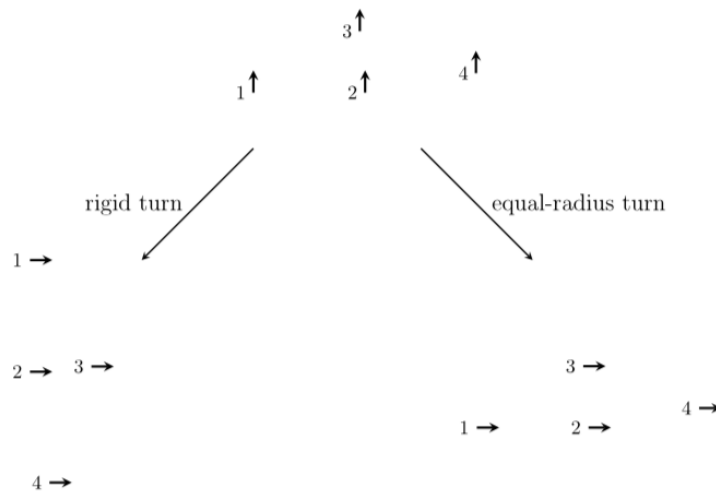


Figure 5.2: Schematic representation of a rigid and an equal-radius turn. Velocities are rotated of 90° degrees in the rigid turn (left) and in the equal-radius case (right). In the latter case the orientational topology of the system is changed. Reprinted from [42].

To see how to make wise use of this symmetry, it is instructive to analyze the two-dimensional case. What changes during an equal radius turning is the direction of the velocity vectors: the rotation takes place in the internal space of velocity and not in the external space of positions. Of course, also in this case,

we can keep on assuming the constraint of constant speed v_0 and then express the directional vector as:

$$v_i = v_0 e^{i\phi_i} \quad (5.15)$$

where now the single phase ϕ_i assumes the role of the new generalized coordinate [42]. The Hamiltonian formalism suggests to pair it to its conjugated momentum, namely the generator of rotation in the internal space that is the *spin* angular momentum s_i [8]. Therefore, the presence of this underlying symmetry allows us to identify a new pair of canonical variables (ϕ, s) that follow the classical equations of motion:

$$\frac{d\phi_i}{dt} = \{\phi_i, H\} \quad (5.16)$$

$$\frac{ds_i}{dt} = \{s_i, H\} \quad (5.17)$$

where the Poisson parenthesis are defined as:

$$\{A, B\} = \sum_i \frac{\partial A}{\partial \phi_i} \frac{\partial B}{\partial s_i} - \frac{\partial A}{\partial s_i} \frac{\partial B}{\partial \phi_i} \quad (5.18)$$

and the Hamiltonian, in the non-interacting case, is:

$$H = \sum_i \frac{s_i^2}{2\chi}. \quad (5.19)$$

Here we can map the parameter χ with a generalized moment of inertia: it embodies the resistance of the active particle to change the instantaneous radius of curvature of its trajectory, thus justifying the name of *behavioral inertial* [8]. In the case of free-particles, we observe a simple circular motion during which particles rotate with constant angular velocity, indeed:

$$\frac{d\phi_i}{dt} = \{\phi_i, H\} = \frac{\partial H}{\partial s_i} = s_i/\chi \quad (5.20)$$

$$\frac{ds_i}{dt} = \{s_i, H\} = -\frac{\partial H}{\partial \phi_i} = 0 \quad (5.21)$$

and the single particle's spin is conserved. We can now add the interaction through a generic potential $V(\{\phi_i\})$ in H , whose derivative describes the alignment interaction force between particles, in such a way that:

$$\frac{d\phi_i}{dt} = \frac{\partial H}{\partial s_i} = s_i/\chi \quad (5.22)$$

$$\frac{ds_i}{dt} = -\frac{\partial H}{\partial \phi_i} = -\frac{\partial V}{\partial \phi_i} = F_i \quad (5.23)$$

and the forces on the phases are mediated by the equation of the spin. A clear

generalization of the interacting Hamiltonian follows,

$$H = \sum_i \frac{s_i^2}{2\chi} + \sum_i V(\{\phi_i\}) \quad (5.24)$$

where we can easily distinguish the kinetic term and the potential V acting on the phases. In order to preserve the complete rotational invariance of the Hamiltonian, V is required to be also rotational symmetric [8]. This means that if the phase of each particle is changed by a global quantity $\delta\phi$, the (5.24) is invariant under this global transformation and, thanks to the Noether's theorem, there exists an associated conserved quantity in the system. It is easy to show that what is preserved along the dynamical evolution is the total spin of the system, namely $S = \sum_i s_i$, since

$$\frac{dS}{dt} = - \sum_i \frac{\partial V}{\partial \phi_i} = 0$$

because of the discrete Laplacian properties and of the symmetry $V(\{\phi_i\}) = V(\{\phi_i + \delta\phi\})$. We stress this symmetry since it will be an important player in all the following field theory analysis.

For the moment, we wrote the dynamical equations for the phase and for the spin, but not for the velocity, which, we remember, is not the canonical variable coupled to the internal angular momentum. The update equation for the \mathbf{v}_i is not trivial, but we can use again the Hamiltonian formalism to compute the time evolution of observable that does not depend explicitly on time, using the Poisson brackets tool. In the simple planar case, where $v_i = v_0 \exp(i\phi_i)$ lies on the 2d plane and s on its orthogonal direction, we get for the first equation:

$$\frac{dv_i}{dt} = \{v_i, H\} = \sum_j \frac{\partial v_i}{\partial \phi_j} \frac{\partial H}{\partial s_j} = i v_i \frac{s_i}{\chi} \quad (5.25)$$

In three dimensions, both \mathbf{v}_i and \mathbf{s}_i become three dimensional vectors. Reinstating back the three different phases that parameterize the rotation around the three axis $\{\phi_i^\alpha\}(\alpha = x, y, z)$, we can use the following relation:

$$\frac{\partial v_i^\alpha}{\partial \phi_i^\beta} = \sum_\gamma \epsilon_{\alpha\beta\gamma} v_i^\gamma, \quad (5.26)$$

where $\epsilon_{\alpha\beta\gamma}$ is the antisymmetric Levi-Civita tensor, to generalize the equations of motion to [8]:

$$\frac{dv_i^\alpha}{dt} = \{v_i^\alpha, H\} = \sum_{j,\gamma} \frac{\partial v_i^\alpha}{\partial \phi_j^\gamma} \frac{\partial H}{\partial s_j^\gamma} = - \sum_{\beta,\gamma} \epsilon_{\alpha\beta\gamma} v_i^\beta \frac{s_j^\gamma}{\chi} \quad (5.27)$$

$$\frac{ds_i^\alpha}{dt} = \{s_i^\alpha, H\} = - \sum_{j,\gamma} \frac{\partial s_i^\alpha}{\partial s_j^\gamma} \frac{\partial H}{\partial \phi_j^\gamma} = \sum_{\beta,\gamma} \epsilon_{\alpha\beta\gamma} v_i^\gamma \frac{\partial H}{\partial v_i^\beta} \quad (5.28)$$

Finally, using a more compact vectorial notation, we can write the underdamped

equations of ISM in the deterministic and conserved case:

$$\frac{d\mathbf{v}_i}{dt} = \frac{\mathbf{s}_i \times \mathbf{v}_i}{\chi} \quad (5.29)$$

$$\frac{d\mathbf{s}_i}{dt} = \mathbf{v}_i \times \mathbf{F}_i \quad (5.30)$$

$$\frac{d\mathbf{r}_i}{dt} = \mathbf{v}_i \quad (5.31)$$

These equations of motion clarify that the spin \mathbf{s}_i assumes a direct kinematic meaning: it is related to the instantaneous radius of curvature of the particle's trajectory $R \sim v_0\chi/|\mathbf{s}_i|$ and it has the main role to mediate a not-instantaneous update of the force on the particles: the alignment interactions manifest on the spin and not directly on the velocity \mathbf{v}_i , hence they cannot change the motion abruptly, but only through a slower and inertial timescale [8].

5.2 Spin dissipation and overdamped limit

The last deterministic formulation of the model is not complete, since we have to enrich the dynamics applying terms of noise and dissipation to the conservative force $\mathbf{F}_i = -\delta H/\delta\mathbf{v}_i$, always preserving the constraint on the fixed modulus of the velocity. A reasonable choice is to insert a dissipation on the spin's dynamics, in a way to reproduce a rectilinear motion in absence of interaction or external forces. Clarifying the social force, we obtain the final equations of the Inertial Spin Model (5.1), that we can report here for the sake of completeness [8]:

$$\frac{d\mathbf{v}_i}{dt} = \frac{\mathbf{s}_i \times \mathbf{v}_i}{\chi} \quad (5.32)$$

$$\frac{d\mathbf{s}_i}{dt} = \frac{\mathbf{v}_i}{v_0} \times \left(\frac{J}{v_0} \sum_j n_{ij} \mathbf{v}_j - \frac{\eta}{v_0} \frac{d\mathbf{v}_i}{dt} + \boldsymbol{\zeta}_i \right) \quad (5.33)$$

$$\frac{d\mathbf{r}_i}{dt} = \mathbf{v}_i \quad (5.34)$$

where $\boldsymbol{\zeta}_i$ is still a Gaussian white noise that satisfies:

$$\langle \boldsymbol{\zeta}_i(t) \boldsymbol{\zeta}_j(t') \rangle = 2d\eta T \delta_{ij} \delta(t - t') . \quad (5.35)$$

Also from a biological point of view, it is reasonable to hypothesize the presence of a spin dissipation of the form $-\eta \delta H/\delta s_i$, such that of eq (5.33), otherwise in absence of interaction and noise ($J = 0$ and $T = 0$) an individual would maintain an everlasting state of circular motion. The dissipation η acts as damping and reinstates a ballistic motion of the agent in this particular situation, modifying its curvature in the long run. Additionally, the presence of this friction actually violates the conservation of the total spin, making the theory not strictly invariant under rotation. However, this violation in the biological systems happens to be always weak, since very small values of η reproduce in a compelling

way the related experimental data [42].

Interestingly, the Vicsek Model can be recovered as the overdamped limit of these equations, that is in the limit for which inertia becomes negligible compared to the spin dissipation,

$$\frac{\chi}{\eta^2} \rightarrow 0. \quad (5.36)$$

To see it more carefully, we can take a further derivative in time of (5.1), obtaining a second order differential equation for the velocity,

$$\begin{aligned} \chi \frac{d^2 \mathbf{v}_i}{dt^2} + \chi \frac{\mathbf{v}_i}{v_0^2} \left(\frac{d\mathbf{v}_i}{dt} \right)^2 + \eta \frac{d\mathbf{v}_i}{dt} = \\ \frac{J}{v_0^2} \left(\sum_j n_{ij} \mathbf{v}_j \right)^\perp + v_0 \boldsymbol{\xi}_i^\perp \end{aligned} \quad (5.37)$$

where with the symbol \perp we mean the orthogonal projection to the direction of motion, i.e.:

$$\boldsymbol{\xi}_i^\perp = \boldsymbol{\xi}_i - \left(\boldsymbol{\xi}_i \cdot \frac{\mathbf{v}_i}{v_0} \right) \frac{\mathbf{v}_i}{v_0} \quad (5.38)$$

used to implement the constraint. The first term on l.h.s. of (5.37) represents the inertial term of the underdamped dynamics, while the second can be interpreted as a centripetal acceleration of the circular motion. Now it is clear that performing the limit of (5.36), we recover directly the continuous version of the Vicsek Model (5.3) where the Lagrange multiplier has been explicitly computed [8].

This mechanism can be interpreted in terms of time-scales and information propagation. In the ISM, we have a fundamental time scale given by:

$$\tau \sim \frac{\chi}{\eta}. \quad (5.39)$$

The overdamped limit corresponds to taking into consideration the asymptotic long-time regime $t \gg \tau$, where the damping kills the inertial terms. This is the time domain described by the VM, which carries only a diffusive propagation [93]. Reinstating the inertial term, we are basically focusing on the underdamped regime, namely, to times $t \ll \tau$ that are those important to describe the fast information which runs through the biological group [42].

Like the VM, also the ISM is a model which undergoes a phase transition from a disordered paramagnetic phase to an ordered one (even in $d = 2$ if the system is not at the equilibrium), indeed it has been derived in order to preserve the static properties of VM. Moreover, looking at the dynamics presented in the deeply polarized phase, we can confirm that the model exhibits propagating modes of spin-waves [93]. To confirm it, it is possible to repeat the same passages we did for the VM under the same assumptions: polarized phase, fixed network and large spatial scales. Managing eq (5.32) and (5.33), we extrapolate the dispersion relation of ISM taking into account, of course, the term of second order in time

derivative. This relation appears:

$$\omega(k) = i\gamma \pm ck\sqrt{1 - k_0^2/k^2} \quad (5.40)$$

where $\gamma = \eta/2\chi$, $k_0 = \gamma/c$ and c is a second sound speed: $c = \sqrt{Jn_c a^2/\chi}$.

Crucial is the presence of a real part for $k > k_0$, which becomes linear in the limit $k \gg k_0$. This confirms that, in this situation, the model admits signal propagation and underdamped modes of information transfer. On the other hand, for $k < k_0$ and in the limit $k \rightarrow 0$, the frequency becomes imaginary and the dynamical regime results diffusive and overdamped. The differences with the case of VM are represented in Fig.5.3 and Fig. 5.4 where the success of this inertial model in reproducing the collective phenomena of turning is clearly visible.

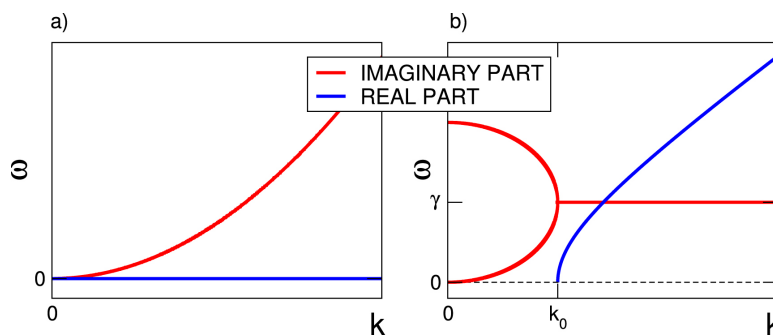


Figure 5.3: Dispersion relations of VM and ISM. Dispersion relation of Vicsek Model (a) and of Inertial Spin Model (b). The blue line represents the real part of the $\omega(k)$ and the red line the imaginary part. In panel (a) we see that the VM has not a propagating part, but the frequency is only dissipative and quadratic in k . On the other hand, for ISM (b) a real propagating part emerges for $k > k_0$, and it becomes linear if $k \gg k_0$; for $k \rightarrow 0$ the real part is zero and the imaginary part goes to zero as k^2 . Figure reprinted from [93].

5.3 Another derivation of the ISM equations

When the interaction matrix n_{ij} is taken symmetric (for instance, in the metric interaction), a formulation in terms of Lagrangian dynamics is possible and formally correct [94]. Indeed, calling $\{\mathbf{r}_i(t), \mathbf{v}_i(t), \mathbf{s}_i(t)\}_{i=1}^N$ the solutions of equations (5.32) (5.33) (5.34), the set $\{\mathbf{v}_i(t)\}_{i=1}^N$ can be proved to be a solution of the constrained mechanical system described by the following time dependent Lagrangian:

$$\mathcal{L}'(\{\mathbf{v}_i\}, \{\dot{\mathbf{v}}_i\}, t) = \frac{m}{2} \sum_i \dot{\mathbf{v}}_i^2 - V(\{\mathbf{v}_i\}, t) \quad (5.41)$$

where again we mean the potential V as the generator of the social force $\mathbf{F}_i = -\partial V/\partial \mathbf{v}_i$ in the equations of motion, and the kinetic term involves a generalized inertia m different from the χ we discussed above. When a Lagrangian problem includes a set of holonomic constraints identified by level curves $f_\alpha(\{\mathbf{v}_i\}) = 0$,

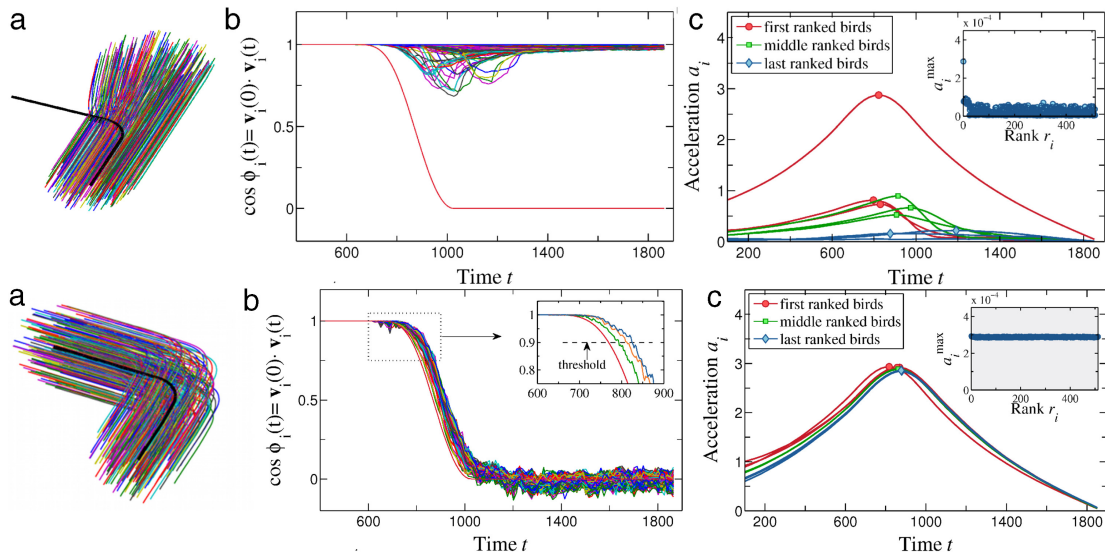


Figure 5.4: Comparison of turning events. Attempts to propagate turning information in a group in the Vicsek Model (top) and Inertial Spin Model (bottom): in the VM the turn cannot propagate and the individual leaves the flock; in ISM the whole group follows the turning individual. Panels a : 2-d trajectories; panels b: cosine of the individual velocities with respect to the original direction; panels c: individual acceleration profiles. Figure reprinted from [8].

it can be mapped in a new Lagrangian function that explicitly contains this information:

$$\mathcal{L} = \mathcal{L}' + \sum_{\alpha} \lambda_{\alpha} \sum_i \dot{\mathbf{v}}_i \frac{\partial f_{\alpha}}{\partial \mathbf{v}_i} \quad (5.42)$$

with λ_{α} a Lagrangian multiplier, one for each constraint [95]. In the case of ISM the holonomic rule is represented by the fixed speed of the particles, i.e. $|\mathbf{v}_i| = v_0$, which can be reformulated as:

$$f(\{\mathbf{v}_i\}) = \sum_j (\mathbf{v}_j^2 - v_0^2) = 0. \quad (5.43)$$

Inserting it in the Lagrangian (5.41) we get,

$$\mathcal{L} = \frac{m}{2} \sum_i \dot{\mathbf{v}}_i^2 - V(\{\mathbf{v}_i\}, t) + 2\lambda \sum_i \mathbf{v}_i \dot{\mathbf{v}}_i. \quad (5.44)$$

At this point, the equations of motion of the system can then be derived either using the standard Euler-Lagrange equation:

$$\frac{d}{dt} \left\{ \frac{\partial \mathcal{L}}{\partial \dot{\mathbf{v}}_i} \right\} - \frac{\partial \mathcal{L}}{\partial \mathbf{v}_i} = 0 \quad (5.45)$$

or using the classical Hamiltonian formalism, which involves the definition of a conjugate momentum related to the generalized variable. In this case, we are addressing this role to the velocity, therefore, by definition, the conjugate mo-

mentum will not be the spin but rather:

$$\boldsymbol{\pi}_i(t) = \frac{\partial \mathcal{L}}{\partial \dot{\mathbf{v}}_i} = m\dot{\mathbf{v}}_i + 2\lambda\mathbf{v}_i \quad (5.46)$$

Certainly, this quantity just introduced now does not assume a direct physical and mechanistic interpretation. What we are doing is only reformulating the problem in a phase space composed by the variables $\{\mathbf{v}, \boldsymbol{\pi}\}$ that could be mathematically connected to the standard $\{\mathbf{q}, \mathbf{p}\}$ of the Hamilton's formalism. Following this analogy, we can express the internal angular momentum as:

$$\mathbf{s}_i = \mathbf{v}_i \times \boldsymbol{\pi}_i \quad (5.47)$$

In these terms, the Hamilton equations look like,

$$\dot{\mathbf{v}}_i = \frac{1}{m}(\boldsymbol{\pi}_i - 2\lambda\mathbf{v}_i) \quad (5.48)$$

$$\dot{\boldsymbol{\pi}}_i = \mathbf{F}_i + \lambda \sum_j \frac{\partial^2 f}{\partial \mathbf{v}_i \partial \mathbf{v}_j} \dot{\mathbf{v}}_j = \mathbf{F}_i + 2\lambda\dot{\mathbf{v}}_i \quad (5.49)$$

where the force \mathbf{F}_i is the derivative of $V(\{\mathbf{v}_i\})$. We can finally write it explicitly solving for the Lagrange multiplier. This latter can be derived by the constraint condition $\mathbf{v}_i \cdot \dot{\mathbf{v}}_i = 0$, which makes the calculation straightforward to obtain,

$$\frac{d\mathbf{v}_i}{dt} = \frac{\mathbf{s}_i \times \mathbf{v}_i}{\chi} \quad (5.50)$$

with the behavioral inertial $\chi = mv_0^2$. To get the equation of the spin, it is sufficient to derive in time eq (5.47), so that:

$$\frac{d\mathbf{s}_i}{dt} = \mathbf{v}_i \times \ddot{\mathbf{v}}_i = \mathbf{v}_i \times \mathbf{F}_i \quad (5.51)$$

finally recalling the original (deterministic) equations of motion of ISM (5.29).

5.4 Why ISM for natural swarms?

Until now we presented this model only referring to the biological system of flocks of birds, actually highlighting its relevance in the context of information propagation in turning movements. We remind that the claimed consistency is evident when the model is studied in its low-temperature phase (i.e. high polarization phase). On the contrary, natural swarms of insects cannot be described by the same set of parameters because they are not a polarized system. They do not show global motion, which means that their global mean velocity is nearly zero. To reproduce the disordered phenomenology of this second biological system, together with the high degree of directional correlation [3], we can transpose the study of ISM in its near critical and paramagnetic region of parameters, i.e. $T \simeq T_c$, to see

if this model is capable to quantitatively reproduce and predict the experimental evidence of natural swarms.

We take into consideration this particular model because of its inertial nature in the dynamics of the velocity. Therefore, the first preliminary thing we can compare with experimental data is the shape of the dynamical correlation functions of orientations when the ISM is posed at criticality from the disordered side of the transition. Before analyzing the comparison between experimental data and correlation functions of ISM, we are going to introduce the analytical method we use to treat the dynamical correlation functions.

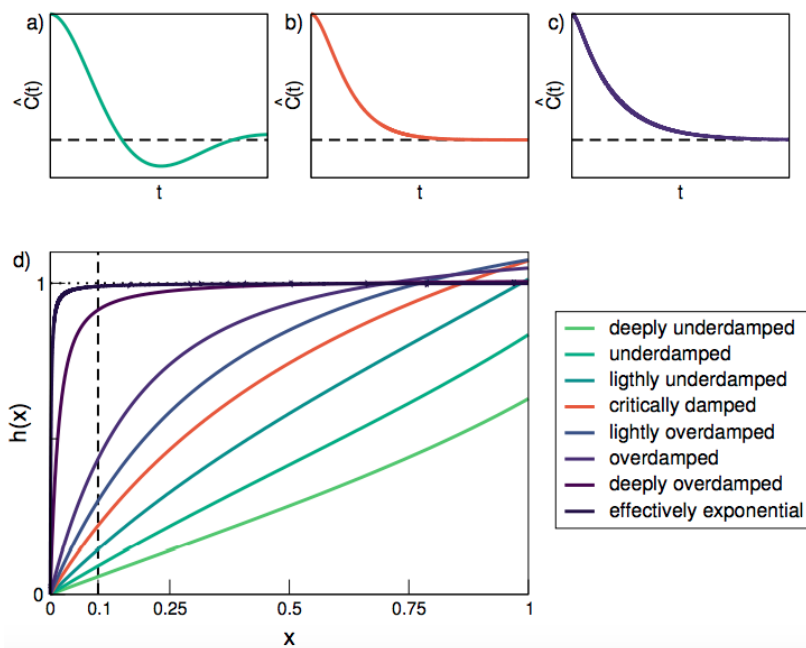


Figure 5.5: Toy model to understand the behavior of $h(x)$: we report the correlation function of the stochastic harmonic oscillator at different values of the damping ratio. a) Underdamped regime: there is a clear oscillatory behavior of the function. b) Critically damped regime: propagating modes are no longer present but the derivative for small times it's clearly flat. c) Overdamped regime: the correlation function are more nearly exponential, but inertial effect are still present for short time. d) The function $h(x)$ shows how the correlation function crosses over from a non-exponential behavior ($h(x) \sim 0$ per $x \sim 0$), to a pure exponential trend ($h(x) \sim 1$ per $x \sim 0$), as the damping grows. Reprinted from [3].

In a more general framework, when the dynamical propagator of a model has more than one pole in the complex ω -plane, the first derivative of the dynamic correlation function vanishes for small times [3]. Therefore, we can take this feature as a good sign of a non-dissipative nature of the dynamics and we can quantitatively measure it computing the form-factor function,

$$h(x) = -\frac{1}{x} \log(\hat{C}(x)) \quad (5.52)$$

where $x = t/\tau$ and \hat{C} is the dynamic correlation function normalized at time

$t = 0$.

We better visualize the information given by this function if we consider a toy model, namely the stochastic harmonic oscillator in $d = 1$, which has a dynamics of second order:

$$m\ddot{u}(t) + \eta\dot{u}(t) + ku(t) = \zeta(t) \quad (5.53)$$

where u is the generalized coordinate, m is the inertia, η is the viscosity, k is the elastic constant (or stiffness), and ζ is the usual white noise. Depending on the strength of the damping, which is determined by the ratio between stiffness and dissipation, the dynamical correlation functions of this model can behave in different ways. In the first three panels of Fig. 5.5 we can appreciate these different regimes. Increasing the damping, the shape of the normalized $\hat{C}(t)$ crosses from a shape with oscillatory modes and flat derivative at time $t = 0$, to a more nearly exponential form, even though non-exponential effects are still present for short times [3].

In panel d of the same figure we can see what is the behavior of the function $h(x)$ applied to this model. Because $\hat{C}(0) = 1$, a purely exponential time correlation implies that:

$$\lim_{x \rightarrow 0} h(x) = 1 \quad (5.54)$$

while, for a non-exponential behavior we have:

$$\lim_{x \rightarrow 0} h(x) = 0 \quad (5.55)$$

Therefore, for a model with a second-order dynamics, $h(x)$ at $x = 0$ is always null. But increasing the damping, the function becomes effectively exponential and the departure from 1 becomes smaller and smaller. This difference can be appreciated in the graphs of this toy model of Fig. 5.5 [3].

In panel a of Fig. 5.6, the spatio-temporal correlation functions of natural swarms, of Vicsek and ISM simulated swarms are compared when time is properly rescaled by their characteristic time scale [10]. The difference between the two types of active dynamics is relevant: the function of ISM fits in a compelling way the experimental data, especially reproducing the curvature of the $C(k, t)$ for small times Fig 5.6. This is even more appreciable when computing the relaxation form factor $h(t/\tau)$ introduced before. This result indicates the type of dynamics described by ISM well reproduces the relaxation of natural swarms from a qualitative point of view. We will therefore work under the hypothesis that the ISM in the paramagnetic phase describes the inertial dynamics of natural swarms.

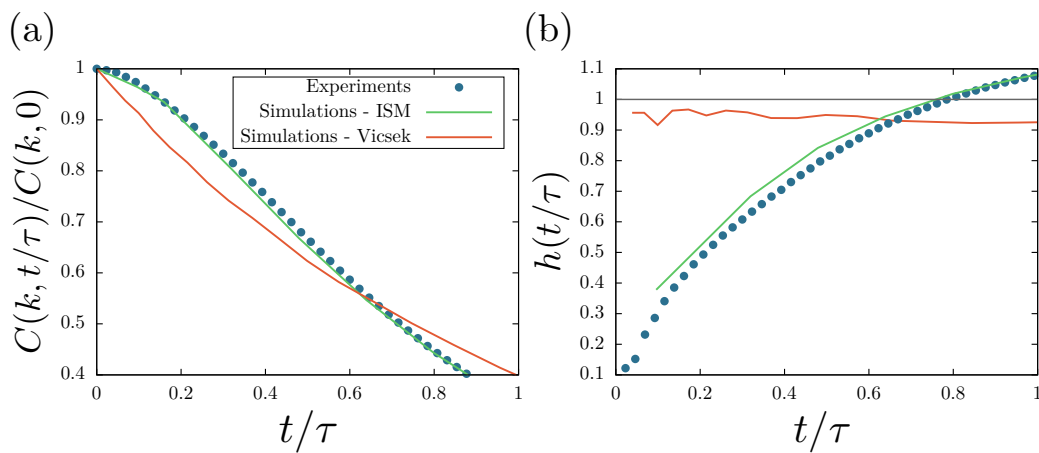


Figure 5.6: Comparison of dynamical correlation functions: models and swarms' data. Panel (a): Normalized dynamical correlation functions $C(k, t)/C(k, 0)$ coming from experimental data on swarms, and from numerical simulations of ISM and of VM. Every curve is evaluated at a proper wave number that verifies $k\xi = 1$. Panel (b): for the same curves of panel (a), the relaxation form factor $h(t/\tau) \equiv \dot{C}(t/\tau)/C(t/\tau)$, which goes to 1 for overdamped exponential relaxation of the VM, while it goes to 0 for inertial relaxation of ISM and swarms [3]. These preliminary simulations suggest that the ISM is able to qualitatively reproduce the dynamics of natural swarms. Figure reprinted from [9].

Chapter 6

Renormalization of the Inertial Spin Model in a fixed network approximation

In this chapter, we perform an RG study on the Inertial Spin Model to test it as a good representative of the natural swarms' dynamics. The analysis is carried out under the relevant approximation of fixed-network, assumed mainly for two reasons: first, it represents the first step of a quite more complex out-of-equilibrium calculation that will follow it; second, we decide to investigate how an inertial dynamics with dissipation influences the dynamical critical exponent of a model at equilibrium, decoupling the problem from the self-propulsion effects studied in the previous chapters.

6.1 ISM in the fixed network approximation

Starting from the microscopic theory of the Inertial Spin Model (5.1), we explore the characteristic critical dynamics of the associated field theory. The first step to achieve this goal is to perform a coarse-graining of the microscopic variables and derive the proper dynamical equations of motion for the fields. However, before introducing them, we can linger for a moment on the complexity of the theory we are going to analyze.

The ISM involves the dynamical evolution of particles' position, velocity, and spin, which should translate in a field theory for three coupled fields, namely the density, the velocity (or polarization), and the spin itself. Moreover, the system described by this model is clearly active, hence out-of-equilibrium, additionally distinguished by a non-trivial coupling between the density and the other fields that in general enriches and complicates a lot its critical nature [11]. To finally assert if this theory can really reproduce the biological system of swarms, we need to take into account all these important features, especially the non-equilibrium ones. However, as a further stepping stone of the analysis, we decide first to treat the simpler (and yet non-trivial) equilibrium case, in which we consider not-moving particles fixed on a lattice [9, 10].

This scenario contains already interesting aspects that deserve attention: first of all, it includes non-dissipative terms and *effective friction*, an interplay that has never been studied before, not even in the equilibrium case. Secondly, we believe it is going to provide useful insights concerning the behavior of swarm's correlation function. It is indeed worth remembering that our main concern is to correctly reproduce both the shape of the dynamical correlation functions and the dynamical critical exponent z of this natural system. We saw that a complete study of the critical dynamics of the self-propelled Vicsek case, even though it led to a lower value of z with respect to the equilibrium case, fails short of the actual experimental value. This fact suggests that self-propulsion may not be the only source of the anomalous natural exponent, but that the inertial dynamics could, instead, play a prominent role in determining it. Finally, we believe that facing the equilibrium problem will give us the right setup and mindset to tackle the more complicated off-equilibrium case and that will definitely clarify the role of dissipative inertial dynamics in the determination of the universality class of a system.

Therefore, here we study a fixed-network version of the ISM, in which the particles belong to a lattice and the connectivity matrix does not depend on time. In this context, we can neglect the dynamical update of the positions, and we can interpret the order parameter no longer as a physical velocity, but just as the polarization of the system. Therefore, we call $\boldsymbol{\psi}_i = \mathbf{v}_i/v_0$ and we write the microscopic equilibrium model in the following way,

$$\frac{d\boldsymbol{\psi}_i}{dt} = \frac{1}{\chi} \mathbf{s}_i \times \boldsymbol{\psi}_i \quad (6.1)$$

$$\frac{d\mathbf{s}_i}{dt} = \boldsymbol{\psi}_i \times J \sum_j n_{ij} \boldsymbol{\psi}_j - \frac{\eta}{\chi} \mathbf{s}_i + \boldsymbol{\psi}_i \times \boldsymbol{\zeta}_i \quad (6.2)$$

where n_{ij} is the fixed interaction matrix, and the modulus of the order parameter is still considered constant $|\boldsymbol{\psi}_i|^2 = 1$. Thanks to these considerations, we can still interpret the equations in a Hamiltonian formalism as,

$$\frac{d\boldsymbol{\psi}_i}{dt} = -\boldsymbol{\psi}_i \times \frac{\partial H}{\partial \mathbf{s}_i} \quad (6.3)$$

$$\frac{d\mathbf{s}_i}{dt} = -\boldsymbol{\psi}_i \times \frac{\partial H}{\partial \boldsymbol{\psi}_i} - \eta \frac{\partial H}{\partial \mathbf{s}_i} + \boldsymbol{\psi}_i \times \boldsymbol{\zeta}_i, \quad (6.4)$$

with microscopic Hamiltonian,

$$H = -J \sum_{i,j} n_{ij} \boldsymbol{\psi}_i \cdot \boldsymbol{\psi}_j + \sum_i \frac{s_i^2}{2\chi}. \quad (6.5)$$

These equations represent the starting point of a coarse-graining procedure that will lead into a corresponding dynamical field theory [10].

6.1.1 Coarse-grained field theory

We are interested in describing the large-scale properties of the system, therefore it is convenient to move onto a description of the model in terms of space and time-dependent fields. Writing hydrodynamics continuous equations of motion for active matter models is a quite well-established procedure that basically follows two different main paths that arrive at similar conclusions.

The first one is called the kinetic (or Boltzmann-Ginzburg-Landau) approach and the central idea is to work out a Boltzmann equation for the one-particle distribution, interpreting active polar interactions as binary collisions between agents [96, 97]. The success of this procedure is that the resulting continuous models consist of field theories characterized by a set of coarse-grained parameters, whose dependence on the microscopic ones is explicit. Thanks to this fact, linear instability analysis of the outcome equations carried the community to demonstrate and predict the nature of ordering transition for many of these models [97–99]. Moreover, recent works highlight the role of fluctuations in this context and they could lead to a revision of the deterministic methodology [100].

The second way to write a field theory for active matter models is a phenomenological approach, coming from Landau-Ginzburg theories [51]. This method was also used by Toner and Tu in their seminal paper [36]. It involves a space-temporal gradient expansion that obeys all symmetries and conservation laws of the system. For instance, a Vicsek-like dynamics is characterized by the rotational symmetry, the conservation of number, and the lack of Galilean invariance. Since the goal is to describe the long-distance, long-time properties of the system, only the lowest terms in gradients and derivatives of the field are inserted in the equations and their relevance is subsequently justified by a renormalization group approach. In our discussion, we are going to follow this second methodology, but it is worth noticing that a calculation with the kinetic approach has been performed also for the original ISM and the result is shown in [101].

We therefore consider smoothly varying polarization and spin fields $\boldsymbol{\psi}(\mathbf{x}, t)$, and $\mathbf{s}(\mathbf{x}, t)$, where \mathbf{x} is interpreted as the center of a small spatial volume in which averages are performed. Since the system is at equilibrium, the original Hamiltonian (6.5) translates into an effective field Hamiltonian $\mathcal{H}[\boldsymbol{\psi}, \mathbf{s}]$ of the classical ferromagnetic-like systems [51, 65], which reads

$$\mathcal{H}[\boldsymbol{\psi}, \mathbf{s}] = \int d^d x \left\{ \frac{1}{2} (\nabla \boldsymbol{\psi})^2 + \frac{1}{2} r_0 \boldsymbol{\psi}^2 + \frac{u_0}{4!} \boldsymbol{\psi}^4 + \frac{s^2}{2\chi_0} \right\}, \quad (6.6)$$

and that is characterized by the following mesoscopic parameters: χ_0 as the effective inertia, r_0 as the bare mass (whose value is negative in the ordered phase), and u_0 that is the bare static coupling constant. We can here briefly remind that the gradient term describes the reciprocal alignment interaction and favors spatially smooth configurations; the quartic and quadratic elements in $\boldsymbol{\psi}$ stand for a confining potential, stemming from the microscopic constraint on the

modulus of ψ_i , and from the coarse-grained entropy. The spin \mathbf{s} contribution is just a Gaussian term as also in the original microscopic model (6.5).

We are now ready to write down the dynamical mesoscopic equation of motion of our model; in the general framework of inertial dynamics (mode-coupling theories [61]), these are formed by two main contributions: the reversible and the dissipative terms. Recalling the notions of chapter 2, the former are those arising from the presence of underlying symmetries and conservation laws, namely describing a deterministic (zero temperature) dynamics for the slow fields. Here we have,

$$\frac{\partial \psi}{\partial t} = \{\psi, \mathcal{H}\} \quad (6.7)$$

$$\frac{\partial \mathbf{s}}{\partial t} = \{\mathbf{s}, \mathcal{H}\} \quad (6.8)$$

that we express for each cartesian component as:

$$\frac{\partial \psi_\alpha(x, t)}{\partial t} = \int d^d x' \frac{\delta \mathcal{H}}{\delta \psi_\beta(x')} \{\psi_\alpha(x), \psi_\beta(x')\} + \int d^d x' \frac{\delta \mathcal{H}}{\delta s_\beta(x')} \{\psi_\alpha(x), s_\beta(x')\} \quad (6.9)$$

$$\frac{\partial s_\alpha(x, t)}{\partial t} = \int d^d x' \frac{\delta \mathcal{H}}{\delta \psi_\beta(x')} \{s_\alpha(x), \psi_\beta(x')\} + \int d^d x' \frac{\delta \mathcal{H}}{\delta s_\beta(x')} \{s_\alpha(x), s_\beta(x')\} \quad (6.10)$$

with repeated indices meaning a sum over the components and $x = \mathbf{x}$ in a d dimensional space. These terms are the only reversible terms allowed when the system is considered at zero temperature. For a different T , one should consider additional terms that ensure the drifts to reproduce an equilibrium Boltzmann distribution $P \sim e^{-\mathcal{H}/T}$ (see [67] and chapter 2). However, thanks to the rotational symmetry of this case, they are zero, therefore we are not going to include them from the beginning.

The only non-zero elements of these Poisson parenthesis are those that express the spin as the infinitesimal generator of rotation of ψ , namely:

$$\{\psi_\alpha(x), s_\beta(x')\} = g_0 \epsilon_{\alpha\beta\gamma} \psi_\gamma(x') \delta^d(x - x') \quad (6.11)$$

$$\{s_\alpha(x), s_\beta(x')\} = g_0 \epsilon_{\alpha\beta\gamma} s_\gamma(x') \delta^d(x - x') \quad (6.12)$$

where $\epsilon_{\alpha\beta\gamma}$ is the Levi-Civita antisymmetric tensor and g_0 assumes the role of non-dissipative mode-coupling constant [61]. In three dimensions the resulting equations read as,

$$\frac{\partial \psi}{\partial t} = g_0 \psi \times \frac{\delta \mathcal{H}}{\delta \mathbf{s}} \quad (6.13)$$

$$\frac{\partial \mathbf{s}}{\partial t} = g_0 \psi \times \frac{\delta \mathcal{H}}{\delta \psi}, \quad (6.14)$$

conserving the same microscopic structure of the dynamics (6.3) (6.4)¹. At this point, we can add the dissipative terms that ensure the relaxation of the system to the equilibrium distribution. This step is somehow different from the microscopic counterpart since we have to include all the possible relevant terms compatible with the dynamics, we then obtain:

$$\frac{\partial \boldsymbol{\psi}}{\partial t} = -\Gamma_0 \frac{\delta \mathcal{H}}{\delta \boldsymbol{\psi}} + g_0 \boldsymbol{\psi} \times \frac{\delta \mathcal{H}}{\delta \mathbf{s}} + \boldsymbol{\theta} \quad (6.15)$$

$$\frac{\partial \mathbf{s}}{\partial t} = (\lambda_0 \nabla^2 - \eta_0) \frac{\delta \mathcal{H}}{\delta \mathbf{s}} + g_0 \boldsymbol{\psi} \times \frac{\delta \mathcal{H}}{\delta \boldsymbol{\psi}} + \boldsymbol{\zeta}, \quad (6.16)$$

where the noise correlators are chosen to have a Boltzmann-like static probability distribution, i.e.:

$$\begin{aligned} \langle \theta_\alpha(\mathbf{x}, t) \theta_\beta(\mathbf{x}', t') \rangle &= 2\Gamma_0 \delta_{\alpha\beta} \delta^{(d)}(\mathbf{x} - \mathbf{x}') \delta(t - t') \\ \langle \zeta_\alpha(\mathbf{x}, t) \zeta_\beta(\mathbf{x}', t') \rangle &= 2(\eta_0 - \lambda_0 \nabla^2) \delta_{\alpha\beta} \delta^{(d)}(\mathbf{x} - \mathbf{x}') \delta(t - t') \end{aligned} \quad (6.17)$$

It is worth noticing that the amplitudes of the noises are described by the same kinetic/transport coefficients of the equations of motion. Since the model fits in an equilibrium scenario, the Einstein relation holds and therefore connects these two quantities, reducing the number of free parameters with respect to the out-of-equilibrium case of chapter 4.

The dissipative terms are accompanied by the bare kinetic and transport coefficients: Γ_0 for the primary field $\boldsymbol{\psi}$, while η_0 and λ_0 for the spin \mathbf{s} . A relevant difference with the microscopic equations of motions (6.15)-(6.16) is that this dynamics shows two additional dissipative terms, namely $-\Gamma_0 \delta \mathcal{H} / \delta \boldsymbol{\psi}$ and $\lambda_0 \nabla^2 \delta \mathcal{H} / \delta \mathbf{s}$, which are fundamental in a hydrodynamic description of the system.

The kinetic coefficient of the first equation contains information of two kinds: first, a derivative of the confining potential $\psi^2 + \psi^4$, and second, a diffusive piece, $\Gamma_0 \nabla^2 \boldsymbol{\psi}(\mathbf{x}, t)$, which describes the role of fluctuations in the dynamical process; altogether this is the item that allows the field to relax to its stationary value. The microscopic theory of ISM can be mapped in the choice $\Gamma_0 = 0$, for which this kind of fluctuations can be considered negligible as in the low-temperature phase [90], however, they become crucial in the near-critical regime and have to be taken into account in a field theory calculation. About the role of this kinetic coefficient, we can also argue that it can be interpreted as the inverse of the characteristic bare time-scale of the order parameter. Therefore, to study a non-trivial critical dynamical behavior, the model has to start with a finite value of Γ_0 , preserving this feature also at the fixed points of the renormalized theory [64].

Definetely less intuitive is the presence of spin transport term, $\lambda_0 \nabla^2 \mathbf{s}(\mathbf{x}, t)$, which has not a microscopic counterpart in the original formulation of the ISM.

¹We reabsorbed the minus sign in front of the cross products in (6.3-6.4) into the definition of the coarse-grained dynamical coupling constant, g_0 , so to obtain in (6.15-6.16) the same field-theory notation as the classic reference papers, [74] and [102].

At the one particle level, the dynamics of the spin is ruled by dissipation, therefore one would have expected to observe in the field-theory equations only the $-\eta_0 \mathbf{s}(\mathbf{x}, t)$ contribution. Nevertheless, as we will explain in the next sections, this additional element arises spontaneously from the first RG coarse-graining step, indicating that it must be included in the starting continuous theory as a relevant term. The physical meaning of the term represented by the kinetic coefficient λ_0 is also evident if we focus on the deterministic version of eq (6.16) with also $g_0 = 0$ and $\eta_0 = 0$,

$$\frac{\partial \mathbf{s}}{\partial t} = \lambda_0 \nabla^2 \frac{\delta \mathcal{H}}{\delta \mathbf{s}} = \lambda_0 \nabla^2 \mathbf{s} . \quad (6.18)$$

This equation is nothing else than a continuity equation for the spin density that, consequently, implies a conservation law for the quantity

$$\mathbf{M} = \int d^d x \mathbf{s}(\mathbf{x}) = \text{const} \quad (6.19)$$

whose value is preserved in time. This conservation law reflects the one regarding the total spin we described for the microscopic case in absence of inter-particle interaction. Hence, we are going to refer to the dynamics depicted by this transport coefficient with the expression *conservative dynamics*. The introduction of the dissipation η_0 has the same effect as in the microscopic theory: it violates the conservation law dissipating the spin but reproducing the more realistic dynamics of biological entities. The coefficient η_0 will be then the representative of a *dissipative dynamics*.

Since the model expresses an equilibrium theory, its static properties only depend on the Hamiltonian \mathcal{H} . As we can see from (6.6), it reads as a Heisenberg model for the order parameter $\boldsymbol{\psi}$, which undergoes a phase transition when the mass assumes the value $r_0 = r_c$, plus a pure Gaussian theory for the spin [61]. This fact makes the angular momentum a non-critical field and, as a consequence, it is possible to know a priori that the inertia χ_0 does not acquire any perturbative contribution from the RG calculation. Hence, to simplify the notation, we choose the units of \mathbf{s} such that $\chi_0 = 1$. Additionally, in contrast to the Toner and Tu theory, here the equilibrium scenario in which we work allows us to take for granted all the results given by the classical theory of critical phenomena on the Heisenberg Hamiltonian, i.e. all the values of static critical exponents [51]. We will see that, since we perform a 1-loop calculation, the statics completely decouples from the critical dynamics, with the effect that the dynamical properties of the model result entirely ruled by the transport and kinetic coefficients we just introduced, and by the reversible mode-coupling terms represented by the g_0 coupling constant.

Finally, we notice that for $\eta_0 = 0$, equations (6.15) and (6.16) are exactly those of Model G (antiferromagnet in $d = 3$) or Model E (liquid Helium in $d = 2$). The dynamical RG study of these models has been performed in [74, 102] and it will be for us an important reference point in the following analysis. Indeed, we will

show that in the regime of small dissipation η_0 , our model can resemble their fully conservative critical dynamics.

6.2 MSR action and Gaussian theory

Before starting the calculation, let's briefly recall the main passages we have to follow in order to compute the dynamical critical exponent:

- write the dynamical equations of motion;
- build the MSR effective action and study the Gaussian theory;
- expand the correlation functions in powers of non-linearities (perturbative expansion);
- apply the main steps of RG to write recursion relations of the parameters and derive the critical exponents at the fixed points.

If we explicitly compute the derivatives of the Hamiltonian in eq (6.15)(6.16) we obtain the dynamical evolution for the singles cartesian component α of the fields, namely:

$$\begin{aligned}\frac{\partial \psi_\alpha}{\partial t} &= \Gamma_0 \nabla^2 \psi_\alpha - \Gamma_0 r_0 \psi_\alpha - \frac{\Gamma_0 u_0}{6} \psi_\alpha (\psi_\gamma \psi_\gamma) + g_0 \epsilon_{\alpha\beta\gamma} \psi_\beta s_\gamma + \theta_\alpha \\ \frac{\partial s_\alpha}{\partial t} &= (\lambda_0 \nabla^2 - \eta_0) s_\alpha - g_0 \epsilon_{\alpha\beta\gamma} \psi_\beta \nabla^2 \psi_\gamma + \zeta_\alpha\end{aligned}\quad (6.20)$$

The non-linearities of the theory are represented by all the terms multiplied by the static and dynamic coupling constant, u_0 and g_0 respectively. Putting them to null values is equivalent to studying the Gaussian theory.

Following the standard manipulations explained in chapter 2, and using the Fourier transforms of the fields defined as,

$$\begin{aligned}\psi_\alpha(\mathbf{x}, t) &= \int d\tilde{\mathbf{k}} e^{-i(\omega t - \mathbf{k} \cdot \mathbf{x})} \psi_\alpha(\tilde{\mathbf{k}}) \\ s_\alpha(\mathbf{x}, t) &= \int d\tilde{\mathbf{k}} e^{-i(\omega t - \mathbf{k} \cdot \mathbf{x})} s_\alpha(\tilde{\mathbf{k}})\end{aligned}\quad (6.21)$$

One can build the Martin-Siggia-Rose action from the dynamical equations of motion (6.15) (6.16),

$$\mathcal{S}[\boldsymbol{\psi}, \hat{\boldsymbol{\psi}}, \mathbf{s}, \hat{\mathbf{s}}] = \mathcal{S}_{0,\psi}[\hat{\boldsymbol{\psi}}, \boldsymbol{\psi}] + \mathcal{S}_{0,s}[\hat{\mathbf{s}}, \mathbf{s}] + \mathcal{S}_I[\boldsymbol{\psi}, \hat{\boldsymbol{\psi}}, \mathbf{s}, \hat{\mathbf{s}}] \quad . \quad (6.22)$$

With $\mathcal{S}_{0,\psi}$ and $\mathcal{S}_{0,s}$ we mean the free actions of the fields $\boldsymbol{\psi}$ and \mathbf{s} , respectively; their explicit expressions are the following

$$\mathcal{S}_{0,\psi} = \int d\tilde{\mathbf{k}} \hat{\psi}_\alpha(-\tilde{\mathbf{k}}) [-i\omega + \Gamma_0(k^2 + r_0^2)] \psi_\alpha(\tilde{\mathbf{k}}) - \Gamma_0 \hat{\psi}_\alpha(-\tilde{\mathbf{k}}) \hat{\psi}_\alpha(\tilde{\mathbf{k}})\quad (6.23)$$

$$\mathcal{S}_{0,s} = \int d\tilde{\mathbf{k}} \hat{s}_\alpha(-\tilde{\mathbf{k}}) [-i\omega + (\eta_0 + \lambda_0 k^2)] s_\alpha(\tilde{\mathbf{k}}) - (\eta_0 + \lambda_0 k^2) \hat{s}_\alpha(-\tilde{\mathbf{k}}) \hat{s}_\alpha(\tilde{\mathbf{k}}) \quad (6.24)$$

where repeated indices are summed as usual. The interaction part of the effective action involves non linear contributions of the dynamics, including mixed terms of both \mathbf{s} , $\hat{\mathbf{s}}$ and $\boldsymbol{\psi}$, $\hat{\boldsymbol{\psi}}$ and it is given by:

$$\begin{aligned} \mathcal{S}_I = & -\frac{g_0}{2} \epsilon_{\alpha\beta\gamma} \int d\tilde{\mathbf{k}}_1 d\tilde{\mathbf{k}}_2 (k_2^2 - k_1^2) \psi_\gamma(\tilde{\mathbf{k}}_2) \psi_\beta(\tilde{\mathbf{k}}_1) \hat{s}_\alpha(-\tilde{\mathbf{k}}_1 - \tilde{\mathbf{k}}_2) \\ & -g_0 \epsilon_{\alpha\beta\gamma} \int d\tilde{\mathbf{k}}_1 d\tilde{\mathbf{k}}_2 \hat{\psi}_\alpha(\tilde{\mathbf{k}}_1) \psi_\beta(\tilde{\mathbf{k}}_2) s_\gamma(-\tilde{\mathbf{k}}_1 - \tilde{\mathbf{k}}_2) \\ & -\frac{\Gamma_0 u_0}{6} \int d\tilde{\mathbf{k}}_1 d\tilde{\mathbf{k}}_2 d\tilde{\mathbf{k}}_3 \hat{\psi}_\alpha(\tilde{\mathbf{k}}_1) \psi_\alpha(\tilde{\mathbf{k}}_2) \psi_\beta(\tilde{\mathbf{k}}_3) \\ & \psi_\beta(-\tilde{\mathbf{k}}_1 - \tilde{\mathbf{k}}_2 - \tilde{\mathbf{k}}_3) . \end{aligned} \quad (6.25)$$

From the free part of the action (6.23)(6.24) it is easy to read the expressions for the bare propagators and correlation functions for the effective field theory:

$$\langle \psi_\alpha(-\tilde{\mathbf{k}}) \hat{\psi}_\beta(\tilde{\mathbf{k}}) \rangle = \delta_{\alpha\beta} G_{0,\psi}(\tilde{\mathbf{k}}) = \delta_{\alpha\beta} [-i\omega + \Gamma_0(k^2 + r_0)]^{-1} \quad (6.26)$$

$$\langle \psi_\alpha(-\tilde{\mathbf{k}}) \psi_\beta(\tilde{\mathbf{k}}) \rangle = \delta_{\alpha\beta} C_{0,\psi}(\tilde{\mathbf{k}}) = 2\delta_{\alpha\beta} \Gamma_0 |G_{0,\psi}|^2 \quad (6.27)$$

$$\langle s_\alpha(-\tilde{\mathbf{k}}) \hat{s}_\beta(\tilde{\mathbf{k}}) \rangle = \delta_{\alpha\beta} G_{0,s}(\tilde{\mathbf{k}}) = \delta_{\alpha\beta} [-i\omega + (\eta_0 + \lambda_0 k^2)]^{-1} \quad (6.28)$$

$$\langle s_\alpha(-\tilde{\mathbf{k}}) s_\beta(\tilde{\mathbf{k}}) \rangle = \delta_{\alpha\beta} C_{0,s}(\tilde{\mathbf{k}}) = 2\delta_{\alpha\beta} (\eta_0 + \lambda_0 k^2) |G_{0,s}|^2 \quad (6.29)$$

Additionally, one could find directly the same quantities starting from eq (6.15) (6.16) and setting to zero the non-linear coupling constants, namely $g_0 = 0$ and $u_0 = 0$. In this way one recovers only the linear dynamical evolution that can be solved with the Green function method in Fourier space. The free equations of motion become,

$$-i\omega \boldsymbol{\psi}(\tilde{\mathbf{k}}) = -\Gamma_0(k^2 + r_0) \boldsymbol{\psi}(\tilde{\mathbf{k}}) + \boldsymbol{\theta}(\tilde{\mathbf{k}}) \quad (6.30)$$

$$-i\omega \mathbf{s}(\tilde{\mathbf{k}}) = -(\eta_0 + \lambda_0 k^2) \mathbf{s}(\tilde{\mathbf{k}}) + \boldsymbol{\zeta}(\tilde{\mathbf{k}}) . \quad (6.31)$$

Therefore inverting (6.30) and (6.31), one obtains:

$$\boldsymbol{\psi}(\tilde{\mathbf{k}}) = G_{0,\psi}(\tilde{\mathbf{k}}) \boldsymbol{\theta}(\tilde{\mathbf{k}}) \quad (6.32)$$

$$\mathbf{s}(\tilde{\mathbf{k}}) = G_{0,s}(\tilde{\mathbf{k}}) \boldsymbol{\zeta}(\tilde{\mathbf{k}}) , \quad (6.33)$$

where the free propagators (or Green functions) are the inverse of the dynamical operators in Fourier space, of course coinciding with(6.26) (6.28):

$$G_{0,\psi}^{-1}(\tilde{\mathbf{k}}) = -i\omega + \Gamma_0(k^2 + r_0) \quad (6.34)$$

$$G_{0,s}^{-1}(\tilde{\mathbf{k}}) = -i\omega + (\eta_0 + \lambda_0 k^2) . \quad (6.35)$$

By using (6.32) and (6.33), and the noise's variances (6.17), we finally get an explicit expression for the correlators,

$$C_{0,\psi} = 2\Gamma_0 |G_{0,\psi}|^2 = \frac{2\Gamma_0}{\omega^2 + \Gamma_0^2(k^2 + r_0)^2} \quad (6.36)$$

$$C_{0,s} = 2(\eta_0 + \lambda_0 k^2) |G_{0,s}|^2 = \frac{2(\eta_0 + \lambda_0 k^2)}{\omega^2 + (\eta_0 + \lambda_0 k^2)^2}. \quad (6.37)$$

These four quantities, propagators and correlators, are the building blocks of the perturbative expansion.

6.3 Vertices and perturbative expansion

From the expression of the interacting part of the action, we see that there are two types of dynamical vertices. Those coming from the mode-coupling dynamics,

$$V_1 = \begin{array}{c} \hat{\psi}_\alpha \\ \nearrow \\ s_\gamma \text{ (wavy)} \\ \bullet \\ \searrow \\ \psi_\beta \end{array} = -g_0 \epsilon_{\alpha\beta\gamma} s_\gamma(\tilde{\mathbf{k}}_1) \hat{\psi}_\alpha(\tilde{\mathbf{k}}_2) \psi_\beta(-\tilde{\mathbf{k}}_1 - \tilde{\mathbf{k}}_2) \quad (6.38)$$

$$V_2 = \begin{array}{c} \psi_\gamma \\ \nearrow \\ \hat{s}_\alpha \text{ (wavy)} \\ \bullet \\ \searrow \\ \psi_\beta \end{array} = -\frac{g_0}{2} \epsilon_{\alpha\beta\gamma} (k_2^2 - k_1^2) \psi_\beta(\tilde{\mathbf{k}}_1) \psi_\gamma(\tilde{\mathbf{k}}_2) \hat{s}_\alpha(-\tilde{\mathbf{k}}_2 - \tilde{\mathbf{k}}_1) \quad (6.39)$$

and one static vertex, i.e. proportional to the static coupling constant u_0 :

$$V_3 = \begin{array}{c} \psi_\alpha \\ \nearrow \\ \hat{\psi}_\alpha \text{ (solid)} \\ \bullet \\ \searrow \\ \psi_\beta \end{array} = -\frac{\Gamma_0 u_0}{6} \hat{\psi}_\alpha(\tilde{\mathbf{k}}_1) \psi_\alpha(\tilde{\mathbf{k}}_2) \psi_\beta(\tilde{\mathbf{k}}_3) \psi_\beta(-\tilde{\mathbf{k}}_1 - \tilde{\mathbf{k}}_2 - \tilde{\mathbf{k}}_3) \quad (6.40)$$

In these graphs, we are indicating with a solid line the fields $\boldsymbol{\psi}$, $\hat{\boldsymbol{\psi}}$, and with wavy lines the fields \mathbf{s} , $\hat{\mathbf{s}}$. Moreover, the representation of the response fields includes an arrow entering the vertex.

At this level, we can notice that the second vertex carries with it a factor $(k_2^2 - k_1^2)$. This is a consequence of the symmetry of the non-linearity of the spin equation (6.16), indeed this mode-coupling term can be rewritten as $-(g_0/2)\epsilon_{\alpha\beta\gamma}(\psi_\beta\nabla^2\psi_\gamma - \psi_\gamma\nabla^2\psi_\beta)$ giving rise to this difference of momenta when in k -space. A practical implication is that every Feynman diagram realized with this vertex and evaluated for $\hat{\mathbf{s}}(\mathbf{k} = 0, \omega)$ is null.

These vertices can now be used to analytically compute a perturbative expansion in the coupling constants around the Gaussian theory. The leftover of this procedure is composed of terms that involve only free propagators and free correlators which are connected through the interaction vertices. To complete the tools we are going to use, it is necessary to assign to each of these bare quantities graphic symbols. We represent propagators with bold or wavy lines with an arrow to reflect the fact that, because of the response fields, they are time-ordered, while the correlators only with simple lines.

$$G_{0,\psi_{\alpha,\beta}} = \text{bold arrow}; \quad C_{0,\psi_{\alpha,\beta}} = \text{simple line} \quad (6.41)$$

$$G_{0,s_{\alpha,\beta}} = \text{bold wavy arrow}; \quad C_{0,\psi_{\alpha,\beta}} = \text{wavy line} \quad (6.42)$$

Finally, from a power counting analysis in the effective action, it is possible to deduce that the parameters g_0 and $\Gamma_0 u_0$ are irrelevant for $d > 4$, thus recovering a mean-field behavior. Therefore the real parameter of expansion can be assumed to be $\epsilon = 4 - d$ as in standard critical phenomena [12]. Moreover, the terms of the expansion that we are going to take into consideration are at first order in ϵ (1-loop).

The first manifestation of this expansion appears with corrections in the expression of the free propagators that we call self-energies. In this model, they are respectively two: one for the field ψ and one for the field \mathbf{s} . The inverse of renormalized propagators can be then defined using the Dyson equation [51] that involves these quantities:

$$G_\psi^{-1}(\tilde{\mathbf{k}})_{\alpha\beta} = G_{0,\psi}^{-1}(\tilde{\mathbf{k}})\delta_{\alpha\beta} - \Sigma_{\alpha\beta}(\tilde{\mathbf{k}}) \quad (6.43)$$

$$G_s^{-1}(\tilde{\mathbf{k}})_{\alpha\beta} = G_{0,s}^{-1}(\tilde{\mathbf{k}})\delta_{\alpha\beta} - \Pi_{\alpha\beta}(\tilde{\mathbf{k}}) \quad (6.44)$$

Σ and Π are the self-energies of the order parameter and of the spin, respectively, and to which we can attribute also a graphical representation:

$$\Sigma_{\alpha\beta} = \hat{\psi}_\alpha \text{ bold arrow } \rightarrow \text{blob} \text{ --- } \psi_\beta \quad (6.45)$$

$$\Pi_{\alpha\beta} = s_\alpha \text{ bold wavy arrow } \rightarrow \text{blob} \text{ --- } s_\beta \quad (6.46)$$

Also here the blobs indicate the sum of all 1PI diagrams with amputated external

legs that take part in the expansion with an incoming $\hat{\psi}$ (or $\hat{\mathbf{s}}$) field and an outgoing ψ (or \mathbf{s}) field; we are going to explicitly compute them in the next section.

Before going on, it is important to highlight a fundamental difference with the out-of-equilibrium case we analyzed in the previous chapters. Also in this context, the Gaussian part of the effective action is not composed only by the $\hat{\psi}\psi$ and $\hat{\mathbf{s}}\mathbf{s}$ parts that take corrections from the perturbative expansion via (6.43) (6.44), but also by the terms coming from the noise's distribution integration, namely $\hat{\psi}\hat{\psi}$ and $\hat{\mathbf{s}}\hat{\mathbf{s}}$. Hence, we should take into account the self energies also for the noise strengths:

$$\tilde{\Sigma}_{\alpha\beta} = \begin{array}{c} \text{---} \hat{\psi}_\alpha \text{---} \text{---} \text{---} \hat{\psi}_\beta \text{---} \\ \text{---} \text{---} \text{---} \text{---} \text{---} \text{---} \end{array} \quad (6.47)$$

$$\tilde{\Pi}_{\alpha\beta} = \begin{array}{c} \text{---} \hat{\mathbf{s}}_\alpha \text{---} \text{---} \text{---} \hat{\mathbf{s}}_\beta \text{---} \\ \text{---} \text{---} \text{---} \text{---} \text{---} \text{---} \end{array} \quad (6.48)$$

which correct respectively the amplitude of the noise Γ_0 and $\eta_0 + \lambda_0 k^2$ through the proper Dyson equations. However, we can skip this part of calculation since the contributions coming from the tilde self-energies have to be identical to those computed using (6.45) (6.46): we are at equilibrium and the Einstein relations must hold.

6.4 Renormalization of the parameters

The coarse-graining is the first stage of RG, which we recall consists of integrating out the short-wavelength fluctuations of the system, namely the modes in the shell $\Lambda/b < k < \Lambda$. It has to be performed through perturbative expansion whose result is not harmless when non-linear interactions are taken into account. The resulting effective theory is characterized by additional terms in the equations of motion and consequently in the propagators, with the effect to renormalize the coefficients both of the linear and non-linear terms [51].

This renormalization procedure starts with the self-energies of eq. (6.43) (6.44) for which we can give a diagrammatic and an analytical expression. Diagrammatically, at one loop level, we have:

$$\Sigma_{\alpha\beta} = \begin{array}{c} \text{---} \hat{\psi}_\alpha \text{---} \text{---} \text{---} \hat{\psi}_\beta \text{---} \\ \text{---} \text{---} \text{---} \text{---} \text{---} \text{---} \end{array} = \begin{array}{c} \text{---} \text{---} \text{---} \text{---} \text{---} \text{---} \\ \text{---} \text{---} \text{---} \text{---} \text{---} \text{---} \end{array} + \begin{array}{c} \text{---} \text{---} \text{---} \text{---} \text{---} \text{---} \\ \text{---} \text{---} \text{---} \text{---} \text{---} \text{---} \end{array} \quad (6.49)$$

$$\Pi_{\alpha\beta} = \begin{array}{c} \text{---} \hat{\mathbf{s}}_\alpha \text{---} \text{---} \text{---} \hat{\mathbf{s}}_\beta \text{---} \\ \text{---} \text{---} \text{---} \text{---} \text{---} \text{---} \end{array} = \begin{array}{c} \text{---} \text{---} \text{---} \text{---} \text{---} \text{---} \\ \text{---} \text{---} \text{---} \text{---} \text{---} \text{---} \end{array} \quad (6.50)$$

where external legs have to be considered amputated. Their respective analytical

expressions read:

$$\begin{aligned} \Sigma_{\alpha\beta}(\tilde{\mathbf{k}}) = & -2g_0^2\delta_{\alpha\beta} \int d\tilde{\mathbf{p}} \left[G_{0,\psi}(\tilde{\mathbf{p}})C_{0,s}(\tilde{\mathbf{k}} - \tilde{\mathbf{p}}) \right. \\ & \left. + (k^2 - p^2)C_{0,\psi}(\tilde{\mathbf{p}})G_{0,s}(\tilde{\mathbf{k}} - \tilde{\mathbf{p}}) \right] \end{aligned} \quad (6.51)$$

$$\Pi_{\alpha\beta}(\tilde{\mathbf{k}}) = -2g_0^2\delta_{\alpha\beta} \int d\tilde{\mathbf{p}} \left[C_{0,\psi}(\tilde{\mathbf{p}})G_{0,\psi}(\tilde{\mathbf{k}} - \tilde{\mathbf{p}})((\mathbf{k} - \mathbf{p})^2 - p^2) \right] \quad (6.52)$$

Performing the frequency integration, whose range is between $-\infty$ and $+\infty$, we get the following expressions:

$$\Sigma_{\alpha\beta}(\tilde{\mathbf{k}}) = -2g_0^2\delta_{\alpha\beta} \int \frac{d^d p}{(2\pi)^d} \frac{(k^2 + r_0)}{(p^2 + r_0)(-i\omega + \Gamma_0(p^2 + r_0) + \lambda_0(\mathbf{k} - \mathbf{p})^2 + \eta_0)} \quad (6.53)$$

$$\Pi_{\alpha\beta}(\tilde{\mathbf{k}}) = -g_0^2\delta_{\alpha\beta} \int \frac{d^d p}{(2\pi)^d} \frac{1}{(p^2 + r_0)((\mathbf{k} - \mathbf{p})^2 + r_0)} \frac{[p^2 - (\mathbf{k} - \mathbf{p})^2]^2}{(-i\omega + \Gamma_0(p^2 + (\mathbf{k} - \mathbf{p})^2 + 2r_0))} \quad (6.54)$$

We can appreciate that these quantities have only diagonal non-zero contributions for $\alpha = \beta$. We can therefore neglect the coordinate index and indicate them simply as Σ_b and Π_b to highlight that the integrals over the momentum are performed on the shell between Λ/b and Λ . Inserting these expressions in the propagators (6.43) (6.44), we can derive the corrections to the kinetic coefficients of the linear part of the dynamics, namely:

$$\Gamma_R \equiv \left. \frac{\partial G_\psi^{-1}}{\partial k^2} \right|_{\substack{k=0 \\ \omega=0}} = \Gamma_0 \left(1 - \frac{1}{\Gamma_0} \left. \frac{\partial \Sigma_b}{\partial k^2} \right|_{\substack{k=0 \\ \omega=0}} \right) \quad (6.55)$$

$$\lambda_R \equiv \left. \frac{\partial G_s^{-1}}{\partial k^2} \right|_{\substack{k=0 \\ \omega=0}} = \lambda_0 \left(1 - \frac{1}{\lambda_0} \left. \frac{\partial \Pi_b}{\partial k^2} \right|_{\substack{k=0 \\ \omega=0}} \right) \quad (6.56)$$

$$\eta_R \equiv \left. G_s^{-1} \right|_{\substack{k=0 \\ \omega=0}} = \eta_0 \left(1 - \frac{1}{\eta_0} \left. \Pi_b \right|_{\substack{k=0 \\ \omega=0}} \right). \quad (6.57)$$

Moreover, one could compute the same quantities looking at the corrections of

the noise amplitudes and using the self-energies (6.47) and (6.48):

$$\Gamma_R = \Gamma_0 \left(1 + \frac{1}{2\Gamma_0} \tilde{\Sigma}_b \Big|_{\substack{k=0 \\ \omega=0}} \right) \quad (6.58)$$

$$\lambda_R = \lambda_0 \left(1 + \frac{1}{2\lambda_0} \frac{\partial \tilde{\Pi}_b}{\partial k^2} \Big|_{\substack{k=0 \\ \omega=0}} \right) \quad (6.59)$$

$$\eta_R = \eta_0 \left(1 + \frac{1}{2\eta_0} \tilde{\Pi}_b \Big|_{\substack{k=0 \\ \omega=0}} \right) . \quad (6.60)$$

since the validity of FDT and of Einstein relation implies:

$$\begin{aligned} \frac{\partial \Sigma_b}{\partial k^2} \Big|_{\substack{k=0 \\ \omega=0}} &= -\frac{1}{2} \tilde{\Sigma}_b \Big|_{\substack{k=0 \\ \omega=0}} \\ \frac{\partial \Pi_b}{\partial k^2} \Big|_{\substack{k=0 \\ \omega=0}} &= -\frac{1}{2} \frac{\partial \tilde{\Pi}_b}{\partial k^2} \Big|_{\substack{k=0 \\ \omega=0}} \\ \Pi_b \Big|_{\substack{k=0 \\ \omega=0}} &= -\frac{1}{2} \tilde{\Pi}_b \Big|_{\substack{k=0 \\ \omega=0}} \end{aligned} \quad (6.61)$$

At this point, the reader could have noticed that we introduced three non-linear vertices for the expansion, but we used only the ones coming entirely from the dynamics (i.e. proportional to g_0) to construct the Σ and Π self-energies. If on the one hand, it is clear that no diagrams involving (6.40) are possible to contribute to Π , one can see that to Σ only the following one-loop diagram can be added:

$$\begin{array}{c} \text{---} \blacktriangleright \text{---} \\ \text{---} \text{---} \text{---} \end{array} \quad = -\frac{\Gamma_0 u_0}{6} \delta_{\alpha\beta} \left[\frac{\Lambda^2}{2} \left(1 - \frac{1}{b^2} \right) - r_0 \ln b \right] \quad (6.62)$$

However, from the direct inspection one can see that it is independent of the external momentum \mathbf{k} , therefore it does not account for corrections for the dynamical quantity Γ_0 but only for the mass r_0 . However, the evolution along RG of this latter quantity follows the standard static path [12, 13] and therefore we are not going to report it here. On the other hand, we are going to deal only with dynamical parameters substituting to the bare mass r_0 its renormalized value $r = 0$, so that we evaluate all the integrals at the critical point, increasing the accuracy of the expansion.

The expressions of the kinetic coefficients finally appear:

$$\Gamma_R = \Gamma_0 \left[1 + 2 \frac{g_0^2}{\Gamma_0} \int_{\Lambda/b}^{\Lambda} \frac{d^d p}{(2\pi)^d} \frac{1}{p^2 [(\Gamma_0 + \lambda_0)p^2 + \eta_0]} \right] \quad (6.63)$$

$$\lambda_R = \lambda_0 \left[1 + \frac{1}{2} \frac{g_0^2}{\Gamma_0 \lambda_0} \int_{\Lambda/b}^{\Lambda} \frac{d^d p}{(2\pi)^d} \frac{1}{p^4} \right] \quad (6.64)$$

$$\eta_R = \eta_0 \quad (6.65)$$

from which we deduce that the effective friction η does not get any correction from the step of coarse-graining. This means that, if the spin's dissipation is present at the microscopic scale, then the RG will follow its flow (that we will see it is going to diverge). On the contrary, if the theory presents a null value $\eta_0 = 0$ at a bare level, the RG will not produce it through shell integration. Therefore, the presence in the theory of this effective friction is completely determined at a microscopic level, and it is more linked to biological motivations than to physical processes. Analytically, this happens because $\Pi_b(k = 0) = 0$, which is a consequence of the structure of the spin's mode-coupling vertex necessary to build the Π . We mentioned this particular feature when introducing (6.39) in the theory. We can then assert that this result is valid at every order of perturbation and it can be interpreted as a manifestation of the strength of symmetry law that rules the system.

Different is the situation for the conservative kinetic coefficient λ_0 . After one step of integration over short wavelengths, a λ_R is inevitably produced, even if the original transport coefficient were $\lambda_0 = 0$, thus absent in the microscopic theory. The fact that the RG structure produces itself a relevant correction of the type $\partial\Pi/\partial k^2$ directly entails that a similar term has to be inserted in the original coarse-grained theory from the beginning of the calculation. The scenario is therefore opposite to that of the friction η and highlights that the *natural* way of the theory to have equilibrium fluctuations is a conservative way.

We can now perform the integrals (6.63) (6.64), however it is convenient to rewrite the first of them as:

$$\Gamma_R = \Gamma_0 \left[1 + 2 \frac{g_0^2}{\Gamma_0(\Gamma_0 + \lambda_0)} \int_{\Lambda/b}^{\Lambda} \frac{d^d p}{(2\pi)^d} \frac{1}{p^2 \left(p^2 + \frac{\eta_0}{\Gamma_0 + \lambda_0} \right)} \right]. \quad (6.66)$$

changing variables with $p = \Lambda x$, we obtain,

$$\Gamma_R = \Gamma_0 \left[1 + 2 \frac{g_0^2 \Lambda^{d-4}}{\Gamma_0 \lambda_0 \left(1 + \frac{\Gamma_0}{\lambda_0} \right)} \int_{1/b}^1 \frac{d^d x}{(2\pi)^d} \frac{1}{x^2 \left(x^2 + \frac{\eta_0}{\lambda_0} \frac{\Lambda^{-2}}{1 + \Gamma_0/\lambda_0} \right)} \right] \quad (6.67)$$

$$\lambda_R = \lambda_0 \left[1 + \frac{1}{2} \frac{g_0^2 \Lambda^{d-4}}{\Gamma_0 \lambda_0} \frac{4}{d} \int_{1/b}^1 \frac{d^d x}{(2\pi)^d} \frac{1}{x^4} \right], \quad (6.68)$$

To simplify these expressions, we can define a set of effective parameters to indicate the prefactors of the perturbative corrections,

$$f_0 = \frac{g_0^2}{\lambda_0 \Gamma_0} K_d \Lambda^{d-4}, \quad w_0 = \frac{\Gamma_0}{\lambda_0}, \quad \mathcal{R}_0 = \sqrt{\frac{\lambda_0}{\eta_0}}, \quad (6.69)$$

where K_d is the unit sphere volume in dimension d . To compute the integrals we use the fact that in the limit $b \rightarrow 1$, indicating an infinitesimal RG transformation, the shell becomes infinitesimal, namely of thickness $1 - 1/b \sim \log b$. Therefore the result of the integral are expressed by this last factor times the integrating

function evaluated at $x = 1$. The three kinetic parameters read,

$$\begin{aligned}\Gamma_R &= \Gamma_0 \left[1 + \frac{2f_0}{1+w_0} \int_{1/b}^1 \frac{d^d x}{x^2} \frac{1}{x^2 + (\mathcal{R}_0\Lambda)^{-2}(1+w_0)^{-1}} \right] \\ &= \Gamma_0 \left[1 + \frac{2f_0}{1+w_0} X_0 \log b \right]\end{aligned}\tag{6.70}$$

$$\lambda_R = \lambda_0 \left[1 + \frac{f_0}{2} \int_{1/b}^1 \frac{d^d x}{x^4} \right] = \lambda_0 \left[1 + \frac{1}{2} f_0 \log b \right]\tag{6.71}$$

$$\eta_R = \eta_0 ,\tag{6.72}$$

In the expression of Γ_R , we introduced the crossover parameter X_0 ,

$$X_0 = \frac{(\mathcal{R}_0\Lambda)^2(1+w_0)}{1 + (\mathcal{R}_0\Lambda)^2(1+w_0)} ,\tag{6.73}$$

which happens to be dimensionless as also the parameter w_0 , but will play a fundamental role in the critical dynamics of the system. The quantity w_0 does not play a real crucial role in the following analysis, in the sense that it represents a useful way to condensate notation, it is finite or null at the fixed points, but no relevant physical information can be extrapolated directly from it [61]. The combination of dynamical parameters f_0 , instead, plays one of the principal roles in the RG calculation. First, it can be noticed that it is proportional to Λ^{d-4} and this suggests its scaling dimension to be $\epsilon = 4 - d$. As we already learned, this fact represents a feature which usually belongs with the real coupling constant of an RG calculation and indeed, f_0 assumes the role of *dynamical coupling constant* of our study: the perturbative expansion is not performed in simple powers of g_0 but rather in a combination of g_0^2 and the other dynamical coefficients.

Finally, we have to comment on the last term of (6.69). \mathcal{R}_0 is given by the ratio between the transport coefficient of the spin and its effective friction. A dimensional analysis reveals that it is a length scale that we can interpret as a measure of the spatial scale under which a conservative dynamics dominates over a dissipative dynamics. Hence, we are going to refer to it as *conservation length scale*. It contains all the information about the interplay between the two different regimes of dynamics that are included in our theory and that will compete in a non-trivial crossover mechanism. To give a small insight of this, we can analyze two opposite limits staying superficially at a bare level: the first one is for $\mathcal{R}_0 = \infty$ that happens when $\eta_0 = 0$. The crossover factor becomes $X_0 = 1$ and the equations reduce to those of the fully conservative Model G [61], describing a scenario where all the system is included in this conservation length scale. On the other hand, when the friction is very large, \mathcal{R}_0 can shrink to zero together with the crossover factor $X_0 \sim 0$, with the consequence that the kinetic coefficient Γ_0 assumes very weak perturbative corrections and the dynamics of ψ becomes purely dissipative.

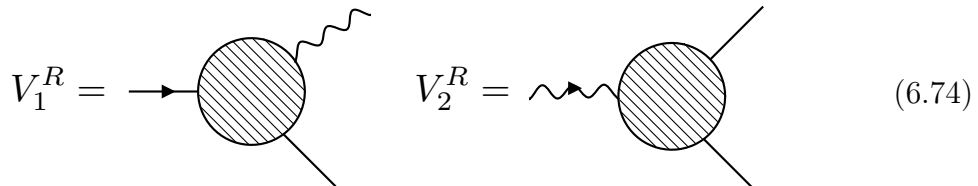
Just following these considerations we can understand how the emergence of a new typical length scale of the system will determine its non-trivial dynamical

large-scale behavior. It is common to discover these particular scenarios characterized by mechanisms of crossover when the problem involves new relevant length scales in addition to the correlation length ξ [103, 104]. This is indeed what we are going to explore in the next sections.

6.5 Vertices corrections and Ward identities

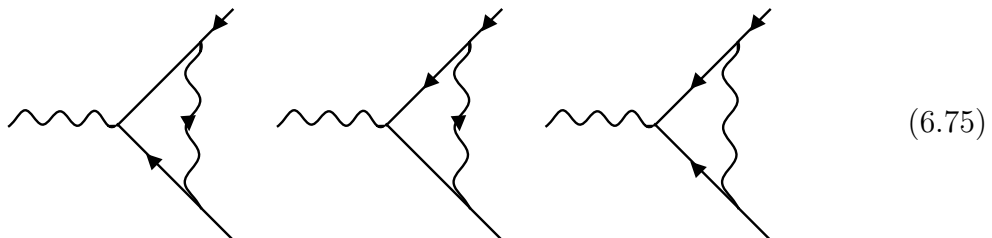
Until now we computed corrections only for the dynamical parameters belonging to the Gaussian part of the action. However, we should also evaluate the Feynman diagrams related to the mode-coupling constant g_0 and to the ferromagnetic coupling constant u_0 , in order to analyze their renormalization under coarse-graining.

Let's start from the latter, u_0 is a parameter of the effective Hamiltonian, therefore, as we did for the mass r_0 , it can be considered a pure static parameter, such that all the knowledge from the standard static RG can be directly applied to it [12, 13]. On the other hand, the renormalization of the dynamical coupling constant is not at all trivial and it deserves some attention. It appears in both the mode-coupling vertices (6.38) (6.39), whose perturbative corrections can be computed as,



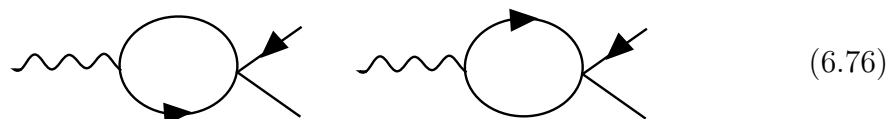
The diagram shows two Feynman diagrams representing the renormalized vertices V_1^R and V_2^R . V_1^R is represented by a shaded circle with a horizontal arrow pointing into it from the left and a diagonal arrow pointing out of it to the bottom-right. V_2^R is represented by a shaded circle with a wavy arrow pointing into it from the left and a diagonal arrow pointing out of it to the bottom-right. The equations are labeled (6.74).

The diagrams that contribute to the correction of the vertex V_1 of the dynamical equation of the order parameter are,



The diagram shows three Feynman diagrams representing corrections to the vertex V_1 . Each diagram features a wavy arrow entering from the left and two diagonal arrows exiting to the right. The first diagram has a loop with a wavy line and a diagonal line. The second diagram has a loop with a wavy line and a diagonal line, with an additional wavy line connecting the two vertices. The third diagram has a loop with a wavy line and a diagonal line, with an additional diagonal line connecting the two vertices. The equations are labeled (6.75).

together with the ones coming from the use of the static vertex V_3 ,



The diagram shows two Feynman diagrams representing corrections to the static vertex V_3 . Each diagram features a wavy arrow entering from the left and two diagonal arrows exiting to the right. The first diagram has a loop with a wavy line and a diagonal line. The second diagram has a loop with a wavy line and a diagonal line, with an additional wavy line connecting the two vertices. The equations are labeled (6.76).

While those contributing to the vertex V_2^R of the spin's equation appear,

(6.77)

From a direct calculation of the integrals they represent, it can be shown that all these corrections are null. It is reasonable to believe that this does not happen by chance or because of the one-loop approximation. In fact, this stands as a non-perturbative result and it is a direct manifestation of the rotational symmetry that characterizes the problem. This result has been proved to be valid in the fully conservative case [74, 102], here we show that it is valuable also including the spin dissipation as we did in our model. The proof comes by the use of the Ward identities that, in the dynamical case, relate response functions of different order [102].

The spin is the generator of the rotational symmetry of the order parameter $\boldsymbol{\psi}$, therefore in absence of dissipation, its total integral is preserved. If we stay for a moment in this case and we imagine applying a homogenous field $\mathbf{H}(t)$ coupled to the spin, the dynamics for the global polarization in an equilibrium state results,

$$\frac{d\langle\boldsymbol{\Phi}\rangle}{dt} = g_0\mathbf{H} \times \langle\boldsymbol{\Psi}\rangle, \quad (6.78)$$

i.e. the effect of this perturbation, as we could have expected, is to simply rotate the polarization. In the more complex situation where we add an additional magnetic field $\mathbf{h}(\mathbf{x}, t)$ coupled to the order parameter, the outcome is that it produces a space-dependent and local polarization $\langle\boldsymbol{\psi}(\mathbf{x}, t)\rangle$ that it is still rotated by \mathbf{H} . If then we consider also a friction acting on the spin, we obtain

$$\frac{d\langle\delta\boldsymbol{\psi}(\mathbf{x}, t)\rangle}{dt} = g_0(\mathbf{H}(t) - \delta\mathbf{s}(t)) \times \langle\boldsymbol{\psi}(\mathbf{x}, t)\rangle \quad (6.79)$$

$$\frac{d\langle\delta\mathbf{s}(t)\rangle}{dt} = -\eta_0\delta\mathbf{s}(t) + \eta_0\mathbf{H}(t) \quad (6.80)$$

where $\delta\mathbf{s}$ is the change of spin per volume due to the dissipation, and where we are considering only the part of the dynamics which changes when both of the fields are applied. The total integral of the spin is not conserved anymore and its variation influences with a further contribution the rotational frequency of the

order parameter. We can now integrate over time the equations, so that,

$$\langle \delta\psi_\alpha(\mathbf{x}, t) \rangle = g_0 \epsilon_{\alpha\beta\gamma} \int_0^t dt'' \langle \psi_\gamma(\mathbf{x}, t'') \rangle [H_\beta(t'') - \eta_0 \int_0^{t''} dt' e^{-\eta_0(t''-t')} H_\beta(t')] \quad (6.81)$$

The average value of the order parameter in the l.h.s. still depends on \mathbf{h} , therefore, deriving with respect to it the entire equation, we get,

$$\begin{aligned} \left. \frac{d\langle \delta\psi_\alpha(\mathbf{x}, t) \rangle}{dh_\delta(\mathbf{x}_1, t_1)} \right|_{h=0} &= g_0 \epsilon_{\alpha\beta\gamma} \int_0^t dt'' H_\beta(t'') \\ &\times \left[R_{\gamma\delta}^h(\mathbf{x}, t''; \mathbf{x}_1, t_1) - \eta_0 \int_{t''}^t dt' e^{-\eta_0(t'-t'')} R_{\gamma\delta}^h(\mathbf{x}, t'; \mathbf{x}_1, t_1) \right] \end{aligned} \quad (6.82)$$

where we are renaming integration variables for convenience and we are indicating the linear response of the order parameter with:

$$R_{\gamma\delta}^h(\mathbf{x}, t; \mathbf{x}_1, t_1) = \left. \frac{\delta\langle \psi_\gamma(\mathbf{x}, t) \rangle}{\delta h_\delta(\mathbf{x}_1, t_1)} \right|_{h, H=0} \quad (6.83)$$

Exploiting further this relation, the l.h.s. of (6.82) can also be written as

$$\left. \frac{d\langle \delta\psi_\alpha(\mathbf{x}, t) \rangle}{dh_\delta(\mathbf{x}_1, t_1)} \right|_{h=0} = \int_0^t dt'' d\mathbf{x}'' H_\beta(t'') R_{\alpha\beta\delta}^{hH}(\mathbf{x}, t; \mathbf{x}_1, t_1; \mathbf{x}'', t'') , \quad (6.84)$$

where now

$$R_{\alpha\beta\delta}^{hH}(\mathbf{x}, t; \mathbf{x}_1, t_1; \mathbf{x}'', t'') = \left. \frac{\delta^2\langle \psi_\alpha(\mathbf{x}, t) \rangle}{\delta h_\delta(\mathbf{x}_1, t_1) \delta H_\beta(\mathbf{x}'', t'')} \right|_{h, H=0} \quad (6.85)$$

is the non-linear quadratic response coupled also to the field acting on the spin. Comparing the r.h.s. of (6.82) and (6.84), we finally obtain

$$\begin{aligned} \int d\mathbf{x}'' R_{\alpha\beta\delta}^{hH}(\mathbf{x}, t; \mathbf{x}_1, t_1; \mathbf{x}'', t'') &= g_0 \epsilon_{\alpha\beta\gamma} \left[R_{\gamma\delta}^h(\mathbf{x}, t''; \mathbf{x}_1, t_1) \right. \\ &\quad \left. - \eta_0 \int_{t''}^t dt' e^{-\eta_0(t'-t'')} R_{\gamma\delta}^h(\mathbf{x}, t'; \mathbf{x}_1, t_1) \right] \end{aligned} \quad (6.86)$$

with $t_1 < t'' < t$, otherwise it is zero. We notice that considering $\eta_0 = 0$ eq (6.86) corresponds to the Ward identity of Model E in [74]. This result is crucial to deduce some information about the renormalization of the mode-coupling constant g_0 , indeed it has been derived without any approximation or expansion; consequently, it has to be preserved at any order of RG calculation. To better understand this fact, let's consider the case $\eta_0 = 0$, from which a generalization for non-zero effective friction can easily follow. If we rewrite eq (6.86) as,

$$\int d\mathbf{x}'' \frac{\delta}{\delta H_\beta(\mathbf{x}'', t'')} R_{\alpha\delta}^h(\mathbf{x}, t; \mathbf{x}_1, t_1) = g_0 \epsilon_{\alpha\beta\gamma} R_{\gamma\delta}^h(\mathbf{x}, t''; \mathbf{x}_1, t_1) \quad (6.87)$$

it is clear that, when we want to consider the perturbative corrections coming from RG to this formula, we need to compute the renormalized version of both the response functions, of g_0 and of a term that dimensionally scales as the spin field (i.e. $\int d\mathbf{x} \delta/\delta H$). Since the system is at equilibrium, the fluctuation dissipation theorem ensures that all the renormalizing corrections of the response functions appearing in eq (6.87) are directly linked to those of correlation functions, thus coming from the renormalized correlators $\langle \psi\psi \rangle$ that we are able to compute. These contributes are then identical on the two sides of the equality and cancel each other; consequently, to state the validity at all orders of perturbation of (6.87), we conclude that the constant g_0 has to renormalize as the field \mathbf{s} does. However, we know a priori that the spin is a non-critical field, meaning that its scaling dimension will not take any perturbative correction from the coarse-graining procedure but will stay equal to its naive static dimension. This implies that the quantity on the r.h.s. of the equation has to behave similarly and, finally, that g_0 is preserved from any type of renormalization.

The validity of the Ward identity is a clear manifestation of the symmetry in the equilibrium system, and it has the effect of protecting the renormalization of the mode-coupling constant g_0 [102]. This result fully agrees with what we saw by direct inspection with the diagrammatic calculation.

6.6 RG flow and fixed points

We now proceed with the second main step of the Renormalization Group, namely the rescaling of space and time to compare the effective theories before and after the coarse-graining. Applying the usual rescaling relations, $k \rightarrow bk$ and $\omega \rightarrow b^z\omega$, all the dynamical parameters acquire some scaling naive dimensions,

$$\begin{aligned} \Gamma_0 &\rightarrow b^{z-2}\Gamma_0 \quad , \quad \lambda_0 \rightarrow b^{z-2}\lambda_0 \\ \eta_0 &\rightarrow b^z\eta_0 \quad , \quad g_0 \rightarrow b^{z-d/2}g_0 \end{aligned} \tag{6.88}$$

that combine in the effective quantities as,

$$f_0 \rightarrow b^{4-d}f_0 \quad , \quad w_0 \rightarrow w_0 \quad , \quad \mathcal{R}_0 \rightarrow b^{-1}\mathcal{R}_0 . \tag{6.89}$$

It is here clearer that the naive dimension of f_0 is equal to $\epsilon = 4 - d$, confirming the role of the dynamical coupling constant of this parameter and the fact that the upper critical dimension is $d_c^u = 4$. Unlike the previous case of the hydrodynamic theory of the Vicsek model, here we can save from the dissertation the rescaling of the fields, especially of ψ , since the first contribute to its anomalous dimension comes from a two-loop static calculation.

Combining eq (6.88) with (6.70)-(6.72), we write the following RG recursion

relations for the dynamical parameters:

$$\begin{aligned}
\Gamma_{l+1} &= b^{z-2} \Gamma_l \left(1 + \frac{2f_l}{1+w_l} X_l \log b \right) \\
\lambda_{l+1} &= b^{z-2} \lambda_l \left(1 + \frac{1}{2} f_l \log b \right) \\
\eta_{l+1} &= b^z \eta_l \\
g_{l+1} &= b^{z-d/2} g_l ,
\end{aligned} \tag{6.90}$$

and for the relevant effective quantities:

$$\begin{aligned}
f_{l+1} &= f_l b^\epsilon \left[1 - f_l \left(\frac{1}{2} + \frac{2X_l}{1+w_l} \right) \log b \right] \\
w_{l+1} &= w_l \left[1 - f_l \left(\frac{1}{2} - \frac{2X_l}{1+w_l} \right) \log b \right] \\
\mathcal{R}_{l+1} &= \mathcal{R}_l b^{-1} \left[1 + \frac{1}{4} f_l \log b \right] ,
\end{aligned} \tag{6.91}$$

where with X_l we simply mean $X_l = [(\mathcal{R}_l \Lambda)^2 (1+w_l)] / [1 + (\mathcal{R}_l \Lambda)^2 (1+w_l)]$.

The scaling dimension of the crossover length scale \mathcal{R} is composed by the first term b^{-1} , that is proper of a naive length scale scaling, and by a non-trivial term proportional to the dynamical coupling constant, namely $b^{\frac{1}{4}f_l}$, which will be crucial in the following study of the crossover. From these expressions, the computation of the related β -functions is straightforward,

$$\begin{aligned}
\beta_f &= -f \left[\epsilon - f \left(\frac{1}{2} + \frac{2X}{1+w} \right) \right] \\
\beta_w &= wf \left[\frac{1}{2} - \frac{2X}{1+w} \right] \\
\beta_{\mathcal{R}} &= \mathcal{R} \left[1 - \frac{1}{4} f \right] .
\end{aligned} \tag{6.92}$$

and the fixed points follow from the searching for their zeros.

Imposing the condition $\Gamma^* = \mathcal{O}(1)$, we obtain the dynamical critical exponent z ,

$$z = 2 - \frac{2f^*}{1+w^*} X^* \tag{6.93}$$

depending from the fixed point values of f, w and X . Solving their β -functions, we discover that the length scale \mathcal{R} has two different fixed points,

$$\mathcal{R}^* = 0 \quad \text{and} \quad \mathcal{R}^* = \infty , \tag{6.94}$$

of which, since we expect $f^* \sim \epsilon$, the first one is IR-stable and the other is IR-unstable. These two values decisively determine the behavior of the other dynamical quantities.

The IR-unstable conservative fixed point

First of all, we analyze the case when $\mathcal{R}^* = \infty$, which happens to be unstable. This fixed point is characterized by the set,

$$f^* = \epsilon, \quad w^* = 3, \quad \mathcal{R}^* = \infty, \quad X^* = 1, \quad \Rightarrow z = d/2 \quad (6.95)$$

The dynamical critical exponent is, therefore, $z = d/2$ as the classic Model G of [61]. Indeed, relations (6.95) imply $\eta^* = 0$: the dissipation becomes irrelevant and the dynamics of the model appears completely conservative. This condition is preserved only if the starting bare effective friction $\eta_0 = 0$, otherwise, as soon as a small dissipation is turned on the system flows to visit the stable fixed point.

The IR-stable dissipative fixed point

The stable fixed point stands out for $\mathcal{R}^* = 0$, which produces:

$$f^* = 2\epsilon, \quad w^* = 0, \quad \mathcal{R}^* = 0, \quad X^* = 0, \quad \Rightarrow z = 2 \quad (6.96)$$

as a consequence of the fact that dissipation completely dominates the dynamics (i.e. $\eta^* = \infty$). As a matter of fact, this fixed point describes a dynamics in which the order parameter field $\boldsymbol{\psi}$ totally decouples from the secondary field \boldsymbol{s} that becomes a fast variable of the system. The mode-coupling terms become negligible and the primary field feels only a dissipative dynamics of the Model A type [61].

The dissipative fixed point is the only stable fixed point of the parameter space. Hence, asymptotically, all the bare theories with non-null starting effective friction belong to its universality class with $z = 2$. However, this kind of scenario can generate a dynamical crossover between the two different fixed points, assuming particular importance for finite-size physical systems. We are going to explain it better in the next chapter.

Chapter 7

The second crossover: from a conservative to a dissipative universality class

In the previous two chapters, we introduced the Inertial Spin Model, an active matter model whose main feature is a second-order dynamics for the degree of freedom of the velocity in an extended Hamiltonian space. Due to its inertial nature, we already tested its ability in reproducing the decay of dynamical correlation functions of natural swarms (Fig 5.6) while, to investigate its dynamical universality class, we performed an RG study on the related field theory under and a fixed-lattice approximation.

The scenario depicted by this calculation highlights the presence of two fixed points on the critical manifold: one unstable with zero effective friction and $z = d/2$, and a stable one characterized by infinite friction and $z = 2$. We can therefore repeat here a similar reasoning we carried out in chapter 4, where we studied the dynamical crossover between an equilibrium to an off-equilibrium universality class [7], and try to understand if a similar phenomenon between these two equilibrium dynamics can give us useful information on the applicability of this model to the natural system.

What really captures our attention is the unstable and conservative fixed point and the reason is twofold. First, natural swarms exhibit an inertial shape of correlation functions [3], therefore, although we cannot totally neglect the presence of dissipation in the system, we can assert that it is not so relevant in the dynamics; second, the dynamic critical exponent of the conservative fixed point is interestingly smaller than the Vicsek-like universality class ($z = 1.7$) getting closer to the one found experimentally, already at the level of equilibrium approximation.

Hence, following these motivations, we are going to carefully explore the crossover between the conservative and the dissipative critical dynamics of the fixed network ISM.

7.1 The crucial role of dissipation

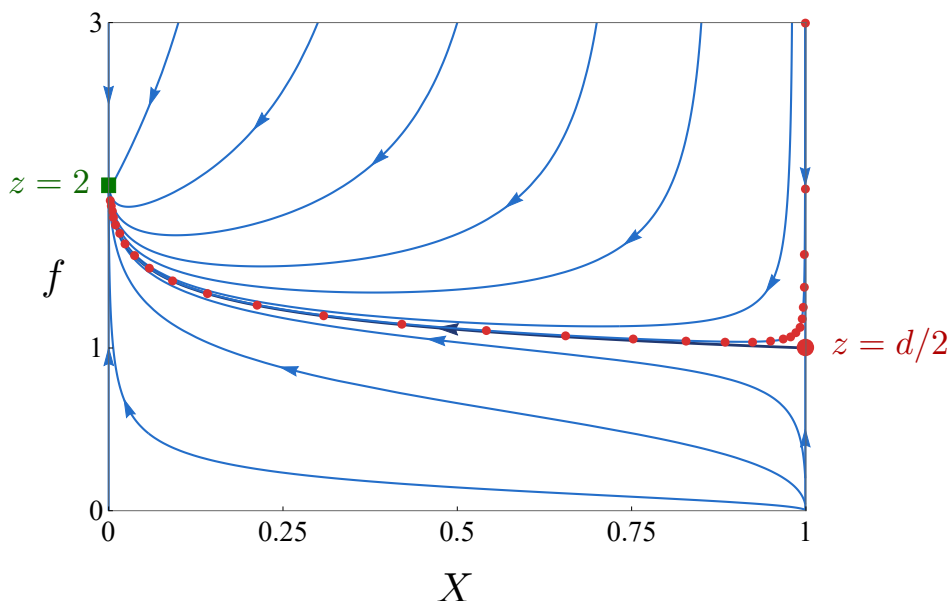


Figure 7.1: Renormalization group flow and crossover (I). Flow diagram on the (X, f) plane. In the plane there are two fixed points: the unstable one (red dot) describes a conservative dynamics with zero effective friction, the second one (green square) represents a dissipative dynamics with infinite friction. When the initial η_0 is small, $X_0 \sim 1$, the flow converges towards the unstable fixed point, $z = d/2$, and remains in its proximity for many iterations, before crossing over to the stable $z = 2$ fixed point. Figure reprinted from [9].

To fully understand this phenomenon and especially the conditions under which it occurs, we start from the RG recursion relations (6.91) we derived in the previous chapter, numerically integrating them and simulating the flow of the parameters in the parameters' space. In the limit of infinitesimal RG transformation ($b \rightarrow 1$), the eq (6.91) can be read as a system of coupled differential equations, from which, calling $x = l \log b$, we perform a continuous limit, mapping for instance $f_l \rightarrow f(x)$. We obtain,

$$\begin{aligned} f'(x) &= \beta_f(f, w, \mathcal{R}) \\ w'(x) &= \beta_w(f, w, \mathcal{R}) \\ \mathcal{R}'(x) &= \beta_{\mathcal{R}}(f, w, \mathcal{R}) , \end{aligned} \tag{7.1}$$

where the prime indicates a derivative with respect to x . These equations can be integrated and represented on the plane (X, f) since they are the most meaningful players of the theory. The result is shown in Fig.7.1 where each line corresponds to different initial values of the set $\eta_0, \lambda_0, \Gamma_0$ (and therefore of f_0 and X_0). The initial condition of X_0 (and then of the bare dissipation η_0) is paramount for the solution of the dynamical system, indeed we can see that when its value is close to one (low friction), the flow starts feeling the attraction of the unstable

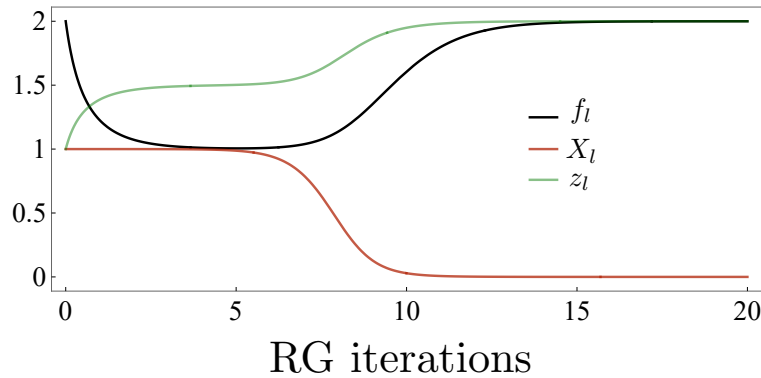


Figure 7.2: Renormalization group flow and crossover (II). Running parameters f_l and X_l , and critical exponent z_l as a function of the iteration step along a flow line at small η_0 . A starting transient regime in which the exponent is $z = 1.5$ in three dimensions is evident. Figure reprinted from [9].

and conservative fixed point ($\eta_0 = 0$), to then end the journey on the stable and dissipative one ($\eta_0 = \infty$).

Moreover, under this condition of small bare dissipation, the flow of the parameters approaches the $z = d/2$ fixed point and spends there many RG iterations. Each red dot of the figure represents an RG step, namely an effective theory describing the system at a particular length scale which increases with the number of steps. Hence, if the flow lingers about the conservative fixed point for many iterations, it means that for many length scales a physical system experiences a conservative-like critical dynamics with a $z = d/2$ dynamical critical exponent. In the asymptotic limit of an infinite system, the RG can be indefinitely applied to explore larger and larger scales. Following the flow, the system is trapped by the stable fixed point, where the nature of the critical dynamics changes becoming dissipative with $z = 2$.

In Fig.7.2 the same dynamical crossover is represented in terms of running values of z , of the coupling constant f and of X . An intermediate and transient regime where the exponent assumes the value of the conservative fixed point can be clearly appreciated before crossing over to the $z = 2$ value.

This crossover has important manifestations on the relaxation properties of the system that we can deduce by looking at the scaling properties of the correlation functions. To make a direct comparison with the study on the critical manifold we have just carried out, we can first analyze the crossover when $\xi = \infty$ and we observe the system at a particular length scale $1/k$. Under RG transformations, the correlation function of the order parameter follows the flow as [64],

$$C(t, k, \mathcal{P}_0) = (b^l)^{2z_l} C(tb^{-lz_l}, kb^l, \mathcal{P}_l) \quad (7.2)$$

where we are indicating with \mathcal{P}_l the set of parameters of the theory after l steps of RG and starting with the bare values \mathcal{P}_0 . The running dynamical critical

exponent has to be interpreted as the quantity,

$$z_l = 2 - \frac{2f_l}{1 + w_l} X_l \quad (7.3)$$

that, at the two fixed points, assumes its physical and macroscopic value (its behavior is also represented in Fig 7.2). As we already noticed, the observation scale fixes the maximum number of RG iterations, that is when the rescaled wave-number becomes $k_l = kb^{l_{STOP}} = \Lambda$ [74]. Assuming that at the end of flow the system is attracted by one fixed point, we use this relation in eq (7.2) obtaining,

$$C(t, k, \mathcal{P}) = \left(\frac{\Lambda}{k}\right)^{2z^*} C(t(k/\Lambda)^{z^*}, \Lambda, \mathcal{P}^*) . \quad (7.4)$$

The leading dependence of this function is therefore on $t(k/\Lambda)^{z^*}$, meaning that the characteristic time scales as,

$$\tau_c(k) \sim k^{-z^*} . \quad (7.5)$$

The value assumed by z^* depends on which of the two fixed points is reached by the flow at the stop condition.

If the bare system is characterized by a very small effective friction, we can state that as long as the crossover parameter remains around $X_l \simeq 1$, the unstable fixed point is the only relevant for the dynamics. This also implies that $\mathcal{R}_l \simeq \Lambda^{-1}$. Hence, the condition to explore only the unstable fixed point can be formulated as,

$$\text{if } \mathcal{R}_l \gg \Lambda^{-1} \implies \omega_c \sim k^{d/2} . \quad (7.6)$$

The conservation length scale $\mathcal{R}_l = \sqrt{\lambda_l/\eta_l}$ rules the condition to observe the conservative dynamics, which appears as an interplay between the correlation length and the ratio of the two transport coefficients. However, even if the flow starts with a very large bare conservation length scale, it can happen that the wave-number in consideration is so small that it allows a great number of iterations reducing the \mathcal{R} by a lot so that

$$\text{if } \mathcal{R}_l \ll \Lambda^{-1} \implies \omega_c \sim k^2 . \quad (7.7)$$

We can then understand that the condition $\mathcal{R}_l \simeq \Lambda^{-1}$ fixes a threshold for making the system to remain around the conservative fixed point. This can be translated in a crossover wave-number: from the recursion relation $\mathcal{R}_l = \mathcal{R}_0 b^{l(-1+f^*/4)}$ we substitute the unstable fixed point value for the coupling constant $f^* = \epsilon$, obtaining:

$$\mathcal{R}_l = \mathcal{R}_0 b^{l(-d/4)} \quad (7.8)$$

so that the threshold wave-number is easily computed,

$$k_c = \Lambda(\Lambda\mathcal{R}_0)^{-4/d} . \quad (7.9)$$

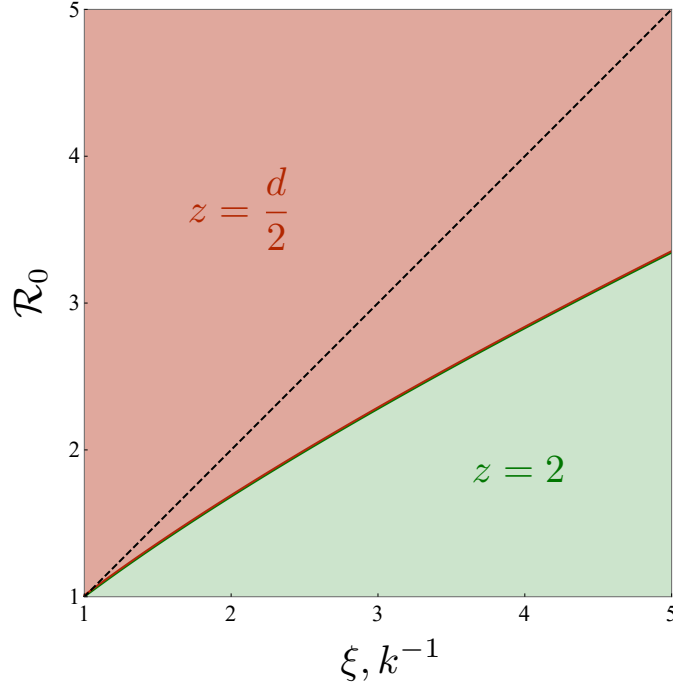


Figure 7.3: Different critical regions. Different values of k , ξ and \mathcal{R}_0 correspond to different critical behaviors. The red region reflects the conservative critical dynamics with $z = d/2$, while the green region corresponds to dissipative critical dynamics with $z = 2$. We set $\Lambda = 1$ so that physical values for lengths are $k^{-1} > 1$, $\xi > 1$ and $\mathcal{R}_0 > 1$. On the critical manifold relaxation is studied in the (k^{-1}, \mathcal{R}_0) plane: the two different regimes are separated by the curve $\mathcal{R}_0 = k^{-d/4}$. Off the critical manifold relaxation is studied in the (ξ, \mathcal{R}_0) plane: the two different regimes are separated by the curve $\mathcal{R}_0 = \xi^{d/4}$. The black dashed line represents, respectively, $\mathcal{R}_0 = k^{-1}$ or $\mathcal{R}_0 = \xi$ (i.e. scaling at the upper critical dimension). The figure refers instead to the $d < d_u^c$ case and it is reprinted from [10].

To summarize, for a system with $\xi = \infty$, the nature of its critical dynamics depends on the interplay between the observation scale and the starting conservation length scale, which is fixed by the level of effective friction of the system, namely:

$$\begin{aligned} k \ll \Lambda(\Lambda\mathcal{R}_0)^{-4/d} &\implies z = 2 \\ k \gg \Lambda(\Lambda\mathcal{R}_0)^{-4/d} &\implies z = d/2. \end{aligned} \quad (7.10)$$

Very similar reasoning can be applied to the case of a finite-size system that stands out to have a large but finite correlation length $\xi < \infty$. The difference is that now the RG takes place out of the critical manifold and also the correlation length changes under rescaling as $\xi_{l+1} = \xi_l/b$. The correlation function along the flow can then be expressed as,

$$C(t, \xi, \mathcal{P}_0) = (b^l)^{2z_l} C(tb^{-lz_l}, \xi/b^l, \mathcal{P}_l) \quad (7.11)$$

where now we can substitute the stopping condition of the flow around the critical fixed points, which reads as $b^{l_{STOP}} = \xi\Lambda$. Following the same steps as before, we

discriminate between the two regimes when

$$\begin{aligned} \mathcal{R}_l \gg \Lambda^{-1}, \quad \xi \ll \xi_c &\implies \omega_c \sim \xi^{-d/2} \\ \mathcal{R}_l \ll \Lambda^{-1}, \quad \xi \gg \xi_c &\implies \omega_c \sim \xi^{-2}. \end{aligned} \quad (7.12)$$

with a crossover length scale,

$$\xi_c \simeq (\mathcal{R}_0 \Lambda)^{4/d} \Lambda^{-1}. \quad (7.13)$$

We can therefore confirm that the relationship between the correlation length and the conservation length scale is crucial to determine the real critical behavior observed in the system. We finally notice that this latter quantity scales with an anomalous dimension $\mathcal{R} \sim b^{-d/4}$ that becomes equal to the naive one only at the upper critical dimension $d = 4$. As long as the dimension is $d < d_u^c$, ξ , and \mathcal{R} behave differently under RG and this has the effect to expand the conservative critical dynamics region with respect to the case of the naive scaling at $d = d_u^c$ (see Fig 7.3).

7.2 More details on the stable dissipative fixed point

The phenomenon we showed in the previous chapters has been derived by an analytical calculation of the integrals on the shell of the self-energies Σ_b and Π_b . However, all come from an assumption we implicitly did when computing the integral (6.66) for the kinetic coefficient Γ_0 . Indeed, we assumed that the effective friction was finite and we managed the calculation under this condition. In fact, this assumption remains valid as long as we are in the vicinity of the conservative fixed point, and, since we are interested in the crossover stemming from it, we can safely state that all the previous results are solid under this approximation.

What crucially drives the flow to explore the dissipative fixed point is the growth of the effective friction under RG transformations (i.e. $\eta_{l+1} = b^z \eta_l$), which can become very large and eventually diverge with the number of iterations. Therefore, the calculation of (6.66) has to be revised when considering the proximity of the stable fixed point, namely:

$$\begin{aligned} \Gamma_{l+1} &= b^{z-2} \Gamma_l \left[1 + 2 \frac{g_l^2}{\Gamma_l} \int_{\Lambda/b}^{\Lambda} \frac{d^d p}{(2\pi)^d} \frac{1}{p^2 [(\Gamma_l + \lambda_l) p^2 + \eta_l]} \right] \\ &= b^{z-2} \Gamma_l \left[1 + 2 \frac{g_l^2}{\Gamma_l \eta_l} \int_{\Lambda/b}^{\Lambda} \frac{d^d p}{(2\pi)^d} \frac{1}{p^2 \left(\frac{\Gamma_l + \lambda_l}{\eta_l} p^2 + 1 \right)} \right] \end{aligned} \quad (7.14)$$

If now we evaluate the last integral for $\eta_l \gg 1$, we obtain

$$\Gamma_{l+1} = b^{z-2} \Gamma_l \left[1 + 2 \frac{g_l^2}{\Gamma_l \eta_l} \int_{\Lambda/b}^{\Lambda} \frac{d^d p}{(2\pi)^d} \frac{1}{p^2} \right] \quad (7.15)$$

describing a logarithmic UV-divergence of order $1/p^2$ instead of the previous $1/p^4$. From the prefactor of the integral we can deduce that the coupling constant to describe the relevance of the mode-coupling interaction is not anymore f_l but rather $q_l = g_l^2 \Lambda^{2-d} / \Gamma_l \eta_l$, whose naive scaling dimension is $d - 2$ and not $d - 4$. This fact suggests that the upper critical dimension for this type of interaction lowers to $\tilde{d}_u^c = 2$.

In the case of our interest, namely for $d = 3$ the scaling dimension of q becomes negative, meaning that it approaches the stable fixed point characterized by $q^* = 0$. Consequently, the perturbative contribution to Γ , given by the mode-coupling self-energy Σ , vanishes and its recursive relation reads,

$$\Gamma_{l+1} = b^{z-2} \Gamma_l . \quad (7.16)$$

At one loop, the dynamical critical exponent is simply $z = 2$, in agreement to the previous result, and the dynamics becomes identical to that of Model A [61]. The effect of imposing $g^* = 0$ or $\eta^* = \infty$ is to make the two equations of motion completely decoupled from each other since the spin can be considered as a fast variable not entering into the hydrodynamics of the system (correlator and propagator of the spin are identically null: $C_s = 0, G_s = 0$).

Finally, the upper critical dimension of the mode-coupling dynamics at the dissipative fixed point is $\tilde{d}_u^c = 2$. This indicates that the fluctuations of the order parameter due to the inertial dynamics are irrelevant at $d = 3$. However, the real upper critical dimension of the whole dynamics and statics remains still $d_u^c = 4$ since the relevant coupling constant becomes unique coinciding with u_l . This brings corrections to the dynamics only at two loops level as it happens for the classic Model A [61]. Certainly, this changing of upper critical dimension could open a deeper future study of the neighborhood of the stable fixed point, however, for the moment, our biological motivations focus our interest mainly on the conservative fixed point, and therefore we are not going to elaborate more on it.

7.3 Numerical simulations

To test the crossover in microscopic systems we performed numerical simulations in $d = 3$ of the on lattice ISM, whose equations we report here again for clarity:

$$\begin{aligned} \frac{d\boldsymbol{\psi}_i}{dt} &= \frac{1}{\chi} \mathbf{s}_i \times \boldsymbol{\psi}_i \\ \frac{d\mathbf{s}_i}{dt} &= \boldsymbol{\psi}_i \times J \sum_j n_{ij} \boldsymbol{\psi}_j - \frac{\eta}{\chi} \mathbf{s}_i + \boldsymbol{\psi}_i \times \boldsymbol{\zeta}_i . \end{aligned}$$

with noise correlator:

$$\langle \boldsymbol{\zeta}_i(t) \cdot \boldsymbol{\zeta}_j(t') \rangle = 2d\eta T \delta_{ij} \delta(t - t')$$

We remind that i is the particle index, η indicates the microscopic dissipation of the spin and the dynamics obeys the constraint $|\mathbf{v}_i| = v_0$. The simulations are performed in the same spirit of fixed-network approximation of the analytical analysis, because we want to emphasize the role of behavioral inertia in the determination of the critical dynamics at an equilibrium level, without necessarily coming to full consistency with experimental data of natural swarms. Particles are disposed on cubic lattices with interaction radius $r_c = 1.05$, PBC are used and the numerical integration follows the RATTLE algorithm which is explained in Appendix B.

The strategy to explore the crossover will be the following: we fix the parameters $J = 1$, $\chi = 1$, and $v_0 = 1$ and we perform simulations at different values of temperature T and of friction η . The T determines the value of the correlation length, while the spin dissipation regulates the conservation length scale \mathcal{R}_0 . We then study the characteristic time scale's τ behavior of the system and we analyze the dynamical scaling in different regions of the (ξ, \mathcal{R}_0) parameters space.

7.3.1 Static behavior and correlation length

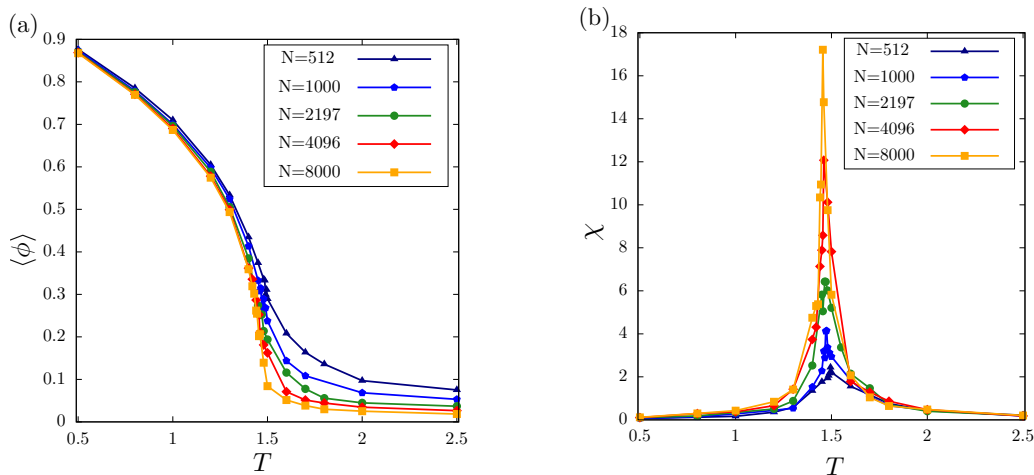


Figure 7.4: Static critical behaviour. Panel (a), average scalar polarization for temperatures $0.5 \leq T \leq 2.5$ and for different sizes ($N = 512, 1000, 2197, 4096, 8000$). An ordering transition occurs at approximately $T_c \simeq 1.5$. Panel (b), susceptibility as a function of temperature, same sizes as in panel (a); the maximum of each curve is located at a temperature that decreases with increasing the size of the system, and approaches the critical temperature T_c in the thermodynamic limit.

Before going into the study of the crossover we need, first of all, to identify the near-critical paramagnetic regime of the system. To achieve this goal we define as order parameter of the system the polarization, namely:

$$\phi = \frac{1}{N} \left| \sum_i \psi_i \right| \quad (7.17)$$

and we compute it for different sizes, $N = 512, 1000, 2197, 4096, 8000$, and for different values of the control parameter, which is clearly the temperature since we are on lattice at fixed density $\rho = 1$. The results are plotted in panel a of Fig. 7.4, while in panel b we show the susceptibility simply computed as for standard ferromagnetic systems from the connected fluctuations of the polarization,

$$\chi = \beta N [\langle \phi^2 \rangle - \langle \phi \rangle^2] \quad (7.18)$$

with $\beta = 1/T$ and the brackets indicate a phase average. From the analysis of these two figures it is evident that the ordering transition occurs at $T_c \simeq 1.5$ and that, due to expected finite-size effects, the critical point moves to lower temperatures when the size of the system increases [60].

Since the model is on the lattice, it has to satisfy the static scaling hypothesis, which tells that the spatial correlation function $C(r)$ has to be a homogeneous function of the distance r and ξ . We, therefore, exploit this concept to extrapolate the characteristic correlation length. We compute the correlation function as introduced in chapter 1 [42],

$$C(r) = \frac{\sum_{i,j} \langle \delta \psi_i(t) \cdot \delta \psi_j(t) \rangle \delta(r - r_{ij})}{\sum_{i,j} \delta(r - r_{ij})} \quad (7.19)$$

with:

$$\delta \psi_i(t) = \psi_i(t) - \langle \psi_i \rangle \quad (7.20)$$

where averages are now phase averages, and r_{ij} the distance between two labeled sites i and j . We expect the behavior of the correlation function to be:

$$C(r) = \frac{e^{-r/\xi}}{r^{d-2}} \quad (7.21)$$

where we are neglecting in the exponent of the denominator the anomalous scaling dimension because we want to compare our results to a one loop calculation. In $d = 3$ we are then able to write the identity:

$$rC(r) = e^{-r/\xi} \quad (7.22)$$

and consequently extrapolate the correlation length ξ from a linear fit of the $\ln(rC(r))$. In Fig. 7.5 we report these equal time correlation functions for the maximum size we took into consideration $N = 8000$, corresponding to the linear size $L = 20$ and considering temperatures just above the ordering transition (for this size $T_c = 1.455$). The maximum correlation length registered is $\xi = 10.15$ for $T = 1.48$, obviously coinciding with the maximum effective distance of the system when PBC are implemented: $L/2$.

To test the reliability of our measure of correlation length, we compute two

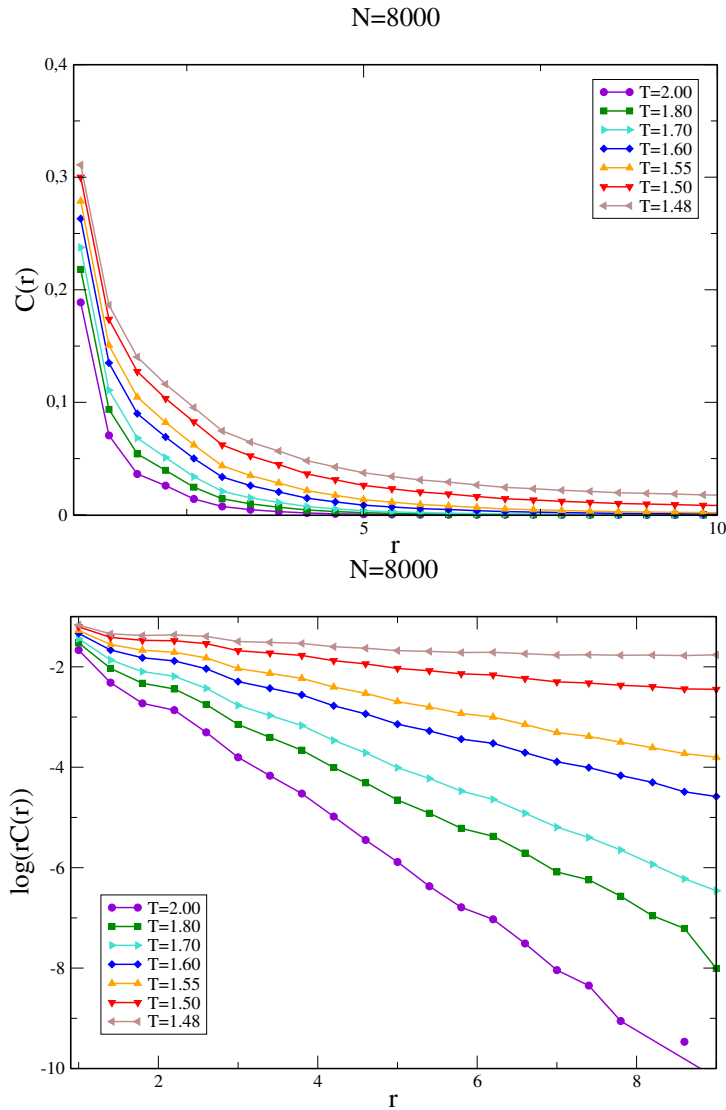


Figure 7.5: Static correlation functions. Top: Spatial correlation functions $C(r)$ for different temperatures at $N = 8000$; the curves stop at $r = 10$ since for $r > L/2$ it is meaningless to compute this quantity because of the periodic boundary conditions used in the simulations. Bottom: we plot $\log(rC(r))$ at different temperatures for the same size: the curves are linear according to theoretical predictions, and we can use them to compute the correlation lengths extrapolated by linear fits.

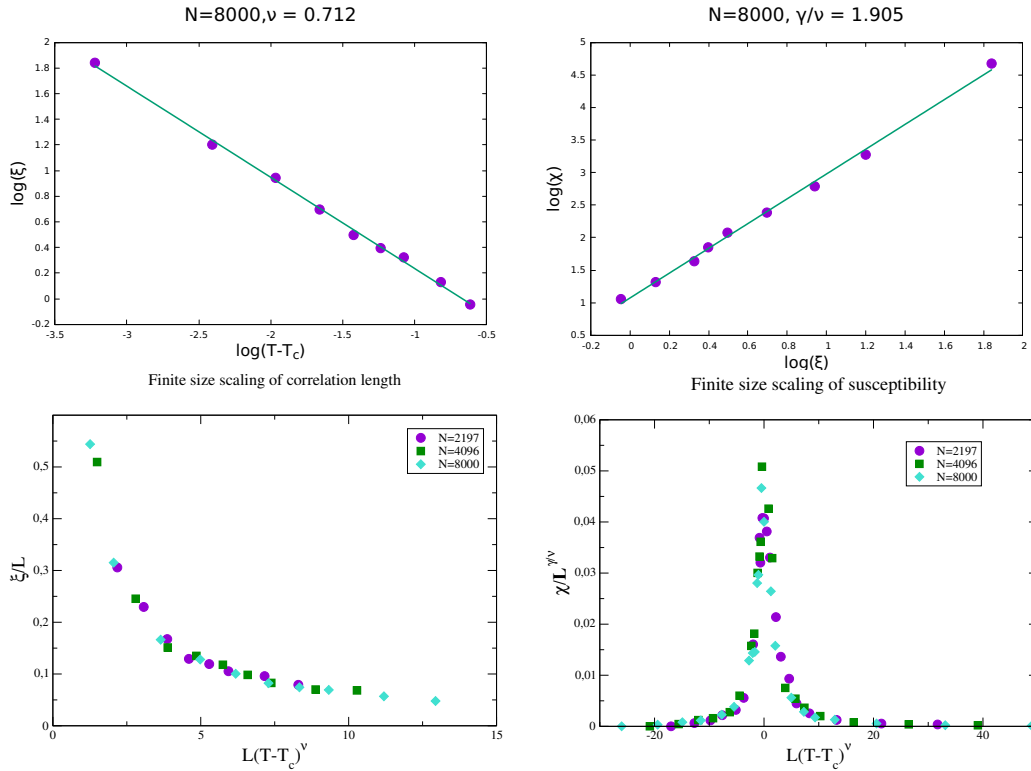


Figure 7.6: Static critical exponents and FFS analysis. Top: extrapolation of static critical exponents: $\nu = 0.712$ and $\gamma/\nu = 1.905$ from the behavior of the correlation length ξ and χ vs $(T - T_c)$, respectively; the size is fixed at $N = 8000$. Bottom: test of the finite size scaling laws for the correlation length and the susceptibility using the above estimate of critical exponents, both the sets of data are evaluated at $N = 2197, 4096, 8000$. All these results confirm that the static of the model belongs to the Heisenberg universality class.

static critical exponents: ν , that describes the divergence of ξ at criticality,

$$\xi \sim \frac{1}{(T - T_c)^\nu} \quad (7.23)$$

and γ that carries the singularity of the susceptibility as,

$$\chi \sim \frac{1}{(T - T_c)^\gamma} . \quad (7.24)$$

Combining these two expressions we obtain that $\chi \sim \xi^{\gamma/\nu}$ [51]. In Fig. 7.6 the extrapolation of these quantities for the maximum size $N = 8000$ are reported, we found $\nu = 0.712$ to be compared with $\nu_H = 0.707$ of the Heisenberg universality class and $\gamma/\nu = 1.905$ to be compared with the theoretical prediction $\gamma/\nu_H = 1.973$.

Finally, using the aforementioned critical exponents we verified the finite size scaling predictions for $N = 2197, 4096, 8000$, namely;

$$\xi = Lg(L(T - T_c)^\nu), \quad \chi = L^{\gamma/\nu}h(L(T - T_c)^\nu) \quad (7.25)$$

where g and h are the respective scaling functions. The results of Fig. 7.6 fully confirm that the static universality class of the fixed network ISM is the Heisenberg one.

7.3.2 Dynamical behavior and relaxation time

The second important and necessary ingredient to investigate the dynamical scaling is the characteristic time scale τ , which represents the scale over which fluctuations of the order parameter become decorrelated. To compute it, we recall the spatio-temporal correlation function in isotropic momentum space, that is:

$$C(k, t) = \frac{1}{N} \sum_{i,j} \frac{\sin(kr_{ij})}{kr_{ij}} \langle \delta\psi_i(t_0) \cdot \delta\psi_j(t_0 + t) \rangle_{t_0},$$

$$\langle (\dots) \rangle_{t_0} = \frac{1}{T_{max} - t} \sum_{t_0=1}^{T_{max}-t} (\dots) \quad (7.26)$$

with T_{max} the length of the simulation. Since we saw that the number of operations to compute it is of order $\sim T_{max}N^2$, we here now exploit the fact that we are on lattice and we use phase averages, therefore we compute the easier:

$$C(k=0, t) = \frac{N}{T_{max} - t} \sum_{t_0=1}^{T_{max}-t} \overline{\delta\psi(t_0)} \cdot \overline{\delta\psi(t_0 + t)}$$

$$\overline{\delta\psi(t_0)} = \frac{1}{N} \sum_i \delta\psi_i(t_0) \quad (7.27)$$

which turned to be identically null in the out-of-equilibrium case, because of the sum rule (4.23). From this latter quantity we compute the characteristic time scale using the same definition given in chapter 1 (1.19), that we report here for simplicity:

$$\frac{1}{2\pi} = \int_0^\infty dt \frac{1}{\tau} \sin\left(\frac{t}{\tau}\right) \frac{C(k=0, t)}{C(k=0, t=0)}. \quad (7.28)$$

We recall that this equality corresponds to requiring that half of the total integrated area of the dynamic correlation function in the frequency domain comes from the interval $-\omega_c < \omega < \omega_c$, with $\omega_c = 1/\tau$. This definition of τ has the advantage of capturing the relevant time-scale both when relaxation is dissipative, and when propagating modes are present, and it is the standard definition adopted in the literature on dynamic critical phenomena [5].

7.4 Dynamical crossover in numerical experiments

We have now all the tools to compute the dynamical critical exponent z . Indeed at $k=0$, the power law that links the correlation in time and space reads,

$$\tau(k=0) \simeq \xi^z \quad (7.29)$$

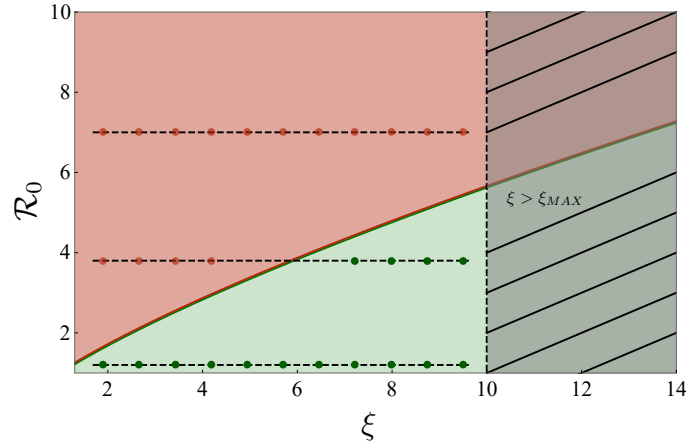


Figure 7.7: Numerical protocol in the (ξ, \mathcal{R}_0) plane. Simulations performed at fixed η and different T correspond to exploring the (ξ, \mathcal{R}_0) plane along with horizontal segments. Since the size of the system is finite ($L \leq 20$), only a limited window of ξ can be accessed and the length of such segments is finite ($1 = \Lambda^{-1} < \xi < \xi_{max} = 10$). According to the RG prediction, for all values of η corresponding to $\mathcal{R}_0 > 10^{3/4}$ the segments belong entirely to the conservative region (upper segment). For larger values of η , such that $1 < \mathcal{R}_0 < 10^{3/4}$, the segments cross from the conservative region to the dissipative one (middle segment): in this case, there is no sufficient span in each region to extract the exponent z from the τ vs ξ plot. Since the minimum physical value of \mathcal{R}_0 is $\Lambda^{-1} = 1$, larger values of η are all equivalent to the $\mathcal{R}_0 = 1$ case (lower segment). Figure reprinted from [10].

Our primary goal is to observe the crossover in the critical dynamics of the model to verify the RG predictions we derived before. From a conceptual point of view, the simplest thing to do would be to follow the analytical path also in the simulations and then, to fix a value of dissipation η , i.e. of \mathcal{R}_0 , and to observe the two different regimes enlarging more and more the correlation length by tuning the temperature T . One would expect to observe a power law with $z = d/2$ for small ξ and then a changing to $z = 2$ for very large values of the correlation length. However, to observe in simulations' data this phenomenon it is necessary to span several orders of magnitudes in ξ , at least three decades, which makes the numerical work quite demanding, especially considering we are studying systems in three dimensions with a large number of particles.

We decide to follow another strategy, certainly more doable from a numerical point of view: we translate the crossover in ξ in a crossover in effective friction fixing the size of the system at $N = 8000$. The reason can be well understood looking at figure Fig 7.7 that represents the (ξ, \mathcal{R}_0) plane. On the x -axis we report the upper limit of the correlation length, which is fixed by the linear size of the system $L/2$, and its lower bound that is determined by the microscopic length scale $\Lambda^{-1} = 1$. This latter belongs also with the conservation length scale, which in turn is fixed once the microscopic value of friction η is chosen. The corresponding values of \mathcal{R}_0 are represented by the horizontal lines in the graph: high values of dissipation correspond to small values of it, which, for very large but finite dissipation, reaches its lower boundary $\mathcal{R}_0 = 1$.

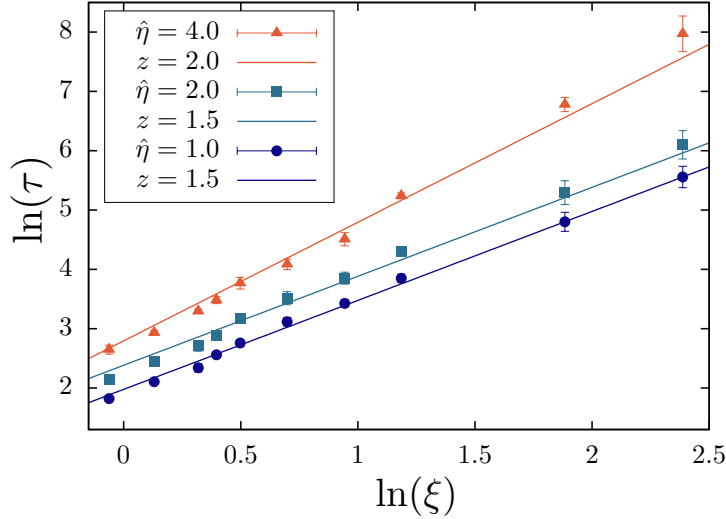


Figure 7.8: Dynamic critical exponents. Relaxation time vs correlation length in $d = 3$, for $L = 20$, $N = 8000$, and $T \in [1.48 : 2.00]$, at various values of the friction coefficient, $\hat{\eta} = 1.0, 2.0, 4.0$. Each point is an average over 10 samples, apart from the lowest T (largest ξ and τ) at $\hat{\eta} = 4$, for which we have 4 samples (one such sample takes 7 days to run on a i7-8700-3.20GHz CPU workstation). Lines are the best fit to $z = 1.5$ (low friction - $\hat{\eta} = 1.0, 2.0$) and $z = 2$ (large friction - $\hat{\eta} = 4.0$). Figure reprinted from [9].

Fig. 7.7 clearly shows that there exists an intermediate region of values of η in which the respective horizontal lines traverse the crossover curve $\mathcal{R}_0 = \xi^{3/4}$, determined by eq (7.13), and where one would observe the transition between the two different power laws. However, the interval in ξ in the two regimes is too narrow to perform reasonable linear fits to extrapolate trustworthy critical exponents. Therefore, it appears more convenient to choose values of η such that the horizontal lines are all included in one or in the other region, where all the disposable data can be used to show a $z = 3/2$ dynamics (for small dissipation) or a $z = 2$ dynamics (for large dissipation), according to the RG predictions.

This is exactly what we find in our numerical simulations, that fully confirm the RG crossover's scenario. Fig. 7.8 shows the results for simulations with $\eta = 1, 2, 4$. It is possible to appreciate the two regimes of critical dynamics: the conservative one is exhibited by the system at low values of $\eta = 1, 2$, while the $z = 2$ emerges when $\eta = 4$. We could not explore larger values of dissipation because the time for the equilibration was numerically too long. The lines reported are the best fit of data points at fixed slopes $z = 1.5$ and $z = 2$.

These values of dynamical critical exponents are also those that have to verify the dynamical scaling hypothesis of spatio-temporal correlation functions. In Fig. 7.9 we present two sets of normalized $C(k = 0, t)$ computed at different temperatures and respectively for $\eta = 1$ (panels a and c) and $\eta = 4$ (panels b and d), from which we extracted the characteristic times reported in Fig. 7.8. When time is rescaled by t/ξ^z with the appropriate value of the exponent, it is possible to appreciate a good collapse of the functions that testifies to the validity

of the dynamical scaling hypothesis in the conservative and in the dissipative regime. We, therefore, conclude that the ISM exhibits a dynamical crossover just as predicted by the RG calculation.

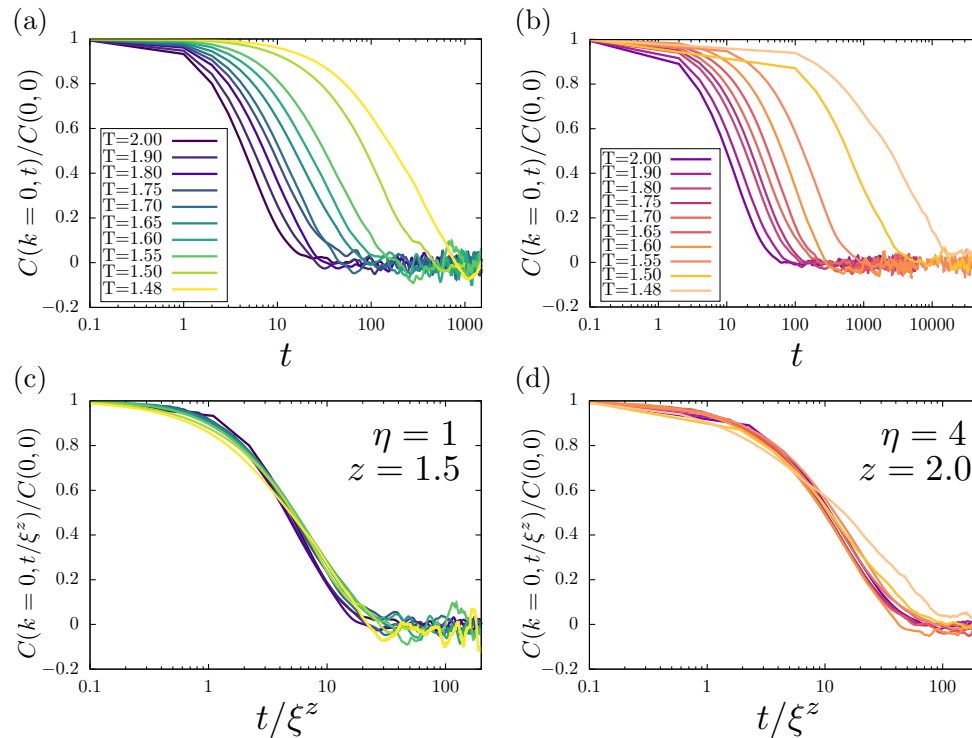


Figure 7.9: Dynamic scaling for correlations. Test of the dynamic scaling hypothesis on the dynamic correlation functions at $k = 0$. Upper panels: spatio-temporal correlation functions at various values of the temperature for $\eta = 1$ (panel a) and $\eta = 4$ (panel b). Lower panels: same curves plotted as a function of t/ξ^z with, respectively, $z = 1.5$ (panel c) and $z = 2$ (panel d): in both cases the functions verify the dynamic scaling hypothesis. Figure reprinted from [9].

7.5 Dynamical scaling at $k\xi = 1$

The behavior of the dynamic correlation function at $k = 0$ is a peculiar case that we tested in the section above. The wavenumber k represents the inverse of the scale of the system which we are looking at, therefore $k = 0$ means that the system is considered in all its entirety, more precisely in the thermodynamic limit. We can explore what happens at these dynamic features when we restrict our attention to smaller scales. The purpose is to test the dynamic scaling hypothesis evaluating the dynamic correlation functions for values of $k\xi$ fixed while the system lives in the conservative regime. As we explained in chapter 1, if the scaling hypothesis is verified for this model, we expect to see the collapse of the dynamic correlation curves one over the other for different temperatures (eq. (1.23)). We, therefore, compute the functions as eq. (1.24) states, using the values of temperatures already reported and changing the wavenumber k in order to maintain the product

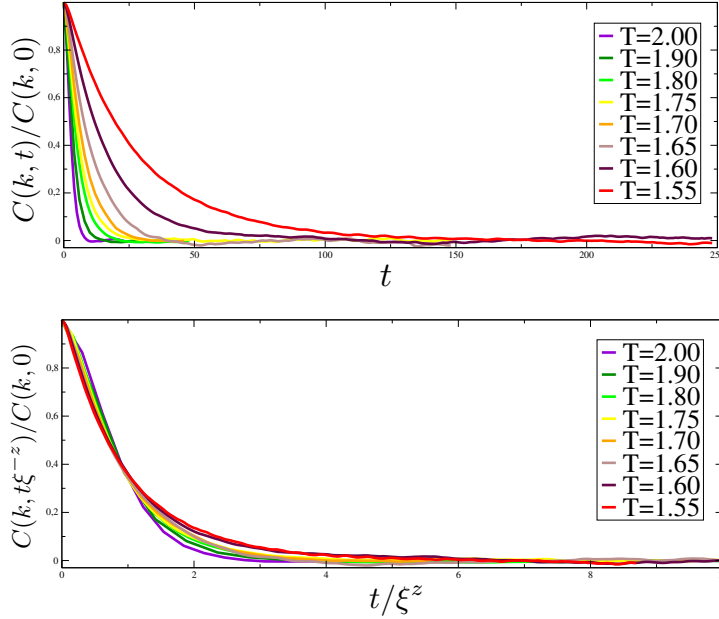


Figure 7.10: Dynamic scaling for correlations at $k\xi = 1$ and $\eta = 1$. Top: dynamic correlation functions at different temperatures but with the wave number that satisfies the product $k\xi = 1$. They are normalized at the value at $t = 0$ and computed for $N=8000$. Bottom: same functions when time is rescaled for t/ξ^z using $z = 1.5$ of the conservative regime. The characteristic collapse is verified, thus stating the validity of the dynamical scaling hypothesis for $k \neq 0$.

fixed. Choosing $k\xi = 1$ and $\eta = 1$, the results of the scaling are reported in Fig. 7.10, from which it can be deduced that the dynamical critical exponent $z = 1.5$ satisfies a robust scaling regime in the conservative case also at different values of wave-number.

To conclude our numerical analysis on the equilibrium ISM, we can finally focus on the qualitative shape of the dynamical correlation functions. In the previous chapters, indeed, we mentioned that this model is able to reproduce the inertial decay of the velocities' correlations of natural swarms. These latter quantities are computed using data satisfying $k\xi = 1$ [3], therefore we can take the last analyzed results as the example for a qualitative comparison.

Even though the shapes of the simulated $C(k, t)$ appear almost exponential, carefully looking at small times we can appreciate a non-vanishing derivative $\dot{C}(t \rightarrow 0) \simeq 0$. Recalling the definition of the relaxation form factor of eq (5.52), we saw that for natural swarms (Fig. 1.9 [3]) $h(x) \rightarrow 0$ for $x \rightarrow 0$, reproducing, for small times, the flat derivative typical of a dynamics of second order. This is a result found in the numerical simulations of ISM as well, as depicted in Fig. 7.11. The analysis has been realized for values of the wave-number satisfying the condition $k\xi = 1$, thus recalling the conditions of natural swarms; the emerging scenario is similar to the experimental one since these functions of the near-critical ISM go to zero as those experimental, highlighting how an inertial nature of the

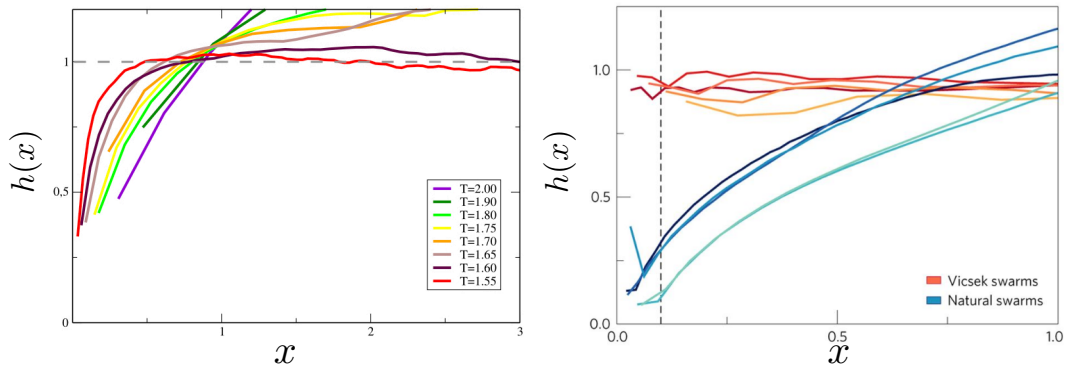


Figure 7.11: ISM reproduces the inertial decay of natural swarms. Left panel: function $h(x)$ computed for ISM numerical simulations at different temperatures and at $N = 8000$; the wave numbers satisfy $k\xi = 1$. It is clear that, for small times, the curves go to zero reflecting the flat derivative of the dynamic correlation functions at $t = 0$, typical of a model with an inertial dynamics. This scenario is similar to the one found in experimental data of natural swarms, which are always in the regime $k\xi \simeq 1$ (right panel).

dynamics is paramount to reproduce the nature of natural systems with respect to the fully dissipative case as the Vicsek model. A meaningful superposition of curves of these three different systems was reported in Fig. 5.6.

7.6 Conclusions on the equilibrium Inertial Spin Model

We conclude here the study of the fixed network ISM. We can say that, even if it involved a relevant equilibrium assumption, quite far from the living system of swarms, this analysis produced very interesting results that we are going to summarize here.

We understood that a microscopic dynamics with a second-order law for the velocity, describing a non-instantaneous update of the alignment force, fits in a compelling way the shape of the dynamical correlation functions of natural swarms; suggesting that an inertial model with small dissipation can be a very good candidate for a theoretical explanation of swarming systems.

Moreover, the microscopic laws transform in a set of dynamical equations with mode-coupling interactions at a field theory level, whose critical dynamics is characterized by a crossover between two dynamical universality classes. The quantity that rules this phenomenon is the effective friction of the spin field that, if it is small, leads the system to show firstly a conservative dynamics with $z = 1.5$, and then to drift asymptotically towards the $z = 2$ fixed point, where mode-coupling interactions become negligible. Therefore, as long as systems are of limited sizes, and inertial dynamical features are relevant, they can exhibit the value of the conservative exponent even if they are microscopically damped.

We believe this is the mechanism that can act on the natural system of swarms of insects, being in part responsible for the low value of their exponent. However, results of equilibrium theories cannot be directly compared to biological systems, since out-of-equilibrium effects are certainly relevant in their context. For this reason, we recently moved to the study of the active case, which totally seems to confirm our intuitions. A brief preliminary summary of this work will be given in the next conclusive chapter.

Chapter 8

In the crossfires of the two crossovers

This chapter concludes the study on the critical dynamics of active matter models, here performed to explain experimental evidence of anomalous relaxation in natural swarms of insects. First, we are going to summarize the results shown in the previous chapters and then we will introduce novel and recent works that completed the investigations on the topic. From a DRG and a numerical perspective, we focused our investigation on the two following models:

- **Vicsek model with an incompressibility constraint:** we started from the corresponding hydrodynamic theory of Toner and Tu with negligible density fluctuations, implemented by the constraint $\nabla \cdot \mathbf{v} = 0$ [6]. This study revealed that the model exhibits a novel critical dynamics, characterized by the emergence of an off-equilibrium universality class with $z = 1.7$ in three dimensions. However, our attention focused on the dynamical crossover involving the stable fixed point characterized by this latter exponent, and the unstable one representing an equilibrium universality class with $z = 2$ and zero activity. We understood that a finite-size active system, depending on its size and on the level of self-propulsion (i.e. the microscopic speed), can experience the attraction of one or both the fixed points showing the respective critical dynamics. In the conditions of relevant activity or sufficiently large size, the relaxation of the system is ruled by the off-equilibrium critical exponent, confirming that activity has the effect of lowering the value of this exponent with respect to the equilibrium case. Additionally, through numerical simulations, we proved that the incompressibility constraint that allows the RG calculation is not essential to verify the crossover in the original microscopic model. Activity rules the same phenomenon also for compressible though homogeneous and limited size systems, and we appreciated it in our simulations of the standard Vicsek model [7]. With this part of the work, we unveiled the real role of the activity in the critical dynamics of out-of-equilibrium systems belonging to the class of polar and dissipative active models. On the other hand, we clarified that this theory is not suitable to explain the dynamical scaling properties of natural swarms. Besides

the single numerical value of the exponent z , also the exponential decay of the dynamical correlation functions, typical of this dissipative dynamics, is not in agreement with experimental data that instead reflect a dynamics of greater order.

- **Inertial spin model under a fixed network approximation:** we then moved to the study of the Inertial Spin Model, different from the dissipative dynamics of Vicsek since it implements a second-order dynamical rule for the velocity. In the coarse-grained version, it produces a mode-coupling field theory for the degrees of freedom of density, velocity, and spin, namely the generator of internal rotations of the orientations. We worked on this theory both numerically and analytically in a fixed network approximation, thus neglecting density fluctuations and studying the system at equilibrium. At this level, the resulting field theory is similar to literature's mode-coupling dynamics but with the original character of dissipative friction in the equation of the spin. The dissipative spin dynamics characterizes also the microscopic equations, in order to reproduce realistic turning movements of biological agents. We, therefore, studied its critical dynamics to understand the effects that this type of dissipation produces on the critical exponent of a mode-coupling field theory. Also for this model, we found a significant result: the interplay of effective friction and system size determines a crossover between two different dynamical universality classes. One is represented by the unstable fixed point, stable only in the zero effective friction's direction and indeed representing a fully conservative critical dynamics with $z = 1.5$ in three dimensions. On the other hand, in case of relevant spin's dissipation or enough large size, the flow reaches the stable fixed point reproducing a fully dissipative dynamics with $z = 2$. We confirmed this scenario with numerical simulations of the fixed-network ISM, thus demonstrating that weakly damped and finite-size systems with an inertial dynamics can show a lower value of the dynamical critical exponent with respect to the dissipative case. We also verified that this model is able to reproduce the same qualitative behavior of the inertial decay of swarms' correlation functions. However, the value of the smaller exponent thus found, $z = 1.5$, is not yet consistent with experimental findings [9, 10].

8.1 How do the crossovers relate to natural swarms?

The main take-home message of the previous discussion is that both activity and inertial dynamics independently have the effect of lowering the value of the dynamical critical exponent. At the same time, they are also both crucial ingredients to reproduce the phenomenology of the biological system of interest. The experimental value of the swarms' exponent is actually smaller than the best estimate obtained $z = 1.5$, thus suggesting that these two ingredients must merge together at the theoretical level in order to explain experiments.

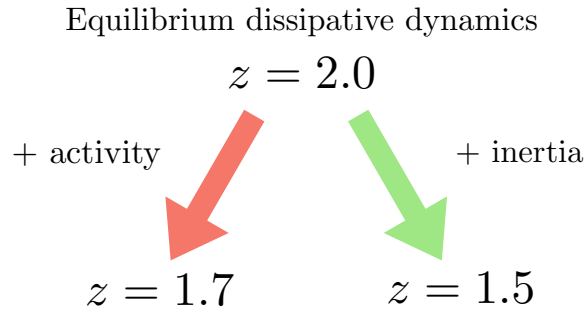


Figure 8.1: Sketch of the DRG results. The figure retraces all the results obtained in this thesis. The reference model to study the critical behavior of a system is the equilibrium dissipative dynamics of the order parameter, described by a critical exponent $z = 2.0$. Adding activity to it, we studied the incompressible Vicsek model that has $z = 1.7$. Considering zero activity but adding inertial coupling we got instead $z = 1.5$. Activity and inertial dynamics have independently the effect of lowering the value of the exponent.

The study carried out on the two crossovers can guide our intuition and provide useful information when we try to translate it to the world of natural swarms. If we want to relate the study of critical phenomena to the behavior of the biological system, some considerations are in order: first, swarms are groups of finite size L and this imposes a limitation to the application of the hydrodynamic limit to their study; second, the same size L determines the degree of correlation in the system, reproducing a quasi-critical behavior when $\xi \sim L$ [2]. A fair interpretation of the crossover phenomena in natural systems can assume, therefore, that the size L is the key parameter to show some peculiar collective properties. Moreover, at the theoretical level, we understood that the interplay between the correlation length and the crossover length scales rules the critical dynamics of the system, ultimately determined by bare values of activity and spin's dissipation. Based on these facts, we can therefore try to connect the main features of this biological system to the dynamical mechanisms we just studied.

Natural swarms are composed by biological living entities, therefore they are really active. To enforce this effect on the critical dynamics of a system, we learnt from the first RG study that its correlation length must satisfy,

$$\xi \gg \xi_c = \left(\frac{\epsilon}{\alpha_0} \right)^{1/\kappa} \Lambda^{-1} \quad (8.1)$$

where we remember that $\kappa = 31/51$ in $d = 3$ [7]. The main physical parameter is hidden in the activity coupling constant α_0 , which directly scales with the microscopic speed $\alpha_0 \sim v_0^2$. With the aim of describing a biological system, activity can be considered very large, thus providing a relation for the system's size $\xi \sim L \gg \xi_c$.

Natural swarms display also an inertial dynamics in the velocity correlation

functions, therefore they are weakly damped. These are the conditions to assume a relevant non-dissipative critical relaxation that, according to the second calculation, is guaranteed when:

$$\xi \ll \xi_c = (\mathcal{R}_0 \Lambda)^{4/d} \Lambda^{-1} \quad (8.2)$$

where the main physical meaning is embedded in the conservation length scale $\mathcal{R}_0 \sim \eta_0^{-1/2}$, with η_0 the friction of the spin [9].

Merging together these limit conditions and considering the finite-size relation $\xi \sim L$, we obtain a *speculative* relation for the system's size of the natural swarm,

$$\alpha \left(\frac{1}{v_0} \right)^{2/\kappa} \ll L \ll \beta \left(\frac{1}{\eta_0} \right)^{2/d} \quad (8.3)$$

where α, β are representative proportionality factors. This relation suggests that, in order to enhance out-of-equilibrium and inertial effects, the size of a swarm must be enclosed in a range determined by relevant activity and low dissipation.

Certainly, this is more speculation than a quantitative result, first of all, because we are comparing out-of-equilibrium features on one side and equilibrium on the other side of the inequality. However, it conveys our idea to explain the phenomenon of dynamical scaling in natural swarms. We, therefore, expect that a theory that takes into account activity and inertial dynamics could provide the right framework to demonstrate this conjecture.

8.2 Next: swarms in 3.99 dimensions

The previous arguments suggest that a combination of activity and inertia is crucial to reproduce the critical dynamics of natural swarms, in particular the value of the dynamical critical exponent $z_{exp} \simeq 1.2$. Even if the best estimate we gave for it is $z = 1.5$ from the equilibrium inertial case, we are convinced that reinstating back the self-propulsion in the equilibrium ISM provides a further lowering of the exponent.

We can gain an insight into this by pondering on the reasons why non-dissipative equilibrium models are characterized by a value of the exponent that is much smaller than the dissipative case $z = 2$. The lower value may be interpreted as a remnant of the spin-wave behavior that the underdamped system exhibits at very low temperatures. In this thermodynamic phase, linear propagating modes emerge and are characterized by a real part of the dispersion relation $\omega = ck$ where c is called the second sound speed. One could naively deduce from it that the dynamical critical exponent is $z = 1$ at all the values of temperature, but this guess would not be correct. Indeed, when moving to the critical region all the corrections coming from the renormalization at criticality have to be taken under consideration. At the critical point, the sound speed c changes its scaling behavior and affects also the value of the exponent that grows to $z = 1.5$, still remaining far from the dissipative one. A similar mechanism could work

when reinstating activity in the inertial dynamics: the primary effect of turning on the self-propulsion is inducing a ballistic, hence linear, motion of the single individuals. The critical exponent certainly does not describe the behavior of the single particles, but rather it measures the collective behavior of the group's velocity fluctuations. Despite this, the idea that a remnant of the ballistic motion influences its value, lowering the $z = 1.5$ like the spin-wave modes do for the dissipative exponent $z = 2$, is interesting.

For these reasons, we decided to conclude our journey by studying the critical dynamics of the full self-propelled Inertial Spin Model, embedding activity in the mode-coupling dynamics. At a field theory level, this produces a hydrodynamic theory for three coupled fields, namely the density, the velocity, and the spin, for which an RG calculation appears quite challenging. A simplification comes from the study we performed on the Toner and Tu theory in chapters 3,4 revealing that suppressing density fluctuations with an incompressibility constraint on the velocity field does not change the dynamical universality class of homogeneous systems. Hence, we evaluated the applicability of this approximation also in the full theory of the hydrodynamic ISM.

8.3 Incompressible ISM

Finally, we faced the calculation of the full field theory of the Inertial Spin Model under the incompressibility constraint [11]. This has been the last work of our group, but the results are still preliminary. For this reason, I will not give here details on the practical DRG calculation. I am going to introduce the equations of motion studied and discuss the principal results. Even if I contributed decisively to this work, all the diagrammatic calculations will be the main topic of the future Ph.D. thesis of another student.

The dynamical field theory we studied combines the hydrodynamic approach of the Toner and Tu equations and the reversible mode-coupling theory introduced in the previous sections. We performed the calculation under incompressibility conditions, thus neglecting density fluctuations and imposing a divergence-free constraint on the velocity field. However, we soon realized that doing it in an inertial field theory was not a piece of cake, therefore we firstly studied the problem at the equilibrium level [105]. Calling $\psi(\mathbf{x}, t)$ the order parameter, which is linked to the velocity field via $\mathbf{v}(\mathbf{x}, t) = v_0\psi(\mathbf{x}, t)$, we obtain the following divergence-free equations of motion in a fixed-network approximation [105]:

$$\begin{aligned}\frac{\partial\psi_\alpha(\mathbf{k}, t)}{\partial t} &= -\Gamma_0 P_{\alpha\beta}(\mathbf{k}) \frac{\delta\mathcal{H}}{\delta\psi_\beta(-\mathbf{k})} + g_0 P_{\alpha\rho}(\mathbf{k}) \mathbb{I}_{\rho\beta\gamma\nu} \int d^d q \psi_\beta(\mathbf{k} - \mathbf{q}) \frac{\delta\mathcal{H}}{\delta s_{\gamma\nu}(-\mathbf{q})} + \theta_\alpha(\mathbf{k}, t) \\ \frac{\partial s_{\alpha\beta}(\mathbf{k}, t)}{\partial t} &= -k^2 \Lambda_{\alpha\beta\gamma\nu}(\mathbf{k}) \frac{\delta\mathcal{H}}{\delta s_{\gamma\nu}(-\mathbf{k})} + 2g_0 \mathbb{I}_{\alpha\beta\gamma\nu} \int d^d q \psi_\gamma(\mathbf{k} - \mathbf{q}) P_{\nu\rho}(\mathbf{q}) \frac{\delta\mathcal{H}}{\delta\psi_\rho(-\mathbf{q})} + \zeta_{\alpha\beta}(\mathbf{k}, t)\end{aligned}\tag{8.4}$$

with noises correlators,

$$\begin{aligned}\langle \theta_\alpha(\mathbf{k}, t) \theta_\beta(\mathbf{k}', t') \rangle &= 2(2\pi)^d \Gamma_0 P_{\alpha\beta}(\mathbf{k}) \delta^d(\mathbf{k} + \mathbf{k}') \delta(t - t') \\ \langle \zeta_{\alpha\beta}(\mathbf{k}, t) \zeta_{\gamma\nu}(\mathbf{k}', t') \rangle &= 4(2\pi)^d \Lambda_{\alpha\beta\gamma\nu}(\mathbf{k}) k^2 \delta^d(\mathbf{k} + \mathbf{k}') \delta(t - t')\end{aligned}\quad (8.5)$$

There are several differences with respect to the equilibrium version of the ISM we already analyzed. First of all, we introduced new operators like the anti-symmetric identity $\mathbb{I}_{\alpha\beta\gamma\nu} = 1/2(\delta_{\alpha\gamma}\delta_{\beta\nu} - \delta_{\alpha\nu}\delta_{\beta\gamma})$, the already met projection operator $P_{\alpha\beta}(\mathbf{k})$ and its compositions; the equation of the order parameter is all projected along the orthogonal direction to \mathbf{k} , including the mode-coupling term, and, what is remarkable, the transport spin coefficient appears modified in,

$$\Lambda_{\alpha\beta\gamma\nu}(\mathbf{k}) = \lambda_0^\perp P_{\alpha\beta\gamma\nu}(\mathbf{k}) + \lambda_0^\parallel (\mathbb{I}_{\alpha\beta\gamma\nu} - P_{\alpha\beta\gamma\nu}(\mathbf{k})) \quad (8.6)$$

where $P_{\alpha\beta\gamma\nu}(\mathbf{k}) = \mathbb{I}_{\alpha\beta\gamma\nu} - \mathbb{I}_{\alpha\beta\sigma\tau} P_{\sigma\gamma}(\mathbf{k}) P_{\tau\nu}(\mathbf{k})$. Equation (8.6) is a manifestation of the solenoidal nature of the system: introducing a spatial anisotropy reflects in the separation of longitudinal and transverse spin relaxation modes. This distinction maintains the RG structure closed and it does not affect the equation of the order parameter since $\psi^\parallel = 0$. Another important difference lies in the mode-coupling element of the equation of the spin when $\delta\mathcal{H}/\delta\psi_\rho$ is explicitly computed: an additional term and then an additional vertex appears, and it is of the form,

$$\partial_t s_{\alpha\beta}(\mathbf{k}) \sim 2g_0 u_0 \mathbb{I}_{\alpha\beta\gamma\nu} \int d^d q d^d h d^d p \psi_\gamma(\mathbf{k} - \mathbf{q}) P_{\nu\rho}(\mathbf{q}) \psi_\rho(\mathbf{p}) \psi_\sigma(\mathbf{h}) \psi_\sigma(\mathbf{q} - \mathbf{p} - \mathbf{h}) . \quad (8.7)$$

This new vertex mixes static and dynamical coupling constants and it is crucial to provide consistency to all the calculation.

We finally added self-propulsion to this theory, enriching the dynamics with new terms that stemmed from activity. The velocity becomes the transporting field and, at the same time, maintains the role of polar order parameter. As a consequence, all the fields are advected by the flow of the velocity and the partial derivatives in time transform into,

$$\begin{aligned}\partial_t \psi_\alpha &\rightarrow D_t \psi_\alpha = \partial_t \psi_\alpha + \gamma_v v_\nu \partial_\nu \psi_\alpha \\ \partial_t s_{\alpha\beta} &\rightarrow D_t s_{\alpha\beta} = \partial_t s_{\alpha\beta} + \gamma_s v_\nu \partial_\nu s_{\alpha\beta}\end{aligned}\quad (8.8)$$

where γ_v and γ_s are the coefficients that break the Galilean invariance. The equation for the velocity contains also a term of pressure $-\partial_\alpha \mathcal{P}$ that enforces the constraint on the density, and the kinetic coefficients, determining the amplitude of the noises, are allowed to be generically different from the equilibrium counterparts ($\Gamma_0 \neq \tilde{\Gamma}_0$, $\lambda_0 \neq \tilde{\lambda}_0$) since activity violates the Fluctuation-Dissipation Relations. Additionally, the equation of the spin's dynamics gains more modifications: first, we add to the transport coefficient a term of dissipation in such a way to reproduce the weak non-conservative dynamics of the microscopic model,

$$\Lambda_{\alpha\beta\gamma\nu} \rightarrow \Lambda_{\alpha\beta\gamma\nu} + \eta_0 \mathbb{I}_{\alpha\beta\gamma\nu} , \quad (8.9)$$

second, we need to include other additional terms in the advective and mode-coupling vertices that go beyond the equilibrium theory introduced before. We realized these elements were necessary to close the RG calculation since they were directly produced by the diagrammatic expansion of the other quantities [11]. A reasonable physical explanation of their presence is that the absence of Galilean invariance allows all the possible combinations of gradients and fields in the equations of motion, if these are forbidden in the equation of the order parameter because of the projection onto the transverse direction, they become permissible in the equation of the spin, and have to be taken under consideration in the bare initial theory to produce a consistent calculation. The new spin's advective vertices are,

$$\begin{aligned} V_{\alpha\beta}^{\text{adv},1} &= v_0\mu_1\gamma_s\partial_\nu(s_{\alpha\nu}\psi_\beta - s_{\beta\nu}\psi_\alpha) \\ V_{\alpha\beta}^{\text{adv},2} &= v_0\mu_2\gamma_s[\partial_\alpha(\psi_\nu s_{\nu\beta}) - \partial_\beta(\psi_\nu s_{\nu\alpha})] , \end{aligned} \quad (8.10)$$

while the new mode-coupling vertices read,

$$\begin{aligned} V_{\alpha\beta}^{\text{mc},1} &= \phi_1 g_0[\partial_\alpha(\psi_\nu\partial_\nu\psi_\beta) - \partial_\beta(\psi_\nu\partial_\nu\psi_\alpha)] \\ V_{\alpha\beta}^{\text{mc},2} &= \phi_2 g_0\partial_\nu[\psi_\nu(\partial_\alpha\psi_\beta - \partial_\beta\psi_\alpha)] . \end{aligned} \quad (8.11)$$

Each term is accompanied by the introduction of a new parameter, namely μ_1, μ_2, ϕ_1 and ϕ_2 . Combining all these ingredients we get the following complete dynamical equations of the incompressible ISM,

$$\partial_t\psi_\alpha + v_0\gamma_v(\psi_\nu\partial_\nu)\psi_\alpha = -\Gamma_0\frac{\delta\mathcal{H}}{\delta\psi_\alpha} + g_0\psi_\beta\frac{\delta\mathcal{H}}{\delta s_{\alpha\beta}} - \partial_\alpha\mathcal{P} + \theta_\alpha , \quad (8.12)$$

$$\begin{aligned} &\partial_t s_{\alpha\beta} + v_0\gamma_s(\psi_\nu\partial_\nu)s_{\alpha\beta} + V_{\alpha\beta}^{\text{adv},1} + V_{\alpha\beta}^{\text{adv},2} = \\ &-(\Lambda_{\alpha\beta\gamma\nu} + \eta_0\mathbb{I}_{\alpha\beta\gamma\nu})\frac{\delta\mathcal{H}}{\delta s_{\gamma\nu}} + 2g_0\mathbb{I}_{\alpha\beta\gamma\nu}\psi_\gamma\frac{\partial\mathcal{H}}{\partial\psi_\nu} + V_{\alpha\beta}^{\text{mc},1} + V_{\alpha\beta}^{\text{mc},2} + \zeta_{\alpha\beta} \end{aligned} \quad (8.13)$$

that we are writing in x -space to condensate notation.

We performed a DRG calculation on this dynamical active field theory producing a closed set of 60 diagrams at one-loop, whose details could be found in a future manuscript [11]. The rich scenario produced by the theory is pictured in Fig. 8.2, where the RG flow is represented in the activity vs conservation plane. These quantities are expressed by the following coupling constants:

$$c_v = \frac{v_0\gamma_v}{\Gamma_0}\sqrt{\frac{\tilde{\Gamma}_0}{\Gamma_0}} \quad (8.14)$$

for the activity, and for the dissipation,

$$q = \frac{f(\lambda_0^\parallel/\eta_0)}{(1 + (\lambda_0^\parallel/\eta_0))} \quad \text{with} \quad f = \frac{\tilde{\lambda}_0^\parallel g_0^2}{(\lambda_0^\parallel)^2\Gamma_0} . \quad (8.15)$$

This last parameter is zero for overdamped dynamics ($\eta_0 \rightarrow \infty$), and equal to one for a perfect conservative dynamics with $\eta_0 = 0$.

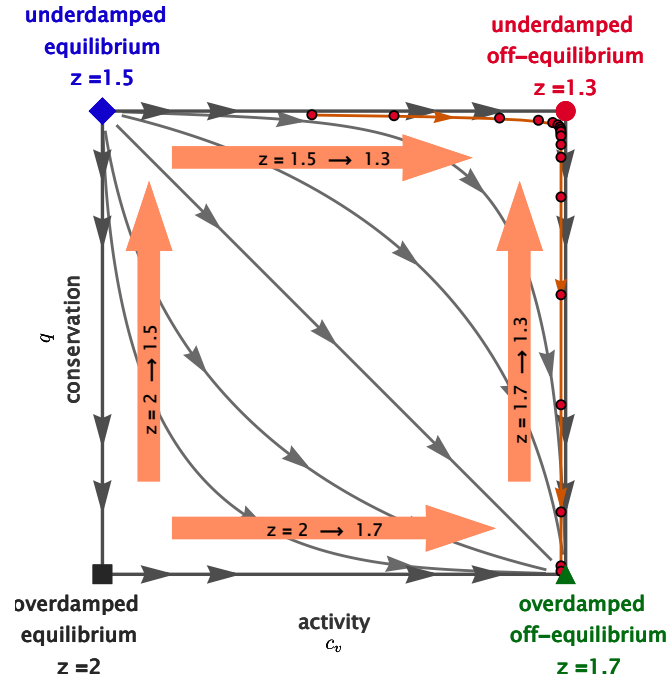


Figure 8.2: Sketch of the RG flow of the incompressible ISM. RG flow of the full ISM’s field theory in the plane activity, c_v , versus spin conservation q . When $c_v = 0$ we recover the equilibrium fixed points and the crossover from a overdamped to underdamped dynamics ($q = 0 \rightarrow q = 1$), while in the axis of relevant activity we have the stable fixed-point under dissipation’s renormalization with $z = 1.7$, and the novel unstable fixed point with underdamped active dynamics and $z = 1.3$. The red arrows indicate the different physical effects of activity and conservation on the value of the dynamical critical exponent z , while the grey arrows show the flow in the activity-conservation plane. Reprinted from [11].

The main novelty is the presence of a new *underdamped off-equilibrium* fixed point, characterized by a value of the dynamical critical exponent equal to $z = 1.3$ in three dimensions. This is IR-unstable in the dissipation direction, but we believe it is the exponent that better describes active homogeneous systems with inertial dynamics, namely natural swarms. Additionally, in this plane, we recover all the fixed points of the previously analyzed models and the two crossovers we have already studied. The path we believe is decisive for natural systems is the one obtained following the red dots of the figure: it starts far from equilibrium (relevant activity) but close to the $q = 1$ axis, where damping is weak. The RG flow carries thus the system to spend many iterations around the novel fixed-point exhibiting a $z = 1.3$ critical dynamics, before eventually crossing over to the overdamped off-equilibrium fixed point where dissipation takes over ($z = 1.7$).

This result confirms all our expectations. The effect of introducing activity in a mode-coupling theory is to lower the critical exponent from $z = 1.5$ to $z = 1.3$, and the mechanism to physically show this last value is again a dynamical crossover involving the size of the system and the physical friction, like for the equilibrium

inertial case. In this phenomenon, activity surprisingly seems to protect the symmetry of conservation against dissipation. Moreover, new recent data, which can be found in [11], enlarged the experimental window on this exponent to $0.88 < z_{exp} < 1.48$ within a two sigma interval of confidence, well including the theoretical prediction $z = 1.3$ and giving robustness to the analytical calculation.

Concluding, this last work finally produced a value of the exponent in agreement with experimental data. We, therefore, believe it represents one of the first examples of perturbative Renormalization Group's applications to the world of biology, being directly confirmed by experimental data on living systems. This result suggests that strongly correlated biological groups, as swarms of insects, can be successfully described with statistical field theory's methods that aim to extend the concept of universality to living matter.

Chapter 9

Collateral projects

This final chapter collects several projects carried on during the doctoral course, some partly concluded and others still ongoing. The topics could appear not in a logical consequential order with respect to the previous research of this thesis, indeed mostly they are not. They in fact come out from collaborations with other members of the group in Rome and in Argentina, and directly from the curiosity of the author, fueled by the lively activity of research of the group.

The common denominator that links the following sections is the attempt of including in the active matter models already introduced along with the dissertation new ingredients that provide a more realistic representation of biological systems displaying collective behavior. For instance, in the context of active matter, one usually refers to systems that dissipate energy at the local level in order to produce work [106]. The motion of single particles is ruled by internal driving forces that can be modeled in different ways, but one of the most common tools is assuming a constant speed of the single individuals, namely using the fixed-parameter v_0 [106, 107]. This constraint is what makes all the microscopic models we analyzed in the previous sections really *active*, in the sense that the locally sustained motion clearly carries an *arrow of time*, breaking the time-reversal symmetry for each active particle.

As we already saw, these descriptions are successful to capture essential traits of natural systems. However, especially for macroscopic biological groups such as flocks of birds and insects swarms, this kind of assumption can appear too distant from the real dynamics of moving animals, lacking some details that could explain additional important features of their groups. In the following, we try to cover some of these issues: in the first two sections, we are going to relax the constraint of constant speed on the Vicsek Model reinstating speed fluctuations, and thus reproducing a more reasonable scenario for birds flocks and insects swarms. The main purpose is to understand the mechanism that explains scale-free correlations in the speed of birds while, in the swarming phase, how this scalar degree of freedom can serve as a tracer to explore an FDT violation. Finally, restoring the constraint on the speed, we move to the ISM and we try to insert in the second-order dynamics of the velocity a confining potential on the positions. The aim is to reproduce the landmark role in the swarming behavior, a type of interaction

not included in the original model.

9.1 A new model to explain anomalous correlations in bird flocks

As long as the speed of the particles is kept constant to v_0 the truly non-trivial behavior of active systems comes directly from the process of mutual imitation of orientations among the individuals. However, when dealing with biological entities, such as flocks of birds, speed fluctuations are concrete and evident, thus need to be taken into account for a complete formal description. It is indeed reasonable to think that an effective natural process of imitation not only favors orientational order, but it also spontaneously carries the elements to adjust their speed to those of the neighbors. We want to model this mechanism, and to reach this goal we need to modify the standard active matter models relaxing the constraint on v_0 and inserting a speed control potential that acts on the single individual. Moreover, we need a description where speed fluctuations are limited around a reference biological value in order to prevent birds to move at an unreasonable value of average velocity.

Finally, we want that the new theoretical formulation matches some evidence coming from experimental data of starling flocks. In [43], the experimental analysis revealed that velocities' vectors exhibit a scale-free behavior ensuring strong correlation on large spatial scales and producing global and collective net motion, whatever the size of the group is. We introduced this feature in chapter 1, showing the vectorial correlation length behavior growing with the linear size of the system (Fig. 1.3). From the same figure, it is evident that also the speed correlation length shows the same scale-free behavior. We already mentioned that the first evidence finds a quite natural explanation in the spontaneous symmetry breaking picture of $\mathcal{O}(n)$ -systems provided by the Goldstone theorem [52], while the behavior showed by the scalar degree of freedom of the speed still lacks a physical modeling interpretation. Here we are going to focus on this latter evidence, which seems to require the introduction of new tools to find an explanation.

The principal mechanism responsible for scale-free behavior of correlation in large interacting systems, apart from the soft Goldstone modes, is the proximity to a critical point in the parameters space. Therefore, we present two models that are characterized by critical points in the degree of freedom of the speed and, at the same time, provide high polarization to the system thus reproducing a realistic thermodynamic phase of flocking. We investigate their positive and negative aspects when compared with experimental data of birds flocks, however we are not going to report the analytical calculations performed on them in the following, since they are reserved to other students thesis and can be found in [54] and [55]. In fact, what we want to highlight here is how powerful self-propelled numerical simulations of these models are to reproduce starlings' experimental data.

Before analyzing them, let's introduce the general dynamics which we are interested in. It recalls the Vicsek-like update rule in its continuous time version, namely:

$$\frac{d\mathbf{v}_i}{dt} = -\frac{\partial H}{\partial \mathbf{v}_i} + \boldsymbol{\eta}_i \quad (9.1)$$

$$\frac{d\mathbf{r}_i}{dt} = \mathbf{v}_i \quad (9.2)$$

where $\boldsymbol{\eta}_i$ is the classic white noise with variance $\langle \boldsymbol{\eta}_i(t) \cdot \boldsymbol{\eta}_j(t') \rangle = 2dT\delta_{ij}\delta(t-t')$ and H is the effective Hamiltonian that generates the social force acting on the velocity's dynamics. We write it in the form,

$$H = \frac{J}{2} \sum_{i,j}^N n_{ij}(t)(\mathbf{v}_i - \mathbf{v}_j)^2 + \sum_i^N V(\mathbf{v}_i) \quad (9.3)$$

recognizing the familiar term of inter-particle interaction with coupling strength J and connectivity matrix n_{ij} . Written in this form, this element describes not only an alignment interaction but also an imitation in the speed's behavior. The original element is the potential of speed control $V(\mathbf{v}_i)$, whose role is to maintain the speed of the single particles confined around a reference value v_0 . Different forms of this potential can be chosen, but we are going to analyze the two simplest formulations compatible with the rotational symmetry of the system.

9.1.1 Linear speed control

The basic proposal that fulfills our requirements to confine the speed around v_0 is of the type,

$$V(\mathbf{v}_i) = g(v_i - v_0)^2 \quad (9.4)$$

where $v_i = |\mathbf{v}_i|$. When computing the derivative in the equation of motion, it produces a linear restoring force that pushes the speed to fluctuate the less around v_0 the stronger is the stiffness g . This model has been already studied in [53], where a spin-wave expansion around the deep ordered state, determined a correlation length for the speed equal to,

$$\xi_{sp} = r_1 \left(\frac{Jn_c}{g} \right)^{1/2} \quad (9.5)$$

where r_1 is the mean inter-particle distance and n_c the average number of interacting neighbors. From eq (9.5) it is visible that $g = 0$ corresponds to a critical point, namely when the correlation length meets its singularity. Therefore, when considering strong correlated finite size systems, for which $\xi_{sp} \sim L$, the condition $g < 1/L^2$ of small enough stiffness ensures an appreciable scale-free behavior of the speed in the deep polarized phase.

This result appears satisfying to reproduce the phenomenology of the speed correlation length found in flocks, however, some troubles emerge when looking

at the behavior of the mean speed of the system. A deeper analysis of the same model that can be found in [55], shows indeed that, when considering the mean speed of the group,

$$s = \frac{1}{N} \sum_i v_i, \quad (9.6)$$

always in the deep polarized phase, its most probable value is given by

$$s_{\text{typical}} = \frac{1}{2}v_0 \left(1 + \sqrt{1 + \frac{4T}{Ngv_0^2}} \right). \quad (9.7)$$

In the thermodynamic limit $N \rightarrow \infty$, s_{typical} is well-behaved and it tends to the reference value v_0 regardless of the values of the other parameters, however some finest considerations are in order when dealing with smaller system sizes. Following (9.5), to achieve the scale-free behavior of the correlation length, we want to tune the model to low values of the stiffness g . This tuning, however, has the effect to increase the second term under the square root of (9.7), producing a growth of s_{typical} which is even more accentuated when the size N is small (because of the requirement $g < 1/L^2$). In this scenario, therefore, the typical speed value can significantly drift apart from v_0 .

These considerations open a dilemma: when the flock is composed by a limited number of agents, to confine its speed's fluctuations around a reference value, a large stiffness g is necessary, but, at the same time, it makes losing the scale free-behavior of the speed. On the other hand, if one wants to preserve the trend $\xi_{sp} \sim L$, it has to deal with an undefined growth of the average speed of the flock that is not realistic. This reasoning suggests that the speed control potential of (9.4) is not properly correct to represent our system and, consistently, also experimental data of flocks confirm this hypothesis. In Fig. 9.1, the black points stand for correlation length and average speed of real flocks in a range of sizes going from $N = 10$ to $N = 2500$: ξ_{sp} always grows with L but the average speed slightly fluctuates around the reference value of 12 m/s, without showing any relevant increase for a small number of individuals.

Numerical simulations

To confirm the above predictions, we perform out-of-equilibrium numerical simulations of the linear model. A simple scheme of Euler integration translates eq (9.1) into,

$$\mathbf{v}_i(t + \Delta t) = \mathbf{v}_i(t) + \Delta t \mathbf{F}_i + \delta \boldsymbol{\eta}_i \quad (9.8)$$

$$\mathbf{r}_i(t + \Delta t) = \mathbf{r}_i(t) + \Delta t \mathbf{v}_i(t) \quad (9.9)$$

where the force \mathbf{F}_i gets two contributions $\mathbf{F}_i = \mathbf{F}_{int} + \mathbf{F}_{sc}$, one from the inter-particles interaction $\mathbf{F}_{int} = -J \sum n_{ij}(\mathbf{v}_i - \mathbf{v}_j)$ and the other from the potential

of speed control,

$$\mathbf{F}_{sc} = -\frac{\partial V(\mathbf{v}_i)}{\partial \mathbf{v}_i} = 2g \frac{\mathbf{v}_i}{|\mathbf{v}_i|} (v_0 - |\mathbf{v}_i|). \quad (9.10)$$

The amplitude of the noise is regulated by the temperature with $\sigma_\eta^2 = 2dT\Delta t$; the density of the system is fixed to $\rho_0 = 1$ and the interaction is implemented according to metrical rules. Even though natural flocks are known to display topological interactions with a fixed number of neighbors, when simulating the low-temperature phase of (9.8) it can be shown that density fluctuations are very small, and the mean number of interacting particles is almost preserved also in a metric system. This fact allows using numerical tricks for the computation of the connectivity matrix such that it has been possible to run simulations up to $N = 3 \times 10^5$ particles. In any case, preliminary tests on the validity of this statement have been performed: the initial condition sees elements on a cubic lattice of size L that interact at time $t = 0$ with $n_c = 6$ particles; the range of interaction is posed at $r_c = 1.05$ and Δt chosen as the maximum value which guarantees a robust numerical integration in terms of errors and stationarity of the system's energy. We compute the distribution of the nearest neighbors along with many time evolutions and we verify that they are always sharply peaked around $n_c = 6$, thus supporting our thesis.

We run simulations for many different parameters, choosing values for J and T to obtain a global polarization of $\phi \simeq 0.9$ and changing g for various N . To provide an estimate of the correlation length, we first compute the spatial correlation function of the speed, namely,

$$C(r) = \frac{\sum_{ij} \langle \delta v_i \delta v_j \rangle \delta(r - r_{ij})}{\sum_{ij} \delta(r - r_{ij})} \quad (9.11)$$

with a definition that recalls that of the velocity [42], also similarly evaluating the speed fluctuations $\delta v_i = v_i - 1/N \sum v_k$. We then extrapolate the correlation length as the quantity,

$$\xi_{sp} = \frac{\int_0^{r_0} dr r C(r)}{\int_0^{r_0} dr C(r)} \quad (9.12)$$

indicating with r_0 the first point when $C(r) = 0$ [42]. This definition appears quite useful when the behavior of the correlation function is not known a priori. If the system is not scale-free, there exists a characteristic length scale, that we call $\hat{\xi}$, which dominates the exponential relaxation of the function, namely $C(r) \sim e^{-r/\hat{\xi}}$. In this case it is possible to extend the integrals of (9.12) over L , thus obtaining a good estimate of the correlation length via the result $\xi_{sp} \sim \hat{\xi}$. On the other hand, when the decay follows the power-law typical of critical regimes, we directly get $\xi_{sp} \sim r_0$, recognizing the procedure for experimental data explained in chapter 1. Finally, correlation length and mean speed (9.6) are then averaged over the stationary states of the numerical simulations.

These quantities are reported in panels a and b of Fig 9.1 in superposition with experimental data. In panel b the average speed is plotted against the number of

a group N and it is computed for a set of sizes similar to the experimental one $N = 8 \div 2744$ and for different stiffness values, namely $g = 1, 0.1, 0.03, 0.001$. In the same range of the control parameter g also the simulations of panel a are run, but to reproduce a linear size L comparable with that of realistic systems L_{exp} we decide to perform another set of simulations. The reason for this choice is that flocks do not move in a cubic shape, their aspect ratio continuously changes in time and they are almost flat in the gravity direction, therefore their linear size is always much larger than $L = N^{1/3}$. Since for the determination of the correlation length what really matters is only the linear extension of a system, we compare the same experimental data with the results of cubic lattice simulations in the range $N = 125 \div 343 \times 10^5$ obtaining what is shown in Fig 9.1 ¹.

Looking at it, evident conclusions can be drawn: for low values of g the scale-free behavior of ξ_{sp} is well reproduced following the black dots, however, the average speed widely grows for small N departing from the reference value; on the other hand, increasing g makes consistent its typical value, but suppresses the divergence of the correlation length. Concluding, numerical simulations fully confirm the unsuitability of the linear speed control to explain flocks experimental evidence; we need therefore to find another theoretical solution and we do it by introducing the marginal speed control.

9.1.2 Marginal speed control

To build up a new speed control potential, we remember that in classical statistical physics the correlation length is always linked to the inverse of the second curvature of the free energy calculated at its minimum. A vanishing second-order derivative implies a divergent correlation length that usually happens when the system is at criticality. The simplest potential that can answer these requirements, being also rotationally symmetric in the complete velocity vector, is of the form,

$$V(\mathbf{v}_i) = \frac{1}{v_0^6} \lambda (\mathbf{v}_i \cdot \mathbf{v}_i - v_0^2)^4 \quad (9.13)$$

where the normalization factor v_0^6 is there to provide the same dimension to all the parameters appearing in the effective Hamiltonian. The crucial feature of (9.13) is that its second derivative in v_0 is always zero irrespective of the value of λ , thus seemingly fulfilling the condition we are looking for.

This potential has been introduced for the first time in [54], where a mean-field analysis revealed that a zero temperature critical point emerges, and the speed correlation length diverges when approaching it:

$$\xi_{sp} \sim \frac{1}{T^{1/2}}, \quad (9.14)$$

¹We can actually demonstrate that using boxes with different aspect ratios, such that to simultaneously reproduce the behavior of ξ and s , is completely equivalent to use cubic lattices. We went for the latter to use standard and identical procedures of calculations for all the simulations.

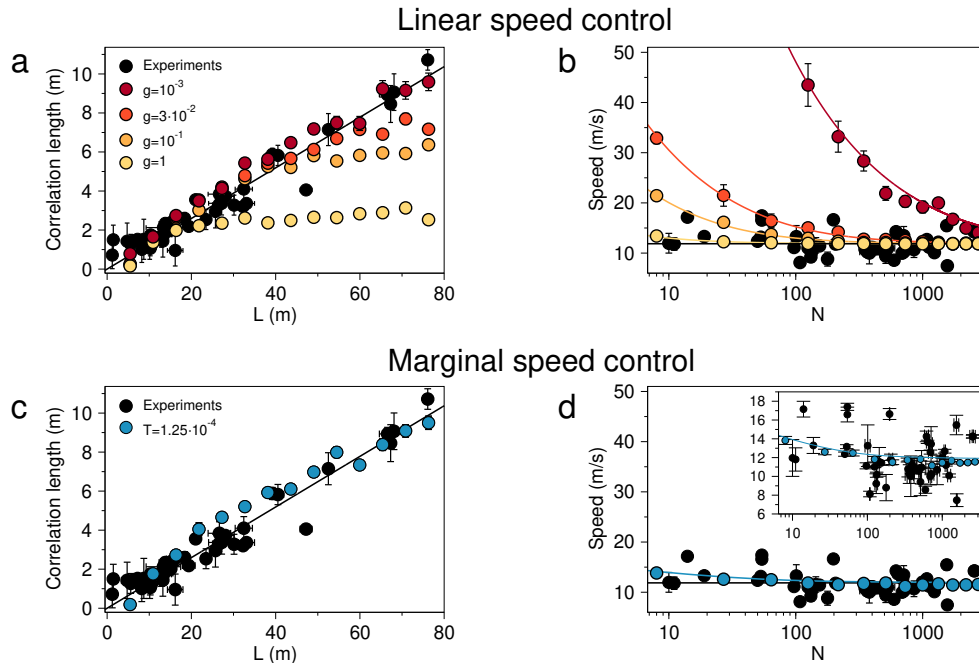


Figure 9.1: Linear vs Marginal speed control for birds flocks. Black dots represent experimental data on starling flocks in the size range $N = 10 \div 2500$. In panels a and c, speed correlation lengths are reported in comparison with those extrapolated from SPP numerical simulations of the linear and marginal speed control, respectively. The scale-free behavior $\xi \sim L$ is reached by the linear control only for the very small value $g = 0.001$, while it is lost when increasing its amplitude (panel a). For the same control parameters g , the mean speed of flocks of numerical simulations with the same number of particles N is calculated and shown in panel b plotted against the system's size. Large values of g reproduce the constant trend of the mean speed of flocks, while for those granting the scale-free behavior of the correlation length the mean speed rapidly grows at small N , deviating from experimental data. In panels c and d, the same quantities are reported for real data and SPP numerical simulations of marginal speed control. Since the zero-temperature critical point is not dependent on the value of λ , one single set of simulations is enough to reproduce both the scale-free behavior of the correlation (c) and the trend of the mean speed with the size. The inset of panel d zooms in the y scale of the same data to appreciate the agreement between theory and experiments. Continuous lines are the theoretical predictions. Reprinted from [55].

a feature interestingly not dependent on the parameter λ , but just naturally generated in the low-temperature phase. This result appeared quite promising since it suggests that low noise conditions and large polarization are sufficient ingredients to reproduce a full scale-free behavior of the system. What is more, carrying out the same analytical analysis contained in [55], it has been possible to derive the probability distribution of the average speed in the low-temperature phase, determining its typical value:

$$s_{\text{typical}} \simeq \begin{cases} v_0 & \text{for } N \gg \frac{T}{\lambda v_0^2} \\ v_0 \left(\frac{T}{4N\lambda v_0^2} \right)^{1/8} & \text{for } N \ll \frac{T}{\lambda v_0^2} \end{cases} \quad (9.15)$$

From this last relation we learn that, again in the thermodynamic limit $N \rightarrow \infty$ the s_{typical} converges to v_0 , while it can assume larger values for $N \ll (T/\lambda v_0^2)$. Nevertheless, the size of transition appears effectively quite small since $\lambda \sim \mathcal{O}(1)$ and the temperature is set to have strong polarization, thus shielding the regime where this increase is appreciable.

In the same spirit of the previous sections, numerical simulations are performed using this marginal speed potential that implements the force,

$$\mathbf{F}_{sc} = \frac{8\lambda}{v_0^6} (v_0^2 - \mathbf{v}_i^2)^3. \quad (9.16)$$

Average speed and its correlation length are computed obtaining panels c and d of Fig 9.1: the scale free-behavior is well reproduced and the average speed is correctly confined around the reference biological value, without any need to tune the amplitude of the potential. Hence, the marginal model seems to provide a way far better speed control mechanism with respect to the linear one.

Certainly, other formal solutions or different models able to properly provide the same level of explanation cannot be excluded a priori, however, the absence of any tuning of parameters and the stunning compatibility with experimental data make this model really sound from a biological point of view, very fit for starling flocks and probably suitable to more extended applications. Concluding, this successful study seems to put a full stop to the open question about the nature of flocks' speed long-range correlation arising in chapter 1 and provides an elegant way to interpret individual fluctuations in a flying flock of starlings [55].

9.2 Violation of Fluctuation-Dissipation Relations in soft-speed active matter models

The study performed in the previous section can be considered as an implementation of the classical active matter Vicsek model plus a relaxation of the speed's constraint, which, as we have just seen, leads to a more realistic representation of a natural phenomenon, like the flocking of birds. Reinserting speed fluctuations carried indeed to the explanation of another important trait of collective behav-

ior in the system, namely scale-free correlations in this scalar degree of freedom. Stimulated by this successful result, we decided to study more in-depth the other thermodynamic phases of this model to see how much it can be extended to our principle system of interest, namely, swarms of insects.

A clarification is in order. Basically, all the work we explained in the previous chapters pointed in a precise direction: swarms are well described by a second-order dynamics in the velocity, for instance by models like the ISM. Additionally, when introducing the latter, we said that also flocks belong to the same category of non-instantaneous interaction. At this point, the situation can appear quite foolish to the reader, which is now probably wondering why we went back to speak about Vicsek's dynamics when still referring to these animals groups. The objection is logical and legitimate. Our answer is twofold: first, the order of the dynamics is paramount when looking at dynamical properties as relaxation or information propagation, while all the static quantities like the correlation length are independent of this trait; second, in this last approach, we are trying to insert completely new ingredients in the mathematical models that are not completely under control. The strategy is therefore to start the investigation on these new tools, applying them to simple and already well-known dynamics, to study all their possible effects, and finally to include them on the proper inertial dynamics obtaining a more complete description of the original biological systems.

With this in mind, we propose to turn our attention to the concept of *response* in a biological system. When in chapter 1 we introduced the experimental evidence on natural swarms, we referred to their quasi-critical nature saying that, in the degree of freedom of velocity, the system shows long-range correlations that help it to maintain cohesion and to efficiently respond to external stimuli [2]. In the last years, it has been clarified that this seems a property common to many different biological systems across several lengths scales [58]. A critical state, in the sense of a functional useful balance between stability and instability, or more properly, between order and disorder, makes the system robust to external perturbation, and, even more, rapidly adaptable to changes of the external environment [59].

Biological examples are the auditory and the sensory systems, the neural activity of the human brain, or the variability of living cells [59]. However, for macroscopic biological systems like groups of animals, a discussion in these terms has not yet been thorough. If on the one hand, dynamical perturbations to the boundaries of flocking events have been already studied in [108], thus providing a description for the movements of birds in response to external predators attacks, on the other, the situation is quite more mysterious for swarms of insects, for which it is still unclear to what they should react, in which terms and what is the quantitative path to approach the issue. Inspired by novel and preliminary data on perturbation-response experiments on this latter system, we try to face the topic through an FDT study.

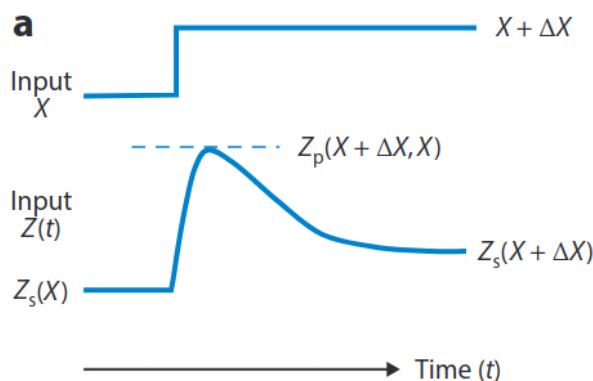


Figure 9.2: Sketch of an adaptive response. The input X represents the external signal which perturbs the system via a step function mechanism. An internal variable Z changes its stationary state to the maximum value $Z_p(X + \Delta X)$ and then descending to a new stationary state $Z_s(X + \Delta X)$ determined by the adaptation error. Reprinted from [109].

9.2.1 Biological motivations: perturbation-response study in swarms of insects

In order to explore and understand the quasi-critical nature of midges swarms, the team CoBBS recently performed perturbation experiments on them. One of these concerns the application of acoustic perturbations to the system formed above a landmark in its natural environment. Sound impulses are emitted from an external source, and the outcome trajectories are tracked and analyzed with the same technology previously used for flocks and swarms [46, 47]².

After processing the data, only a quantity seemed to register the event of perturbation with a significant change, namely the average speed of the group. Experimental data are preliminary, but we can already state that no changes of polarization in the direction of the source, or of the linear size of the swarm have been observed; the net effect of applying a sound disturbance is to slow down the system to smaller speeds³. In more detail, the appreciated reaction is a sudden decrease of the average system's speed as soon as the perturbation is turned on, and then a following slower ascent to the original stationary state, even before the sound stops.

This phenomenology appears very interesting since it seems to describe a process with *adaptability* happening in a collective biological system. With this word we mean the ability of a living system to change its internal state in response to environmental changes, in order to maintain proper features to ensure survival and biological functions [109]. The preliminary evidence thus obtained suggests

²More details on the experimental setup will be given in future publications.

³Experimental data will not be shown in this thesis to protect the originality and the preliminary nature of the results.

that performing response experiments like the usual physical ones is doable also for these systems, and it may pave the way for highlighting and quantifying this crucial property that distinguishes alive from not-alive systems.

Fig 9.2 sketches a simple example of a perturbation event when a biological system experiences adaptability [109]. The external signal is represented by the input X that, at a certain time, increases to $X + \Delta X$ like a step function. The system reacts changing the state of an internal variable Z , from an original stationary state $Z_s(X)$ to a maximum value depending on the intensity of the signal $Z_p(X + \Delta X, X)$. Finally, the system adapts itself to the new background signal and reaches a new stationary state at $Z_s(X + \Delta X)$, which can be generally different from the unperturbed state. In equilibrium physical systems what happens is that $Z_s(X + \Delta X) = Z_p(X + \Delta X, X)$ since there is no adaptability, while we can say that the adaptation is perfect when, despite the disturbance, the system manages to return to the starting state and $Z_s(X + \Delta X) = Z_s(X)$.

We can therefore give a quantitative measure of this phenomenon, defining the adaptation error [109],

$$\varepsilon = \frac{|Z_s(X + \Delta X) - Z_s(X)|}{|Z_p(X + \Delta X, X) - Z_s(X)|} \quad (9.17)$$

which is $\varepsilon = 1$ for equilibrium system, while it is $\varepsilon = 0$ for perfect adaptability. By multiplying and deviding (9.17) for $|\Delta X|$, we can express ε in terms of two response functions, namely:

$$\varepsilon = \frac{R_a(X, \Delta X)}{R_p(X, \Delta X)} \quad (9.18)$$

where we introduced the adapted response,

$$R_a(X, \Delta X) = \frac{|Z_s(X + \Delta X) - Z_s(X)|}{|\Delta X|} \quad (9.19)$$

and the physical response,

$$R_p(X, \Delta X) = \frac{|Z_p(X + \Delta X, X) - Z_s(X)|}{|\Delta X|} \quad (9.20)$$

If now we postulate that the adaptation error is an inner structural property of a biological system and that it can be measured directly from the experimental data, then all the information on the adaptation process comes from,

$$R_a(X, \Delta X) = \varepsilon R_p(X, \Delta X) , \quad (9.21)$$

and then from the out-of-equilibrium physical response function of the system.

Motivated by these considerations, we decided to start an investigation on response functions in active matter models that can help in reproducing the swarming scenario. The final aim is to arrive at a good quantitative measure of out-of-equilibrium effects in this kind of active system and then to go back

to compare the acquired knowledge with experimental data. Since this topic for polar active matter models is quite an open ground, we are proceeding by simple steps: first (what is discussed here), we study the out-of-equilibrium speed response in the modified Vicsek-like model of the previous sections; second, we will repeat the study reinstating the second-order dynamics using the ISM and finally, we will study the adaptive dynamics of the natural system. We here start our investigation by studying response and FDT in equilibrium conditions to test procedures and protocols, and, to conclude, we show some preliminary results on the out-of-equilibrium case.

9.2.2 The model: speed perturbations

As we said before, to study speed's response properties we have to allow fluctuations of this degree of freedom and control them with a suitable potential as we did for the flocking case. For simplicity, we start here with the simplest Gaussian form of speed control (9.4), since we are not interested in the study of scale-free correlations of the polarized phase. We are instead mainly interested in the near-critical phase of the model and in mild speed fluctuations, features ensured for large values of the stiffness g .

The starting point is therefore assuming a microscopic effective Hamiltonian with Gaussian speed control:

$$\mathcal{H} = \frac{J}{2} \sum_{ij} n_{ij} (\mathbf{v}_i - \mathbf{v}_j)^2 + g \sum_i (|\mathbf{v}_i| - v_0)^2 \quad (9.22)$$

where J is the usual parameter that controls the interaction, and g sets the amplitude of the speed's potential, exactly as presented in (9.4). The implemented dynamics also follows equations (9.1).

The novelty appears in the introduction of the perturbation, which we model as an additional term in the Hamiltonian, namely:

$$\mathcal{H} \rightarrow \mathcal{H} - h(t) \sum_i |\mathbf{v}_i|. \quad (9.23)$$

We are calling $h(t)$ the source of the disturbance, equal for all the individuals, in analogy with the magnetic field of classical Heisenberg dynamics. However, contrary to this case, in (9.23) the scalar field is coupled to the total speed of the system and not to the directional degree of freedom. We study two different time-dependent fields, namely

$$h(t, t_0) = h_0 \theta(t - t_0) \quad \text{and} \quad h(t, t_0) = h_0 \theta(t - t_0) \theta(t_0 + \delta t - t) \quad (9.24)$$

a step function and a square wave of amplitude δt , respectively (panels a and b of Fig 9.3); the t_0 is the switch-on time of the field and h_0 sets its amplitude. It is useful to immediately look at the effect this perturbation produces on the average speed of the system: when considering negatives amplitudes ($h_0 < 0$) the reaction

is naively similar to that of natural swarms, namely s , the mean system's speed (9.6), decreases proportionally to the magnitude of h_0 following the step function (panel c of Fig 9.3), or going back to the original stationary state according to the square wave (panel d of Fig 9.3). Therefore we believe that, especially in the impulsive case, this theoretical scheme can reproduce, at least qualitatively, the picture of the natural system. However, in experimental data, an overshooting of reaction is not visible, and this is probably due to second-order dynamics that we are going to implement later. Moreover, the model does not include adaptability that will be also studied in the future.

Adding the speed's perturbation, the final equations of motion become,

$$\begin{aligned}\frac{d\mathbf{v}_i}{dt} &= -J \sum_j n_{ij}(t)(\mathbf{v}_i - \mathbf{v}_j) - 2g(|\mathbf{v}_i| - v_0) \frac{\mathbf{v}_i}{|\mathbf{v}_i|} + h(t) \frac{\mathbf{v}_i}{|\mathbf{v}_i|} + \boldsymbol{\xi}_i \\ \frac{d\mathbf{r}_i}{dt} &= \mathbf{v}_i\end{aligned}\tag{9.25}$$

from which it is visible that adding this field term is equivalent to shift the center of the Gaussian control speed potential, from v_0 to $v_0(1 + h(t)/2gv_0)$. As a consequence, considering fields that vary locally, namely $h_i(t)$, could lead to a model where the individual center of the potential v_0 is not fixed but fluctuates. This is also another interesting feature that can go closer to a realistic description of natural systems, but for the moment we will leave it to upcoming research.

9.2.3 Response function and equilibrium study

Our purpose is to study the response function of the speed when subject to external perturbations. To do this, we are going to explore the validity of the linear response theory and of the Fluctuation Dissipation Relations (FDR) [68] for this active system following a Vicsek-like dynamics.

We certainly know that a polar active system is out-of-equilibrium since the time-dependence of the connectivity matrix breaks the detailed balance condition. The consequence of adding self-propulsion to the particles reflects in a space-time dependence of the $n_{ij}(t)$, whose variation is responsible for out-of-equilibrium effects. In two limiting cases, we expect to observe equilibrium and therefore the validity of the FDR relations: i) in the non-interacting case $J = 0$ since the system is composed by N particles in a potential $V(\mathbf{v}_i)$; ii) in the equilibrium on lattice case, when we consider $d\mathbf{r}_i/dt = 0$ and the effective Hamiltonian contributes to the usual Boltzmann weight $P \sim e^{-\beta\mathcal{H}}$.

In both these cases, we expect to observe the validity of the FDR [68]. For clarity, let's briefly recall the main concepts for a Langevin equilibrium dynamics of a scalar quantity $A(t)$ [110]:

$$\frac{dA(t)}{dt} = -\gamma \frac{\partial \mathcal{H}[A(t)]}{\partial A(t)} + \sqrt{2\gamma T} \eta(t)\tag{9.26}$$

where η is a white noise, namely with zero mean and variance $\langle \eta(t)\eta(t') \rangle = \delta(t-t')$,

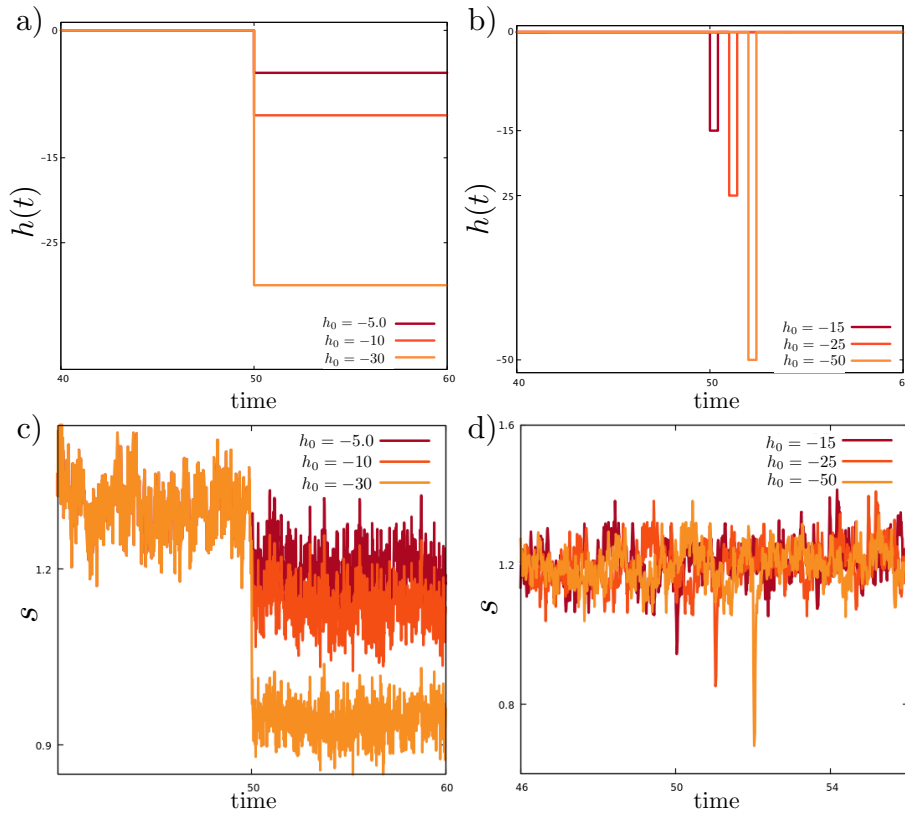


Figure 9.3: Types of speed perturbations. Panels a and b represent fields with different amplitudes h_0 , which follow a step function and a square wave mechanism, respectively. Panels c and d, temporal series of mean speed $s = (1/N) \sum v_i$ in the reaction of the corresponding perturbation. All these numerical simulations are run with $J = 5$, $T = 20$, $g = 10$, $v_0 = 1$, $r_c = 1.05$. The duration of the impulse on the left is $\delta t = 50$ time steps.

γ is the friction coefficient and \mathcal{H} is a generic functional of A . A perturbation coupled to the same degree of freedom can be added to the cost function obtaining:

$$\mathcal{H}^h[A] = \mathcal{H}[A] - h(t)A(t) . \quad (9.27)$$

The response is then computed by evaluating the change of the average value of the observable with the field, leading to the definition of the two times response function,

$$R(t, t') = \frac{\delta \langle A(t) \rangle}{\delta h(t')} \quad (9.28)$$

where we are considering $t > t'$. The Fluctuation Dissipation Theorem (FDT) connects this quantity to the correlation function of the same observable in absence of perturbation, namely $C(t, t') = \langle A(t)A(t') \rangle$, through the formula [110],

$$R(t, t') = \frac{1}{\gamma T} \theta(t - t') \frac{\partial C(t, t')}{\partial t'} . \quad (9.29)$$

The connection is deeper if we evaluate the integrated response. In the case of a field turned on with a step function at time $t = 0$ of the type $h(t) = h_0 \theta(t)$, and with a small amplitude h_0 , we can say that from (9.28) it follows,

$$\langle A(t) \rangle - \langle A(0) \rangle = h_0 \int_0^t dt' R(t, t') \quad (9.30)$$

thus obtaining the dynamical susceptibility as,

$$\chi(t) = \int_0^t dt' R(t, t') . \quad (9.31)$$

Finally using (9.29), we appreciate the connection between susceptibility and correlation function given by,

$$\chi(t) = \frac{1}{\gamma T} [C(0) - C(t)] \quad (9.32)$$

where the proportionality factor that links correlation and response is given by the amplitude of the noise term, namely the temperature. This statement is known as the Fluctuation Dissipation Theorem [68, 110] and it lies at the core of the equilibrium physics. We, therefore, expect that, if we consider the model (9.25), under one of the two equilibrium conditions, we should be able to verify it for any observable $A(\{\mathbf{v}_i\})$, as for instance the average speed s of the system.

The FDT relation (9.32) has to be fulfilled in the equilibrium case that can be recovered in the two situations we explained above. Therefore, as a preliminary step towards a future study of the off-equilibrium case, we decide to numerically verify the theorem simulating the dynamics (9.25) stopping particles on a cubic lattice, and implementing both the sources of disturbance. In this case, the terms of speed and velocity lose their kinematic meaning, they just represent the

modulus and the direction of spin vectors on a site, but, for the sake of upcoming consistency, we are going to preserve the same names of the off-equilibrium case.

However, since the speed is a scalar degree of freedom that has never been considered yet for these active models, before starting the simulations, we give a brief theoretical insight of what we should expect looking at the non-interacting case. The purpose is to understand how the stochastic equation for the speed looks like and what is the effective noise regulating its dynamics. For simplicity, we refer to the case $d = 2$, but everything can be generalized in $d = 3$.

When $J = 0$, the N coupled equations of the velocities (9.25) separate in N dynamics for single particles, hence we get:

$$\frac{d\mathbf{r}_i}{dt} = \mathbf{v}_i \quad (9.33)$$

$$\frac{d\mathbf{v}_i}{dt} = -2g(|\mathbf{v}_i| - v_0) \frac{\mathbf{v}_i}{|\mathbf{v}_i|} + \sqrt{2T}\boldsymbol{\xi}_i \quad (9.34)$$

where we are considering the white noise $\langle \boldsymbol{\xi}_i(t) \rangle = 0$ and $\langle \boldsymbol{\xi}_i(t) \cdot \boldsymbol{\xi}_i(t') \rangle = 2d\delta(t-t')$. We can now transform these equations using polar coordinates, namely identifying $\mathbf{v}_i(t) = s_i(t)(\cos \phi_i(t), \sin \phi_i(t))$, where $s_i(t)$ is speed and $\phi_i(t)$ is the phase of the velocity vector. Using the Stratonovich convention [31] of standard derivatives, the resulting equations read,

$$\frac{d\mathbf{r}_i}{dt} = s_i(t)\mathbf{e}_i(t) \quad (9.35)$$

$$\frac{d\phi_i(t)}{dt} = \frac{1}{s_i(t)}\sqrt{2T}\xi_i^\phi(t) \quad (9.36)$$

$$\frac{ds_i(t)}{dt} = -2g(s_i(t) - v_0) + \sqrt{2T}\xi_i^s(t) \quad (9.37)$$

where the two new noises just introduced are multiplicative in the form,

$$\xi_i^\phi(t) = \cos \phi_i(t)\xi_i^y(t) - \sin \phi_i(t)\xi_i^x(t) \quad (9.38)$$

$$\xi_i^s(t) = \cos \phi_i(t)\xi_i^x(t) + \sin \phi_i(t)\xi_i^y(t) . \quad (9.39)$$

The Stratonovich calculus implies that the average values of the above expressions are different from zero, making difficult to compute the stochastic differential equation for the global degree of freedom. It is, indeed, simpler if we pass to the Ito 's scheme [31], remembering that,

$$\frac{ds_i(t)}{dt} = \frac{1}{2s_i} \frac{d(s_i^2)}{dt} - \frac{T}{s_i} \quad (9.40)$$

and

$$\frac{d(s_i^2)}{dt} = 2v^x \frac{dv^x}{dt} + 2v^y \frac{dv^y}{dt} + 4T \quad (9.41)$$

where the temperature terms are the additional elements of the derivatives [31].

The equation for the speed modifies into,

$$\frac{ds_i(t)}{dt} = -2g(s_i(t) - v_0) + (d-1)\frac{T}{s_i} + \sqrt{2T}\xi_i^s(t) \quad (9.42)$$

with a generalization to d dimensions. The advantage is that now, the same noise term of the previous equation has zero mean, and it is easier to compute

$$\frac{ds(t)}{dt} = \frac{d}{dt} \left(\frac{1}{N} \sum_i s_i \right)$$

which follows,

$$\frac{ds(t)}{dt} = -2g(s(t) - v_0) + (d-1)T(\overline{1/s}) + \sqrt{\frac{2T}{N}}\eta(t) \quad (9.43)$$

where with $(\overline{1/s})$ we mean $1/N \sum_i (1/s_i)$ and $\eta = (1/N) \sum_i \xi_i^s(t)$. As we expected, the effective temperature that rules the equilibrium dynamics of s is T/N .

This result can be generalized to the case $J \neq 0$, which we decide to numerically implement by means of lattice simulations. To test the validity of the FDT, we thus have to compute correlation and response function. For the former we define,

$$C(t) = \frac{1}{T_{max} - t} \sum_{t_0=1}^{T_{max}-t} \frac{1}{N} \sum_{ij} \delta s_i(t_0) \delta s_j(t_0 + t) \quad (9.44)$$

which, expressed in terms of the global degree of freedom, reads

$$C(t) = \frac{N}{T_{max} - t} \sum_{t_0=1}^{T_{max}-t} \delta s(t_0) \delta s(t_0 + t), \quad (9.45)$$

T_{max} is the length of the simulation, and the fluctuations are calculated with respect to a phase average, namely:

$$\delta s_i(t) = s_i(t) - \langle s_i \rangle_t; \quad \delta s(t) = s(t) - \langle s \rangle_t. \quad (9.46)$$

The factor N in (9.45) ensures that the proportionality factor with the response will be given only by the temperature T .

To compute the susceptibility we then realize the following protocol [111], for each simulation and set of parameters explored:

1. we run a simulation without field and we compute the correlation function over it;
2. we run a simulation with the same seed of point 1., but switching on the field at time t_0 ;
3. we evaluate the difference between the trajectories generated by the two

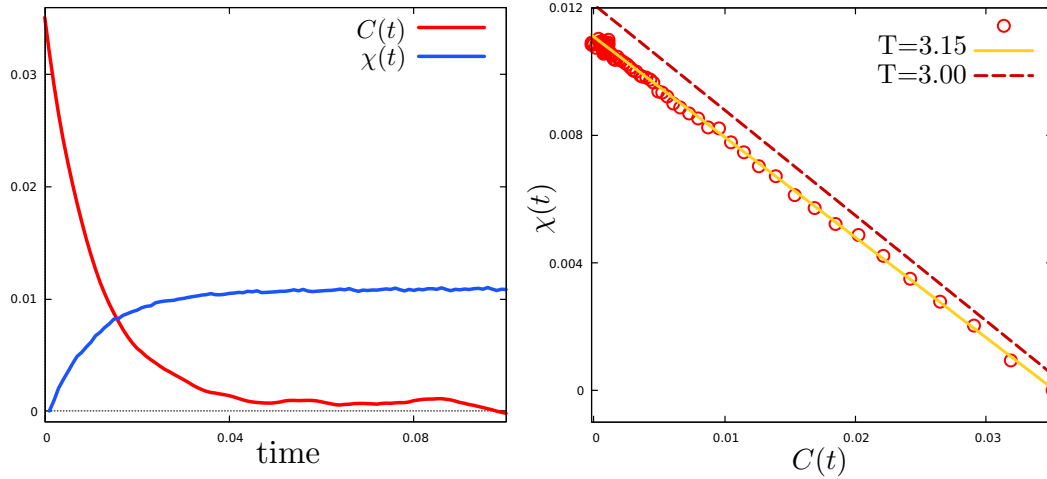


Figure 9.4: Equilibrium FDT test for step-function field. Left: correlation function and integrated response function in time of cubic lattice numerical simulations performed with $N = 216$, $J = 1.5$, $T = 3$, $g = 40$, $v_0 = 1$, $r_c = 1.05$, $h_0 = 0.1$. The two curves are used to realize the parametric plot of the right panel: the slope of the line gives an estimate of the temperature compared to the real value $T = 3$.

previous points divided by the intensity of the field for $t > t_0$;

4. we average over 400 realization of the starting time t_0 .
5. we obtain the integrated response as,

$$\chi(t) = \left\langle \frac{1}{N} \frac{|\sum_i^N s_i(t)^h - \sum_i^N s_i(t)|}{|h_0|} \right\rangle_{t_0} \quad (9.47)$$

for $t > t_0$. We are indicating with $s_i(t)^h$ the copy of the system which evolves with the field, and with $s_i(t)$ the copy with $h_0 = 0$;

6. we finally average over a sample of independent simulations.

To test the validity of (9.32), we realize the parametric plot $\chi(t)$ vs $C(t)$ whose slope can be identified as the inverse of the temperature of eq (9.25).

In the left panel of Fig 9.4, we report the correlation function in red and the integrated response in blue of a simulation of $N = 216$ particles with a step function field of amplitude $h_0 = 0.1$. On the right panel, we show the parametric plot realized with the same curves: we observe a straight line, whose fitted slope provides a measured temperature equal to $T = 3.15$, very consistent with the theoretical prediction $T = 3$. In the range of errors, statistics, and a small number of particles, we can state that we appreciate the validity of FDT in this case.

We repeat the same experiment for a square wave perturbation and the results are shown in Fig 9.5. In the left panel, we show the response and the correlation for a simulation of $N = 216$ particles, when the duration of the wave lasts $\delta t = 0.05$, a representative value to enhance the procedure.

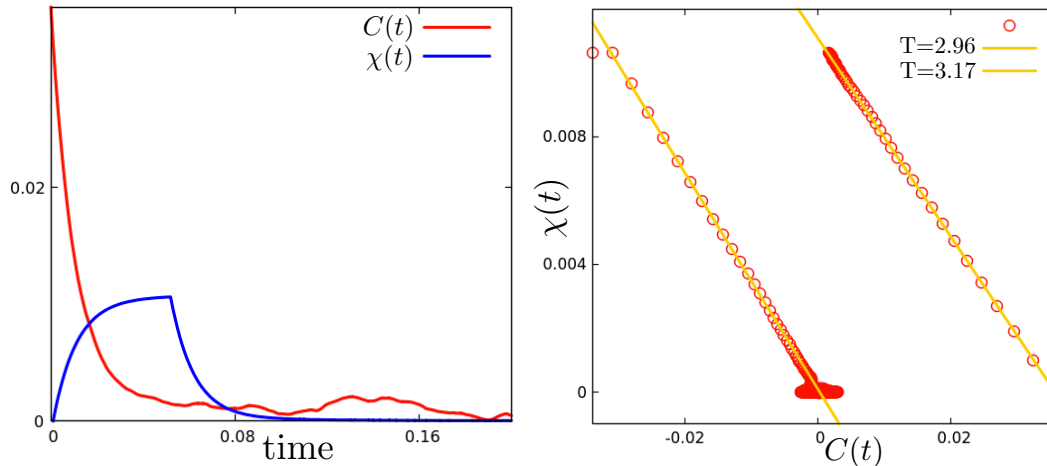


Figure 9.5: Equilibrium FDT test for square wave field. Left: correlation function and integrated response function in time of cubic lattice numerical simulations performed with $N = 216$, $J = 1.5$, $T = 3$, $g = 40$, $v_0 = 1$, $r_c = 1.05$, $h_0 = 3.0$, and $\delta t = 50$ time steps. The two curves are used to realize the parametric plot of the right panel: the slope of the lines give an estimate of the temperature compared to the real value $T = 3$. The right line corresponds to times $t < \delta t$, while the left line to $t > \delta t$.

The right panel shows two lines in the parametric plot of χ vs C . This is due to the fact that we need to distinguish the cases,

$$\begin{cases} t < \delta t & \rightarrow & \chi(t) = \beta(C(0) - C(t)) & \text{right line} \\ t > \delta t & \rightarrow & \chi(t) = \beta(C(t - \delta t) - C(t)) & \text{left line} \end{cases}$$

Both the slopes of Fig 9.5 give a good estimate of the equilibrium temperature $T = 3$.

9.2.4 Out-of-equilibrium preliminary results

After testing the protocols to compute the correlation and response of the model, we decide to move the study to the out-of-equilibrium case. In the vision of a possible application to the metric biological system of natural swarms, we use as control parameter the density and we keep fixed the temperature T in all the thermodynamic phases.

The first thing we analyze is the comparison between the on lattice and the off-lattice case when a step function field is applied, choosing $v_0 = 1$ and keeping the same set of the other parameters ($N = 216$). In the left panel of Fig 9.6, we present the curve of polarization when the density moves a continuous phase transition, certainly due to the small system's size. A quick interpolation suggests that the critical point is located around $\rho_c \simeq 1$, where we expect that the major manifestations of the out-of-equilibrium nature of the system appear. What indeed carries this active model to the violation of equilibrium is the reshuffling of the interaction network, especially its variation in time $\dot{n}_{ij}(t)$. The more the

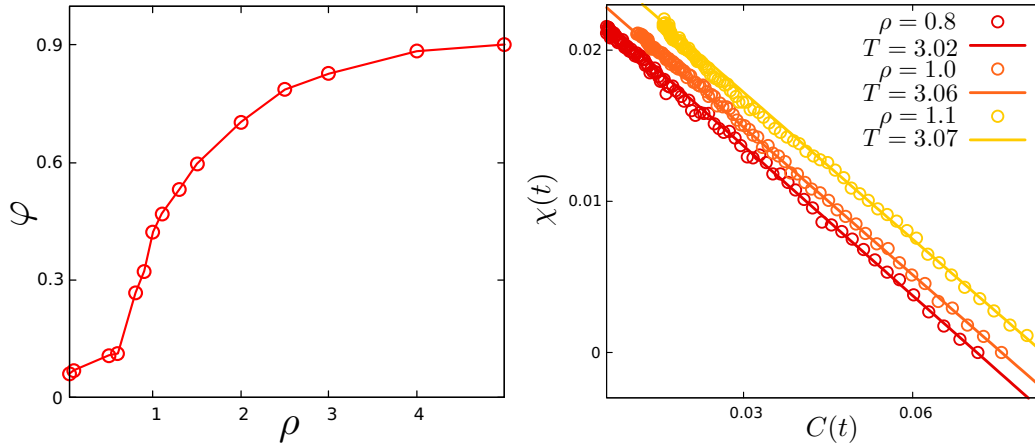


Figure 9.6: Off-equilibrium FDT for small activity. Left: polarization vs density, the control parameter, whose critical point is located around $\rho_c \simeq 1$. Right: parametric plot response vs correlation for densities close to the critical point. Out-of-equilibrium effects are not visible and the estimate temperature is always very close to the equilibrium value. The parameters used for the numerical simulations are $N = 216$, $J = 1.5$, $T = 3$, $g = 40$, $v_0 = 1$, $r_c = 1.05$, $h_0 = 0.1$, and the field taken as a step function.

particles exchange their neighbors, the more we should observe out-of-equilibrium effects. In the two limiting phases, of a deeply polarized and completely disordered system, we expect to observe effective equilibrium situations, since, in the high-density case the particles form a coherent flock thus almost preserving the same neighbors, while in the strongly sparse case the level of the interaction is poor and an effective equilibrium dominates.

Therefore, it seems reasonable to assume that the near-critical region is a good candidate to make manifest effects of FDT violation. In the right panel of Fig 9.6 we take three densities around polarization 0.3–0.4 and we analyzed the parametric plot of integrated response vs correlation. However, for this set of parameters, we still observe a good validity of the theorem, since the relation between the two quantities is perfectly linear and the slopes provide values very close to the real temperature of the system. We would have expected a discrepancy in the linear trend or in the fitted value of T .

The study of chapter 4 teaches us that this is not really surprising, but that can exist regions in the parameters space where the system is characterized by effective equilibrium dynamics even if microscopically active. This could be even more evident when the system’s size is small, together with the effective activity. Hence, we decide to pump both the effects exploring a larger size ($N = 512$) and multiplying the speed by a factor of 4. We repeat the study explained above, but, before going on and showing the results, we would like to clarify that these are just preliminary and that for sure need more investigation.

We fix a set of parameters that produces the curve of polarization, like the one shown in Fig 9.6, but locating the critical point around $\rho \sim 0.25$. For den-

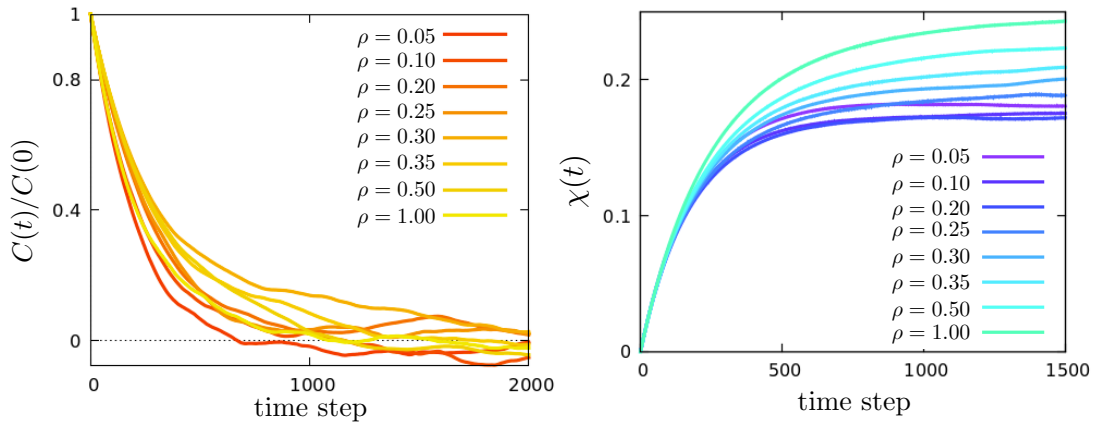


Figure 9.7: Off-equilibrium correlation and response function for large activity. Left: speed normalized correlation functions of SPP simulations spanning the control parameter in $\rho \in [0.05, 1.00]$. Right: for the same density values, integrated response functions. The numerical simulations are run with $N = 512$, $J = 1.5$, $T = 10$, $g = 2$, $v_0 = 4$, $r_c = 1.05$, $h_0 = 0.1$ in a step-function scheme.

sities spanning the range $\rho \in [0.05, 1.00]$ we compute correlation functions and integrated responses on a sample of 10 independent runs lasting $T_{max} = 3 \times 10^4$ time steps each. These curves are pictured in Fig 9.7 where the smooth behaviors in time can be appreciated. However, when we realize the parametric plots we finally notice some differences with the equilibrium case.

In Fig 9.8 some of them are reported. We can see that most of these curves are linear for small times, namely starting from the right corner, but then they develop a curvature towards what seems another linear regime. This trend is more evident in the example case of the left panel of Fig 9.9 where we are able to fit two different slopes of the curve: what we call T_1 , for small times and T_2 for larger times. Applying this operation to the data of different densities, we get the right panel of Fig 9.9: the estimate values of T_1 seem to reproduce the temperature of the thermal bath applied, thus still reflecting an effective equilibrium dynamics for small time scales; on the other hand, the values of T_2 appear always greater than the former, especially around the critical point where we can observe a maximum.

Even though the interpretation of these results still needs more work to be found, the second slope seems to suggest a violation of the FDT happening through a definition of an effective temperature, which measures these out-of-equilibrium effects enhanced at the critical point. Moreover, the fact of observing a violation only for very large temporal scales seems to be in agreement with the crossover in the Vicsek dynamics of [7], a field theory that should also be valid for this microscopic model. However, we are still lacking a complete analytical calculation that confirms this intuition and a good exploration of the model's parameters space and system's size. We hope that an intense future work will clarify if this is a good way to quantify out of equilibrium effects in the speed of swarming systems.

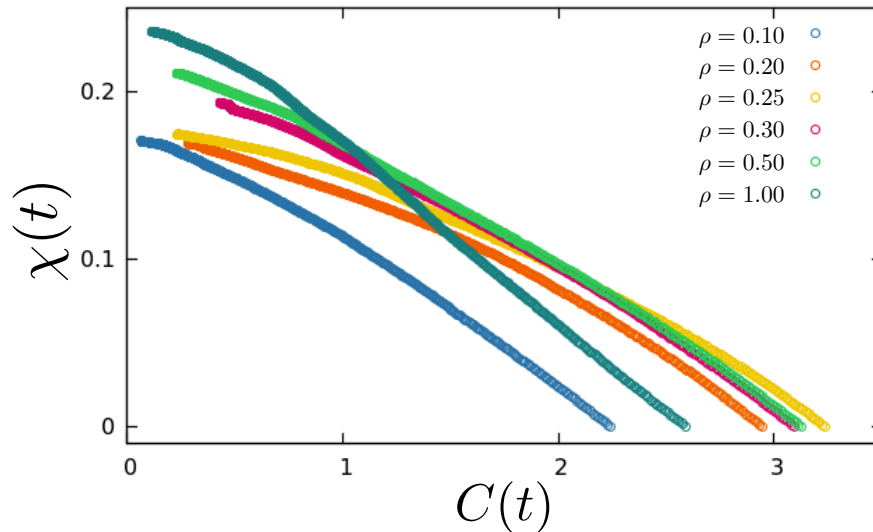


Figure 9.8: Off-equilibrium FDT for large activity. Parametric plot integrated response vs correlation of speed for different values of density, going from the disordered phase $\rho = 0.10$ to the ordered phase $\rho = 1.0$. The behavior of the lines manifests differences with the equilibrium or the small speed regimes. The trend is linear for small times (right bottom corner), and then curves towards another linear regime (top left corner). The point of curvature is more accentuated for densities close to the critical point. The numerical simulations are run with $N = 512$, $J = 1.5$, $T = 10$, $g = 2$, $v_0 = 4$, $r_c = 1.05$, $h_0 = 0.1$ in a step-function scheme.

9.3 How to spatially confine ISM swarms

We finally introduce the last topic of this dissertation which, as the previous one, belongs to the set of ongoing and still open projects. It also goes in the direction of adding more realistic ingredients to the active matter models we use to reproduce the behavior of swarming systems. The purpose of this section is indeed to understand how to model an inertial dynamics in the velocity including a force acting on the particles' positions.

With the study we carried out in the previous chapters, we understood the relevance of a second-order dynamics in the velocity to reproduce the critical behavior of natural swarms, starting from the shape of the dynamical correlation functions to the value of the dynamical critical exponent. We found out that the ISM is a good candidate to achieve this goal, and that it could be taken as a good reference point to explain the dynamics of the system. However, if from one hand it takes into account the main features of a velocity inertial dynamics, of an alignment force between the individuals and of their self-propulsion, on the other, it neglects one of the most evident interactions present at the swarming phase of these animals: the attraction to a landmark.

It has indeed been found that midges form collective movements in the proximity of some visual markers, like natural water pools or street lamps with the reproductive purpose of attracting females [56]. Experiments on these systems are therefore realized placing in proper natural environments artificial landmarks,

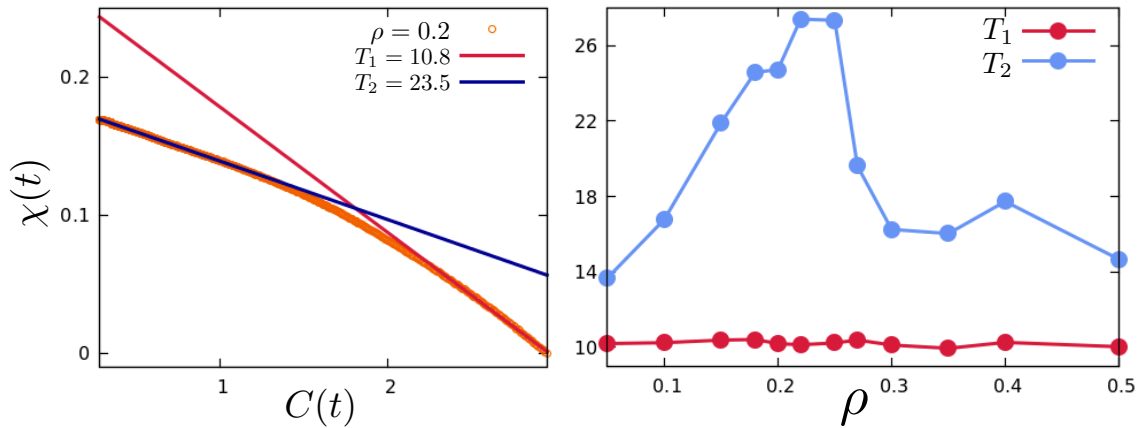


Figure 9.9: Effective temperatures for off-equilibrium FDT. Left: parametric plot for $\rho = 0.2$, the curve is fitted by two linear laws with different slopes that can reflect different measures of effective temperatures. The red line says that the temperature ruling the system for small time-scales is that of the standard thermal bath, while the blue line fits a bigger temperature for large temporal scales. The same procedure is repeated for all the values of density studied and the extrapolation of the two temperatures is reported on the right panel. The T_2 shows a trend in control parameter and it is peaked around the transition point. The numerical simulations are run with $N = 512$, $J = 1.5$, $T = 10$, $g = 2$, $v_0 = 4$, $r_c = 1.05$, $h_0 = 0.1$ in a step-function scheme.

able to induce spontaneous aggregations above them, and then starting the stereo video acquisitions [1, 2]. Here we want to model this scenario, representing the landmark's attraction as a confining potential on the midges positions in an inertial model for the velocities. A possible future perturbation-response experiment could be that of moving the landmark and try to understand how the dynamics of the swarm changes when changing the reference position. This model could serve as a solid ground to validate the experimental results.

On a first order Vicsek-like dynamics, it is very easy and natural to implement the presence of a Landmark: we can represent it as a harmonic force $\mathbf{F}(\mathbf{r}_i) = -\beta\mathbf{r}_i(t)$ acting of the velocity update equation,

$$\frac{d\mathbf{v}_i}{dt} = J \sum_j n_{ij} \mathbf{v}_j - \beta \mathbf{r}_i + \lambda \mathbf{v}_i + \boldsymbol{\zeta}_i \quad (9.48)$$

where $\boldsymbol{\zeta}_i$ is the usual source of white noise, λ is the Lagrange multiplier implementing the constant speed v_0 constraint, and finally β is the stiffness of the force which attracts each particle ideally towards the origin of the landmark. In the discrete time version, this model has already been studied in [1, 2], where it is shown that it preserves the same collective properties of the classical Vicsek model. Moreover the positional dependent force has a direct kinematic meaning: in absence of alignment interaction $J = 0$, eq (9.48) reads as a standard Newton equation with a harmonic force acting on a particle of mass $m = 1$.

Things get more complicated when we try to extend it to a second-order dynamics in the velocity since we want to include a non-standard Hamiltonian degree of freedom which generates the spin angular momentum. The first approach we try starts from the ISM derivation we carried out in section 5.4, namely passing through a Lagrangian formulation in terms of conjugated variables $\{\mathbf{v}_i, \boldsymbol{\pi}_i\}$, such that, in absence of external forces and noise, we get the dynamical equations:

$$\begin{aligned}\dot{\mathbf{r}}_i &= \mathbf{v}_i \\ \dot{\mathbf{v}}_i &= \frac{1}{m}(\boldsymbol{\pi}_i - 2\lambda\mathbf{v}_i) \\ \dot{\boldsymbol{\pi}}_i &= 2\lambda\dot{\mathbf{v}}_i \\ \mathbf{s}_i &= \mathbf{v}_i \times \boldsymbol{\pi}_i\end{aligned}\tag{9.49}$$

where λ still implements $|\mathbf{v}_i| = v_0$. In the same mechanistic view of the Vicsek formulation, we add the positional force on the first equation of the real particle acceleration, namely:

$$\dot{\mathbf{v}}_i = \frac{1}{m}(\boldsymbol{\pi}_i - 2\lambda\mathbf{v}_i + \mathbf{F}(\mathbf{r}_i))\tag{9.50}$$

from which the Lagrange multiplier can be solved,

$$\lambda = \frac{(\mathbf{v}_i \cdot \boldsymbol{\pi}_i) + (\mathbf{v}_i \cdot \mathbf{F}(\mathbf{r}_i))}{2v_0^2}.\tag{9.51}$$

Repeating then the same passages of section 5.4 we arrive to the equations of motion for the velocity and for the spin, which appear

$$\begin{aligned}\dot{\mathbf{r}}_i &= \mathbf{v}_i \\ \dot{\mathbf{v}}_i &= \frac{\mathbf{s}_i \times \mathbf{v}_i}{\chi} + \frac{\mathbf{v}_i}{\chi} \times \left(\mathbf{F}(\mathbf{r}_i) \times \mathbf{v}_i \right) \\ \dot{\mathbf{s}}_i &= \mathbf{F}(\mathbf{r}_i) \times \dot{\mathbf{v}}_i.\end{aligned}\tag{9.52}$$

From this, it is clear that the positional force seems to enter in a non-trivial way in the dynamics of the spin and of the velocity itself, due to the implementation of the speed constraint. However, a numerical solution of these differential equations for several initial conditions shows that this mechanism does not work, since the dynamics of the single-particle happens not to be confined.

To understand why this naive choice does not fulfill our expectations, let's briefly look at the situation where no confining force is implemented, i.e. $\mathbf{F} = 0$. The trajectory of the single-particle strongly depends on the initial conditions $\mathbf{r}_i(t=0)$, $\mathbf{v}_i(t=0)$ and $\mathbf{s}_i(t=0)$. We can have three different outcomes which are illustrated in Fig 9.10, where the result of numerical integration of the above differential equations is shown using projections on the xy -plan of the single particle's trajectory. In the first panel a, the system starts with null initial spin $\mathbf{s}_i(t=0) = 0$, and consequently, the particle does a simple linear motion; in b the initial spin is not zero, but its value is preserved along with the dynamical evolu-

tion, moreover since $\mathbf{v}_i(0) \cdot \mathbf{s}_i(0) = 0$ the resulting motion is circular with radius fixed by the modulus of the spin; finally the last case happens when $\mathbf{v}_i(0) \cdot \mathbf{s}_i(0) \neq 0$ producing a helical trajectory that we can call "corkscrew" solution (panel c).

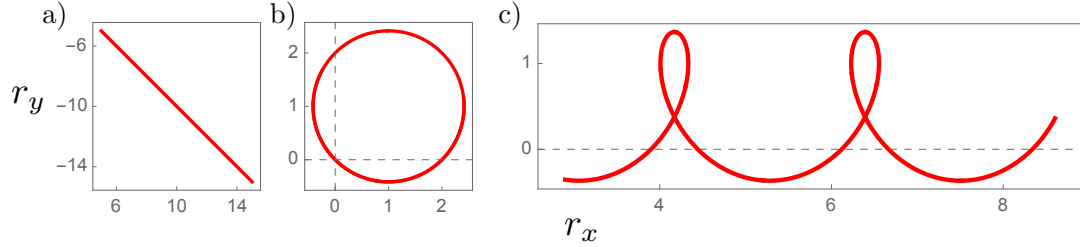


Figure 9.10: Numerical integration of single particle with $\mathbf{F}(\mathbf{r}_i) = 0$. Depending on the initial conditions the 3d particle trajectory can be of three different types which are reported in a projection on the plane (r_x, r_y) . Panel a: $\mathbf{s}_i(t=0) = 0$, the particle performs a simple linear motion; panel b: $\mathbf{s}_i(t=0) \neq 0$ and $\mathbf{v}_i(0) \cdot \mathbf{s}_i(0) = 0$, these conditions produce a circular motion on the plane orthogonal to the spin; panel c: $\mathbf{s}_i(t=0) \neq 0$ and $\mathbf{v}_i(0) \cdot \mathbf{s}_i(0) \neq 0$, the particle's trajectory is helical and we call it "corkscrew solution".

Now that this scenario is clear, we can reintroduce the confining force and reformulate eq (9.52) as,

$$\dot{\mathbf{v}}_i = \frac{1}{\chi} \left(\mathbf{s}_i - (\mathbf{F}(\mathbf{r}_i) \times \mathbf{v}_i) \right) \times \mathbf{v}_i . \quad (9.53)$$

If we introduce the pseudo spin,

$$\mathbf{T}_i = \mathbf{s}_i - (\mathbf{F}(\mathbf{r}_i) \times \mathbf{v}_i) , \quad (9.54)$$

the equations of motion can then be expressed,

$$\begin{aligned} \dot{\mathbf{r}}_i &= \mathbf{v}_i \\ \dot{\mathbf{v}}_i &= \frac{\mathbf{T}_i \times \mathbf{v}_i}{\chi} \\ \dot{\mathbf{T}}_i &= \frac{\mathbf{v}_i \times \dot{\mathbf{F}}(\mathbf{r}_i)}{\chi} \end{aligned} \quad (9.55)$$

identifying \mathbf{T}_i as the new torque of the velocity. It is clear that, when considering only harmonic confining forces, namely $\mathbf{F}(\mathbf{r}_i) = -\beta \mathbf{r}_i$, the implemented dynamics is of the type,

$$\begin{aligned} \dot{\mathbf{r}}_i &= \mathbf{v}_i \\ \dot{\mathbf{v}}_i &= \frac{\mathbf{T}_i \times \mathbf{v}_i}{\chi} \\ \dot{\mathbf{T}}_i &= 0 \end{aligned} \quad (9.56)$$

which looks very similar to the deterministic evolution with conserved angular

momentum of Fig 9.10. Indeed, the analogy is complete and it is represented by the trajectories of Fig 9.11, which come from a numerical integration of eq (9.55) with the explicit version of the pseudo-spin. Also in presence of a harmonic force on the particle's position, the effect is only to contribute to the value of the angular momentum which is fixed by the initial conditions reproducing the effects of the not-confined case. In Fig 9.11, we show in a the case where $\mathbf{T}_i(0) = 0$, in b when $\mathbf{T}_i(0) \cdot \mathbf{v}_i(0) = 0$ and finally in c when $\mathbf{T}_i(0) \cdot \mathbf{v}_i(0) \neq 0$. We used also different initial conditions from Fig 9.10 to test the generality and the accuracy of the equations.

Concluding, we can say that this way of implementing a confining quadratic force in ISM is not correct and we need to find a new method that goes beyond the classical mechanistic approach.

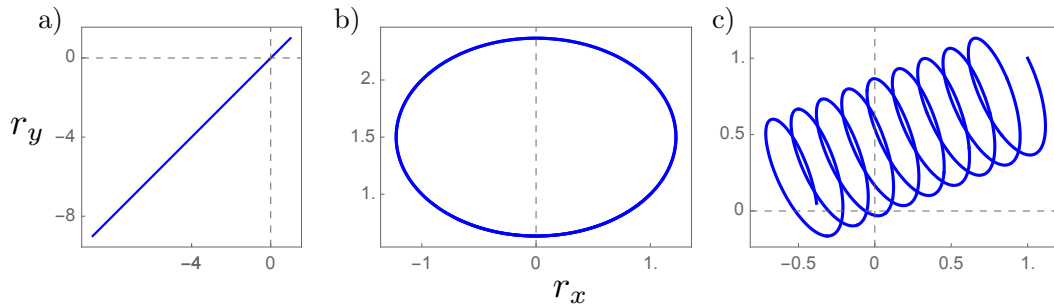


Figure 9.11: Numerical integration of single particle with $\mathbf{F}(\mathbf{r}_i)$ in the velocity's update. Implementing the confining force in the equation of the velocity update produces the same non-confined scenario of Fig 9.10. Initial conditions are given with respect to the pseudo-spin $\mathbf{T}_i = \mathbf{s}_i - (\mathbf{F}(\mathbf{r}_i) \times \mathbf{v}_i)$ and the trajectories are projected on the (r_x, r_y) plane. Panel a: linear motion when $\mathbf{T}_i(0) = 0$; panel b: circular motion for $\mathbf{T}_i(0) \neq 0$ and $\mathbf{T}_i(0) \cdot \mathbf{v}_i(0) = 0$; panel c: corkscrew motion for $\mathbf{T}_i(0) \neq 0$ and $\mathbf{T}_i(0) \cdot \mathbf{v}_i(0) \neq 0$.

9.3.1 Force on the angular momentum

The idea we present follows the intuition of assuming the spin as the mediator of all the forces acting on the single particle, therefore also including those involving positional degrees of freedom. This mean we insert the $\mathbf{F}(\mathbf{r}_i)$ on the equation of the generalized conjugated momentum, namely starting with equations,

$$\begin{aligned}
 \dot{\mathbf{r}}_i &= \mathbf{v}_i \\
 \dot{\mathbf{v}}_i &= \frac{1}{m}(\boldsymbol{\pi}_i - 2\lambda\mathbf{v}_i) \\
 \dot{\boldsymbol{\pi}}_i &= 2\lambda\dot{\mathbf{v}}_i + \mathbf{F}(\mathbf{r}_i) \\
 \mathbf{s}_i &= \mathbf{v}_i \times \boldsymbol{\pi}_i
 \end{aligned} \tag{9.57}$$

thus leading to,

$$\begin{aligned}\dot{\mathbf{r}}_i &= \mathbf{v}_i \\ \dot{\mathbf{v}}_i &= \frac{\mathbf{s}_i \times \mathbf{v}_i}{\chi} \\ \dot{\mathbf{s}}_i &= \mathbf{v}_i \times \mathbf{F}(\mathbf{r}_i) .\end{aligned}\tag{9.58}$$

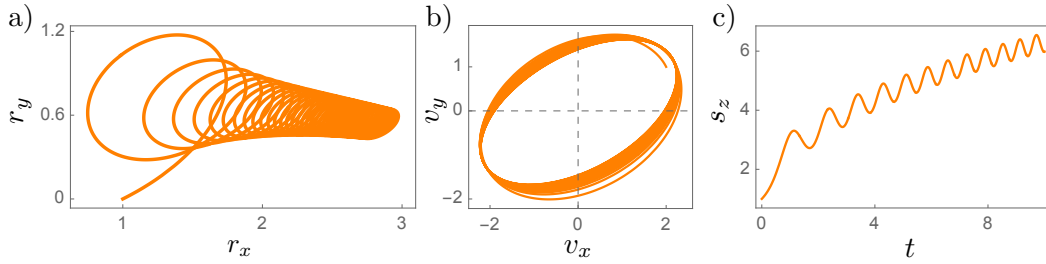


Figure 9.12: Numerical integration of single particle with $\mathbf{F}(\mathbf{r}_i)$ in the spin's update. The trajectory produced by this way of imposing the confining force is always of the corkscrew type, since the spin is never perpendicular to the velocity. Panel a: projection on the (r_x, r_y) of the trajectory for one set of initial conditions, panel b: projection of the (v_x, v_y) plane of the velocity's trajectory; panel c: trend in time of z component of the spin.

The numerical implementation of these equations of motion is reproduced in Fig 9.12, where we show the case for only one initial condition. Indeed, whatever starting values are chosen, the resulting trajectory is always of the corkscrew type, because, due to the positional force, the spin cannot align orthogonally to the velocity and it produces the characteristic helicoidal movement. Therefore, also in this case, it seems we do not find the right solution for confinement.

However, in the standard case of zero forces, we already know a way to dominate this type of trajectories, and to restore the particle to move in a circular motion: the spin dissipation [8]. It has been actually demonstrated that inserting a dissipation drives the solutions with $\mathbf{v}_i(0) \cdot \mathbf{s}_i(0) \neq 0$ for long time to the well-behaved trajectories of the case $\mathbf{v}_i(0) \cdot \mathbf{s}_i(0) = 0$ [94]. We, therefore, enrich the model with the usual thermal couple, noise plus dissipation, in the generalized momentum's equation:

$$\dot{\boldsymbol{\pi}}_i = 2\lambda\dot{\mathbf{v}}_i + \mathbf{F}(\mathbf{r}_i) - \frac{\eta}{\chi}\boldsymbol{\pi}_i + \frac{1}{v_0}\boldsymbol{\xi}_i\tag{9.59}$$

finally arriving to the dynamics,

$$\begin{aligned}\dot{\mathbf{r}}_i &= \mathbf{v}_i \\ \dot{\mathbf{v}}_i &= \frac{\mathbf{s}_i \times \mathbf{v}_i}{\chi} \\ \dot{\mathbf{s}}_i &= \mathbf{v}_i \times \left(\mathbf{F}(\mathbf{r}_i) + \frac{1}{v_0}\boldsymbol{\xi}_i \right) - \frac{\eta}{\chi}\mathbf{s}_i\end{aligned}\tag{9.60}$$

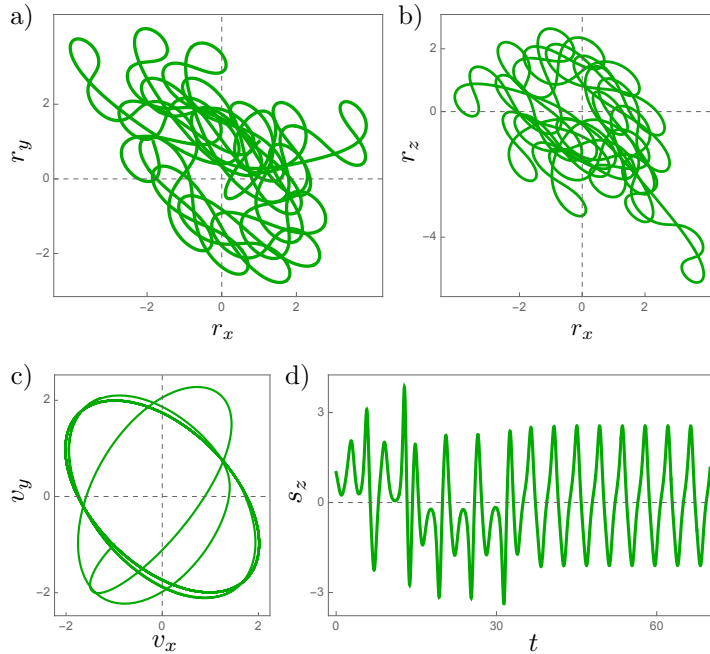


Figure 9.13: Numerical integration of single particle with $\mathbf{F}(\mathbf{r}_i)$ and dissipation in the spin's update. When we add dissipation to the evolution of the spin, the spatial trajectory of one ISM particle is correctly confined around the origin of the space, panels a and b are sections in the (r_x, r_y) and (r_x, r_z) planes. Panel c: projection of the (v_x, v_y) plane of the velocity's trajectory; panel d: trend in time of the z component of the spin.

where η is the friction coefficient, and ξ_i is the white noise source.

This scenario seems to have the right features to reach our final objective, because if now we compute the second order differential equation for the velocity, we get,

$$\chi \ddot{\mathbf{v}}_i + \eta \dot{\mathbf{v}}_i + \frac{\chi}{v_0^2} \mathbf{v}_i (\dot{\mathbf{v}}_i)^2 = \left(v_0^2 \mathbf{F}(\mathbf{r}_i) + v_0 \xi_i \right)^\perp \quad (9.61)$$

where with the expression \mathbf{w}^\perp we mean $\mathbf{w}^\perp = \mathbf{w} - (\mathbf{v}_i (\mathbf{w} \cdot \mathbf{v}_i) / v_0^2)$. From this equation, it is possible to easily perform the overdamped limit considering time scales $t \gg \chi / \eta$ or vanishing inertia, thus obtaining,

$$\eta \dot{\mathbf{v}}_i = \left(v_0^2 \mathbf{F}(\mathbf{r}_i) + v_0 \xi_i \right)^\perp \quad (9.62)$$

which, when we add also a social alignment force, reads correctly as the above Vicsek model simulated in [2]. This fact suggests that we are building up a good underdamped theory.

We finally numerically integrate eq (9.60) with zero noise, and we confirm that now the positional force acts properly to confine the particle around the origin of the space for all the initial conditions. Results for one set of starting coordinates are shown in Fig 9.13, where we look at two sectional planes of positions, at a projection of the velocity's space and at the time series of a component of the

spin. This result confirms that dissipation is crucial to reproduce the correct movement of turning and confined particles.

Certainly, deeper studies have to be carried out on this topic, above all reinstating stochasticity and alignment forces, thus testing if this scheme is maintained by the inter-particle interaction. Additionally, more investigations on the Hamiltonian nature of the degrees of freedom are necessary, since this dynamics seems to mix in a non-trivial way the different levels of positions and velocity, with that of velocity and spin. New physical interpretations of the spin could indeed be still hidden by these formulations. Nevertheless, this preliminary study seems to build an interesting way to go.

Conclusions

We started from experimental evidence of dynamical scaling in natural swarms of insects, with a dynamical critical exponent $z_{exp} = 1.2$ not predicted by any statistical theory. Data also revealed that the shape of swarms' dynamical correlation functions follows an underdamped dynamics not compatible with a dissipative exponential relaxation [3]. Our purpose was to find a physical model able to describe these experimental findings, reproducing a consistent value of the dynamical critical exponent and the typical decay of the swarms' temporal correlation functions. Since this biological system satisfies scaling laws and reflects a near-critical behavior, we decided to use a field theory approach to describe its properties. Therefore, we combined Dynamical Renormalization Group calculations with extensive numerical simulations to study the critical relaxation of active matter models.

We went through several stages. The first step was to study the critical dynamics of the Vicsek model. To begin with, we tackled the problem from an analytical point of view, retracing the calculation of the incompressible hydrodynamic theory of Chen et al [6]. From this study, we learned that dissipative polar active systems belong to a dynamical universality class described by the exponent $z = 1.7$ in three dimensions. The theory produces also an equilibrium unstable fixed point characterized by zero activity and relevant ferromagnetic interaction with $z = 2$. Investigating the crossover between these two dynamical universality classes, we unveiled how the interplay between the system's size and the activity level determines the dynamical relaxation of active systems. In the limit of small sizes and activity, the system only shows an effective equilibrium critical dynamics, while for large sizes or large activity levels the out-of-equilibrium critical dynamics emerges with the exponent $z = 1.7$. The crossover is regulated by a crossover length scale $\mathcal{R}_c = (1/\alpha_0)^\kappa \Lambda^{-1}$ with $\kappa = 31/51$ in $d = 3$, above which the non-equilibrium dynamics takes over. Moreover, we performed numerical simulations of the original Vicsek model in three dimensions and in the paramagnetic near-critical regime without imposing any incompressibility constraint. We verified the same crossover phenomenon tuning the speed of the particles v_0 , demonstrating that the active fixed point is not an artifact of incompressibility but an authentic characteristic of polar active systems. Finally, we confirmed that activity has the effect to lower the dynamical critical exponent from $z = 2$ to $z = 1.7$. Unfortunately, even though closer to it, this latter value is not compatible with the experimental one. The exponential dynamical relaxation is also

not in agreement with the dynamics of natural swarms [7].

These reasons prompted us to study the critical behavior of the Inertial Spin Model, an active matter model with inertial dynamics in the velocity coupled to the conjugated momentum [8]. We studied it under a fixed-network approximation to focus on the role of inertia and dissipation in determining the critical dynamics of a system. A one-loop DRG calculation showed that the violation of momentum conservation generates a crossover between an unstable fixed point, characterized by a dynamic critical exponent $z = 1.5$ for $d = 3$, and a stable fixed point with $z = 2$. The fixed point with the lower exponent describes a conservative dynamics that finite-size and weakly damped systems can experience at a macroscopic level. The phenomenon is regulated by a crossover length scale $\mathcal{R}_c = \mathcal{R}_0^{4/d}$, which importantly depends on \mathcal{R}_0 . This latter represents an additional characteristic length scale of the system that describes the interplay between the conservative and the dissipative relaxation. Numerically we verified this crossover at equilibrium varying the microscopic momentum's dissipation in a three-dimensional system of fixed size. Moreover, simulations confirmed that the second-order of the ISM's dynamics is fundamental to reproducing the underdamped relaxation of natural swarms. Even if the on-lattice approximation did not reproduce the out-of-equilibrium phenomenology of the swarming system, this study confirmed that a theory with inertial couplings goes in the right direction for lowering the value of the critical exponent with respect to the fully dissipative case [9, 10].

Finally, we performed a DRG calculation on the out-of-equilibrium incompressible hydrodynamic theory of the ISM. Results are preliminary and we postponed a detailed discussion to a colleague's future thesis. However, we anticipated the main outcome, which concludes the investigation on natural swarms of insects: a novel fixed-point with $z = 1.3$ emerges, and it expresses a conservative out-of-equilibrium critical dynamics. We believe this point describes the critical dynamics of the system of our interest. This study confirmed that, in a non-equilibrium mode-coupling theory, activity levels and inertia cooperate to lower the value of the dynamical critical exponent. The obtained value agrees with experimental measurements on natural swarms. The crossovers described in this thesis are recovered in this calculation, and they represented important stepping stones to arrive at the final result [11].

Future studies are necessary to have a full comprehension of this theory: more work is needed to clarify the physical role of all the terms of the hydrodynamic equations. Out-of-equilibrium simulations of the near-critical ISM are also necessary to validate the analytical results at microscopic scales. Moreover, the models and the approximations we used are definitely not the only methods to provide possible explanations to the phenomenon under consideration. Different microscopic formulations of the models we analyzed could involve additional interaction terms or non-trivial sources of noise, arriving at more realistic descriptions of the swarming system. A possible future study concerns the role of density fluctuations, which, for this kind of active model at the edge of the phase transition,

surely deserves more attention. Additionally, the application of the same calculations to the case of ordered polarized systems as bird flocks is an interesting project to carry out. New experimental techniques will soon allow deeper studies of the flocks' dynamics, providing data on which to test the dynamical scaling hypothesis. A DRG computation in the deeply ordered phase of the ISM could confirm if this model is able to quantitatively reproduce this possible evidence. If this was the case, we would have a single minimal model describing the collective behavior of very different biological systems. This could confirm that the search for universality in this field is achievable, thus stimulating additional experiments on new living and collective systems.

In the last chapter, we introduced some side projects dedicated to modifications of standard active matter models. We firstly explored speed fluctuations in Vicsek-like dynamics relaxing the fixed speed constraint. We analyzed the low-temperature phase of two different speed control potentials and we verified with extensive numerical simulations that the marginal model reproduces experimental features of bird flocks [55]. We then used the linear potential to explore the near-critical regime of an active system and we developed a model to study external perturbation in speed fluctuations in swarms. Preliminary results showed that for large activity levels, we observe a violation of the Fluctuation-Dissipation relations in speed's dynamics, with an effective temperature maximum at the critical point. More in-depth studies have to be performed on the same topic, especially to understand which are the main factors that increase the out-of-equilibrium nature of the system and to what extent they can be measured. Finally, we studied how to reproduce the presence of an external attracting landmark on the ISM with a rigid speed constraint. The non-trivial solution opens many questions about the mechanistic nature of the dynamical variables of the model, but it allows to perform additional studies of landmark perturbations that could find also experimental confirmation.

Concluding, the approach taken in this thesis combined a statistical description of collective behavior with experimental evidence from field studies. We are convinced that bridging theory and experiment is fundamental to increasing our knowledge of living systems. We hope that this work not only contributes to the corpus of research in the active matter but also lays down fruitful scientific directions for future studies.

Appendix A

Angular averages

In this section we present the angular averages used for the calculation of the incompressible and near-critical hydrodynamic equation of the Vicsek model, which can also be found in [6]. In generic d dimensions, we begin with the identity,

$$\left\langle \frac{k_\alpha k_\beta}{k^2} \right\rangle_{\hat{\mathbf{k}}} = \frac{1}{d} \delta_{\alpha\beta} \quad (\text{A.1})$$

where $\langle \rangle_{\hat{\mathbf{k}}}$ indicates the average over the directions $\hat{\mathbf{k}}$ around the wave-vector \mathbf{k} . This identity is proved by symmetry: it has to be null when $\alpha \neq \beta$ because the average becomes odd, while it has to be identical to 1 when evaluating the same component. The dimension factor in the denominator comes from the evaluation of the trace: $\langle \frac{k_\alpha k_\alpha}{k^2} \rangle_{\hat{\mathbf{k}}} = 1$. From this result the average of a projector directly follows,

$$\langle P_{\alpha\beta}(\mathbf{k}) \rangle_{\hat{\mathbf{k}}} = \langle \delta_{\alpha\beta} - \frac{k_\alpha k_\beta}{k^2} \rangle_{\hat{\mathbf{k}}} = \left(1 - \frac{1}{d}\right) \delta_{\alpha\beta} . \quad (\text{A.2})$$

The last useful formula to report concerns the average of the product of two projectors $\langle P_{\alpha\beta}(\mathbf{k}) P_{\gamma\nu}(\mathbf{k}) \rangle_{\hat{\mathbf{k}}}$, which can be rewritten as,

$$\langle P_{\alpha\beta}(\mathbf{k}) P_{\gamma\nu}(\mathbf{k}) \rangle_{\hat{\mathbf{k}}} = \delta_{\alpha\beta} \delta_{\gamma\nu} - \delta_{\alpha\beta} \langle \frac{k_\gamma k_\nu}{k^2} \rangle_{\hat{\mathbf{k}}} - \delta_{\gamma\nu} \langle \frac{k_\alpha k_\beta}{k^2} \rangle_{\hat{\mathbf{k}}} + \langle \frac{k_\alpha k_\beta k_\gamma k_\nu}{k^4} \rangle_{\hat{\mathbf{k}}} . \quad (\text{A.3})$$

The first three terms can be evaluated with the tools already introduced, while the last term needs more attention. This is different from zero only if the indices are equal in pair, otherwise the average is performed over odd quantities and then it is null. Taking into consideration the case of all 4 identical labels, and the other possible mixed combinations, it can be proved that [6],

$$\left\langle \frac{k_\alpha k_\beta k_\gamma k_\nu}{k^4} \right\rangle_{\hat{\mathbf{k}}} = \frac{1}{d(d+2)} (\delta_{\alpha\beta} \delta_{\gamma\nu} + \delta_{\gamma\beta} \delta_{\alpha\nu} + \delta_{\alpha\gamma} \delta_{\beta\nu}) \quad (\text{A.4})$$

Using this last and the first formula in (A.3), we finally get:

$$\langle P_{\alpha\beta}(\mathbf{k}) P_{\gamma\nu}(\mathbf{k}) \rangle_{\hat{\mathbf{k}}} = \left(\frac{d^2 - 3}{d(d+2)} \right) \delta_{\alpha\beta} \delta_{\gamma\nu} + \frac{1}{d(d+2)} (\delta_{\gamma\beta} \delta_{\alpha\nu} + \delta_{\alpha\gamma} \delta_{\beta\nu}) . \quad (\text{A.5})$$

Appendix B

Numerical implementation of ISM algorithm

If for the Vicsek model, in its original derivation, the numerical implementation is almost straightforward, for the ISM the discretized equations are more complicated, due also to the presence of the constraint on v_0 . The algorithm used is a RATTLE [112], and the original simulation code has been written by Prof. Tomas Grigera. We resume here the numerical scheme.

The starting point is the second order differential equation for the velocity, that can be derived in the same spirit of eq (9.61) namely,

$$\frac{d^2 \mathbf{v}_i}{dt^2} = \frac{v_0^2}{\chi} [\mathbf{F}_s^i + \mathbf{F}_v^i + \mathbf{f}_c^i] \quad (\text{B.1})$$

where, the first term on the r.h.s. is the social force, and the second is the thermal bath force:

$$\mathbf{F}_s^i = \frac{J}{v_0^2} \sum_j n_{ij}(t) \mathbf{v}_j \quad (\text{B.2})$$

$$\mathbf{F}_v^i = -\frac{\eta}{v_0^2} \frac{d\mathbf{v}_i}{dt} + \frac{\boldsymbol{\xi}_i}{v_0} . \quad (\text{B.3})$$

The last term is instead the force implementing the constraint which is enforced with Lagrange multipliers according to the RATTLE scheme. To discretize it, we define $\mathbf{a}_i = d\mathbf{v}_i/dt$ and $\mathbf{b}_i = d\mathbf{a}_i/dt$ which allow to arrive to [93],

$$\mathbf{r}_i(t + \Delta t) = \mathbf{r}_i(t) + \Delta t \mathbf{v}_i(t) \quad (\text{B.4})$$

$$\mathbf{v}_i(t + \Delta t) = \mathbf{v}_i(t) + \Delta t c_1 \mathbf{a}_i(t) + (\Delta t)^2 c_2 \mathbf{b}_i(t) + (\Delta t)^2 c_2 \lambda_i(t) + \boldsymbol{\Xi}_v(t) \quad (\text{B.5})$$

$$\begin{aligned} \mathbf{a}_i(t + \Delta t) = & c_0 \mathbf{a}_i(t) + (c_1 - c_2) \Delta t [\mathbf{b}_i(t) + \lambda_i \mathbf{v}_i(t)] + \\ & + c_2 \Delta t [\mathbf{b}_i(t + \Delta t) + \mu_i \mathbf{v}_i(t + \Delta t)] + \boldsymbol{\Xi}_a(t) \end{aligned} \quad (\text{B.6})$$

$$\mathbf{b}_i(t + \Delta t) = \frac{v_0^2}{\chi} \mathbf{F}_s^i(\{\mathbf{r}_j(t + \Delta t), \mathbf{v}_j(t + \Delta t)\})$$

where λ_i and μ_i are related to the constraint and their expression will be given

in a moment. The other constant result from the time integration and they are given by,

$$c_0 = e^{-\eta v_0^2 \Delta t / \chi} \quad (\text{B.7})$$

$$c_1 = \frac{\chi}{v_0^2 \eta \Delta t} (1 - c_0) \quad (\text{B.8})$$

$$c_2 = \frac{\chi}{v_0^2 \eta \Delta t} (1 - c_1) , \quad (\text{B.9})$$

while we are indicating with Ξ_v and Ξ_a the random variables with variance,

$$\langle \Xi_v^2 \rangle = \frac{T \chi}{v_0^2 \eta} \left(2 \frac{\eta v_0^2 \Delta t}{\chi} - 3 + 4e^{-\eta v_0^2 \Delta t / \chi} - e^{-2\eta v_0^2 \Delta t / \chi} \right) \quad (\text{B.10})$$

$$\langle \Xi_a^2 \rangle = \frac{T v_0^2}{\chi} \left(1 - e^{-2\eta v_0^2 \Delta t / \chi} \right) \quad (\text{B.11})$$

$$\langle \Xi_a \Xi_v \rangle = \frac{T}{\eta} \left(1 - e^{-\eta v_0^2 \Delta t / \chi} \right) . \quad (\text{B.12})$$

Finally the implementation of the N independent constraints on the velocities' moduli allows to derive analytically the Lagrange multipliers, just imposing $v_i^2(t + \Delta t)^2 = v_0^2$ and $\mathbf{v}_i(t + \Delta t) \cdot \mathbf{a}_i(t + \Delta t) = 0$. They read,

$$\lambda_i = \frac{w_+ - 1}{(\Delta t)^2 c_2} \quad (\text{B.13})$$

$$\mu_i = - \frac{\mathbf{v}_i(t + \Delta t) \cdot \mathbf{a}'_i(t + \Delta t)}{c_2 v_0^2 \Delta t} \quad (\text{B.14})$$

where w_+ is the positive solution of,

$$v_0^2 w^2 + 2\mathbf{v}_i(t) \cdot \Delta \mathbf{v}_i(t) w + \Delta v_i^2 = v_0^2 \quad (\text{B.15})$$

with $\Delta \mathbf{v}_i(t)$ indicating the Δt dependent part of $\mathbf{v}_i(t + \Delta t)$, and $\mathbf{a}'_i(t + \Delta t)$ the expression of $\mathbf{a}'_i(t + \Delta t)$ without the μ part. Finally, the dynamical implementation follows the velocity Verlet scheme [113].

Bibliography

- [1] A. Attanasi, A. Cavagna, L. Del Castello, I. Giardina, S. Melillo, L. Parisi, O. Pohl, B. Rossaro, E. Shen, E. Silvestri, *et al.*, “Collective behaviour without collective order in wild swarms of midges,” *PLoS Comput Biol*, vol. 10, no. 7, p. e1003697, 2014.
- [2] A. Attanasi, A. Cavagna, L. Del Castello, I. Giardina, S. Melillo, L. Parisi, O. Pohl, B. Rossaro, E. Shen, E. Silvestri, *et al.*, “Finite-size scaling as a way to probe near-criticality in natural swarms,” *Physical Review Letters*, vol. 113, no. 23, p. 238102, 2014.
- [3] A. Cavagna, D. Conti, C. Creato, L. Del Castello, I. Giardina, T. S. Grigera, S. Melillo, L. Parisi, and M. Viale, “Dynamic scaling in natural swarms,” *Nature Physics*, vol. 13, no. 9, p. 914, 2017.
- [4] B. I. Halperin and P. C. Hohenberg, “Generalization of scaling laws to dynamical properties of a system near its critical point,” *Phys. Rev. Lett.*, vol. 19, pp. 700–703, Sep 1967.
- [5] B. I. Halperin and P. C. Hohenberg, “Scaling laws for dynamic critical phenomena,” *Phys. Rev.*, vol. 177, pp. 952–971, Jan 1969.
- [6] L. Chen, J. Toner, and C. F. Lee, “Critical phenomenon of the order–disorder transition in incompressible active fluids,” *New Journal of Physics*, vol. 17, no. 4, p. 042002, 2015.
- [7] A. Cavagna, L. Di Carlo, I. Giardina, T. S. Grigera, and G. Pisegna, “Equilibrium to off-equilibrium crossover in homogeneous active matter,” *Physical Review Research*, vol. 3, no. 1, p. 013210, 2021.
- [8] A. Cavagna, L. Del Castello, I. Giardina, T. Grigera, A. Jelic, S. Melillo, T. Mora, L. Parisi, E. Silvestri, M. Viale, *et al.*, “Flocking and turning: a new model for self-organized collective motion,” *Journal of Statistical Physics*, vol. 158, no. 3, pp. 601–627, 2015.
- [9] A. Cavagna, L. Di Carlo, I. Giardina, L. Grandinetti, T. S. Grigera, and G. Pisegna, “Dynamical renormalization group approach to the collective behavior of swarms,” *Physical Review Letters*, vol. 123, no. 26, p. 268001, 2019.

- [10] A. Cavagna, L. Di Carlo, I. Giardina, L. Grandinetti, T. S. Grigera, and G. Pisegna, “Renormalization group crossover in the critical dynamics of field theories with mode coupling terms,” *Physical Review E*, vol. 100, no. 6, p. 062130, 2019.
- [11] A. Cavagna, L. Di Carlo, I. Giardina, T. S. Grigera, S. Melillo, L. Parisi, G. Pisegna, and M. Scandolo, “Natural swarms in **3.99** dimensions,” *arXiv preprint arXiv:2107.04432*, 2021.
- [12] K. G. Wilson, “Renormalization group and critical phenomena. i. renormalization group and the kadanoff scaling picture,” *Physical review B*, vol. 4, no. 9, p. 3174, 1971.
- [13] K. G. Wilson, “Renormalization group and strong interactions,” *Physical Review D*, vol. 3, no. 8, p. 1818, 1971.
- [14] B. Widom, “Equation of state in the neighborhood of the critical point,” *The Journal of Chemical Physics*, vol. 43, no. 11, pp. 3898–3905, 1965.
- [15] F. Ginelli, F. Peruani, M. Bär, and H. Chaté, “Large-scale collective properties of self-propelled rods,” *Physical review letters*, vol. 104, no. 18, p. 184502, 2010.
- [16] P. A. Lebowitz and G. Lasher, “Nematic-liquid-crystal order? a monte carlo calculation,” *Physical Review A*, vol. 6, no. 1, p. 426, 1972.
- [17] V. Schaller, C. Weber, C. Semmrich, E. Frey, and A. R. Bausch, “Polar patterns of driven filaments,” *Nature*, vol. 467, no. 7311, pp. 73–77, 2010.
- [18] B. Szabo, G. Szöllösi, B. Gönci, Z. Jurányi, D. Selmeczi, and T. Vicsek, “Phase transition in the collective migration of tissue cells: experiment and model,” *Physical Review E*, vol. 74, no. 6, p. 061908, 2006.
- [19] D. Bi, X. Yang, M. C. Marchetti, and M. L. Manning, “Motility-driven glass and jamming transitions in biological tissues,” *Physical Review X*, vol. 6, no. 2, p. 021011, 2016.
- [20] A. Sokolov, I. S. Aranson, J. O. Kessler, and R. E. Goldstein, “Concentration dependence of the collective dynamics of swimming bacteria,” *Physical review letters*, vol. 98, no. 15, p. 158102, 2007.
- [21] I. D. Couzin and N. R. Franks, “Self-organized lane formation and optimized traffic flow in army ants,” *Proceedings of the Royal Society of London. Series B: Biological Sciences*, vol. 270, no. 1511, pp. 139–146, 2003.
- [22] C. K. Hemelrijk and H. Kunz, “Density distribution and size sorting in fish schools: an individual-based model,” *Behavioral Ecology*, vol. 16, no. 1, pp. 178–187, 2005.

- [23] J. K. Parrish, S. V. Viscido, and D. Grunbaum, “Self-organized fish schools: an examination of emergent properties,” *The biological bulletin*, vol. 202, no. 3, pp. 296–305, 2002.
- [24] M. Ballerini, N. Cabibbo, R. Candelier, A. Cavagna, E. Cisbani, I. Giardina, A. Orlandi, G. Parisi, A. Procaccini, M. Viale, and V. Zdravkovic, “Empirical investigation of starling flocks: a benchmark study in collective animal behaviour,” *Anim Behav*, vol. 76, pp. 201–215, Jan 2008.
- [25] I. L. Bajec and F. H. Heppner, “Organized flight in birds,” *Animal Behaviour*, vol. 78, no. 4, pp. 777–789, 2009.
- [26] C. K. Hemelrijk and H. Hildenbrandt, “Some causes of the variable shape of flocks of birds,” *PloS one*, vol. 6, no. 8, p. e22479, 2011.
- [27] D. J. Sumpter, *Collective animal behavior*. Princeton University Press, 2010.
- [28] T. Vicsek and A. Zafeiris, “Collective motion,” *Physics Reports*, vol. 517, no. 3, pp. 71–140, 2012.
- [29] T. Vicsek, A. Czirók, E. Ben-Jacob, I. Cohen, and O. Shochet, “Novel type of phase transition in a system of self-driven particles,” *Phys Rev Lett*, vol. 75, pp. 1226–1229, Aug 1995.
- [30] F. Ginelli, “The physics of the Vicsek model,” *The European Physical Journal Special Topics*, vol. 225, no. 11-12, pp. 2099–2117, 2016.
- [31] C. W. Gardiner *et al.*, *Handbook of stochastic methods*, vol. 3. springer Berlin, 1985.
- [32] H.-K. Janssen, “On the nonequilibrium phase transition in reaction-diffusion systems with an absorbing stationary state,” *Zeitschrift für Physik B Condensed Matter*, vol. 42, no. 2, pp. 151–154, 1981.
- [33] G. Ódor, “Universality classes in nonequilibrium lattice systems,” *Reviews of modern physics*, vol. 76, no. 3, p. 663, 2004.
- [34] G. Baglietto and E. V. Albano, “Nature of the order-disorder transition in the Vicsek model for the collective motion of self-propelled particles,” *Physical Review E*, vol. 80, no. 5, p. 050103, 2009.
- [35] G. Grégoire and H. Chaté, “Onset of collective and cohesive motion,” *Physical review letters*, vol. 92, no. 2, p. 025702, 2004.
- [36] J. Toner and Y. Tu, “Long-range order in a two-dimensional dynamical xy model: How birds fly together,” *Phys Rev Lett*, vol. 75, pp. 4326–4329, Dec 1995.
- [37] Y. Tu, J. Toner, and M. Ulm, “Sound waves and the absence of galilean invariance in flocks,” *Phys. Rev. Lett.*, vol. 80, pp. 4819–4822, May 1998.

- [38] G. Grégoire and H. Chaté, “Onset of collective and cohesive motion,” *Phys Rev Lett*, vol. 92, p. 025702, Jan 2004.
- [39] H. Chaté, F. Ginelli, G. Grégoire, F. Peruani, and F. Raynaud, “Modeling collective motion: variations on the Vicsek model,” *The European Physical Journal B*, vol. 64, no. 3-4, pp. 451–456, 2008.
- [40] R. Grossmann, L. Schimansky-Geier, and P. Romanczuk, “Self-propelled particles with selective attraction–repulsion interaction: from microscopic dynamics to coarse-grained theories,” *New Journal of Physics*, vol. 15, no. 8, p. 085014, 2013.
- [41] P. Romanczuk and L. Schimansky-Geier, “Swarming and pattern formation due to selective attraction and repulsion,” *Interface focus*, vol. 2, no. 6, pp. 746–756, 2012.
- [42] A. Cavagna, I. Giardina, and T. S. Grigera, “The physics of flocking: Correlation as a compass from experiments to theory,” *Physics Reports*, vol. 728, pp. 1–62, 2018.
- [43] Andrea, A. Cimorelli, I. Giardina, G. Parisi, R. Santagati, F. Stefanini, and M. Viale, “Scale-free correlations in starling flocks,” *Proc Natl Acad Sci USA*, vol. 107, pp. 11865–70, Jun 2010.
- [44] P. F. Major and L. M. Dill, “The three-dimensional structure of airborne bird flocks,” *Behavioral Ecology and Sociobiology*, vol. 4, no. 2, pp. 111–122, 1978.
- [45] F. Heppner, “Three-dimensional structure and dynamics of bird flocks,” *Animal groups in three dimensions*, pp. 68–89, 1997.
- [46] A. Cavagna, I. Giardina, A. Orlandi, G. Parisi, A. Procaccini, M. Viale, and V. Zdravkovic, “The starflag handbook on collective animal behaviour: 1. empirical methods,” *Anim Behav*, vol. 76, pp. 217–236, Jan 2008.
- [47] A. Cavagna, I. Giardina, A. Orlandi, G. Parisi, and A. Procaccini, “The starflag handbook on collective animal behaviour: 2. three-dimensional analysis,” *Anim Behav*, vol. 76, pp. 237–248, Jan 2008.
- [48] A. Cavagna, A. Cimorelli, I. Giardina, A. Orlandi, G. Parisi, A. Procaccini, R. Santagati, and F. Stefanini, “New statistical tools for analyzing the structure of animal groups,” *Math Biosci*, vol. 214, pp. 32–37, Jan 2008.
- [49] M. Ballerini, N. Cabibbo, R. Candelier, A. Cavagna, E. Cisbani, I. Giardina, V. Lecomte, A. Orlandi, G. Parisi, A. Procaccini, *et al.*, “Interaction ruling animal collective behavior depends on topological rather than metric distance: Evidence from a field study,” *Proceedings of the national academy of sciences*, vol. 105, no. 4, pp. 1232–1237, 2008.

- [50] C. K. Hemelrijk and H. Hildenbrandt, “Scale-free correlations, influential neighbours and speed control in flocks of birds,” *Journal of Statistical Physics*, vol. 158, no. 3, pp. 563–578, 2015.
- [51] J. J. Binney, N. Dowrick, A. Fisher, and M. Newman, *The theory of critical phenomena: an introduction to the renormalization group*. Oxford University Press, Inc., 1992.
- [52] J. Goldstone, “Field theories with superconductor solutions,” *Il Nuovo Cimento (1955-1965)*, vol. 19, no. 1, pp. 154–164, 1961.
- [53] W. Bialek, A. Cavagna, I. Giardina, T. Mora, O. Pohl, E. Silvestri, M. Viale, and A. Walczak, “Social interactions dominate speed control in driving natural flocks toward criticality,” *arXiv*, vol. physics.bio-ph, Jul 2013.
- [54] A. Cavagna, A. Culla, L. Di Carlo, I. Giardina, and T. S. Grigera, “Low-temperature marginal ferromagnetism explains anomalous scale-free correlations in natural flocks,” *Comptes Rendus Physique*, vol. 20, no. 4, pp. 319–328, 2019.
- [55] A. Cavagna, A. Culla, X. Feng, I. Giardina, T. S. Grigera, W. Kion-Crosby, S. Melillo, G. Pisegna, L. Postiglione, and P. Villegas, “Marginal speed confinement resolves the conflict between correlation and control in natural flocks of birds,” *arXiv preprint arXiv:2101.09748*, 2021.
- [56] J. Downes, “The swarming and mating flight of diptera,” *Annual review of entomology*, vol. 14, no. 1, pp. 271–298, 1969.
- [57] D. H. Kelley and N. T. Ouellette, “Emergent dynamics of laboratory insect swarms,” *Scientific reports*, vol. 3, no. 1, pp. 1–7, 2013.
- [58] T. Mora and W. Bialek, “Are biological systems poised at criticality?,” *J Stat Phys*, vol. 144, pp. 268–302, Jul 2011.
- [59] M. A. Munoz, “Colloquium: Criticality and dynamical scaling in living systems,” *Reviews of Modern Physics*, vol. 90, no. 3, p. 031001, 2018.
- [60] J. Niel and J. Zinn-Justin, “Finite size effects in critical dynamics,” *Nuclear Physics B*, vol. 280, pp. 355–384, 1987.
- [61] P. C. Hohenberg and B. I. Halperin, “Theory of dynamic critical phenomena,” *Reviews of Modern Physics*, vol. 49, no. 3, p. 435, 1977.
- [62] J. Cardy, *Scaling and renormalization in statistical physics*, vol. 5. Cambridge university press, 1996.
- [63] L. Kadanoff, “The introduction of the idea that exponents could be derived from real-space scaling arguments,” *Physics*, vol. 2, pp. 263–273, 1966.

- [64] S. keng Ma, *Modern theory of critical phenomena*. Advanced book classics, Perseus Pub, 2000.
- [65] N. Goldenfeld, *Lectures on Phase Transitions and the Renormalization Group*. Reading, Massachusetts: Perseus Books, 1992.
- [66] L. Van Hove, “Correlations in space and time and born approximation scattering in systems of interacting particles,” *Physical Review*, vol. 95, no. 1, p. 249, 1954.
- [67] U. C. Täuber, *Critical dynamics: a field theory approach to equilibrium and non-equilibrium scaling behavior*. Cambridge University Press, 2014.
- [68] R. Kubo, “The fluctuation-dissipation theorem,” *Reports on progress in physics*, vol. 29, no. 1, p. 255, 1966.
- [69] H. Risken, “Fokker-planck equation,” in *The Fokker-Planck Equation*, pp. 63–95, Springer, 1996.
- [70] K. G. Wilson and J. Kogut, “The renormalization group and the ϵ expansion,” *Physics Reports*, vol. 12, no. 2, pp. 75–199, 1974.
- [71] P. C. Martin, E. Siggia, and H. Rose, “Statistical dynamics of classical systems,” *Physical Review A*, vol. 8, no. 1, p. 423, 1973.
- [72] H. Janssen, “Field-theoretic method applied to critical dynamics,” in *Dynamical critical phenomena and related topics*, pp. 25–47, Springer, 1979.
- [73] B. Halperin, P. Hohenberg, and S.-k. Ma, “Calculation of dynamic critical properties using wilson’s expansion methods,” *Physical Review Letters*, vol. 29, no. 23, p. 1548, 1972.
- [74] B. Halperin, P. Hohenberg, and E. Siggia, “Renormalization-group treatment of the critical dynamics of superfluid helium, the isotropic antiferromagnet, and the easy-plane ferromagnet,” *Physical Review B*, vol. 13, no. 3, p. 1299, 1976.
- [75] B. Halperin and P. Hohenberg, “Hydrodynamic theory of spin waves,” *Physical Review*, vol. 188, no. 2, p. 898, 1969.
- [76] H. Chaté, “Dry aligning dilute active matter,” *Annual Review of Condensed Matter Physics*, vol. 11, pp. 189–212, 2020.
- [77] G. Baglietto and E. V. Albano, “Finite-size scaling analysis and dynamic study of the critical behavior of a model for the collective displacement of self-driven individuals,” *Physical Review E*, vol. 78, no. 2, p. 021125, 2008.
- [78] H. Chaté, F. Ginelli, G. Grégoire, and F. Raynaud, “Collective motion of self-propelled particles interacting without cohesion,” *Phys Rev E Stat Nonlin Soft Matter Phys*, vol. 77, p. 046113, Mar 2008.

- [79] N. D. Mermin and H. Wagner, “Absence of ferromagnetism or antiferromagnetism in one- or two-dimensional isotropic heisenberg models,” *Phys. Rev. Lett.*, vol. 17, pp. 1133–1136, Nov 1966.
- [80] J. Toner, Y. Tu, and S. Ramaswamy, “Hydrodynamics and phases of flocks,” *Annals of Physics*, vol. 318, no. 1, pp. 170–244, 2005.
- [81] R. Kürsten and T. Ihle, “Dry active matter exhibits a self-organized cross sea phase,” *Physical Review Letters*, vol. 125, no. 18, p. 188003, 2020.
- [82] M. E. Fisher and A. Aharony, “Dipolar interactions at ferromagnetic critical points,” *Physical Review Letters*, vol. 30, no. 12, p. 559, 1973.
- [83] D. Forster, “Hydrodynamic fluctuations, broken symmetry, and correlation functions,” in *Reading, Mass., WA Benjamin, Inc. (Frontiers in Physics. Volume 47), 1975. 343 p.*, vol. 47, 1975.
- [84] E. Bertin, M. Droz, and G. Grégoire, “Boltzmann and hydrodynamic description for self-propelled particles,” *Phys. Rev. E*, vol. 74, p. 022101, 2006.
- [85] E. Bertin, M. Droz, and G. Grégoire, “Hydrodynamic equations for self-propelled particles: microscopic derivation and stability analysis,” *J. Phys. A*, vol. 42, p. 445001, 2009.
- [86] A. Cavagna and I. Giardina, “Bird flocks as condensed matter,” *Annu. Rev. Condens. Matter Phys.*, vol. 5, no. 1, pp. 183–207, 2014.
- [87] J. K. Taylor and C. Cihon, *Statistical techniques for data analysis*. CRC Press, 2004.
- [88] L. Pitaevskii and E. Lifshitz, *Physical kinetics*, vol. 10. Butterworth-Heinemann, 2012.
- [89] A. Attanasi, A. Cavagna, L. Del Castello, I. Giardina, T. S. Grigera, A. Jelić, S. Melillo, L. Parisi, O. Pohl, E. Shen, *et al.*, “Information transfer and behavioural inertia in starling flocks,” *Nature physics*, vol. 10, no. 9, pp. 691–696, 2014.
- [90] A. Cavagna, I. Giardina, T. S. Grigera, A. Jelic, D. Levine, S. Ramaswamy, and M. Viale, “Silent flocks: constraints on signal propagation across biological groups,” *Physical Review Letters*, vol. 114, no. 21, p. 218101, 2015.
- [91] T. Mora, A. M. Walczak, L. Del Castello, F. Ginelli, S. Melillo, L. Parisi, M. Viale, A. Cavagna, and I. Giardina, “Local equilibrium in bird flocks,” *Nature Physics*, vol. 12, no. 12, pp. 1153–1157, 2016.
- [92] A. Attanasi, A. Cavagna, L. Del Castello, I. Giardina, A. Jelic, S. Melillo, L. Parisi, O. Pohl, E. Shen, and M. Viale, “Emergence of collective changes in travel direction of starling flocks from individual birds’ fluctuations,” *Journal of The Royal Society Interface*, vol. 12, no. 108, p. 20150319, 2015.

- [93] A. Cavagna, D. Conti, I. Giardina, T. S. Grigera, S. Melillo, and M. Viale, “Spatio-temporal correlations in models of collective motion ruled by different dynamical laws,” *Physical Biology*, vol. 13, p. 065001, 2016.
- [94] D. Benedetto, P. Buttà, and E. Caglioti, “Some aspects of the inertial spin model for flocks and related kinetic equations,” *Mathematical Models and Methods in Applied Sciences*, vol. 30, no. 10, pp. 1987–2022, 2020.
- [95] S. W. de Leeuw, J. W. Perram, and H. G. Petersen, “Hamilton’s equations for constrained dynamical systems,” *Journal of statistical physics*, vol. 61, no. 5, pp. 1203–1222, 1990.
- [96] E. Bertin, M. Droz, and G. Grégoire, “Boltzmann and hydrodynamic description for self-propelled particles,” *Physical Review E*, vol. 74, no. 2, p. 022101, 2006.
- [97] A. Peshkov, E. Bertin, F. Ginelli, and H. Chaté, “Boltzmann-ginzburg-landau approach for continuous descriptions of generic vicsek-like models,” *The European Physical Journal Special Topics*, vol. 223, no. 7, pp. 1315–1344, 2014.
- [98] T. Ihle, “Towards a quantitative kinetic theory of polar active matter,” *The European Physical Journal Special Topics*, vol. 223, no. 7, pp. 1293–1314, 2014.
- [99] E. Bertin, A. Baskaran, H. Chaté, and M. C. Marchetti, “Comparison between smoluchowski and boltzmann approaches for self-propelled rods,” *Physical Review E*, vol. 92, no. 4, p. 042141, 2015.
- [100] D. Martin, H. Chaté, C. Nardini, A. Solon, J. Tailleur, and F. Van Wijland, “Fluctuation-induced phase separation in metric and topological models of collective motion,” *Physical Review Letters*, vol. 126, no. 14, p. 148001, 2021.
- [101] X. Yang and M. C. Marchetti, “Hydrodynamics of turning flocks,” *Physical review letters*, vol. 115, no. 25, p. 258101, 2015.
- [102] C. De Dominicis and L. Peliti, “Field-theory renormalization and critical dynamics above t_c : Helium, antiferromagnets, and liquid-gas systems,” *Physical Review B*, vol. 18, no. 1, p. 353, 1978.
- [103] E. Frey, “Crossover scaling functions and an extended minimal subtraction scheme,” *Physica A: Statistical Mechanics and its Applications*, vol. 221, no. 1-3, pp. 52–67, 1995.
- [104] E. Frey and F. Schwabl, “Renormalized field theory for the static crossover in uniaxial dipolar ferromagnets,” *Physical Review B*, vol. 42, no. 13, p. 8261, 1990.

- [105] A. Cavagna, L. Di Carlo, I. Giardina, T. S. Grigera, G. Pisegna, and M. Scandolo, “Dynamical renormalization group for mode-coupling field theories with solenoidal constraint,” *arXiv preprint arXiv:2103.10914*, 2021.
- [106] M. Marchetti, J. Joanny, S. Ramaswamy, T. Liverpool, J. Prost, M. Rao, and R. A. Simha, “Hydrodynamics of soft active matter,” *Reviews of Modern Physics*, vol. 85, no. 3, p. 1143, 2013.
- [107] S. Ramaswamy, “The mechanics and statistics of active matter,” *Annu. Rev. Condens. Matter Phys.*, vol. 1, p. 323, 2010.
- [108] N. Kyriakopoulos, F. Ginelli, and J. Toner, “Leading birds by their beaks: the response of flocks to external perturbations,” *New Journal of Physics*, vol. 18, no. 7, p. 073039, 2016.
- [109] Y. Tu and W.-J. Rappel, “Adaptation in living systems,” *Annual review of condensed matter physics*, vol. 9, pp. 183–205, 2018.
- [110] U. M. B. Marconi, A. Puglisi, L. Rondoni, and A. Vulpiani, “Fluctuation–dissipation: response theory in statistical physics,” *Physics reports*, vol. 461, no. 4–6, pp. 111–195, 2008.
- [111] A. Puglisi, A. Baldassarri, and V. Loreto, “Fluctuation-dissipation relations in driven granular gases,” *Physical Review E*, vol. 66, no. 6, p. 061305, 2002.
- [112] H. C. Andersen, “Rattle: A “velocity” version of the shake algorithm for molecular dynamics calculations,” *Journal of Computational Physics*, vol. 52, pp. 24–34, Oct. 1983.
- [113] M. Tuckerman, *Statistical mechanics: theory and molecular simulation*. Oxford university press, 2010.

Acknowledgements

I would like to start expressing my gratitude to Prof. Luca Giomi and Prof. Francesco Ginelli to have kindly accepted to read and evaluate this manuscript.

My greatest acknowledgment goes to my advisor and my mentor Dr. Andrea Cavagna. To him, I owe all my interest and my dedication to statistical physics, born with the study of the Ising model way back in 2016, and then grew up till the deepest concepts of the statistical field theory. I thank him for all the knowledge, the teachings, the working method, the passion for work he transmitted to me during these years. These are precious gifts, and I feel blessed to have received them.

I thank also Prof. Tomas Grigera that from Argentina has been always present to follow and guide my work. His teachings and the period of collaboration in La Plata completely determined my knowledge of the numerical techniques, giving me exceptional tools to achieve my results. My thanks go also to Prof. Irene Giardina for having participated in the intense blackboard sessions and discussions, for having offered me the opportunity to work on recent novel projects, and for having represented to me a model of a successful woman in science.

Finally, I need to thank all the group CoBBS: Massimiliano, Leonardo, and especially Stefania for the fruitful scientific discussions but also for existential and life advice along the streets of San Lorenzo. Among the *kids*, I need to firstly thank Luca Di Carlo, which is one of the main co-authors of all the publications explained in this work. Thanks to our collaboration it was possible to reach these results. To conclude I thank Antonio, Federica, Mattia, and Mario for the work we have done together and the things I learned through our discussions. I am sincerely grateful to have had the incredible and rare opportunity to collaborate with each of them.

Work never comes by itself, I thank family and friendships to have been the essential cure to the bitter moments of these last three years.

Giulia Pisegna, Rome, January 2022
